N69-18665
32

NASA CR-72360

R7338

CASE FILE COPY

INTERIM REPORT

SPACE STORABLE REGENERATIVE COOLING INVESTIGATION

PREPARED FOR

NATIONAL AERONAUTICS AND SPACE ADMINISTRATION

CONTRACT NAS3-11191

ROCKETDYNE
A DIVISION OF NORTH AMERICAN ROCKWELL CORPORATION
6633 CANOGA AVENUE, CANOGA PARK, CALIFORNIA 91304

NOTICE

This report was prepared as an account of Government sponsored work. Neither the United States, nor the National Aeronautics and Space Administration (NASA), nor any person acting on behalf of NASA:

A.) Makes any warranty or representation, expressed or implied, with respect to the accuracy, completeness, or usefulness of the information contained in this report, or that the use of any information, apparatus, method, or process disclosed in this report may not infringe privately owned rights; or

B.) Assumes any liabilities with respect to the use of, or for damages resulting from the use of any information, apparatus, method, or process disclosed to this report.

As used above, "person acting on behalf of NASA" includes any employee or contractor of NASA, or employee of such contractor, to the extent that such employee or contractor of NASA, or employee of such contactor prepares, disseminates, or provides access to, any information pursuant to his employment or contract with NASA, or his employment with such contractor.

Requests for copies of this report should be referred to

National Aeronautics and Space Administration
Office of Scientific and Technical Information
Attention: AFSS-A
Washington, D.C. 20546

NASA CR-72360
R7338

INTERIM REPORT

SPACE STORABLE REGENERATIVE COOLING INVESTIGATION

by

R. P. Pauckert

prepared for

NATIONAL AERONAUTICS AND SPACE ADMINISTRATION

September 25, 1968

CONTRACT NAS3-11191

Technical Management
NASA Lewis Research Center
Cleveland, Ohio
Liquid Rocket Propulsion Office
John W. Gregory

ROCKETDYNE
A Division of North American Rockwell Corporation
6633 Canoga Avenue
Canoga Park, California 91304

ACKNOWLEDGMENTS

The contributions of the following personnel are gratefully acknowledged: R. Tobin, T. Vahedi, and W. Wagner for heat transfer analysis; J. Shoji for performance analysis and nozzle contour design; A. Axworthy and M. Ladacki for coolant decomposition research and analysis; W. Anderson and H. Griggs for program management advice and direction.

FOREWORD

The results of the Parametric and Detailed Heat Transfer Analyses are presented in this report. These studies comprise Task I of Contract NAS 3-11191 conducted by Rocketdyne, a division of North American Rockwell Corporation. Technical direction of the effort was supplied by John W. Gregory of the NASA Lewis Research Center.

The analysis reported herein were conducted from July through December of 1967. The results for other tasks of this contract will be reported separately.

ABSTRACT

Analyses were conducted to determine the regenerative cooling capabilites of light hydrocarbon fuels when used with FLOX and OF_2 oxidizers over a wide range of operating conditions. Limits based on propellant decomposition, pressure drop, and coolant passage dimensions were applied. The presence or absence of a gas-side carbon layer was found to be significant. All of the hydrocarbons were suitable coolants with the carbon layer. Without the carbon layer only methane was applicable for regenerative cooling under all conditions; the other hydrocarbons were generally limited to low chamber pressures or high thrust levels.

TABLE OF CONTENTS

Acknowledgements iii

Foreword v

Abstract vii

Introduction 1

Summary 5

Parametric Analysis 5

Detailed Analysis 8

Conclusions 13

Parametric Analysis 15

Heat Input 16

Thrust Chamber Design and Analysis 16

Heat Transfer Analysis 20

Carbon Deposition on the Walls 31

Heat Absorption Capabilities 42

Subcritical Pressure Operation 49

Supercritical Pressure Operation 51

Operating Limits 58

Supercritical Operation 58

Subcritical Operation 70

Operating Limits Summary 96

Detailed Analysis. 101

Ground Rules and Preliminary Observations 103

Pressure Drop, Thermal, and Geometric Limits . . . 103

Thrust Chamber Wall Materials 107

Thrust Chamber Wall Coatings 110

TABLE OF CONTENTS (continued)

FLOX/Methane Analysis Results 112
Pressure Drops for Nickel Walls 112
Wall Material and Coating Effects 117
Coolant Temperature and Channel Dimensions 120
OF_2/Propane Analysis Results 123
Pressure Drops for Nickel Walls 123
Wall Material and Coating Effects 126
Coolant Temperature and Channel Dimensions 126
OF_2/1-Butene Analysis Results 131
Nickel-200 Wall Material with Carbon Coating . . . 131
Hastelloy-X Wall Material with Carbon Coating . . . 138
347 CRES Wall Material with Carbon Coating 138
Nickel-200 without Carbon Coating and 139
with Refractory Coating
Nomenclature 147
References 151
Appendix A
Gas-Side Heat Transfer Coefficient Calculations A-1
Appendix B
Gas-Side Carbon Layer Thermal Resistance B-1
Appendix C
Thermal Decomposition of Light Hydrocarbon C-1
Kinetics and Products of Pyrolysis C-1
Decomposition Temperature C-5
Inhibition and Catalysis C-9
Pyrolytic Carbon Formation C-10

TABLE OF CONTENTS (continued)

Appendix D

Calculation of Coolant Transport Properties D-1

Methane D-1

Propane D-2

1-Butene D-3

Appendix E

Detailed Analysis Technique E-1

ILLUSTRATIONS

1. Bell Nozzle Design 18
2. Bell Nozzle Contours 19
3. Temperature Ratio Variation 22
4. Wall Mach Number Variation 23
5. Thrust Influence Coefficient 25
6. Chamber Pressure Influence Coefficient 26
7. Area Ratio Influence Coefficients 27
8. Gas-Side Wall Temperature Influence Coefficient. 28
9. Comparison of Heat Transfer Coefficients - FLOX/Methane 33
10. Comparison of Heat Transfer Coefficients - FLOX/Propane 34
11. Comparison of Heat Transfer Coefficients - FLOX/Butene 35
12. Comparison of Heat Transfer Coefficients - FLOX/Pentane Blend 36
13. Variation of Combustion-Side Film Coefficient with Axial Location: Injector S/N IF 764 37
14. Variation of Combustion-Side Film Coefficient with Axial Location: Injector S/N HK 713 38
15. Measured Heat Loss Per Pound of Propellant vs Mixture Ratio 40
16. Heat Transfer Rate Reduction for Various Hydrocarbons . . 41
17. Mixture Ratio Effect on Performance, Area Ratio = 40 . . . 44
18. Mixture Ratio Effect on Performance, Area Ratio = 100 . . 45
19. Area Ratio Effect on Performance 46
20. Chamber Pressure Effect on Performance 47

ILLUSTRATIONS (continued)

21. Thrust Effect on Delivered Performance 48
22. Regenerative Cooling Limits Based on Propellant Decomposition $\epsilon_c = 2$, $\epsilon = 100$ 65
23. Regenerative Cooling Limits Based on Propellant Decomposition $\epsilon_c = 2$, $\epsilon = 40$ 66
24. Regenerative Cooling Limits Based on Propellant Decomposition, $\epsilon_c = 4$, $\epsilon = 100$ 67
25. Regenerative Cooling Limits Based on Propellant Decomposition, $\epsilon_c = 4$, $\epsilon = 60$ 68
26. Regenerative Cooling Limits Based on Propellant Decomposition, $\epsilon_c = 4$, $\epsilon = 40$ 69
27. Normalized Nozzle Heat Input vs Local Heat Flux 73
28. Total Heat Input vs Thrust and Propellant Combination . . 75
29. Propellant Mixture Ratio and Geometry Tradeoffs Based on Ethane Boiling Limits with Carbon Layer 77
30. Minimum Thrust Limits for Propane at $P_c = 100$ psia 78
31. Minimum Thrust Limits for FLOX/Propane at $P_c = 100$ psia. . 79
32. Minimum Thrust Limits for Ethane at Chamber Pressure of 250 psia 88
33. Minimum Thrust Limits for Propane at Chamber Pressure of 250 psia 90
34. Minimum Thrust Limits for FLOX/Propane at Chamber Pressure of 250 psia. 91
35. Operating Envelopes at 250 psia Chamber Pressure with Carbon Layer 99
36. Channel Isotherm Profiles in Throat Region 106
37. Effect of Material and Heat Flux on Throat Coolant - Side Wall Temperature. 109

ILLUSTRATIONS (continued)

38. Coating Temperature Drop vs Heat Flux 111
39. Coating Thickness Requirements as a Function of Heat Flux Level 112
40. Methane Cooling Jacket Pressure Drop with Nickel Walls 114
41. Coolant Jacket Pressure Drop - Nickel Walls with Carbon Layer 116
42. Comparison of Nickel and Steel Chambers 118
43. Methane Cooling Jacket Pressure Drop with Hastelloy X Walls 119
44. Coolant Exit Bulk Temperature for FLOX/Methane Thrust Chambers 121
45. Minimum Channel Dimensions for the FLOX/Methane Regenerative-Cooled Thrust Chambers 122
46. Coolant Jacket Pressure Drops for OF_2/Propane with Nickel Walls 124
47. Coolant Jacket Pressure Drops for OF_2/Propane with Hastelloy X Walls 127
48. Wall Temperature Profiles for OF_2/Propane 128
49. Coolant Exit Bulk Temperatures for OF_2/Propane Chambers . 129
50. Minimum Channel Dimension for the OF_2/Propane Regenerative Cooled Thrust Chambers 130
51. 1-Butene Coolant Jacket Pressure Drops with Gas-Side Carbon Layer 133
52. Maximum Coolant Velocity Requirements for 1-Butene with Gas-Side Carbon Layer 134

ILLUSTRATIONS (continued)

53. Wall Thickness vs Chamber Pressure for Various Materials 130
54. Channel Dimension vs Chamber Pressure for OF_2/1-Butene 137
55. Bulk Temperature Rise vs Chamber Pressure for OF_2/1-Butene 140
56. Pressure Drop vs Chamber Pressure for OF_2/1-Butene with No Carbon Layer 142
57. Wall Temperature for 1-Butene with No Carbon Layer . . . 143
58. Coolant Velocity Requirements for 1-Butene with No Carbon Layer 144
B1. Nondimensionalized Heat Transfer Rate vs Axial Coordinate for FLOX/Methane B-3
B2. Nondimensionalized Heat Transfer Rate vs Axial Coordinate for FLOX/Propane B-4
B3. Nondimensionalized Heat Transfer Rate vs Axial Coordinate for FLOX/1-Butene B-5
B4. Nondimensionalized Heat Transfer Rate vs Axial Coordinate for FLOX/Pentane-Blend B-6
B5. Carbon Layer Resistance Correlation for FLOX/Methane B-8
B6. Carbon Layer Resistance Correlation for FLOX/Propane . . B-9
B7. Carbon Layer Resistance Correlation for FLOX/Butene-1 . . B-10
B8. Carbon Layer Resistance Correlation for FLOX/Pentane-Blend B-11
B9. Carbon Layer Resistance Correlation for FLOX/Methane . . B-13
E1. Coolant-Side Curvature Enhancement Factor E-6
E2. Effect of Temperature on Coolant Mass Velocity Requirements E-7

TABLES

S-1. Subcritical Operation Summary 9
1. Ranges of Operating Parameters 15
2. Propellant Combustion Products Properties 21
3. Variation of Heat Transfer Characteristics with Propellant Combination and Mixture Ratio 24
4. Temperature Data for Light Hydrocarbon Fuels 50
5. Subcritical Heat Absorption Capabilites 52
6. Kinetic Parameters 54
7. Decomposition Temperatures 55
8. Supercritical Heat Absorption Capabilities 57
9. Nominal Design Parameters 59
10. Coolant Jacket Discharge Temperatures 61
11. Heat Absorption Capability/Heat Input Ratio 62
12. Maximum Chamber Pressure (psia) for 1000 Pound Thrust . . 63
13. Throat Heat Flux Values 72
14. 1-Butene Boiling Conditions 80
15. Regenerative Cooling Circuits for Subcritical Operation . 82
16. FLOX/1-Butene Cooling Limits at 250 psia Chamber Pressure with $T_{Bulk} \leq T_{Sat}$ 92
17. Applicable Thrust Regimes for Regenerative Cooling at 100 psia Chamber Pressure 97
18. Applicable Thrust Regimes for Regenerative Cooling at 250 psia Chamber Pressure 98
19. Operating Conditions for Detailed Analysis 102
20. Limiting Conditions for Regenerative Cooling 105
C-1. Kinetic Parameters C-6
C-2. Decomposition Temperatures C-8
E-1. Correlation Constants for Maximum Nucleate Boiling Heat Flux E-8

INTRODUCTION

Propellant combinations with overlapping liquidus ranges are attractive for extended-duration space missions because of the elimination or reduction of interpropellant heat transfer. Both propellants may be maintained at the same temperature and need to be insulated only from external heat sources, i.e., payload and environment. Space storable propellant combinations using FLOX or OF_2 as the oxidizer and a light hydrocarbon as the fuel have the additional advantages of high theoretical performance and good availability of the fuel.

Because of the promising characteristics of these propellant combinations, initial theoretical and experimental studies were conducted (e.g., Contracts NAS 3-4195, NAS 3-6296, NAS 3-7950) to select the most suitable fuels and to determine actual combustion chamber performance and heat transfer characteristics. These theoretical studies indicated the lighter hydrocarbons to be the most attractive from a performance standpoint; however, the lighter hydrocarbons were found to be inadequate for use as nonboiling regenerative coolants under subcritical operating conditions. Moderate C* efficiencies were demonstrated and, most significantly, the experimental heat flux values were found to be significantly lower than theoretically predicted. The reduction in heat flux was found to be approximately proportional to the carbon-to-hydrogen atomic ratio so that the denser hydrocarbons became attractive as regenerative coolants. These analytical and experimental investigations were conducted over the 100- to 250-psia chamber pressure range at thrust levels of 5000 to 12,500 pounds.

Application of space storable propellants at higher chamber pressures and over broader thrust ranges now appears promising. The present investigation was therefore undertaken to extend the ranges of operating conditions considered in the earlier studies for regeneratively cooled thrust chambers. The

chamber pressure and thrust ranges covered in the present study were 100 to 1000 psia for chamber pressure and 1000 to 20,000 pounds for thrust. Effects of variations of thrust chamber contraction ratio from 2 to 4 and expansion area ratio from 40 to 100 were evaluated. The implications of reducing propellant mixture ratio to as low as 70 percent of the optimum (maximum C*) value and of using various thrust chamber construction materials were evaluated. On the basis of the earlier study results, methane, ethane, and a blend of 55 percent methane and 45 percent ethane were selected for evaluation because of their high performance; propane and 1-butene were selected because of their superior heat transfer characteristics with a gas-side carbon layer.

The purpose of the present effort is to define regenerative cooling limits over the above ranges of operating parameters. Recognizing that a high performance injector is essential to obtaining meaningful thrust chamber heat transfer data, a second purpose of the present effort was the development of an injector delivering a C* efficiency of at least 96 percent.

The heat transfer analysis was divided into two tasks: (1) Parametric Analysis; and (2) Detailed Analysis. In the Parametric Analysis, the 10 propellant combinations (two oxidizers, five fuels) were evaluated over the entire range of variables by comparing heat absorption capabilities of the regenerative coolant with the heat input to the entire thrust chamber. Based upon the results of the Parametric Analysis, three propellant combinations were selected for Detailed Heat Transfer Analysis. Actual thrust chamber designs were made to determine heat transfer limits resulting

from excessive coolant pressure drops, minimum fabrication dimensions, or thermal decomposition of the coolant. The results of the heat transfer analyses contained in this report provide regenerative cooling design data for a wide range of potential thrust chamber operating conditions for space storable propellant combinations and specify those conditions under which regenerative cooling is practical.

SUMMARY

The present analytical study was undertaken to define the operating conditions and limits for regenerative cooling as applied to the light hydrocarbon fuels when used with FLOX or OF_2 as oxidizers. The ranges of operating parameters, particularly chamber pressure and thrust level, investigated previously were extended in this study. The effort was conducted in two major areas, the Parametric Analysis and the Detailed Analysis.

PARAMETRIC ANALYSIS

The purpose of the Parametric Analysis was to determine regenerative cooling limits, based upon coolant temperature limits, for a wide variety of operating parameters. Ten propellant combinations were investigated: FLOX and OF_2 as oxidizers with methane, ethane, propane, 1-butene, and a blend of methane and ethane as fuels. Chamber pressures ranged from 100 to 1000 psia, thrust levels from 1000 to 20,000 pounds, propellant mixture ratios from 70 to 100 percent of the optimum values, and nozzle area ratios from 40 to 100. The total heat input input to the chamber was also varied by varying the contraction ratio from 2 to 4 and the gas-side wall temperature from 1700 to 3200F. Two assumptions were made concerning the gas-side carbon layer: 1) the assumption of no gas-side carbon layer was made, and alternately 2) the assumption was made that the heat input computed analytically was reduced by the carbon layer by an amount based on existing experimental data.

The total heat input to the chamber was first calculated without considering carbon layer effects. Little variation in heat input with propellant combination or propellant mixture ratio was found. The effects of other variables (thrust, chamber pressure, area ratios, and gas-side wall) temperature) were then determined. The nozzle area ratio had a comparatively small effect over the range investigated.

Experimental data taken at 100 psia chamber pressure and relatively low characteristic velocity efficiency were then correlated with total heat input determined by application of the analytical model to the experimental conditions. Significant heat input reductions were found and the ratio of experimental-to-analytical values of heat input was nearly linear with the hydrogen-to-carbon atomic ratio of the fuel. Propellant mixture ratio effects on the carbon layer effectiveness were found to be uncertain. Values of heat flux reduction used in subsequent analyses were based upon the average of experimental data obtained with solid-wall and regeneratively cooled thrust chambers.

The heat absorption capability of the regenerative coolants was based upon the enthalpy change of the coolant between the inlet and exit of the coolant jacket. The inlet enthalpy was evaluated at ten degrees (F) above the freezing point of the fuel. The exit enthalpy depended upon the allowable maximum bulk temperature of the fuel which in turn, depended upon the pressure at the coolant jacket exit.

For high chamber pressure operation, the limiting temperature was that which resulted in decomposition of the fuel. A literature search was conducted to determine the most accurate values of kinetic constants to relate decomposition rates to coolant bulk temperature. Decomposition temperatures used in the analysis were: methane, 1500F; ethane and the methane-ethane blend, 900F,; propane, 850F; and 1-butene, 800F.

For low-chamber-pressure operation the conditions in the coolant jacket were subcritical and the restriction that bulk boiling should not occur limited the exit temperature to the saturation value. The saturation temperature was based upon a pressure which was 20 percent higher than chamber pressure to account for a reasonable injector pressure drop.

Removal of the saturation temperature limit at low pressures was also investigated. However, it was then required that (1) complete vaporization of the fuel be accomplished to avoid mixed-phase flow in the injector, and (2) that bulk boiling be confined to the low flux (< 1 Btu/in^2-sec) region of the nozzle. A nucleate boiling flux of 3 Btu/in^2-sec was established as a practical maximum value.

A comparison of the heat inputs and the heat absorption capabilities was then made to determine the conditions under which regenerative cooling could be accomplished. Regenerative cooling was found to be applicable to practically all combinations of parameters investigated on the basis of propellant decomposition if the assumed gas-side carbon layer was present. The temperature of the 1-butene at the exit of the coolant jacket was furthest below the decomposition temperature. The exit temperature of the methane-ethane blend was closest to the decomposition value. Without the carbon layer, methane could still be used as a regenerative coolant under all conditions. For the other fuels, however, reduction of propellant mixture ratio and/or nozzle area ratio would be required to prevent propellant decomposition at low thrust levels and high chamber pressures, or the gas-side wall temperature would have to be raised to 3200F.

Combinations of parameters may be selected for the chamber pressures which result in subcritical pressure operation (100 and 250 psia chamber pressures were investigated) which will permit use of regenerative cooling with all of the fuels at most thrust levels. Methane can be used as a regenerative coolant with complete vaporization under all conditions. The same conclusions apply to the methane-ethane blend except that the minimum thrust level is approximately 3500 pounds at 250 psia chamber

pressure if a carbon layer does not exist. Ethane can be used as a liquid at the higher thrust levels and completely vaporized at the low thrust levels if a carbon layer exists. Without a carbon layer, ethane can be vaporized at all thrust levels but is decomposition-limited to thrust levels above 3500 pounds at 250 psia chamber pressure. Propane may be used as a liquid at all thrust levels with a carbon layer and may be completely vaporized without decomposition at all thrust levels above 5000 pounds without a carbon layer. Butene may be used at all thrust levels with a carbon layer as a liquid and may be completely vaporized at all thrust levels without a carbon layer at 100-psia chamber pressure. Regenerative cooling without a carbon layer at 250-psia chamber pressure is limited to the 20,000 pound thrust level for 1-butene (Table S-1).

DETAILED ANALYSIS

The purpose of the Detailed Analysis was to further investigate regenerative cooling limits for propellant combinations which were the most attractive on the basis of performance and the results of the Parametric Analysis. Detailed analysis and designs were accomplished for FLOX/methane at thrust levels of 1000, 5000 and 20,000 pounds for OF_2/propane at 5000 and 20,000 pounds, and for OF_2/1-butene at 1000 pounds. Channel-type coolant passages in nickel, stainless steel (CRES), and Hastelloy X walls were assumed. The nickel and CRES operated at a maximum gas-side wall temperature of 1700F, the Hastelloy X at 2100F. The case of a refractory coating operating at 3200F on a nickel wall chamber was also evaluated. Analyses were again conducted both with and without the assumption of a gas-side carbon layer. A contraction ratio of 4, a nozzle area ratio of 100, and optimum propellant mixture ratio were generally assumed. Single-pass counterflow coolant circuits were found to be practical for most cases.

TABLE S-1

SUBCRITICAL OPERATION SUMMARY

Coolant	Carbon Layer	Coolant Exit State	Minimum Thrust Level,* pounds
Methane	Yes	Vapor	< 1000
	No	Vapor	< 1000
Methane-Ethane	Yes	Vapor	< 1000
	No	Vapor	3500 pounds at P_c = 250 psia
Ethane	Yes	Liquid ($F \gtrsim 10000$ pounds)	< 1000
		Vapor ($F \lesssim 10000$ pounds)	
	No	Vapor	3500 pounds at P_c = 250 psia
Propane	Yes	Liquid	< 1000
	No	Vapor	5000 pounds at P_c = 250 psia
1-Butene	Yes	Liquid	< 1000
	No	Vapor	20000 pounds at P_c = 250 psia

*Based on thermal decomposition temperature limit

ROCKETDYNE

Regenerative cooling limits were based upon coolant jacket pressure drop, minimum channel dimensions, and coking of the coolant. The allowable pressure drop varied linearly from 100 psi at a chamber pressure of 100 psia to 500 psi at 1000 psia. Minimum channel dimensions occurred at the throat where the channels were square for dimensions greater than 0.040 inches. The configuration of smaller channels was a constant width of 0.040 inches and a variable depth. A minimum depth of 0.025 was selected on the basis of manufacturing tolerances and plugging considerations. Coolant-side wall temperatures were limited to 1500F for propane and 1-butene and to 2000F for methane to prevent coking of the coolant.

Regenerative cooling was practical for the FLOX/methane propellant combination with nickel walls at all chamber pressures and thrust levels investigated whether or not a gas-side carbon layer exists. Only at the most severe condition (1000 psia chamber pressure and 1000 pounds thrust level with no carbon layer) were the pressure drop and minimum channel dimension limits slightly exceeded. The coating was approximately as effective as the gas-side carbon layer in reducing the heat flux.

Pressure drop limits were slightly exceeded for the OF_2/propane propellant combination only at 1000 psia chamber pressure with no carbon layer. The carbon layer was more effective in reducing the heat flux than the 3200F coating. The 1500F decomposition temperature limit on the coolant-side wall did not permit use of the 2100F capability of the Hastelloy X. The gas-side wall temperatures of all materials were established by nucleate boiling conditions for subcritical pressure operation with a carbon layer. Minimum channel dimensions were less than 0.025 inches at chamber pressures greater than 750 psia with no carbon layer. Propellant mixture ratio reductions (to as low as 74 percent of the optimum value at 1000 psia chamber pressure) would be required to maintain a

minimum channel depth of 0.025 inches. Regenerative cooling is therefore practical for OF_2/propane at all chamber pressures and thrust levels if the assumed gas-side carbon layer exists. Regenerative cooling is possible without the carbon layer but operating parameters are sometimes restricted.

The OF_2/1-butene propellant combination can be regeneratively cooled at the 1000-pound thrust level for all chamber pressures and materials investigated if the assumed gas-side carbon layer exists. Without the carbon layer, pressure drops with a nickel wall were generally acceptable, although slightly above the 500 psi limit at the highest (1000 psia) chamber pressure analyzed. Use of CRES or Hastelloy X would result in even higher pressure drops at the high chamber pressures. The minimum channel dimensions were satisfactory for subcritical operation without a carbon layer but were below the limit under supercritical operating conditions. The exit temperature of the coolant was above the decomposition value, 800F, for all chamber pressures without a carbon layer or refractory coating. Application of a coating to increase the gas-side wall temperature to 3200F or reduction of propellant mixture ratio would prevent coolant decomposition.

Nickel 200 was found to be the most suitable material for thrust chamber walls at high flux levels, i.e, high chamber pressures with no carbon layer. Hastelloy X was slightly superior at moderate heat flux conditions. CRES was inferior to the other two materials because of its low thermal conductivity and operating temperature. However, under low heat flux conditions, the differences between the three materials was not sufficient to base a selection on the regenerative cooling characteristics.

As a general conclusion, it may be stated that regenerative cooling with the light hydrocarbons appears practical over the ranges of chamber pressures and thrust levels investigated in this study. Regenerative cooling is, generally, greatly facilitated by the presence of a gas-side carbon layer.

CONCLUSIONS AND RECOMMENDATIONS

The following conclusions may be made based upon the results of the Parametric and Detailed Analyses.

1. Regenerative cooling is feasible for all of the ten propellant combinations investigated with respect to coolant decomposition if the assumed gas-side carbon layer exists. Thrust levels from 1000 to 20,000 pounds and chamber pressures from 100 to 1000 psia are included.

2. If a gas-side carbon layer does not exist, coolant decomposition occurs under some conditions for most of the fuels. Conditions which tend to cause decomposition are high chamber pressure and low thrust.

3. Methane is particularly suitable for regenerative cooling inasmuch as it is not decomposition-limited at any thrust level or chamber pressure investigated, even without a carbon layer.

4. Coolant pressure drops are acceptable for methane, propane, and 1-butene for all chamber pressures and thrust levels investigated either with or without a gas-side carbon layer if nickel is used as the hot-gas wall material.

5. Use of Hastelloy-X as a wall material would result in lower pressure drops than nickel except at high chamber pressures without a carbon layer. Use of CRES would result in higher pressure drops than nickel. However, for the low heat fluxes associated with the gas-side carbon layer, all three materials result in acceptable pressure drops.

6. Coolant channel minimum dimensions are acceptable for methane, propane, and 1-butene if the carbon layer is present. Without the carbon layer the coolant channel dimensions at the throat are smaller than acceptable at higher chamber pressures for propane at 5000 pounds thrust and 1-butene at 1000 pounds thrust.

7. Although conservative estimates were used in the present analysis, experimental verification of coolant side heat transfer coefficients by means of heated tube experiments in the following areas is desirable:

   a. Methane at low bulk temperatures and high pressures
   b. Propane and 1-butene at high coolant velocities in the subcritical region

8. Further development and experimental verification of the regenerative cooling capabilities of FLOX/methane or OF_2/methane is desirable because of the high specific impulse and analytically demonstrated cooling capability of these propellant combinations. Experiments should be conducted in the 500 to 1000 psia chamber pressure range with a high performance injector.

PARAMETRIC HEAT TRANSFER ANALYSIS

The purpose of this analytical effort was to specify regenerative cooling limits for a wide variety of operating conditions on the basis of the heat absorption capabilities of the regenerative coolant. The operating parameter ranges are shown in Table 1. The propellants represent combinations found to have attractive features on the basis of the results of previous studies. Mission analysis and application studies have indicated the range of thrust levels, nozzle area ratios, and chamber pressures shown in Table 1. The contraction area ratios, propellant mixture ratios, and gas-side wall temperatures represent possible design compromises which may be employed to improve regenerative cooling capabilities.

TABLE 1

RANGES OF OPERATING PARAMETERS

Fuels: Methane(CH_4)
Ethane(C_2H_6)
Blend of 45 percent Ethane and 55 percent Methane
Propane(C_3H_8)
Butene-1(C_4H_8)

Oxidizers: FLOX (optimum mixture)
OF_2

Chamber Pressure, psia: 100, 250, 500, 750, 1000
Vacuum Thrust, pounds: 1000, 2500, 5000, 10,000, 20,000
C* Efficiency: 96 percent of theoretical shifting equilibrium
Mixture Ratio (o/f): 70, 80, 90 and 100 percent of optimum
Contraction Ratio: 2:1, 3:1, 4:1
Chamber Characteristic Length (L*), inches: 30
Nozzle Area Ratio (Regeneratively Cooled Portion): 40:1, 60:1, 100:1

Temperature of wall on gas side, F: 1700, 2100, 3200.

The basic approach to the parametric phase of the analysis consisted of the calculation and comparison of the heat rejected to the thrust chamber walls (heat input) with the heat absorption capability of the coolant under the various operating conditions. Nozzles and combustion chambers were initially designed and analyzed to determine heat inputs with no gas-side carbon layer. Experimentally determined carbon effects were superimposed upon the analytical heat inputs. The heat absorption capabilities of the regenerative coolant were detemined on the basis of boiling limits for subcritical operation and coolant decomposition for the supercritical operation.

HEAT INPUT

Determination of thrust chamber inputs was first made on the basis of theoretical calculations including gas-side boundary layer effects but without inclusion of the carbon layer effects. Combustion chamber and nozzle designs were accomplished to provide a basis for the heat transfer calculations.

Thrust Chamber Design and Analysis

On the basis of previous experience, a nozzle convergence angle of 15 degrees and a ratio of throat radius of curvature to throat radius of 0.7 were selected. The angle selected represents a compromise between minimizing the combustion chamber surface (large angle) and providing for suitable boundary layer growth to reduce the peak heat flux at the throat (small angle).

The analysis was conducted by first developing a transonic input line from point T to point A (Fig. 1). This transonic line forms an input to the design program. Prandtl-Meyer flow was assumed around the wall defined by the downstream radius, R_2, to the Point T'. The flow field was calculated by applying the method of characteristics to the right-running characteristic line from T'. The point T' was obtained by specifying the wall angle Θ_m. Using the right-running characteristic line emanating from T' and designated as line Θ_m, a value of M^*_D was selected. From this value, an optimum impulse control surface was formed using the optimization criteria of Ref. 1 and 2. The control surface determines the exit point, E, which, in turn, defines the nozzle length, L, and area ratio, ϵ. The contour was developed by forming left-running characteristics from optimum control surface, terminating each line by satisfying the continuity equation. A rapid computerized, iterative procedure was used to select the values of Θ_M and M^*_D which would result in an 80-percent-length nozzle of the required area ratio.

Past Rocketdyne studies have indicated that optimum nozzle contours are relatively insensitive to chemical kinetics of the combustion products, chamber pressure, and mixture ratio for the cases presently under consideration. Since the propellant combinations presently being investigated have similar exhaust gas properties, the nozzle design is not expected to vary significantly with propellant combination, and therefore the nozzle designs were performed for the FLOX/methane propellant combination. A method-of-characteristics analysis was then used to determine the temperature, density, and Mach number profiles along the nozzle wall.

The nozzle contours designed for FLOX/methane at a chamber pressure of 1000 psia are shown in Fig. 2. The contour for an area ratio of 100 was used to analyze the effects of propellant combination and mixture ratio on the combustion product properties and flow characteristics along the wall.

M* = MACH NUMBER REFERRED TO SONIC VELOCITY AT MACH 1

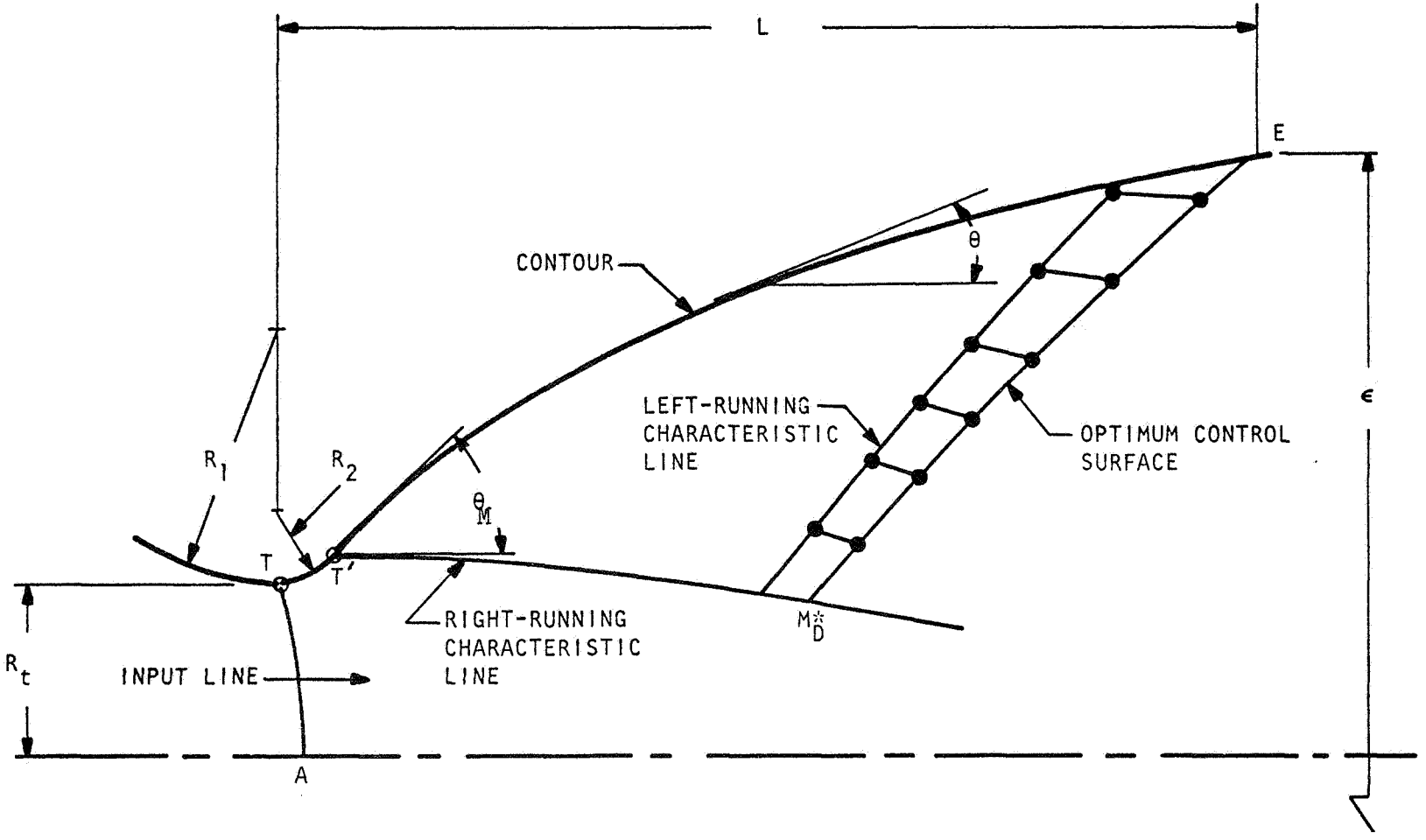

Figure 1. Bell Nozzle Design

DESIGN CONDITIONS:

PROPELLANT = FLOX (82.6)/CH_4

o/f = 5.7 Pc = 1000 psia

80 percent Bell Nozzle

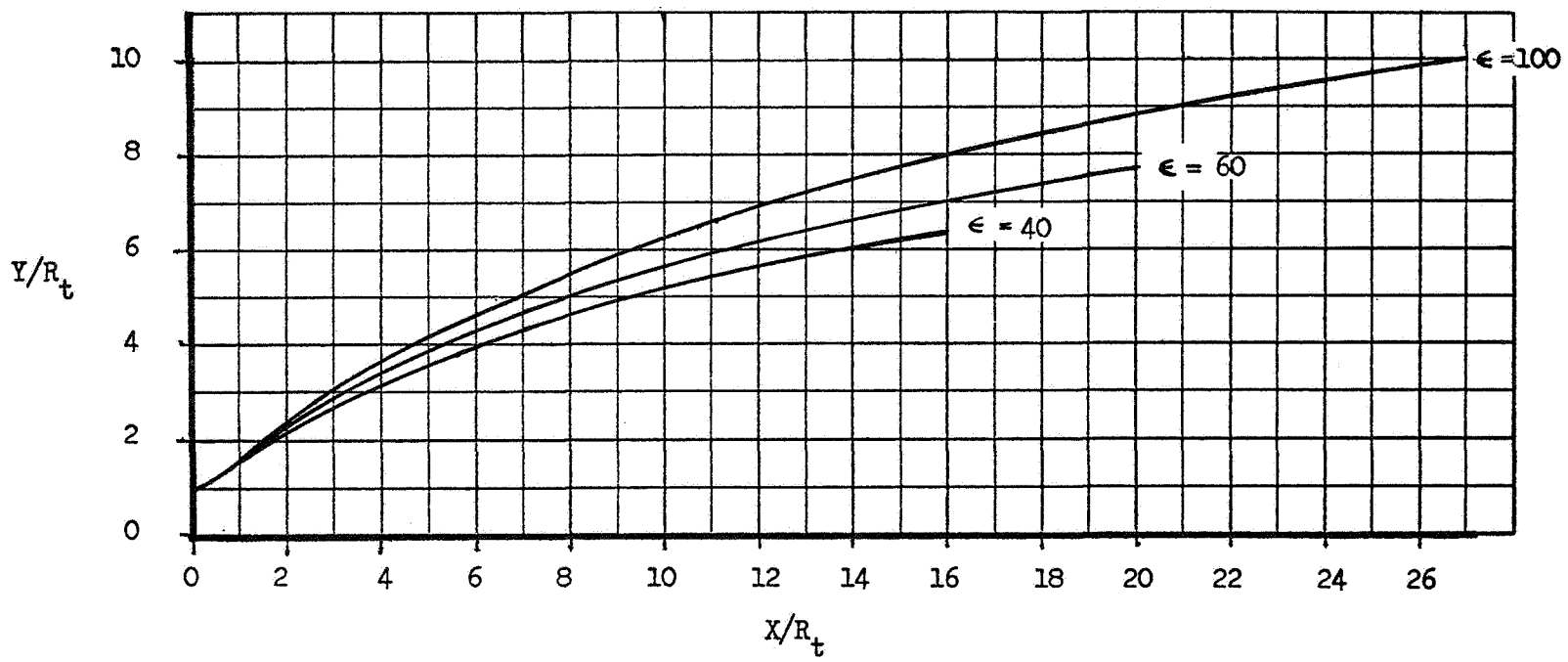

Figure 2. Bell Nozzle Contours

The propellant combination FLOX/butene-1 was selected as the combination most different from the reference propellants. The effect of propellant mixture ratio was investigated by analyzing the FLOX/methane propellants at a mixture ratio of 4.0 (70 percent of optimum).

The results of these analyses, as shown in Table 2 for the combustion chamber, throat, and nozzle exit regions imply small effects because of mixture ratio variations and negligible (for heat transfer calculation purposes) effects resulting from propellant combination differences. The manner in which the local-to-throat static temperature ratio and Mach number vary along the nozzle are shown in Fig. 3 and 4 respectively. Similarity of results for all cases is again evident. The data generated by these analyses were used in the heat transfer analysis to obtain a comparison of the three cases on the basis of the total heat rejected to the thrust chamber walls.

Heat Transfer Analysis

Gas-side heat transfer coefficient profiles along the thrust chamber walls were computed for the two propellant combinations, FLOX/methane and FLOX/butene-1, and for two propellant mixture ratios, 5.7 and 4.0, for FLOX/methane. The chamber pressure and nozzle area ratio were 500 psia and 100 respectively. The total integrated heat rejection rates were then calculated. The approach employed to obtain the heat transfer coefficient profiles was to solve the von Karman boundary layer integral momentum equation and the integral energy equation to describe the wall skin friction and Stanton number behavior along the chamber length as described in Appendix A. This approach has been found to yield results which are in better agreement with experimental data than the more simplified closed-form Bartz solution (Ref. 3) frequently used for conservative, rapid estimates.

TABLE 2

PROPELLANT COMBUSTION PRODUCTS PROPERTIES

Properties	Combustion Chamber			Throat			Nozzle Wall Exit	
Propellant	T_o, R	Chem Equilib	Mol Wt	T*, R	C_p*	Chem Equilib	M*	P/P*
FLOX (82.6 percent F_2)/CH_4 (77 F) MR = 5.7 (optimum)	8440	1.169	19.56	7930	0.423	1.166	2.800	0.00584
FLOX (82.6 percent F_2)/CH_4 (77F) MR = 4 (0.7 optimum)	7530	1.185	18.46	7000	0.482	1.189	2.753	0.00587
FLOX (70.4 percent F_2) /C_4H_8 (77 F) MR = 3.85 (optimum)	8440	1.172	20.76	7920	0.402	1.169	2.786	0.00580

Chamber Pressure = 1000 psia ϵ = 100

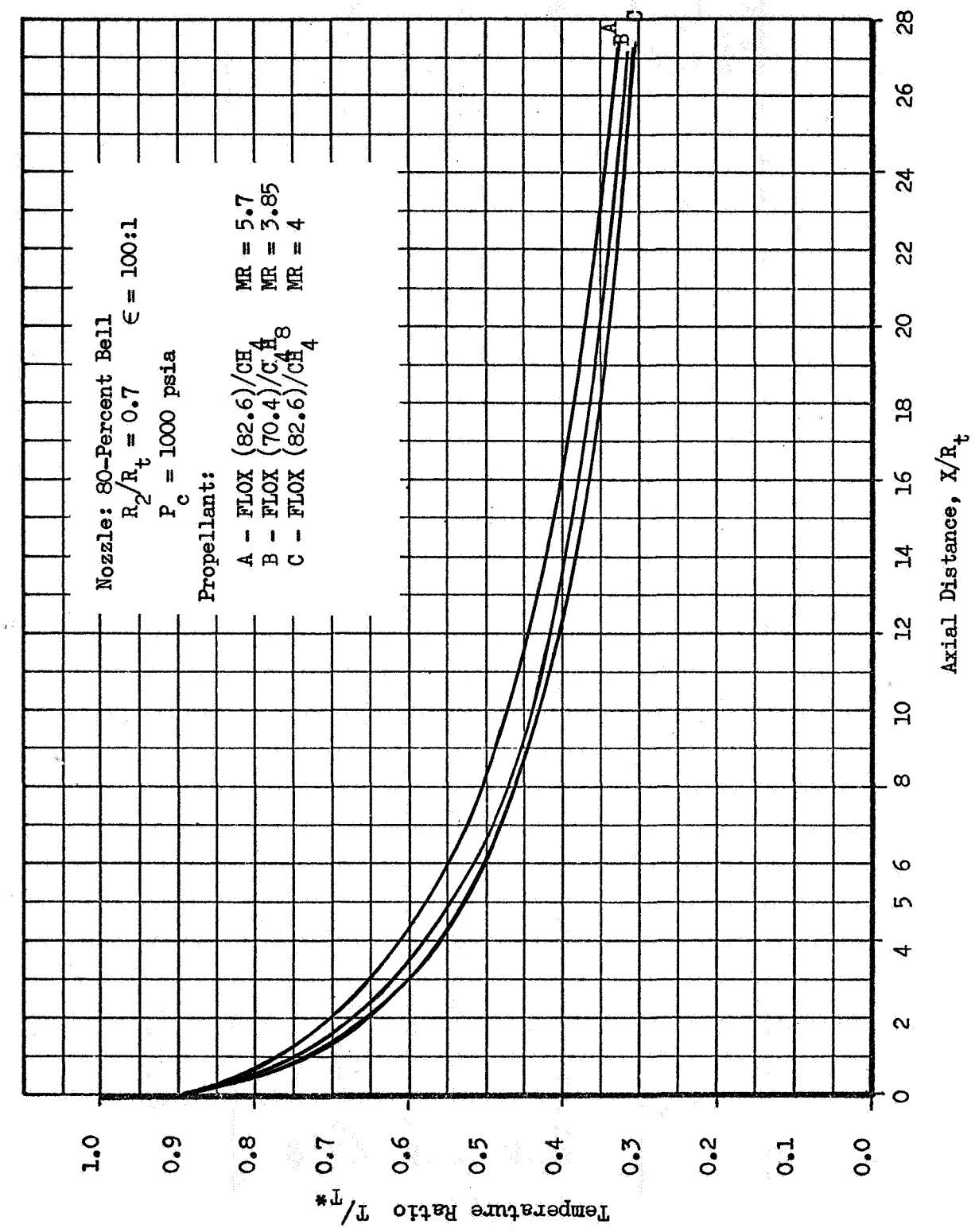

Figure 3. Temperature Ratio Variation

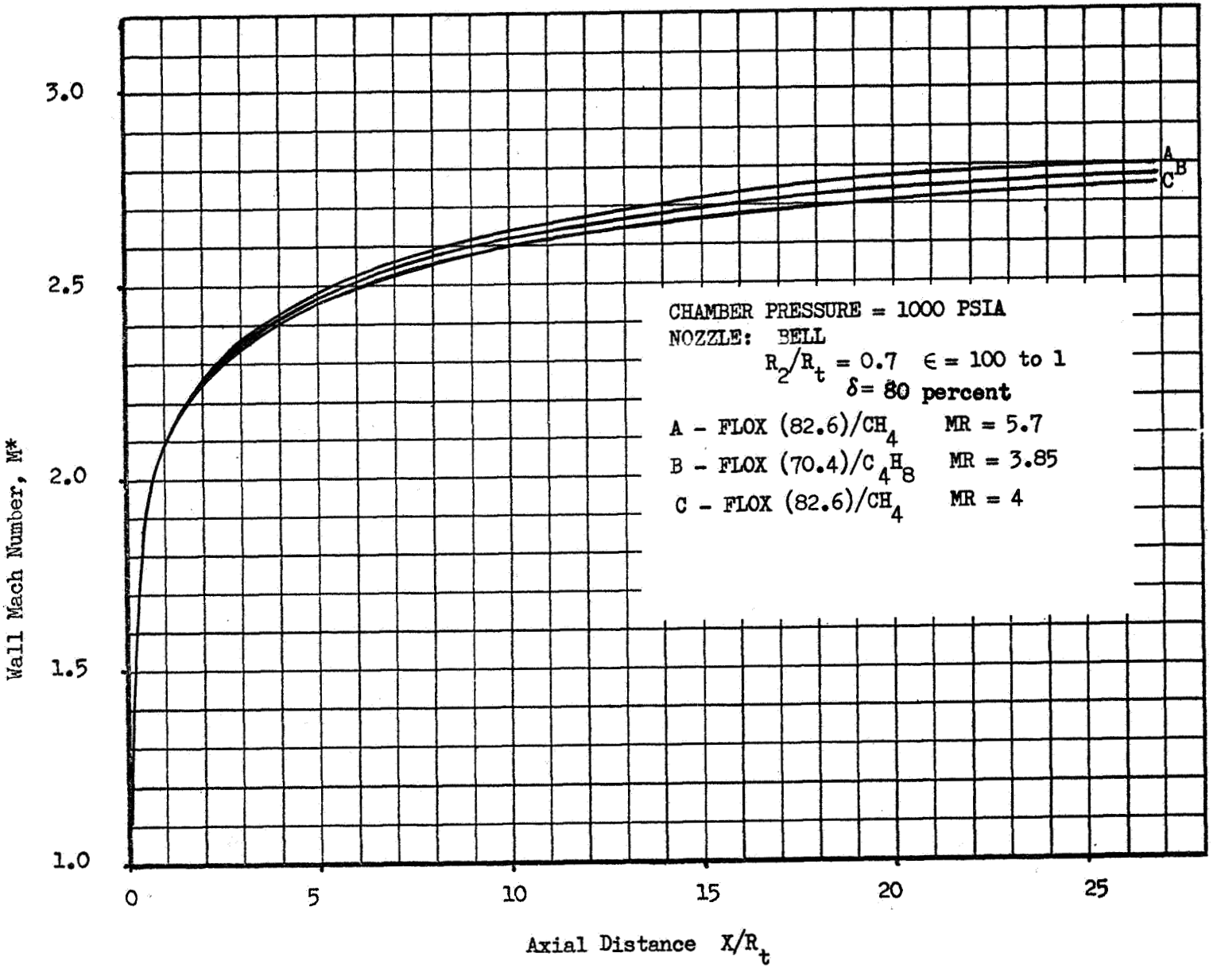

Figure 4. Wall Mach Number Variation

TABLE 3

VARIATION OF HEAT TRANSFER CHARACTERISTICS
WITH PROPELLANT COMBINATION AND MIXTURE RATIO

Propellants	Mixture Ratio (o/f)	Btu/in^2-sec	Total Heat Input Btu/sec
FLOX/methane	5.7	9.4	1570
FLOX/methane	4.0	9.3	1540
FLOX/butene-1	3.85	9.3	1575

The results of the analysis for the three cases are shown in Table 3 and indicate that the total heat flux values are similar for the propellant combinations being considered in this analysis when carbon layer effects are not included. The effect of propellant mixture ratio on the integrated heat flux and on the local throat heat flux is also seen to be very small. The heat transfer analyses for the remaining variables were then conducted for the no-carbon layer case and the experimental values of heat transfer reduction caused by carbon layer effects were superimposed upon the results of these analysis.

The total heat inputs calculated for the various combinations of thrust, chamber pressure, expansion and contraction area ratios, and gas-side wall temperature are presented in Fig. 5 through 8 in the form of influence coefficients. These coefficients illustrate the effect of a single variable on the heat input and, as such, they are useful in showing the significance of variations of a particular parameter with respect to the heat input. Furthermore, they provide a convenient means of approximating the total heat input for any given set of conditions. The total heat input, Q, in terms of the reference value, Q_{ref}, and influence coefficient, η, is:

$$Q = \left[Q_{ref_N} \times \eta_{F_N} \times \eta_{P_{c_N}} \times \eta_{T_{wg}} \times \eta_{\epsilon_c}\right] + \left[Q_{ref_{CZ}} \times \eta_{F_{CZ}} \times \eta_{P_{c_{CZ}}} \times \eta_{T_{wg}} \times \eta_{\epsilon}\right]$$

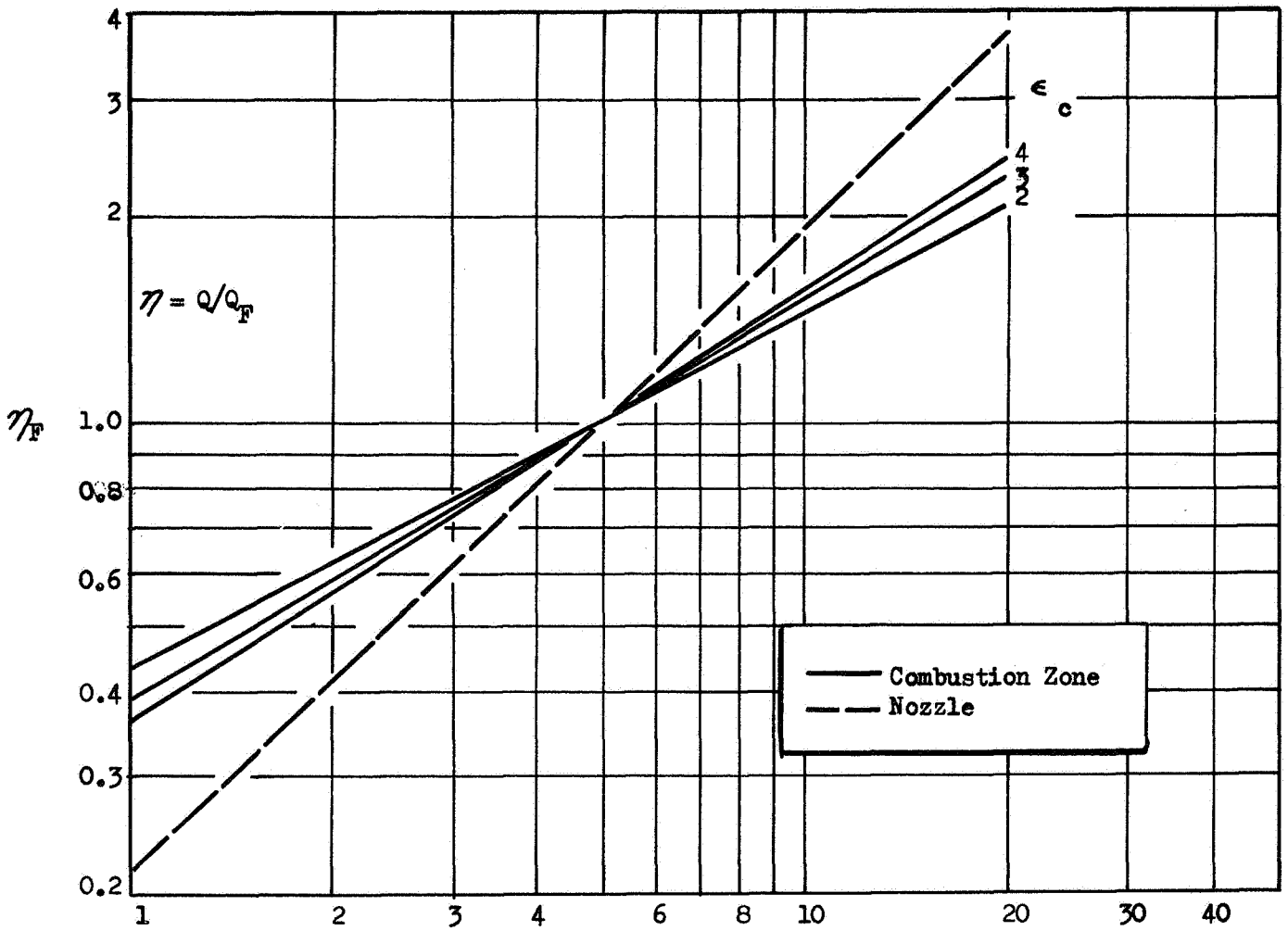

Thrust, 1000 Pounds

Figure 5 . Thrust Influence Coefficient

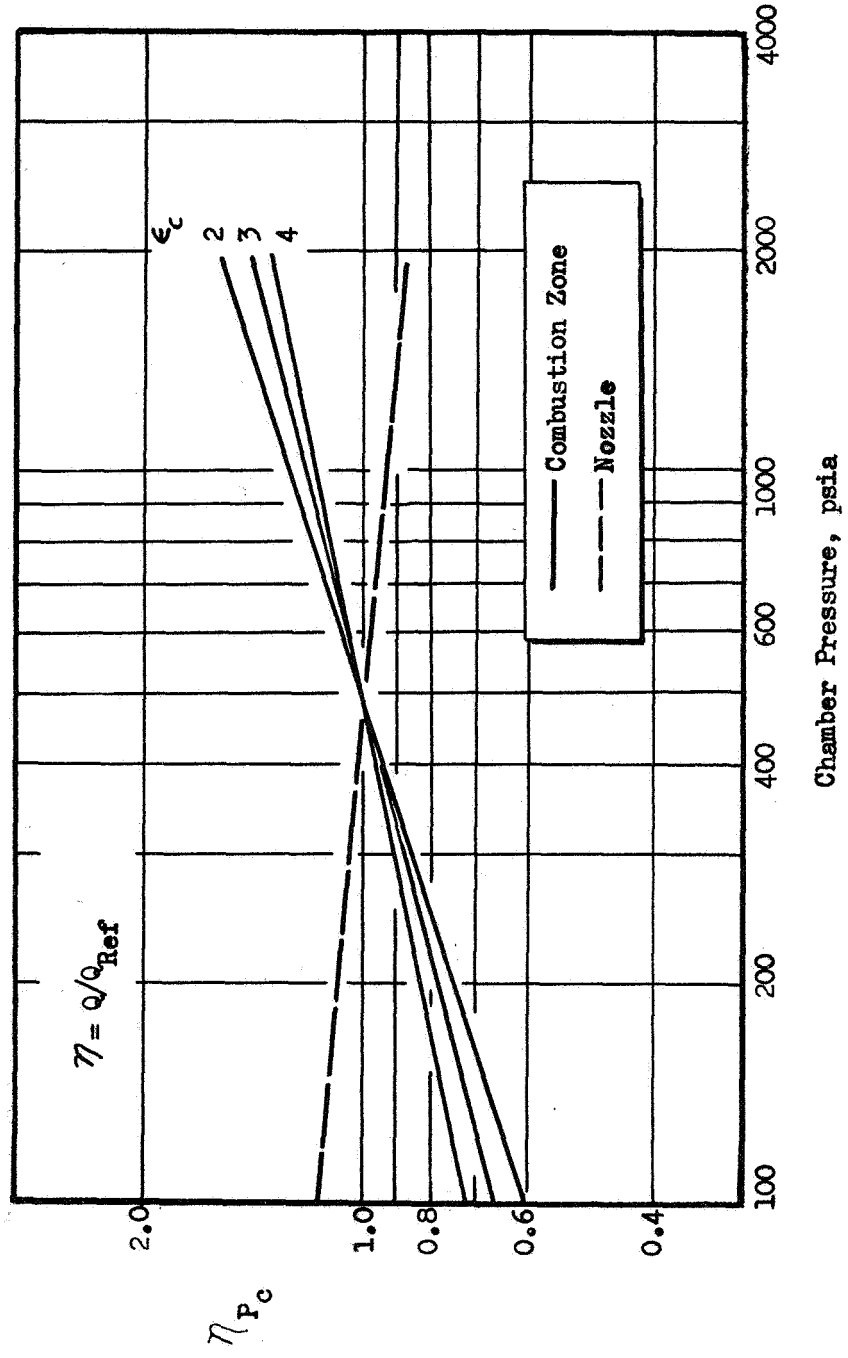

Figure 6 . Chamber Pressure Influence Coefficient

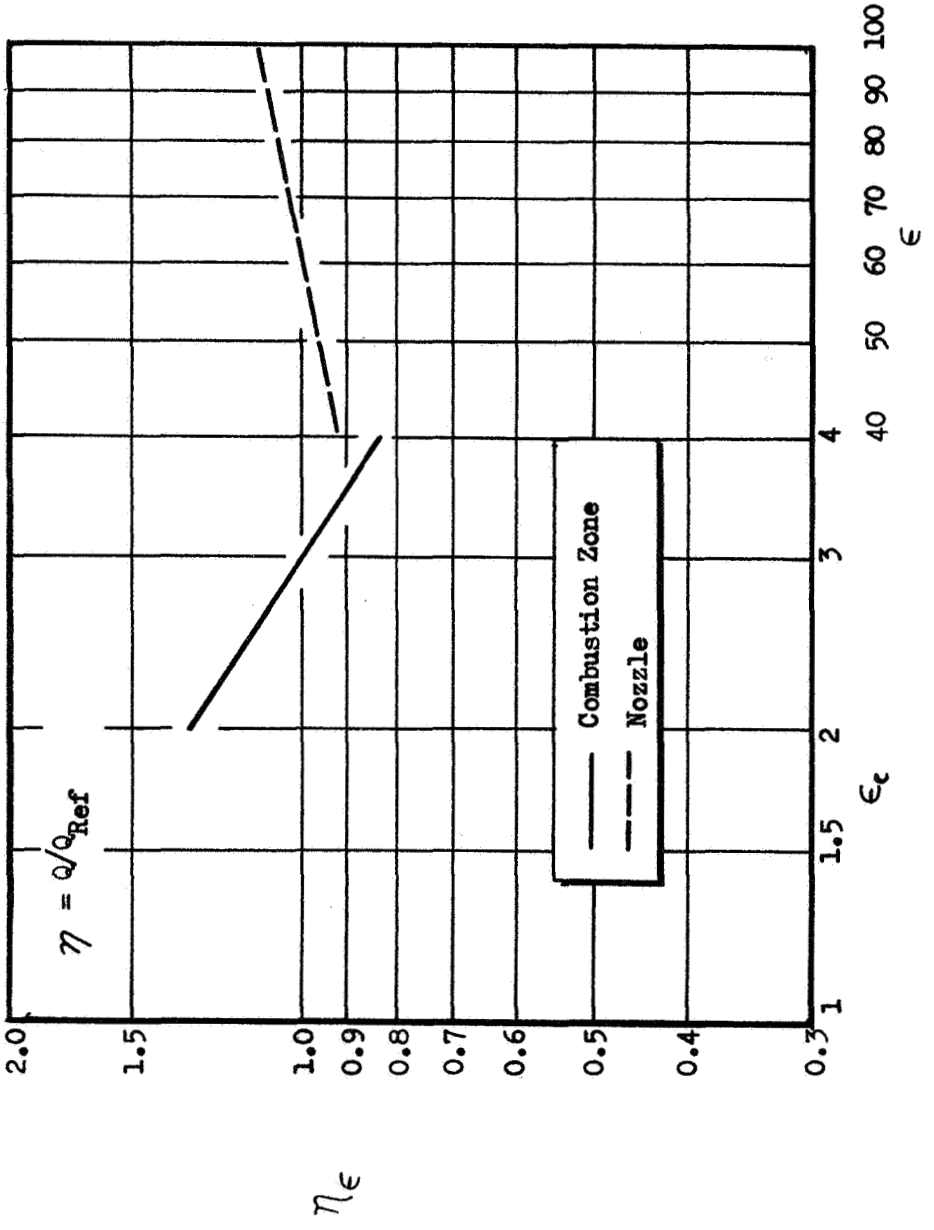

Figure 7. Area Ratio Influence Coefficients

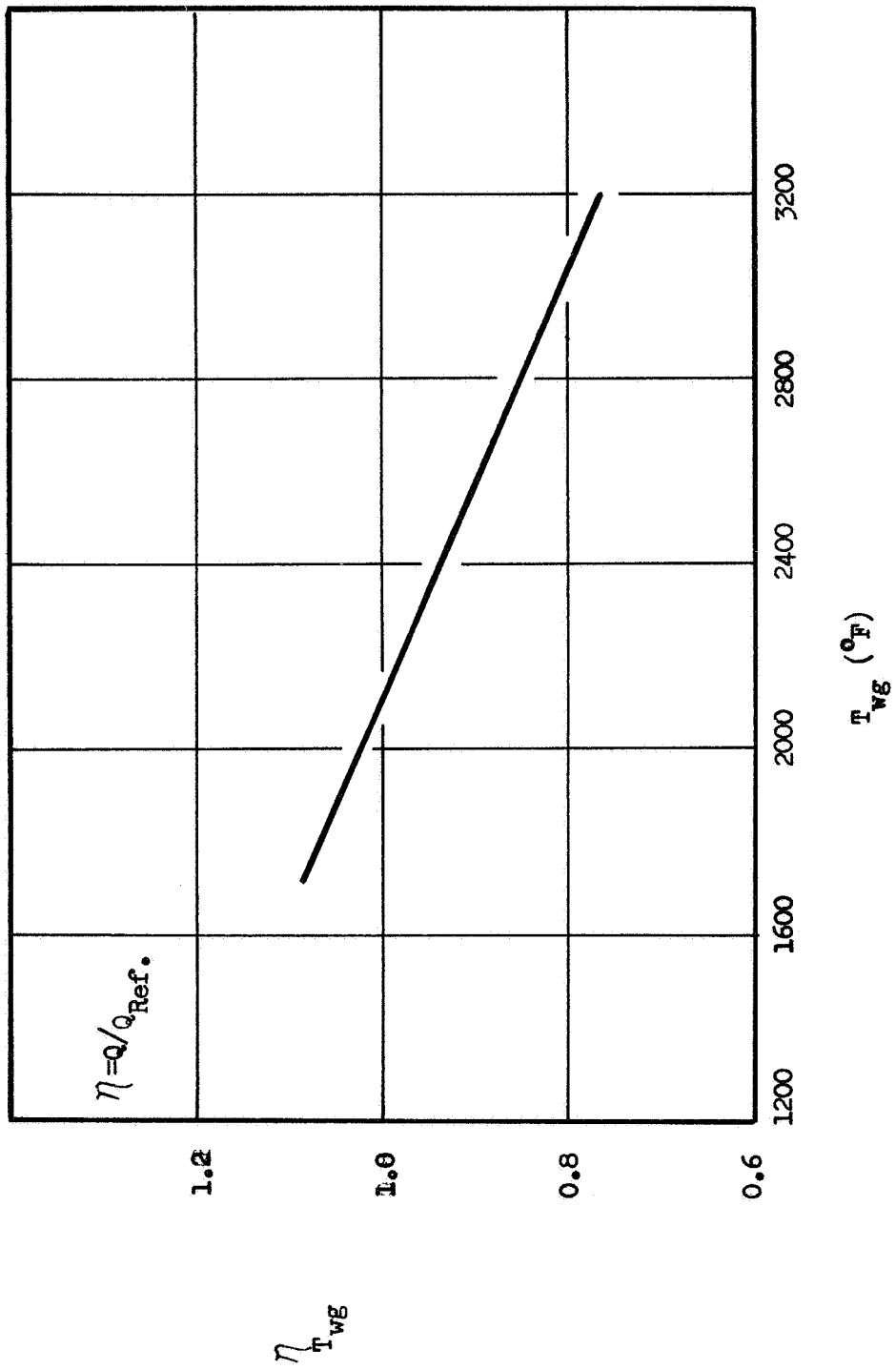

Figure 8 . Gas-Side Wall Temperature Influence Coefficient

The subscript CZ refers to the thrust chamber region upstream of the throat and the subscript N refers to the region downstream. The value of Q_{ref_N} was 649 Btu/sec and $Q_{ref_{CZ}}$ was 846 Btu/sec. The reference values of total heat input were calculated for the conditions shown below:

OPERATING CONDITIONS FOR Q_{ref}

Propellants	FLOX (82.6)/Methane
Mixture Ratio	5.7
Thrust, pounds	5000
Chamber pressure, psia	500
Nozzle Area Ratio	60
Contraction Area Ratio	3
Gas-side Wall Temperature, F	2100
Carbon Layer	None

The effect of thrust on the total heat input was found to differ for the combustion zone and the nozzle. Accordingly, influence coefficients are presented in Fig. 5 for each section of the chamber. The thrust influence coefficient for the combustion zone depends upon the contraction ratio ϵ_c, because the value ϵ_c affects the heat transfer rate to the cylindrical portion of the chamber (all analyses were conducted for a constant L* value of 30 inches). These coefficient indicate that the heat input to the nozzle is approximately proportional ($Q_N \propto F^{0.95}$) while the combustion zone heat input is less than proportional to thrust ($Q_{c_z} \propto F^{0.60}$). Since coolant flowrate is almost proportional to thrust, the total heat absorption capability-to-heat input ratio may be expected to improve with increasing thrust level.

The chamber pressure influence coefficients shown in Fig. 6 were also separated into combustion zone and nozzle coefficients. The coefficients have a positive slope in the combustion zone region and a negative slope in the nozzle although the heat transfer rates are approximately proportional to $P_c^{0.8}$ in both regions. This occurs because the nozzle surface area varies approximately inversely with chamber pressure, while the variation of combustion zone surface areas with chamber pressure depends upon the contraction ratio because of the fixed L* constraint.

The influence coefficients for the nozzle contraction and expansion area ratios are shown in Fig. 7. The contraction area ratio coefficient was found to be sensitive to the thrust level and chamber presssure. For values of F and P_c at the extremes of the matrix under investigation, the error in the contraction area ratio coefficient could be as much as 15 percent. In the parametric and detailed analyses, actual computed heat flux values were used.

The effect of nozzle expansion area ratio on the combustion zone heat input is small over the range of area ratios investigated. This geometric effect can be appreciated by comparing the contours shown in Fig. 2. Because the lower area ratio optimum contours approach the axial direction more rapidly, more of their surface (for a given length) is exposed to high heat flux conditions. The gas-side tube wall temperature affects the heat inputs to the nozzle and combustion zone similarly so that the total heat input effect may be presented as shown in Fig. 8.

Carbon Deposition on the Hot Gas Wall

Combustion of hydrocarbons in the thrust chamber results in deposition of a layer of carbon upon the walls of the combustion chamber and nozzle. This carbon could provide a significant contribution to the total resistance to heat transfer and must, therefore, be considered in calculation of heat inputs for the various operating conditions. The extent of carbon layer formation depends upon complex chemical and mechanical equilibrium in the boundary layer. Since analytical determination of the carbon layer resistance is not possible at this time, experimental data must be used. Ideally, the data should indicate the axial profiles of the carbon layer resistance as functions of the variables being investigated in the present study; i.e., chamber pressure, thrust level, contraction and expansion area ratios, propellant combination, propellant mixture ratio, gas-side wall temperature, and combustion efficiency. Experimental data applicable to the light hydrocarbon fuels are those of Ref. 4 and 5. The tests were conducted with FLOX and several hydrocarbons at 100-psia chamber pressure and with FLOX/methane at 250 psia. These data, although not encompassing the complete range of operating conditions, were used and extrapolated to provide the best available estimates of carbon layer resistance.

Analysis Method and Results. The axial profiles of the measured heat transfer coefficients were presented in Ref. 4 and 5. These were compared with the gas-side film coefficient profiles calculated by the closed-form Bartz equation (Ref. 3). Although this equation is simple to apply and results in conservative values for design purposes, the use of the integral energy equation as described in Appendix A yields values in closer agreement with experimental results as indicated in Ref. 6 and was the method of analysis used throughout this study. Accordingly, these equations were applied to the experimental conditions of Ref. 4

and 5, and the resulting theoretical gas-side heat transfer coefficients correlated with the experimental values. These correlations resulted in carbon-layer resistance profiles and overall heat transfer rate reduction factors.

The computerized integral energy equations were first applied to test data taken at a chamber pressure of 100 psia in uncooled thrust chambers. Actual thrust chamber geometrical parameters were used in the analysis. Details of the analysis are given in Appendices A and B.

The axial profiles of the gas-side heat transfer coefficients are shown in Fig. 9 through 12. The Bartz equation, as is typical, results in higher values of the film coefficient than the integral energy equation in the throat region. The experimental results are significantly lower than either of the two theoretical curves. The maximum values of the measured heat transfer coefficient occur approximately half an inch downstream of the throat for propane, pentane-blend, and butene-1 tests. Normally, the maximum heat transfer coefficient occurs slightly upstream of the throat.

The variation in film coefficient profiles with injector configuration is illustrated by comparison of Fig. 13 and 14. The data presented in these two figures demonstrate the dependence of thrust chamber heat transfer rates on injector design parameters. Experimental heat-transfer coefficients in the combustion chamber differ by as much as a factor of 3 and the peak values near the throat vary by approximately 35 percent. Various injectors were used throughout the tests evaluated. Some injector patterns resulted in fuel-rich mixture ratio near the wall which provided a protective film-coolant layer and reduced the heat flux and the effective film coefficient. Some configurations resulted in injection of oxidizer near the thrust chamber wall surface resulting in heat-flux values above the normal case (uniform mixture ratio throughout).

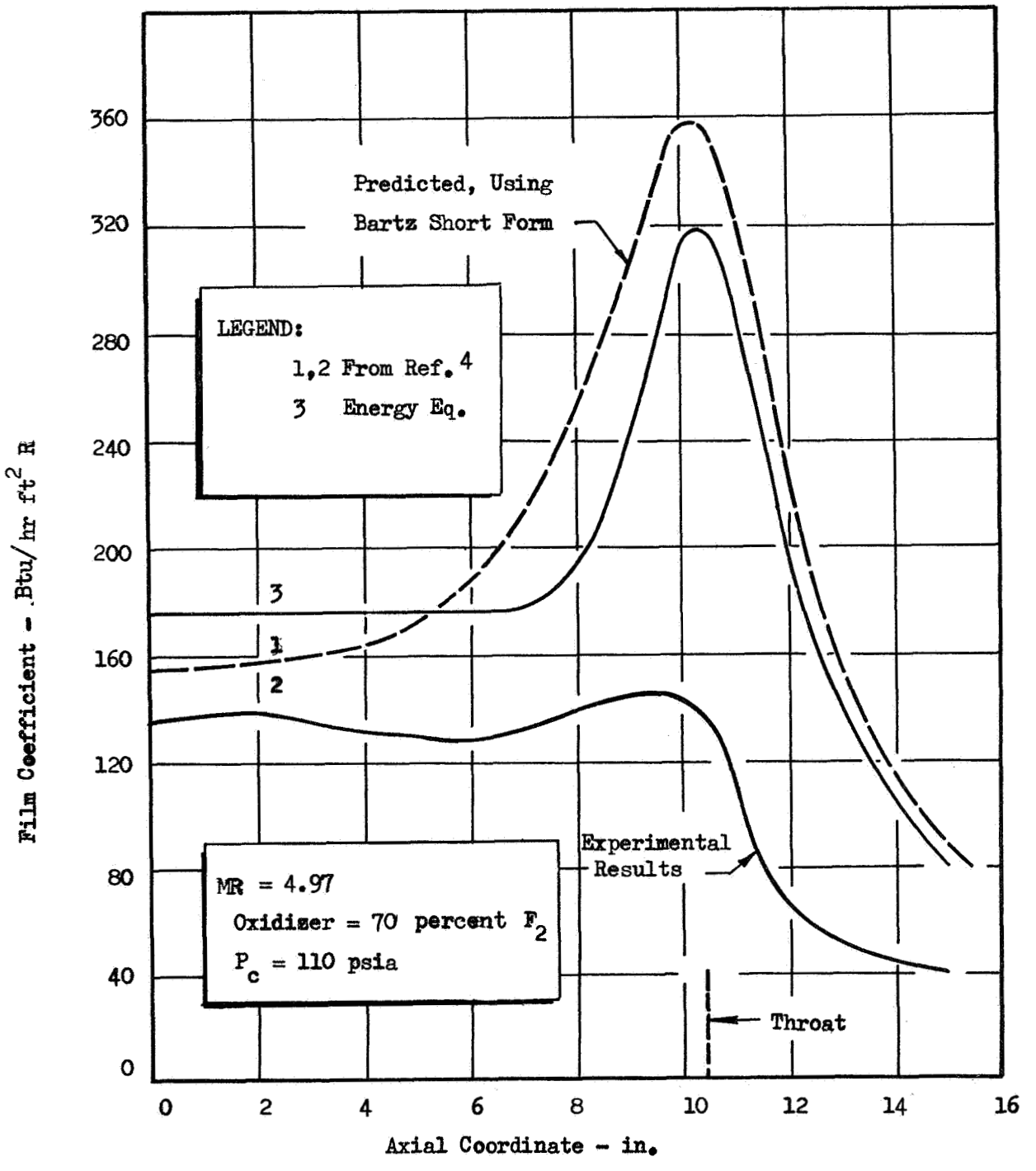

Figure 9. Comparison of Heat Transfer Coefficients - FLOX/Methane

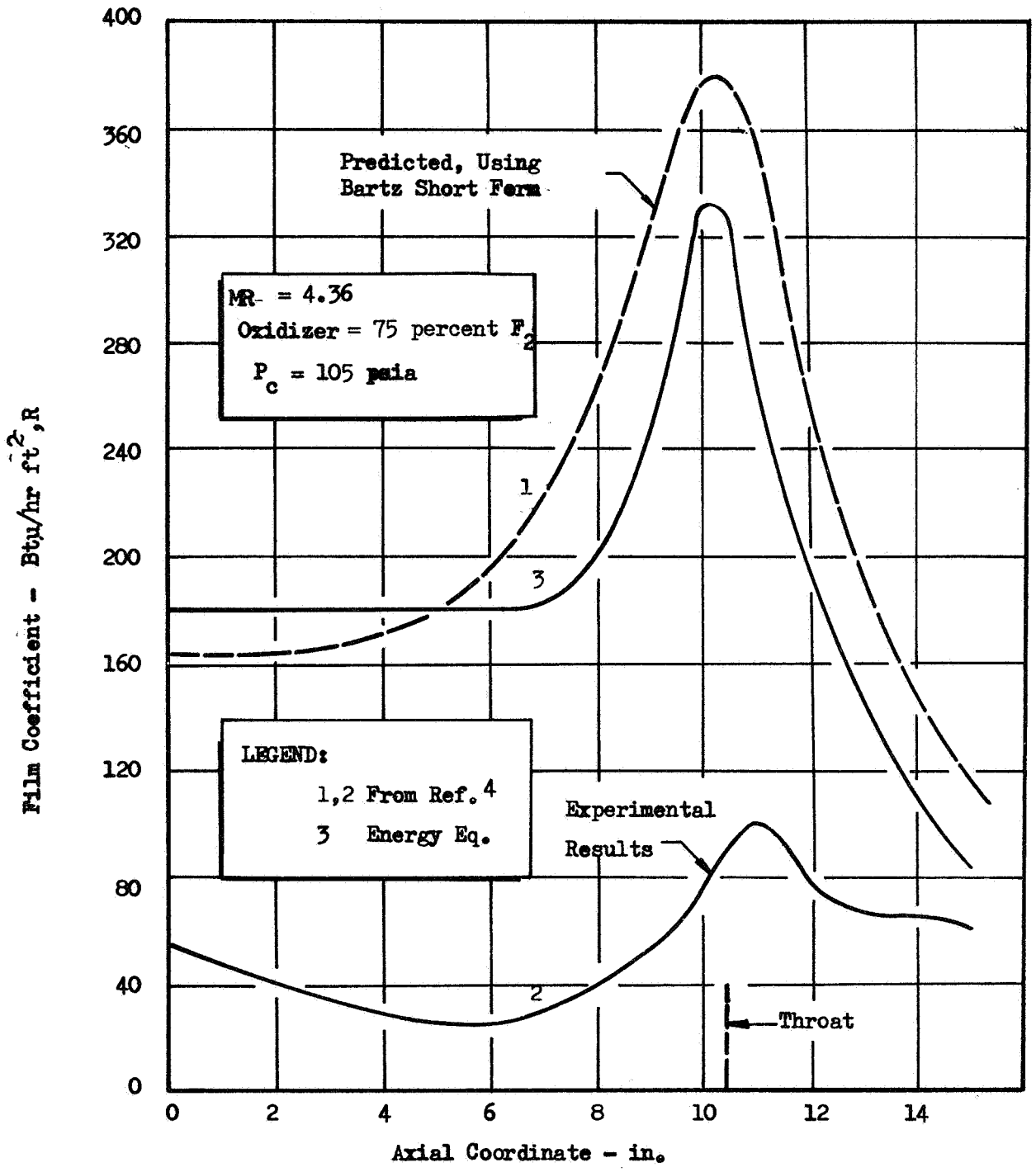

Figure 10. Comparison of Heat Transfer Coefficients - FLOX/Propane

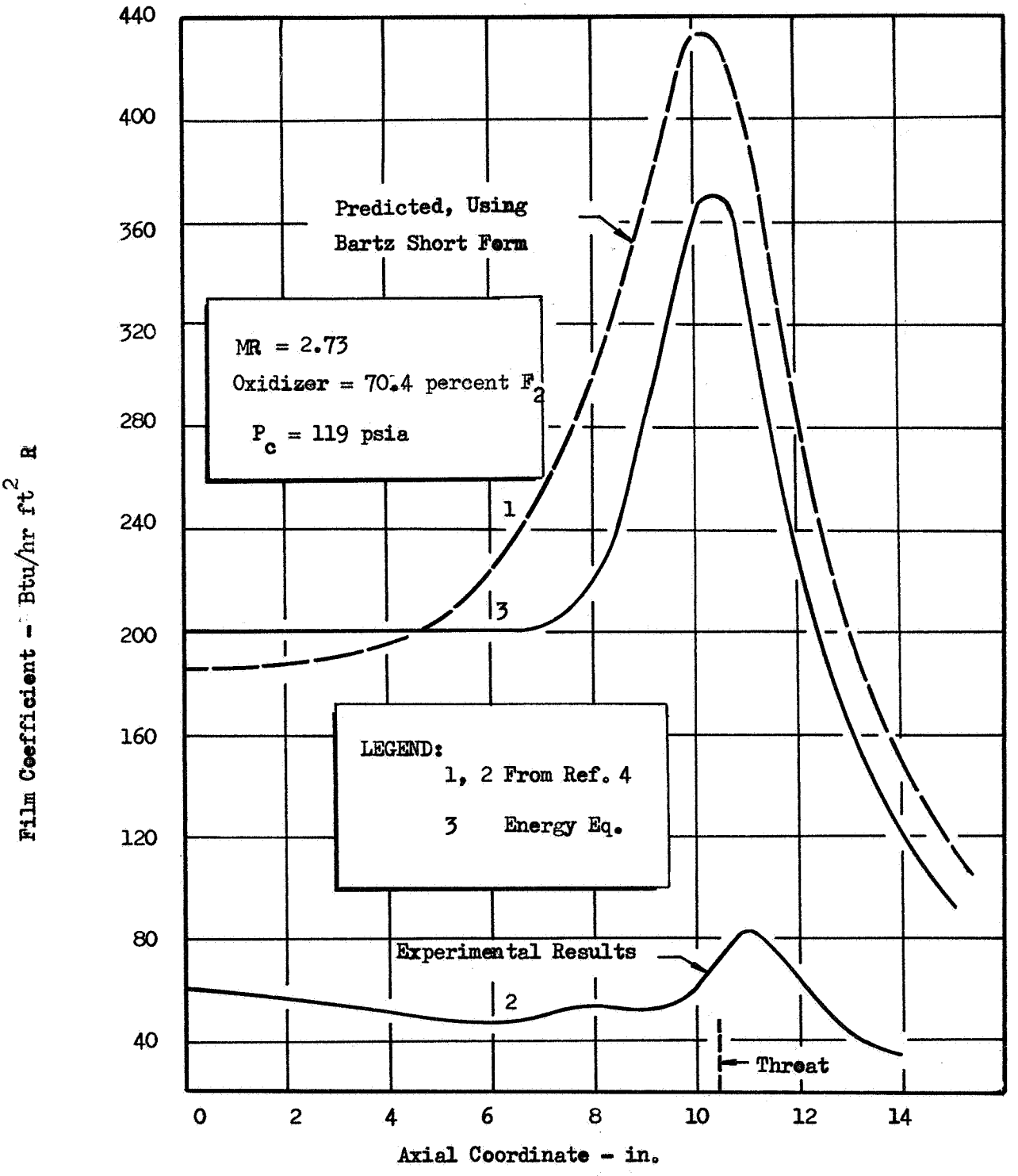

Figure 11. Comparison of Heat Transfer Coefficients - FLOX/Butene

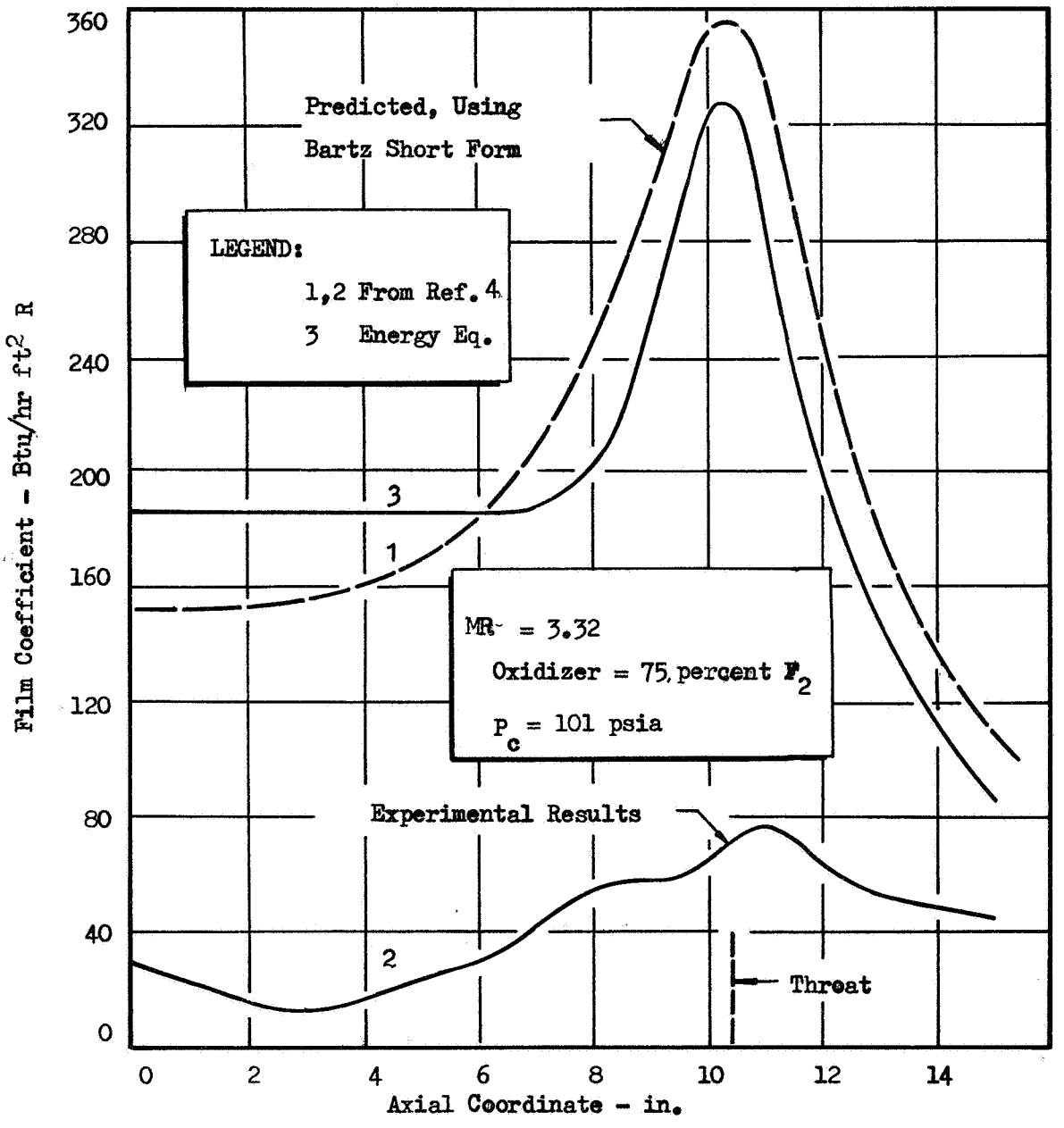

Figure 12 . Comparison of Heat Transfer Coefficients - FLOX/Pentane Blend

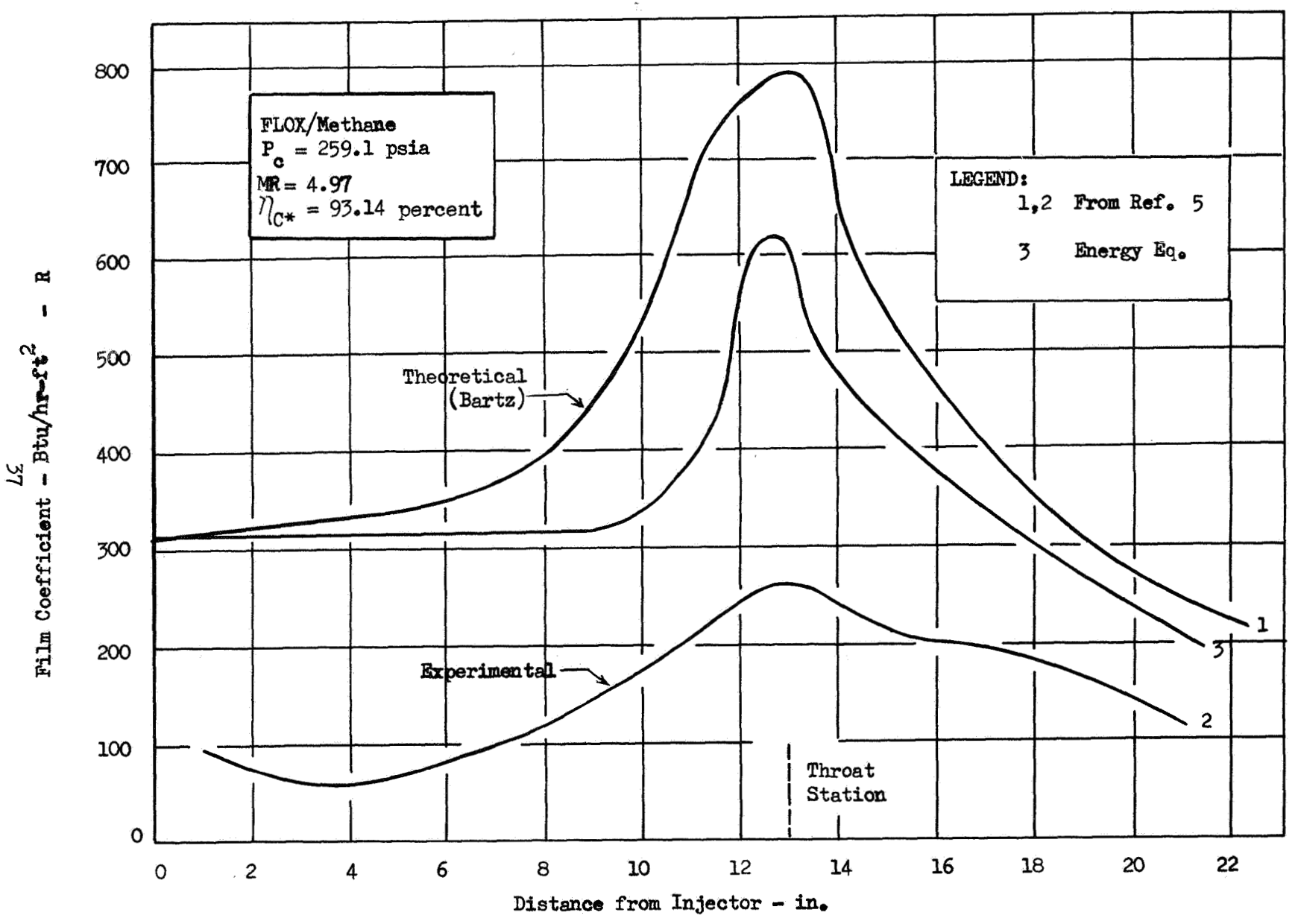

Figure 13. Variation of Combustion-Side Film Coefficient with Axial Location: Injector S/N IF 764

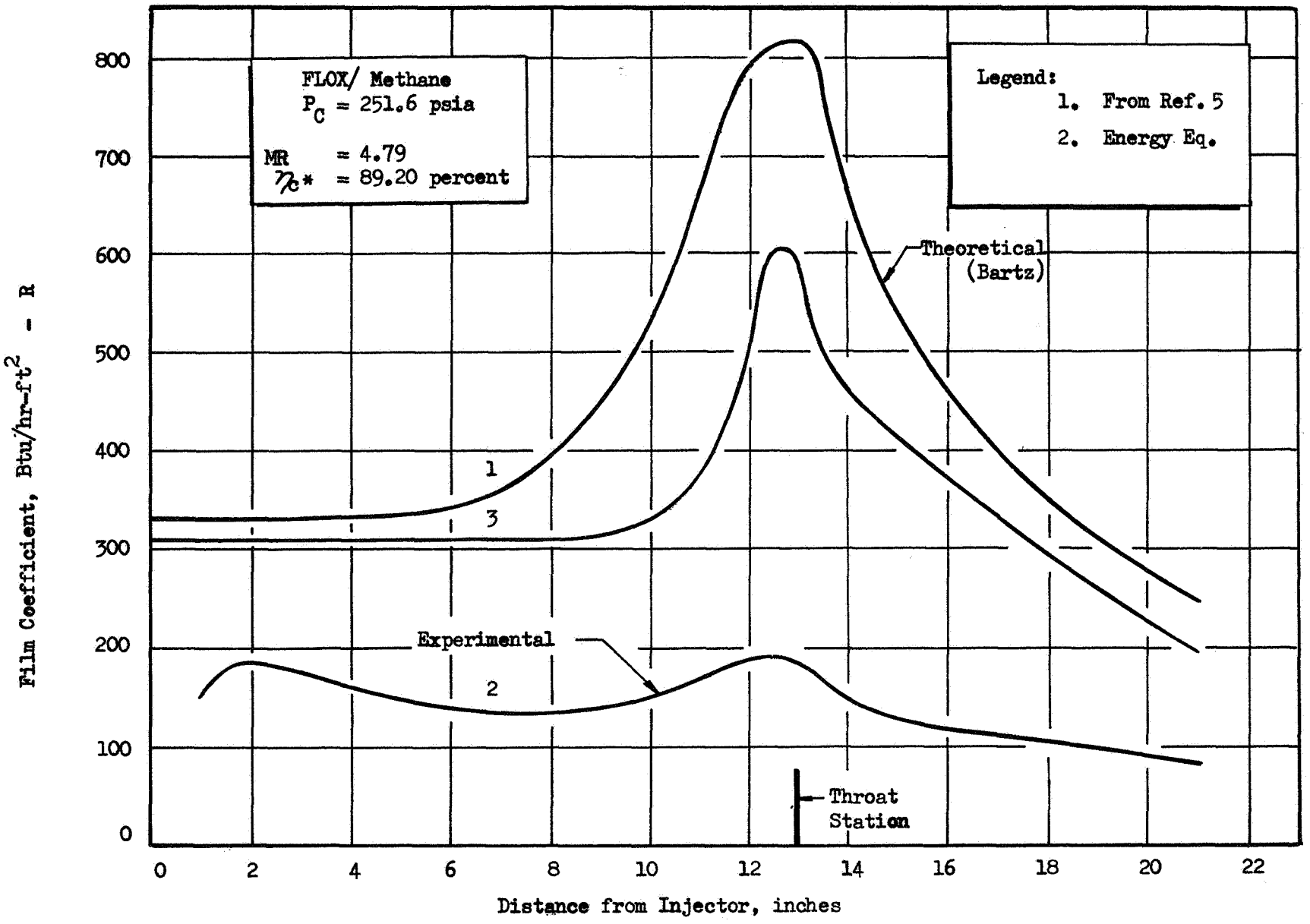

Figure 14 . Variation of Combustion-Side Film Coefficient with Axial Location: Injector S/N HK 713

Recent data generated under Contract NAS 7-304 for FLOX/1-butene have demonstrated that high performance (98 percent η_{c*}) could be achieved with this propellant combination but that heat fluxes comparable to the theoretical (no-carbon layer) values could accompany the high performance. The goal of the present program is a high-combustion-efficiency (96 to 98 percent) injector which will maintain, as far as possible, the beneficial carbon layer deposit.

The amount of heat loss to the thrust chamber per pound of propellants vs mixture ratio is shown in Fig. 15. No significant trend in heat loss per pound of propellants vs mixture ratio was noticed. Since the theoretical heat inputs were also not appreciably affected by mixture ratio variations, it was concluded that the carbon layer resistance is insensitive to mixture ratio variations.

The data taken at 250 psia chamber pressure in Ref. 5 were also compared with theoretical heat-transfer coefficients. The ratio of measured-to-theoretical total heat input for an uncooled thrust chamber using FLOX-methane at approximately 250 psia chamber pressure was 0.38. This value is lower than that at 100 psia (0.67) and appears to be in contrast to the results of previous studies with RP-1 (Ref. 7). For this reason, and because no data for other fuels such as propane or butene-1 was available at 250 psia chamber pressure at this time to verify the increase in carbon build-up with pressure, the calculated heat inputs at higher pressures were based upon data taken at 100 psia chamber pressure.

The ratio of the experimental total heat inputs to the analytically determined values is presented in Fig. 16 as a function of the hydrogen-to-carbon atomic ratio of the various fuels. The similar plot of Ref. 4 based upon use of the Bartz equation is included. Although the

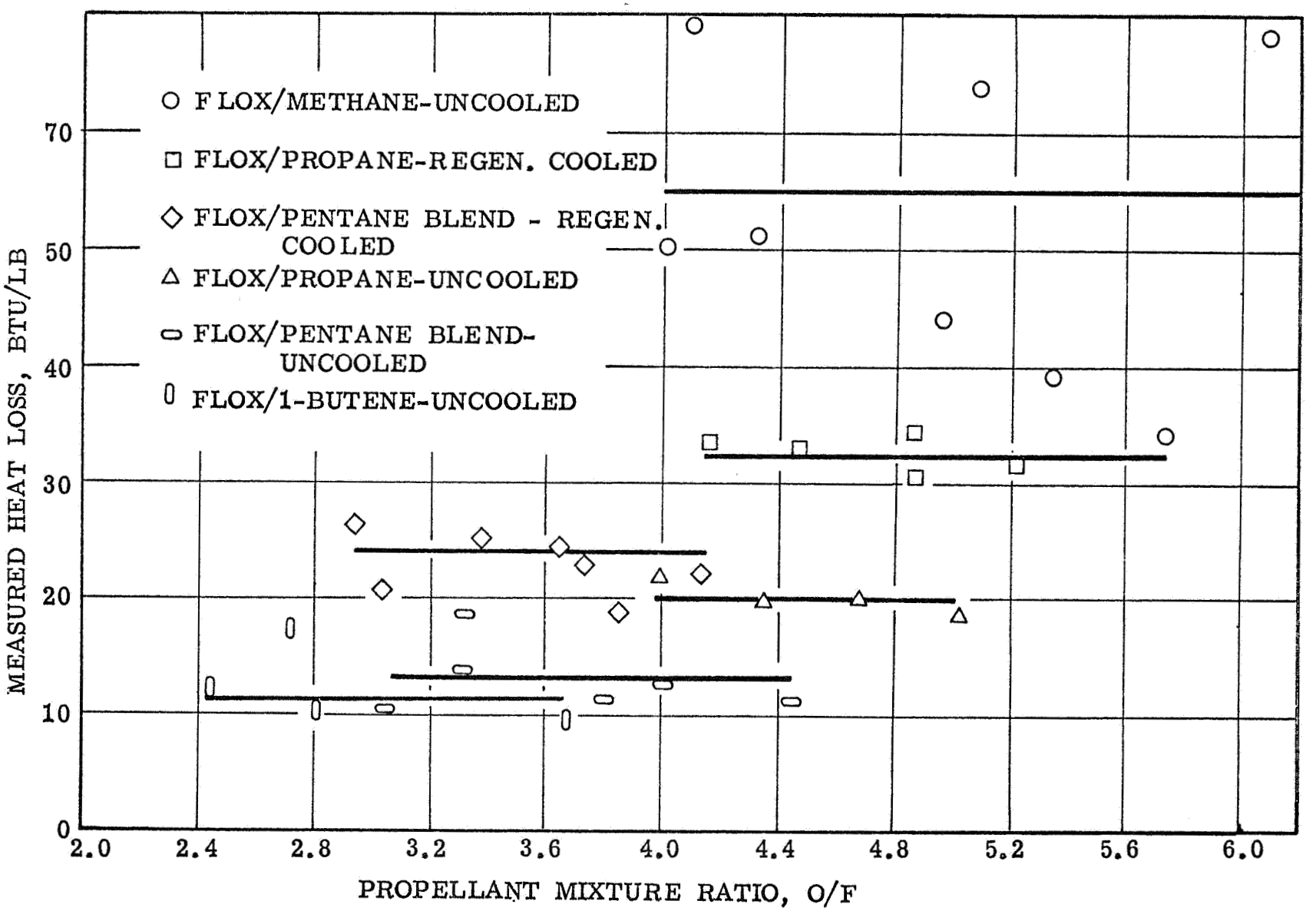

Figure 15 . Measured Heat Loss Per Pound of Propellant vs Mixture Ratio (Ref. 4)

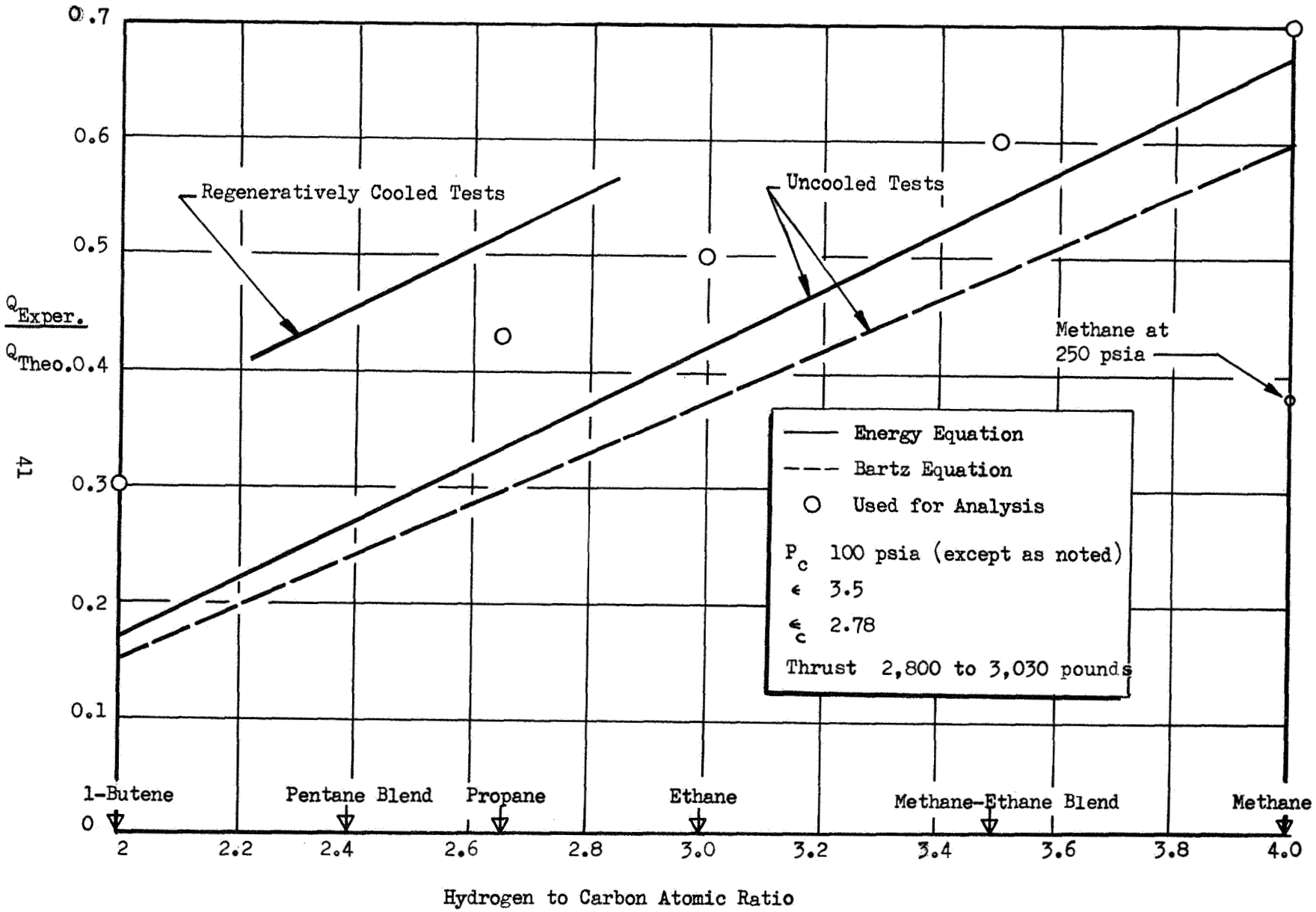

Figure 16 . Heat Transfer Rate Reduction for Various Hydrocarbons

ROCKETDYNE

presently determined ratio is higher because of the lower heat transfer coefficients predicted by the integral energy equation, both results indicate the very significant effects of the carbon layer.

The effect of the carbon layer for data based upon experimental results with a regeneratively cooled chamber is also shown in Fig. 16. Factors contributing to the higher heat fluxes measured with the regeneratively cooled chamber are: (1) the circumferentially integrating nature of the regenerative data may have included hot spots undetected in the uncooled chamber, (2) the regeneratively cooled chamber had slightly more surface area because of the corrugated tube surface and the slightly longer (1.3 inches) combustion zone. A linear relationship considering both sets of data (uncooled and regenerative) was used to evaluate regenerative limits in the subsequent Parametric and Detailed Heat Transfer Analysis. The values used for the various fuels are also shown in Fig. 16.

An analysis was conducted to determine the actual thermal resistance of the carbon layer. The results of this analysis, presented in Appendix B indicated definite trends but considerable scatter. Therefore, the overall heat-transfer coefficient values were used to determine heat inputs in the subsequent analyses. Because of the uncertainty of the effectiveness of the carbon layer, analyses were also conducted without considering carbon layer resistance for comparison purposes.

HEAT ABSORPTION CAPABILITES

Having determined the heat inputs to the walls of the thrust chamber, the next step in the parametric analysis was the calculation of the heat-absorption capacity of the various fuels. The heat-absorption capacity

is expressed as

$$Q_f = \dot{W}_f \, (H_{out} - H_{in})$$

where H_{in} is the enthalpy of the fuel entering the coolant jacket and evaluated at 10 degrees (F) above its freezing point, H_{out} is the enthalpy at the maximum allowable fuel temperature, T_f, and $\dot{W}_f$ is the fuel flowrate.

$$\dot{W}_f = \dot{W}/(1 + o/f) = F/I_s \, (1 + o/f)$$

Q_f is, therefore, dependent upon F, o/f, I_s, T_f, and the enthalpy rise of the fuel between T_{in} and T_f.

Values of chemical equilibrium specific impulse were generated for several propellant combinations over the ranges of chamber pressure, thrust level, expansion area ratio, and propellant mixture ratio of interest. These data are presented in Fig. 17 through 21. The specific impulse is shown in terms of the percent of the value at 1000 psia chamber pressure, expansion area ratio of 100, and optimum propellant mixture ratio. The effects of variations of these three operating parameters on specific impulse are similar for the propellant combinations which represent the extreme variations in the fuels and oxidizers under investigation. For the Heat Transfer Analysis, therefore, specific impulse values were calculated by detailed thermodynamic methods for each of the propellant combinations for one set of operating parameters. Values of specific impulse for other operating parameter values were obtained using Fig. 17 through 21. The optimum fluorine concentration was used in the FLOX for each of the fuels: i.e., 82.6 percent fluorine for methane, 80.8 percent for the methane-ethane blend, 78.1 percent for the ethane, 76 percent for the propane, and 70.4 percent for the 1-butene.

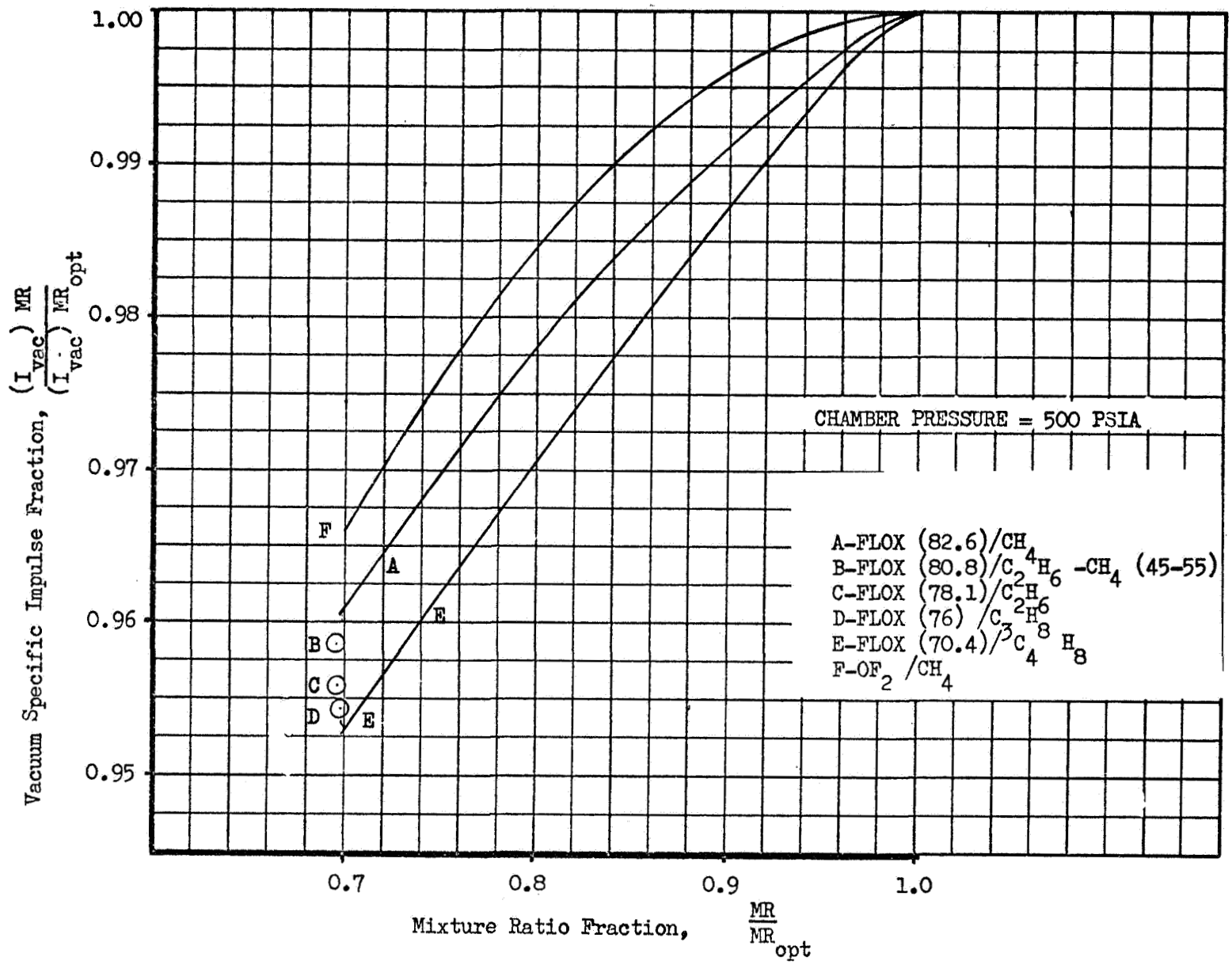

Figure 17. Mixture Ratio Effect on Performance, Area Ratio = 40

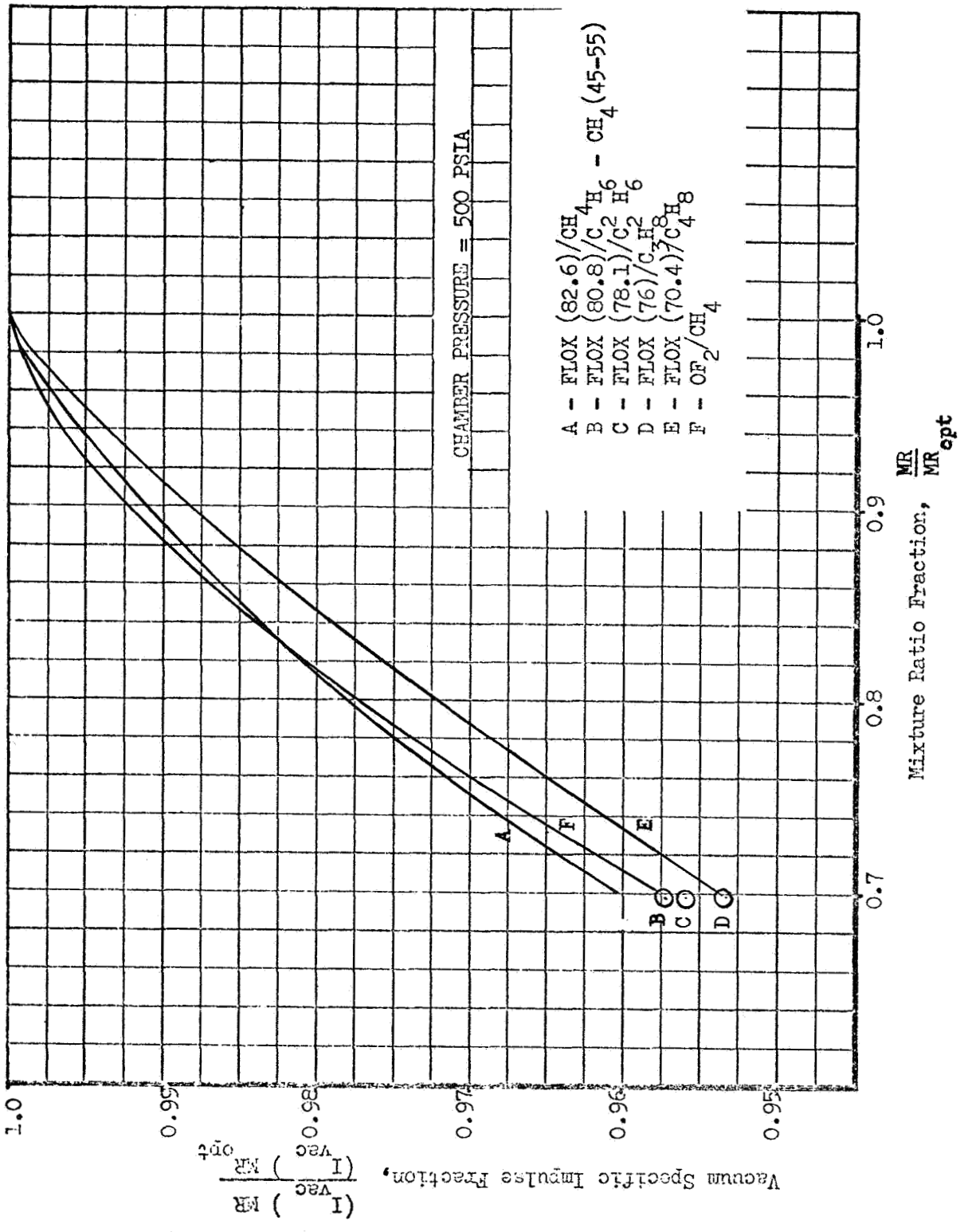

Figure 18. Mixture Ratio Effect on Performance, Area Ratio = 100

Mixture Ratio Effecto on Performance, Area Ratio = 100

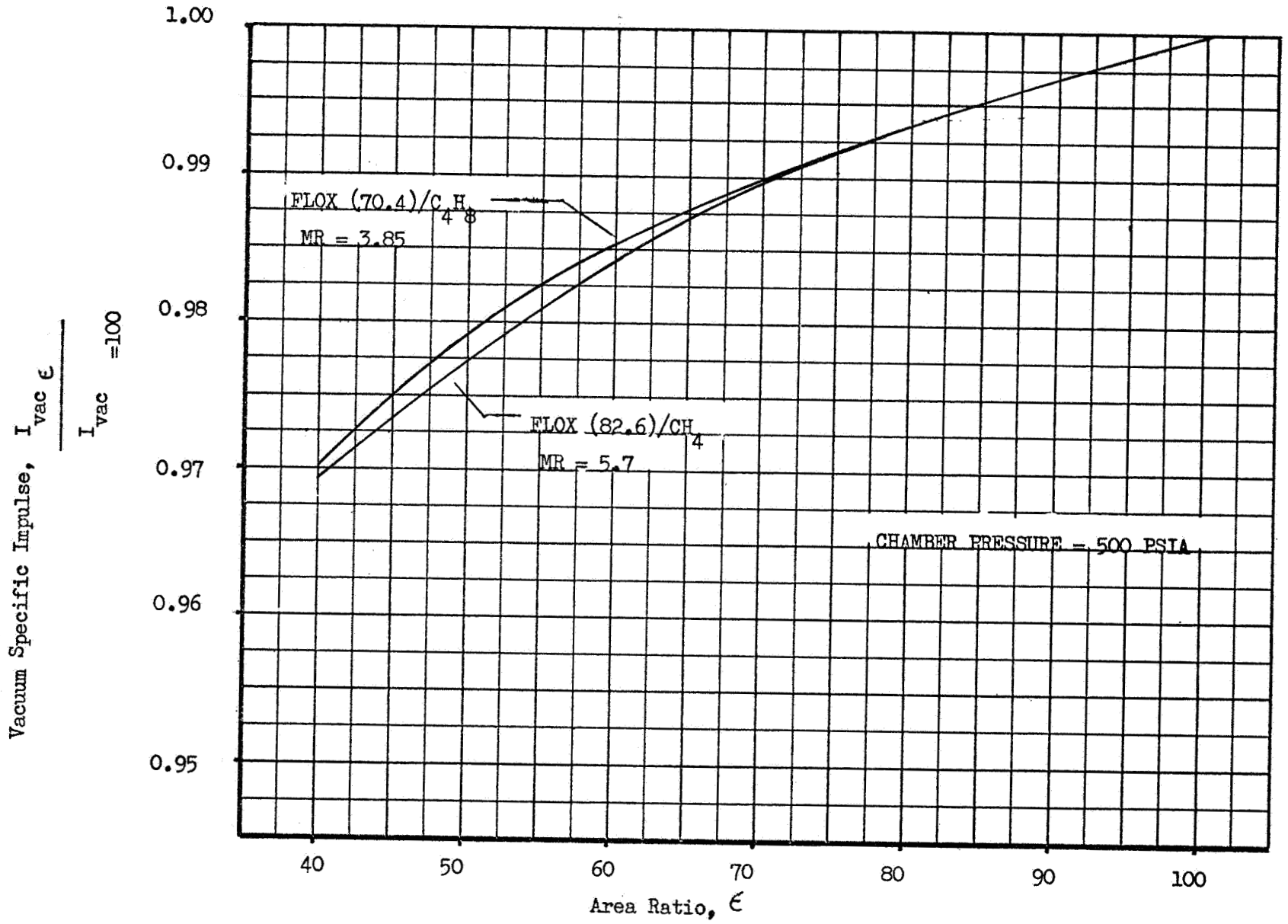

Figure 19. Area Ratio Effect on Performance

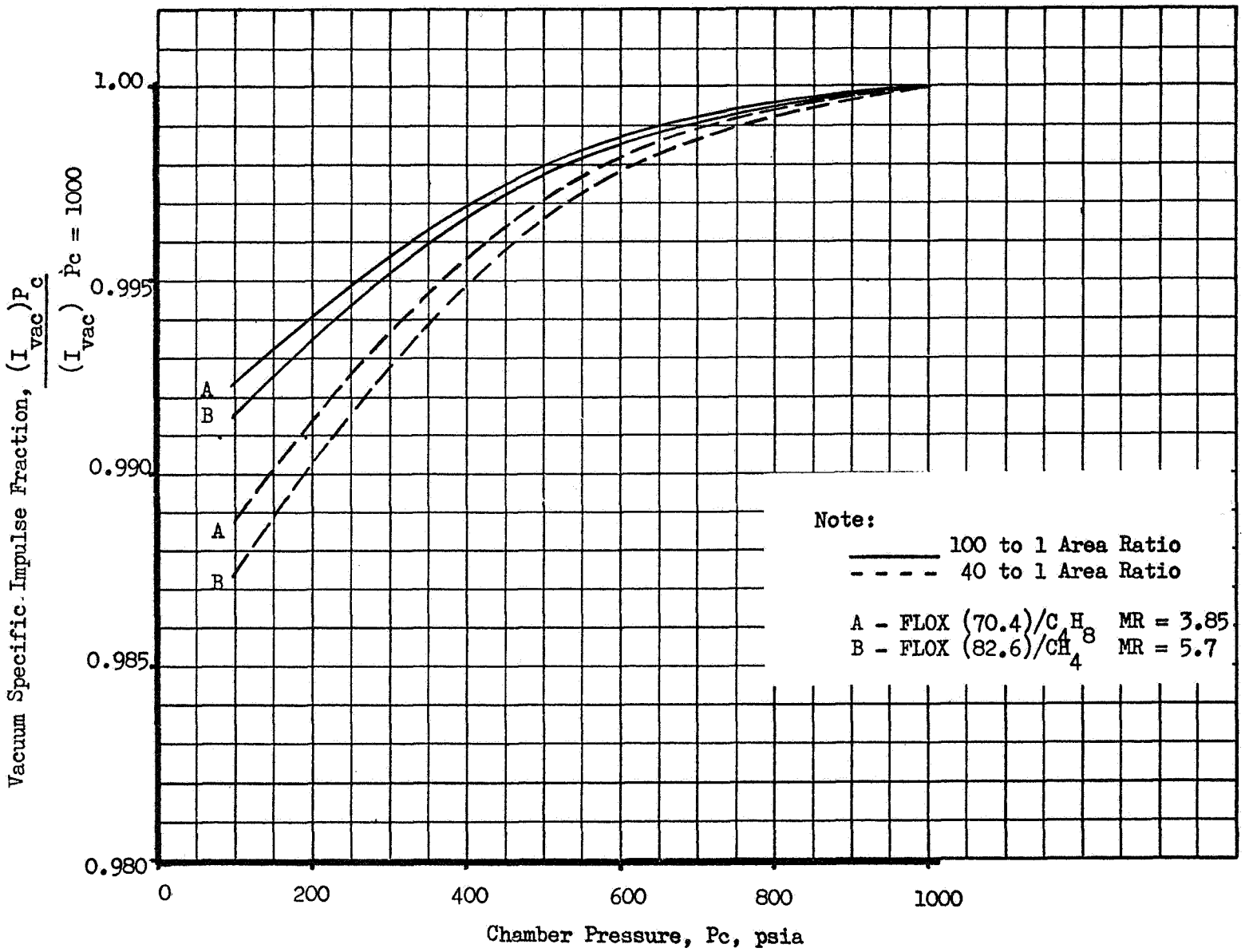

Figure 20 . Chamber Pressure Effect on Performance

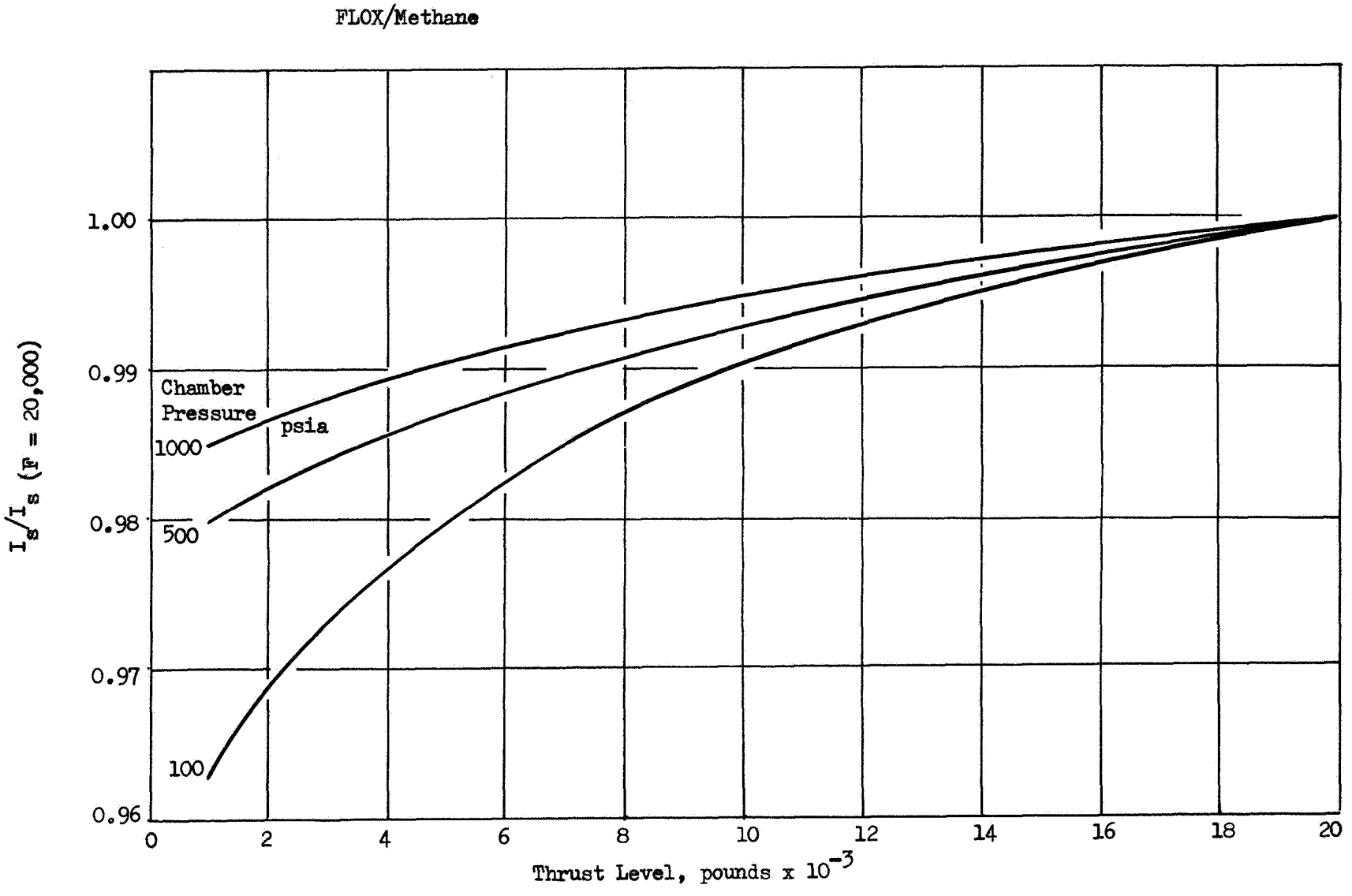

Figure 21. Thrust Effect on Delivered Performance

The maximum fuel bulk temperature, T_f, is a significant factor in determining the heat absorbing capability of the fuel. For supercritical coolant pressure cases, the temperature is limited by decomposition of the fuel. For subcritical cases, the effect of limiting the coolant temperature to prevent boiling was also investigated. In all cases, the value of T_{in} was assumed to be 10 degrees (F) above the freezing point of the particular fuel.

Subcritical Pressure Operation

For subcritical cases (P_c = 100 and 250 psia), T_f was limited to the saturation temperature of the fuel at a pressure 20 percent greater than chamber pressure to allow for injector pressure loss, i.e., P_{sat} = 120 and 300 psia. Values of $T_f = T_{sat}$ and $T_{critical}$ for the light hydrocarbon gases are shown in Table 4. The allowable temperature rises and corresponding enthalpy changes from 10 degrees (F) above the freezing point of each fuel are also shown. The heat absorption capacities were also calculated. The heat absorption capacity of each fuel may be written as

$$Q/F = \Delta H/I_s \, (1 + o/f)$$

The values of optimum propellant mixture ratio, nominal specific impulse, and resulting Q/F for each propellant combination are given in Table 5. This tabulation presents a good comparison of the heat absorption capabilites of the various propellant combinations because, as previously shown, the effects of P_c, F, ϵ, and o/f on performance are similar for the various propellant combinations. Furthermore, since the heat input to the walls was found to be essentially independent from propellant combination when gas-side carbon layer effects were not considered, the relative standing of the propellant combinations in Table 5 is indicative of the relative operating-parameter limits for each propellant combination

TABLE 4

TEMPERATURE DATA FOR LIGHT HYDROCARBON FUELS

Fuel	Critical Temp (F)	Freezing Temp (F)	Saturation Temp (F)		Allowable Temp. Rise (F)		ΔH (Btu/lb)	
			P_{sat} = 120 psia	P_{sat} = 300 psia	P_{sat} = 120 psia	P_{sat} = 300 psia	P_{sat} = 120 psia	P_{sat} = 300 psia
Methane	-116.3	-296.5	-199	-160	88	127	73	105
Methane (55) -Ethane (45) Blend	-54	-327.5	≈ -186	≈ -142	132	176	93	125
Ethane	90.1	-297.8	-37	22	251	310	140	174
Propane	206.3	-305.7	69	138	365	434	193	230
Butene-1	293	-301.6	147	222	439	514	236	286

under these conditions. The increasing values of saturation temperature with molecular weight of the fuels shown in Table 4 result in the increasing heat absorption capabilities shown in Table 5. The trends in specific impulse and optimum propellant mixture ratio also enhance the heat-absorption capabilites of the propellant combinations using the hydrocarbon fuels which have higher carbon-to-hydrogen atomic ratios. The heat absorption capability of the 1-butene is thus approximately four times that of methane when used with OF_2 or FLOX and subject to the nonboiling constraint at subcritical pressures.

Supercritical Operation

The critical pressures for the fuels studied range from 583 psia for 1-butene to 710 psia for ethane. For a chamber pressure of 500 psia and an injector pressure drop equal to 20 percent of chamber pressure, the coolant jacket outlet pressure (600 psia) is below the critical pressures of methane (673 psia) and ethane, and just below the critical pressure of propane (617 psia). The coolant jacket pressure and temperature profiles are such that the coolant would generally be heated to the critical temperature before the pressure decays to the critical value. Thus, chamber pressures of 500 psia through 1000 psia were considered for evaluating regenerative cooling limits under supercritical fuel bulk temperature restrictions. These coolant temperature limits could result from either material strength reduction or coolant decomposition. Decomposition of the fuels was found to impose the lowest bulk temperature limits on the coolant.

Decomposition Rates. A literature search was undertaken to obtain existing data which would permit estimation of the temperatures at which the hydrocarbons methane, ethane, propane, and 1-butene would begin to decompose.

TABLE 5
SUBCRITICAL HEAT ABSORPTION CAPABILITIES

Propellants	Optimum Propellant Mixture Ratio (o/f)	Nominal Specific Impulse*, sec	Maximum Heat Absorption Capability, Q/F P_{sat} = 120psia	P_{sat}=300psia
FLOX/Methane	5.70	389	0.028	0.040
FLOX/Methane-Ethane	5.33	385	0.038	0.051
FLOX/Ethane	4.82	381	0.063	0.078
FLOX/Propane	4.50	378	0.093	0.111
FLOX/Butene-1	3.85	374	0.130	0.157
OF_2/Methane	5.30	390	0.030	0.043
OF_2/Methane-Ethane	5.00	388	0.040	0.054
OF_2/Ethane	4.60	386	0.065	0.081
OF_2/Propane	4.60	381	0.090	0.107
OF_2/1-Butene	3.85	379	0.129	0.156

*F = 5000 pounds, P_c = 250 psia, ϵ = 60

For uncatalyzed thermal decomposition, lower hydrocarbons ($C_1 - C_4$) require temperatures of the order of 800 to 1500 F. The products are not only the smaller fragments, down to elemental carbon, but also some larger species. First-order kinetics are generally found to be obeyed. The decomposition rates are described by

$$\frac{a}{a - x} = \exp (kt)$$

where a is the original concentration of the component; x is the fraction decomposed in time, t; and k is the reaction rate constant. This constant depends upon temperature, T, and is conventionally expressed as

$$k = A \exp (E/RT)$$

where R is the universal gas constant and A and E are characteristic constants for the particular reaction. Values of A and E have been determined experimentally by several investigators. Typical results are shown in Table 6. Although the variations in A and E are sometimes large, they are compensating so that the values of k in the usual working temperature range generally are more consistent.

Decomposition Temperatures. Pyrolysis takes place over a range of temperatures. However, for practical reasons, it is important to know the temperature at which the decomposition starts, i.e., becomes measureable, or begins to exert some noticeable effects. Such a "decomposition temperature" has to be defined somewhat arbitrarily. A value of 1 percent per hour appears in the literature (Ref. 8) as the limiting rate. The decomposition temperatures calculated on this basis as well as on the basis of 1 percent per minute and 1 percent per second from the kinetic parameters listed in Table 6, are given in Table 7.

TABLE 6

KINETIC PARAMETERS

Hydrocarbon	Investigators	E, cal/mole	A, sec^{-1}	log A
Methane	Kassel (1935)	79,000	10^{12}	12.00
Ethane	Laidler & Wojciechowski (1961)	73,060	1.07×10^{15}	15.02
Propane	1) Kershenbaum & Martin (1967)	52,100	2.4×10^{11}	11.38
	2) Laidler et al (1962)	54,500	8.5×10^{13}	13.92
	3) Laidler et al (1962)	67,100	2.6×10^{14}	14.41
1-Butene	1) Bryce & Kebarle (1958)	66,000	$10^{13.2}$	13.20
	2) Sehon & Szwarc (1950)	61,500	10^{13}	13.00
	3) Karr et al (1965)	59,100	$10^{12.71}$	12.71

$$k = A \exp(-E/RT)$$

TABLE 7

DECOMPOSITION TEMPERATURES

Hydrocarbon		Calculated temperature, F, for 1 - percent decomposition in		
		1 hour	1 minute	1 second
Methane		1310	1510	1760
Ethane		937	1069	1230
Propane	1) Kershenbaum & Martin (1967)	750	892	1072
	2) Laidler et al (1962)	640	752	887
	3) Laidler et al (1962)	861	991	1148
1-Butene	1) Bryce & Kebarle (1958)	925	1069	1248
	2) Sehon & Szwarc (1950)	844	982	1153
	3) Karr et al (1965)	813	950	1120

The following decomposition temperatures were given (without specification of the reaction rate) in Ref. 9: methane, 1900 F; ethane, 900 F; propane, 850 F. Values of decomposition temperature used in the heat transfer analysis are as follows:

Methane	1500 F
Methane-Ethane Blend	900 F
Ethane	900 F
Propane	850 F
1-Butene	800 F

These values were arrived at prior to completion of the literature survey and are in fair agreement with the final results shown in Table 7. The effect of variations in the decomposition temperature on operating limits is discussed in the following section.

The heat absorption capabilites of the coolant when used with FLOX and OF_2 are shown in Table 8. The values represent the heat absorbed when the temperature of the coolant is raised from its inlet value of 10 degrees(F) above the freezing point to the temperatures listed above. Under these conditions, it can be seen that a completely different trend occurs from that found in the subcritical pressure analysis. The methane has a significantly higher heat absorption capability than the other coolants under supercritical operating conditions.

TABLE 8

SUPERCRITICAL HEAT ABSORPTION CAPABILITES

Propellant Combination	Mixture Ratio	Heat Absorption Capability Q/F, Btu/lb-sec
FLOX/Methane	5.70	0.61
FLOX/Methane-Ethane	5.33	0.40
FLOX/Ethane	4.82	0.40
FLOX/Propane	4.50	0.40
FLOX/1-Butene	3.85	0.40
OF_2/Methane	5.30	0.65
OF_2/Methane-Ethane	5.00	0.42
OF_2/Ethane	4.60	0.41
OF_2/Propane	4.60	0.39
OF_2/1-Butene	3.85	0.40

OPERATING LIMITS

The operating limits imposed by the restriction of the fuel bulk temperature may be discussed in terms of the maximum allowable propellant mixture ratio for fixed values of other parameters. Graphical presentations of $P_{c_{max}}$ vs thrust are also frequently used to show the operating envelope when other parameters are fixed. Both methods are used in the following discussion.

Supercritical Operation

The values of the parameters shown in Table 9 were fixed for the nominal case and regenerative cooling capabilities were determined for each propellant combination. The parameters were then allowed to vary individually to show the effect of the specific parameter on the operating limits. The effects of simultaneous variation of more than one parameter are also shown.

A thrust level of 1000 pounds and a chamber pressure of 1000 psia (extreme values considered in this study) impose the most severe limits on regenerative cooling. Values of exit bulk temperature were calculated for each of the 10 propellant combinations for the decomposition-limited conditions. Under these conditions, the decomposition temperatures were not exceeded for any of the propellant combinations even at a chamber pressure of 1000 psia. Therefore, operation in the region of $P_c \leq 1000$ psia and $F \geq 1000$ pounds is not limited by fuel decomposition for the nominal values of the parameters of Table 9 as well as for the values which result in less severe heat inputs, i.e., $\epsilon_c \geq 3$, $\epsilon \leq 60$, $T_{wg} \geq 1700$ F, and o/f less than the optimum values.

TABLE 9

NOMINAL DESIGN PARAMETERS

Propellant Mixture Ratio	Optimum
Combustion efficiency, percent	96
Contraction Area Ratio	3
Expansion Area Ratio	60
Gas Side Wall Temperature, F	1700
Carbon Layer Resistance	Fig. 16

Bulk Temperature Limit for Supercritical Operation

Value from Page 56

As noted in a previous section various values of decomposition temperature may be found in the literature for the different fuels. Therefore, the fuel jacket exit temperatures were determined which would result from a chamber pressure of 1000 psia and a thrust level of 1000 pounds. The results, shown in Table 10, indicate that temperature limits much lower than the values used would have to be effected in order to reduce $P_{c_{max}}$ to 1000 psia.

Although all propellants could be used at the lowest thrust and highest chamber pressure values under consideration, the propellant combinations may be rated by considering their safety factors (heat absorption capability/heat input) under these conditions. The results are presented in Table 11 and show that all combinations (except possibly the methane-ethane blend) have comfortable safety factors and that the safety factor for 1-butene is much greater than those for the other fuels.

The effects of parameter variations which tend to cause thermal decompositions of the fuel were then investigated at the 1000-pound-thrust level. Increasing the nozzle area ratio to 100 did not result in any $P_{c_{max}}$ values less than 1000 psia. Reducing the contraction ratio from 3 to 2 did result in values of $P_{c_{max}}$ less than 1000 psia for propellant combinations using ethane and ethane-methane blend fuels as shown in Table 12. However, the value of $P_{c_{max}}$ for all propellants was again above 1000 psia at a thrust level of 2000 pounds or greater.

The importance of the carbon layer is evident from the results shown in Table 12 for the case where the carbon layer resistance was not included. Although the maximum chamber pressure for methane with either FLOX or OF_2 is still above 1000 psia, values of $P_{c_{max}}$ for the other propellants, which

TABLE 10

COOLANT JACKET DISCHARGE TEMPERATURES

Propellants	Discharge Temperature, F
FLOX/CH_4	1005
FLOX/CH_4-C_2H_6	795
FLOX/C_2H_6	635
FLOX/C_3H_8	430
FLOX/C_4H_8	300
OF_2/CH_4	935
OF_2/CH_4-C_2H_6	750
OF_2/C_2H_6	610
OF_2/C_3H_8	445
OF_2/C_4H_8	310

Chamber Pressure = 1000 psia
Thrust = 1000 pounds
Other parameters given in Table 9

TABLE 11

HEAT ABSORPTION CAPABILITY/HEAT INPUT RATIO

FLOX/CH_4	1.43
FLOX/CH_4-C_2H_6	1.11
FLOX/C_2H_6	1.32
FLOX/C_3H_8	1.63
FLOX/C_4H_8	2.21
OF_2/CH_4	1.52
OF_2/CH_4-C_2H_6	1.16
OF_2/C_2H_6	1.36
OF_2/C_3H_8	1.59
OF_2/C_4H_8	2.17

Chamber Pressure = 1000 psia
Thrust = 1000 pounds
Other parameters given in Table 9

TABLE 12

MAXIMUM CHAMBER PRESSURE (PSIA) FOR 1000 POUND THRUST

Propellants	$\epsilon_c = 2$			No Carbon Resistance
	ϵ=40	ϵ =60	ϵ =100	
FLOX/CH_4	*	*	*	*
FLOX/CH_4-C_2H_6	497	453	398	137
FLOX/C_2H_6	916	844	758	130
FLOX/C_3H_8	*	*	*	116
FLOX/C_4H_8	*	*	*	141
OF_2/CH_4	*	*	*	*
OF_2/CH_4-C_2H_6	572	520	420	174
OF_2/C_2H_6	980	906	816	148
OF_2/C_3H_8	*	*	*	100
OF_2/C_4H_8	*	*	*	125

* $Pc_{max} \geq$ 1000 psia

Nominal Conditions Except as Noted

have (and require) more effective carbon layers, are significantly reduced. The carbon layer permits an order of magnitude increase in chamber pressure for these propellants. The reason for the strong effect of the carbon layer on maximum chamber pressure is readily apparent upon consideration of the influence coefficients shown in Fig. 6. The combination of combustion zone and nozzle influence coefficients indicates that chamber pressure has a small effect on total heat input. Conversely, slight changes in heat input are reflected in large changes in chamber pressure limits. This effect also accounts for the much higher chamber pressure limits determined for methane in that it magnifies the differences in heat absorption capabilities of the fuels (Table 8).

The results of the no-carbon layer analysis are shown in more detail in Fig. 22 through 26. Maximum chamber pressures vs thrust are shown in Fig. 22 for the most severe condition, a contraction ratio of 2 and expansion ratio of 100. Under these conditions, 1000 psia chamber pressure operation is not possible at thrust levels lower than 7000 pounds for most propellant combinations. Even the propellant combinations using methane cannot be operated at thrust levels under 2200 pounds at a 1000 psia chamber pressure. Propellant combinations using propane are most severely limited (F_{min} = 9700 pounds for OF_2/propane) under these conditions. The limits can be slightly relaxed by reducing the nozzle area ratio from 100 to 40 as shown in Fig. 23. However, except for methane, the operating conditions are still restricted.

Much more significant extension of the operating envelope can be achieved by increasing the contraction ratio from 2 to 4. As shown in Fig. 24, the operating limits for methane-cooled chambers are well above 1000 psia even at the 1000 pound thrust level. Regenerative cooling of the OF_2/propane system can be accomplished at 1000 psia for thrust levels as low as

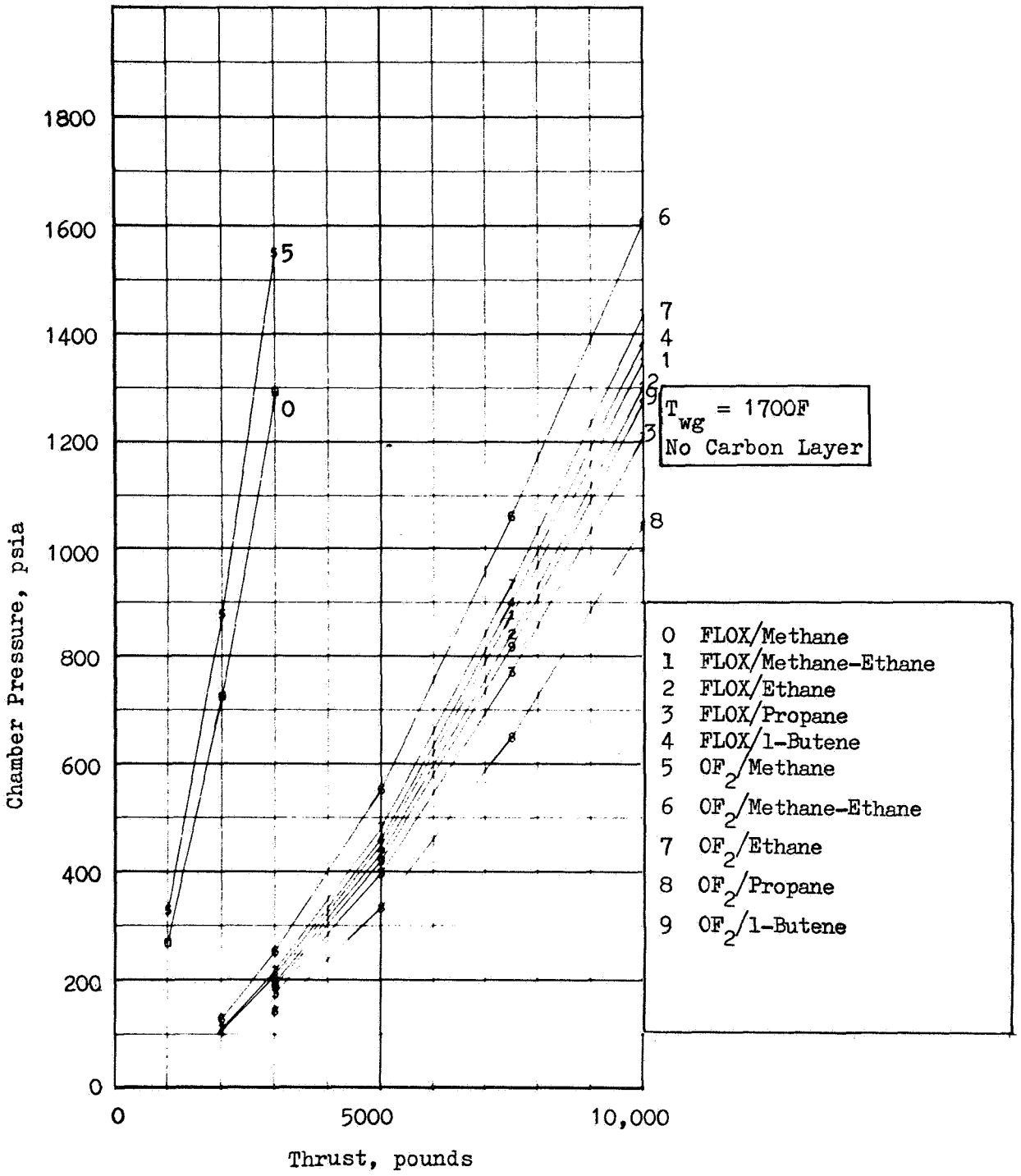

Figure 22. Regenerative Cooling Limits Based Upon Propellant Decomposition $\epsilon_c = 2$, $\epsilon = 100$

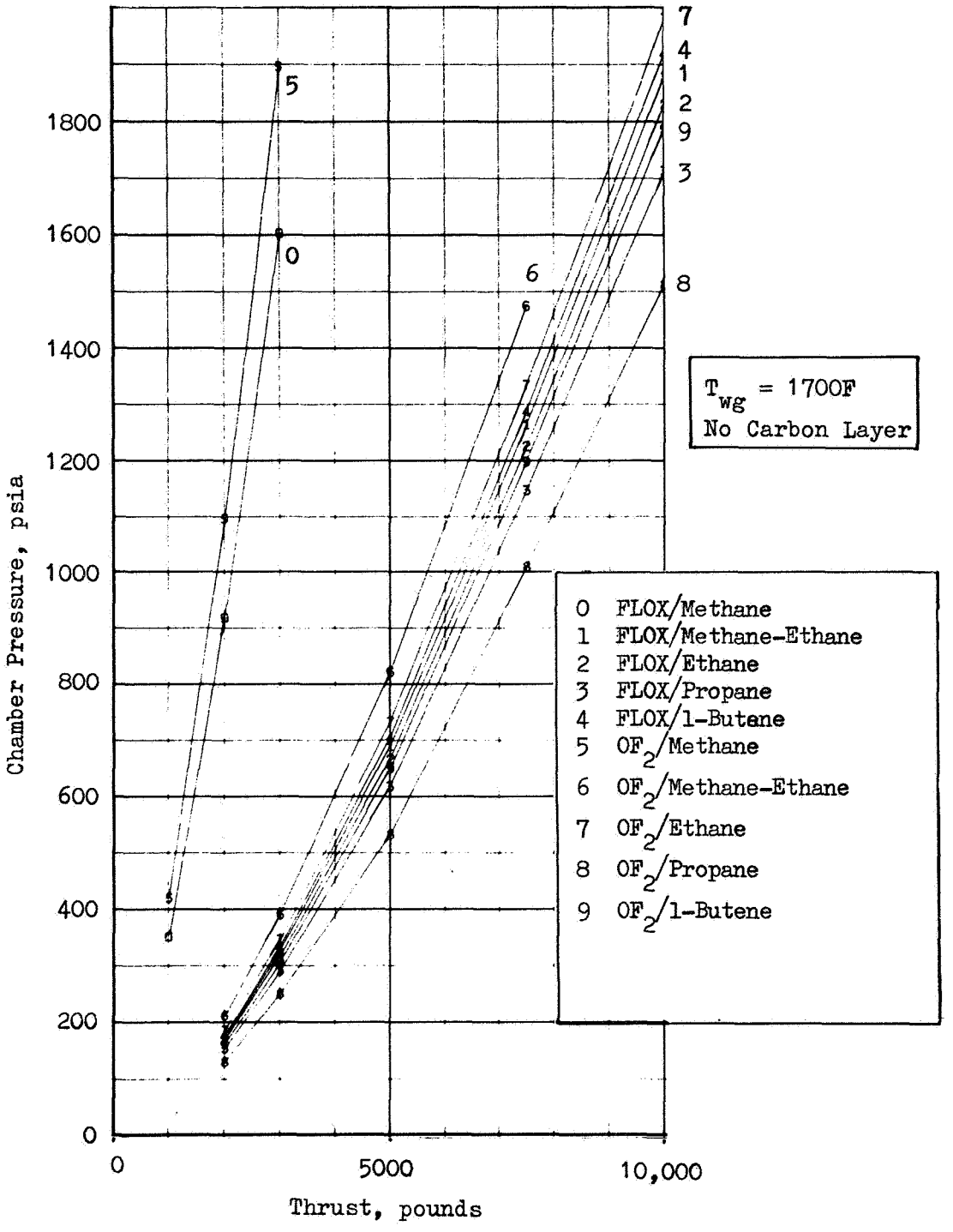

Figure 23. Regenerative Cooling Limits Based Upon Propellant Decomposition $\epsilon_c = 2$, $\epsilon = 40$

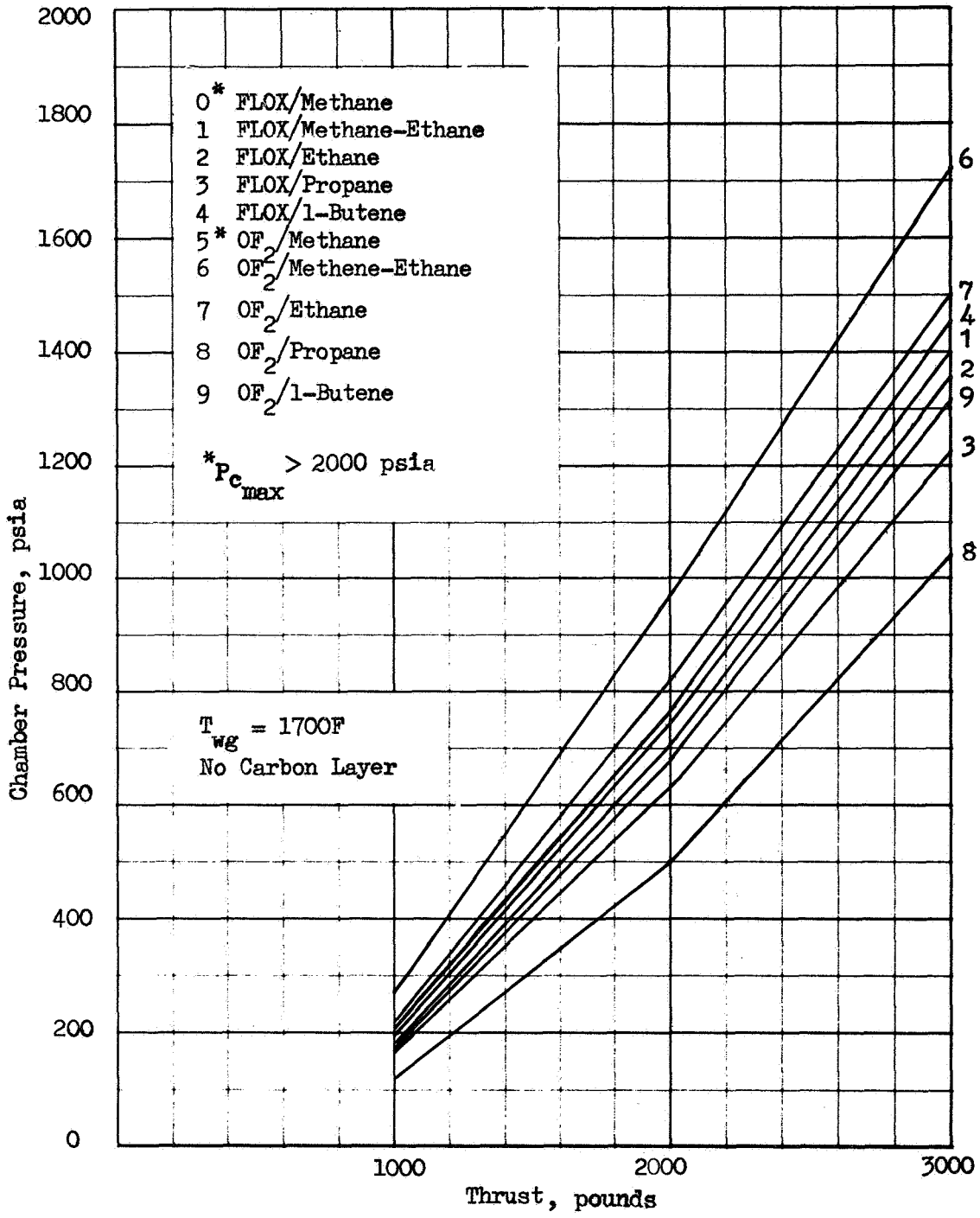

Figure 24. Regenerative Cooling Limits Based on Propellant Decomposition, $\epsilon_c = 4$, $\epsilon = 100$

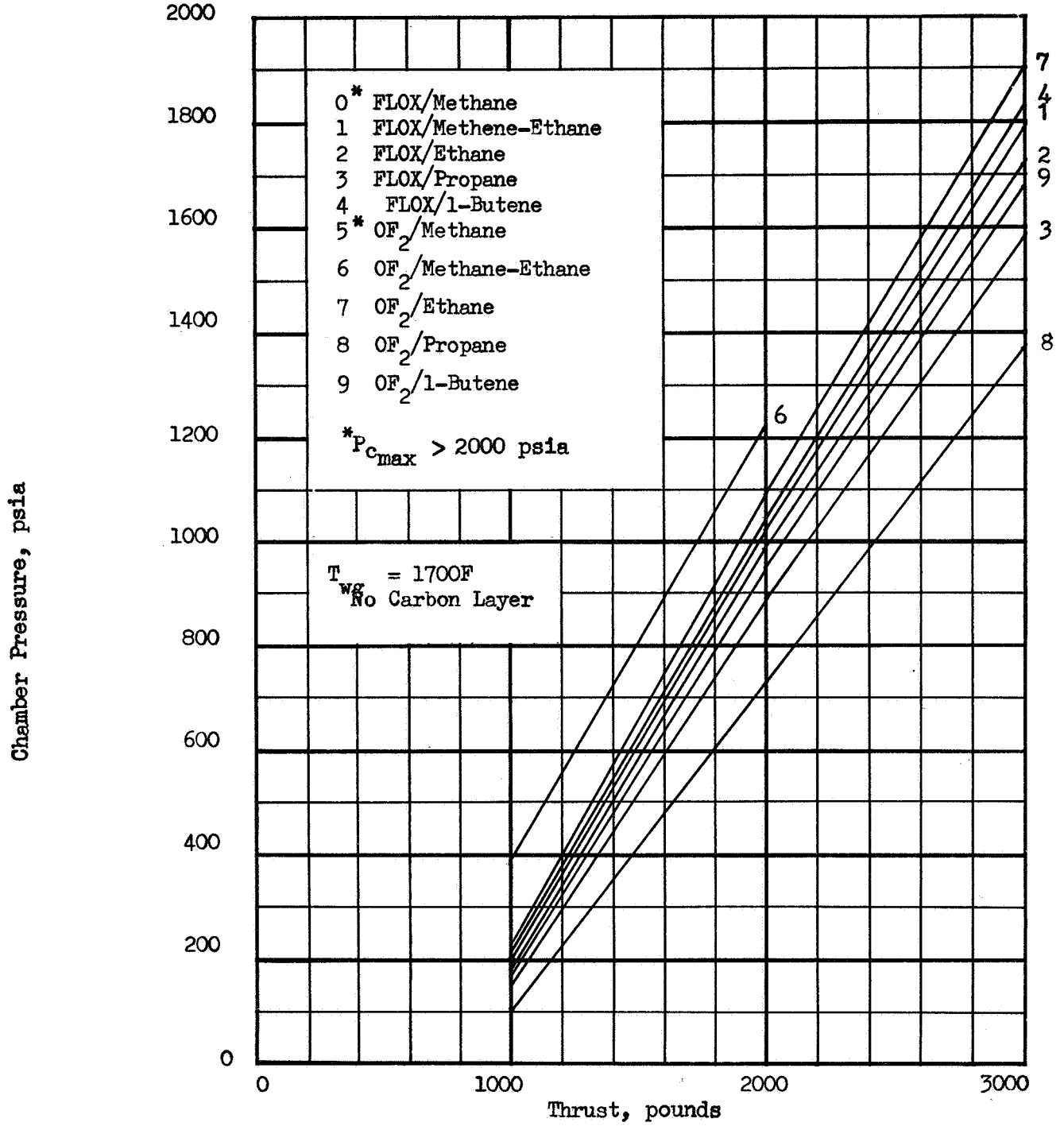

Figure 25 . Regenerative Cooling Limits Based on Propellant Decomposition, $\epsilon_c = 4$, $\epsilon = 60$

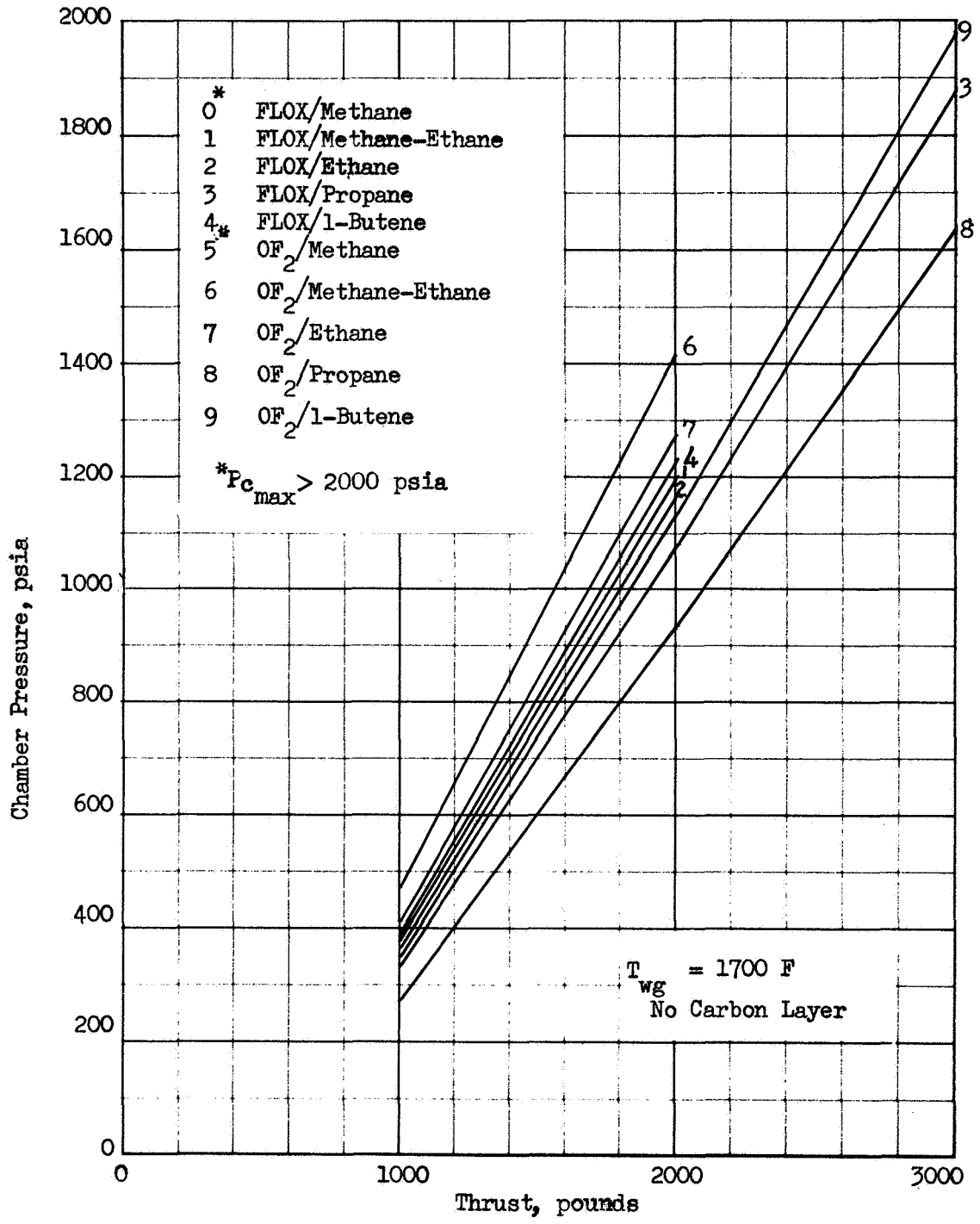

Figure 26. Regenerative Cooling Limits Based on Propellant Decomposition, $\epsilon_c = 4$, $\epsilon = 40$

3000 pounds. However, supercritical operation is not possible at the 1000-pound thrust level for any of the propellants except FLOX/methane and OF_2/methane. The further benefits of nozzle area ratio reduction (at $\epsilon_c = 4$) are shown in Fig. 25 and 26. Thrust levels as low as 2100 pounds can be regeneratively cooled with propane (OF_2 oxidizer) at a chamber pressure of 1000 psia. Results similar to those obtained by increasing the contraction ratio to 4 could also have been obtained by increasing the gas-side wall temperature from 1700 to approximately 2200 F. Propellant mixture ratio could also have been reduced to enlarge the operating envelope. The percent reduction would be different for each propellant combination because of the various optimum mixture ratios. However, a reduction to roughly 85 to 90 percent of the optimum value would achieve the same result as increasing the contraction area ratio to 4. All propellant combinations can operate at a thrust level of 1000 psia and chamber pressure of 1000 pounds without a carbon layer if the nozzle area ratio is reduced to 60 and the propellant mixutre ratio is reduced to 70 percent of optimum with ϵ_c of 4 and T_{wg} of 1700 F. If T_{wg} is increased to 3200 F, all propellant combinations can operate without a carbon layer at the 1000 pound thrust level and optimum propellant mixutre ratio with $\epsilon = 100$ and $\epsilon_c = 4$.

Subcritical Operation

Regenerative cooling limits were investigated for 100- and 250-psia chamber pressure applications. Under these conditions, the coolant pressure in the jacket would be below the critical pressure for all of the fuels and boiling would occur if the coolant temperature exceeded the saturation temperature. Cooling limits based upon prevention of bulk boiling were determined for both chamber pressures. Cooling limits based upon the alternative requirement that all of the coolant be vaporized prior to injection were also determined. In addition to the comparison of heat

absorption with heat input values, it was also necessary to evaluate the boiling heat-flux limits to determine the coolant characteristics required.

Boiling Heat-Flux Limits. Data from Ref. 4 indicate that peak nucleate boiling heat-flux values were in the order of 1 Btu/in^2-sec for coolant velocities of 25 fps. Film boiling heat-flux values were approximately 0.5 Btu/in^2-sec. Film boiling results in a lower heat flux capability as compared to nucleate boiling due to the formation of a high thermal resistance vapor blanket between the wall and the liquid core. Transition to film is greatly dependent on the coolant velocity and sub-cooling ($T_{saturation}-T_{Bulk}$). Although the slopes of the peak flux-vs-velocity curves decrease with increasing coolant velocity, peak nucleate-flux values of approximately 2 to 3 Btu/in^2-sec and film boiling fluxes of approximately 1 Btu/in^2-sec should be attainable at reasonable design velocities of 100 fps. The exact values of the heat flux limits depend upon the particular conditions. The above values are typical and are useful in defining the type of coolant circuit applicable for the various operating parameters.

Throat heat-flux values for 100 psia chamber pressure are shown in Table 13. The heat-flux values for all propellant combinations are below the peak nucleate-boiling value. The heat-flux values are above the film-boiling value for all propellants except 1-butene and, perhaps, propane at high thrust levels. Thus at 100 psia, all propellants may pass through the throat regions as liquids even without a gas-side carbon layer. Propane and 1-butene may also be allowed to vaporize in the throat if the assumed carbon resistance exists.

The values of maximum (throat) heat flux are also shown in Table 13 for the various propellant combinations at 250 psia chamber pressure. These values are all well above the film-boiling fluxes so that vaporization

TABLE 13

THROAT HEAT FLUX VALUES

Fuel*	Throat Heat Flux, Btu/in.^{2}-sec			
	Chamber Pressure;psia			
	100		250	
	Thrust, pounds 1000	20,000	Thrust, pounds 1000	20,000
All Fuels - no carbon layer	2.54	2.22	5.54	5.10
Methane	1.77	1.56	3.88	3.57
Methane-Ethane	1.52	1.34	3.32	3.06
Ethane	1.27	1.11	2.77	2.55
Propane	1.09	0.94	2.38	2.20
1-Butene	0.76	0.67	1.66	1.53

*Oxidizer is either FLOX or OF_2

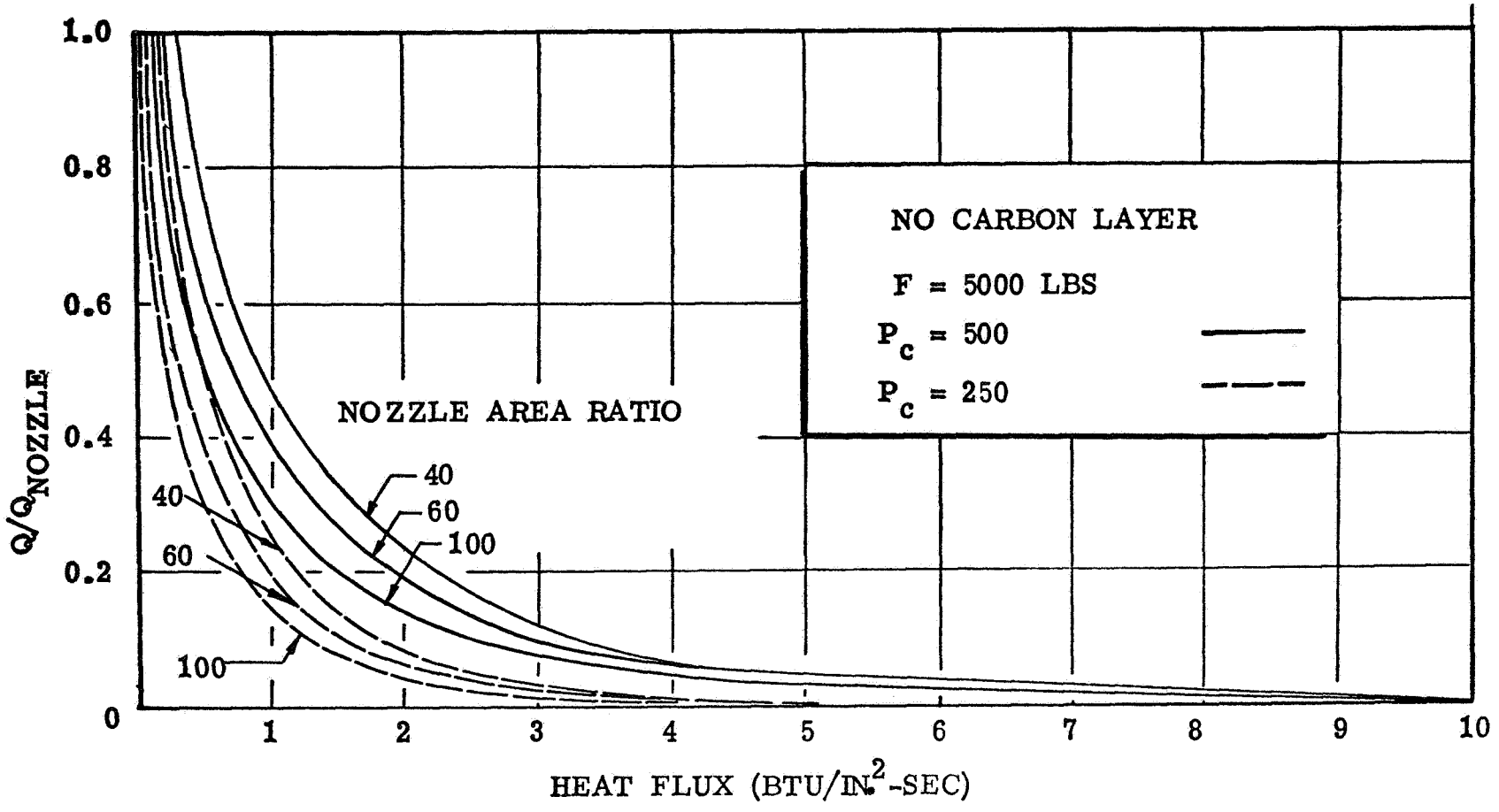

Figure 27. Normalized Nozzle Heat Input vs Local Heat Flux

in the throat region is not permissible for any of the propellant combinations. The throat heat fluxes are below the peak nucleate-boiling flux levels for 1-butene, propane, and probably, ethane, and indicate that these fuels could pass through the throat region as liquids provided that the gas-side carbon layer is present.

The heat flux decays rapidly downstream of the throat as shown in Fig. 27. The maximum heat flux shown is the value at the throat; the minimum flux shown occurs at the nozzle exit. Most of the nozzle heat input occurs in the low flux region; e.g., for a chamber pressure of 250 psia and a nozzle area ratio of 100, 86 percent of the nozzle heat input is accumulated in the region of the nozzle where the flux is less than 1 Btu/in.^{2}-sec. This implies that those fuels which cannot be vaporized in the throat might be completely vaporized in the nozzle.

Operation at 100-psia Chamber Pressure without Vaporization. The restriction that the fuel bulk temperature be below the saturation temperature for the 100-psia chamber pressure case results in the heat absorption limits given in Table 5. The total heat input data, including the gas-side carbon resistance, is shown in Fig. 28 for the various fuels.

Methane and Methane-Ethane Blend. The heat absorption capability of methane is such that bulk boiling cannot be prevented under any of the conditions investigated. The same conclusion applies to the methane-ethane blend. The presence of the assumed carbon layer does not prevent bulk boiling.

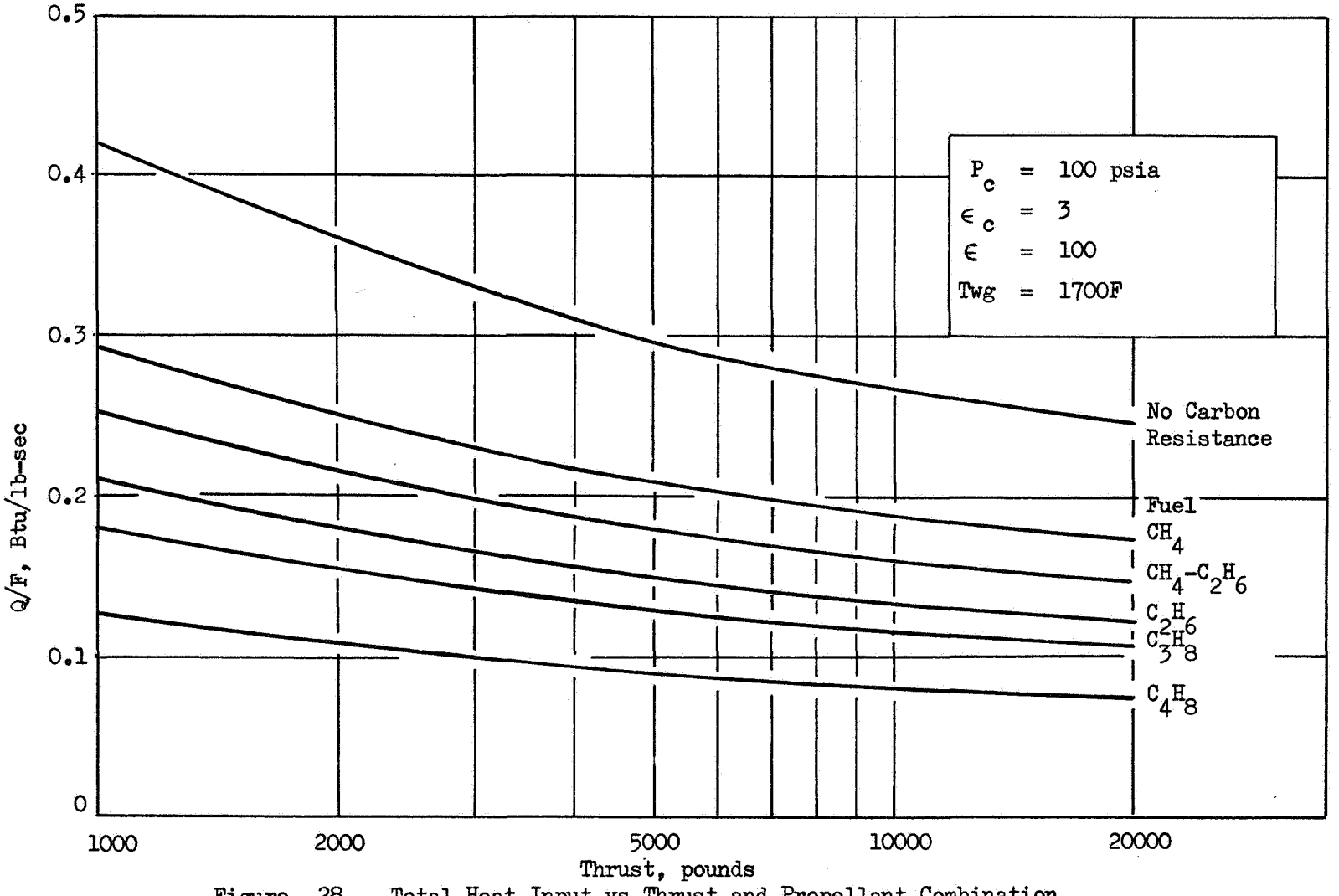

Figure 28. Total Heat Input vs Thrust and Propellant Combination

Ethane. Comparison of the heat absorption capabilites and heat inputs of FLOX/methane and OF_2/ethane results in the conclusion that either propellant combination can be used, without bulk boiling at the 10,000-pound thrust level only under the most mild conditions (T_{wg} = 3200 F, ϵ = 40, o/f = 70 percent of optimum, gas-side carbon layer present). Operation at lower thrust levels is not possible. Operation at the 20,000-pound thrust level is possible only for T_{wg} of 3200 F and o/f $\leq$ 85 percent of the optimum specific impulse value. The tradeoffs between contraction area ratio, nozzle area ratio, and propellant mixture ratio are shown in Fig. 29. Fairly severe limits are shown to exist even at these conditions of high wall temperature and high thrust level. Without the carbon layer, ethane cannot be prevented from boiling under any condition investigated.

Propane. Tradeoffs between the various parameters required to prevent bulk boiling of propane at 100-psia chamber pressure with a carbon layer are shown in Fig. 30 and 31. The results shown in Fig. 30 indicate the similarity of the tradeoffs for FLOX and OF_2. Use of OF_2 results in slightly more severe limits than FLOX because of the higher optimum propellant mixture ratio and specific impulse of the OF_2/propane combinations. Both of these factors reduce the fuel-coolant flowrate available at a given thrust level.

The tradeoffs shown in Fig. 30 for FLOX/propane indicate that operation at the 1000-pound thrust level is just barely possible (o/f = 70 percent, ϵ = 40, T_{wg} = 3200 F). Operation at even the highest (20,000 pound) thrust level investigated is somewhat limited; i.e., operation at T_{wg} = 1700 F, ϵ = 100, o/f = 100 percent is not possible. Either

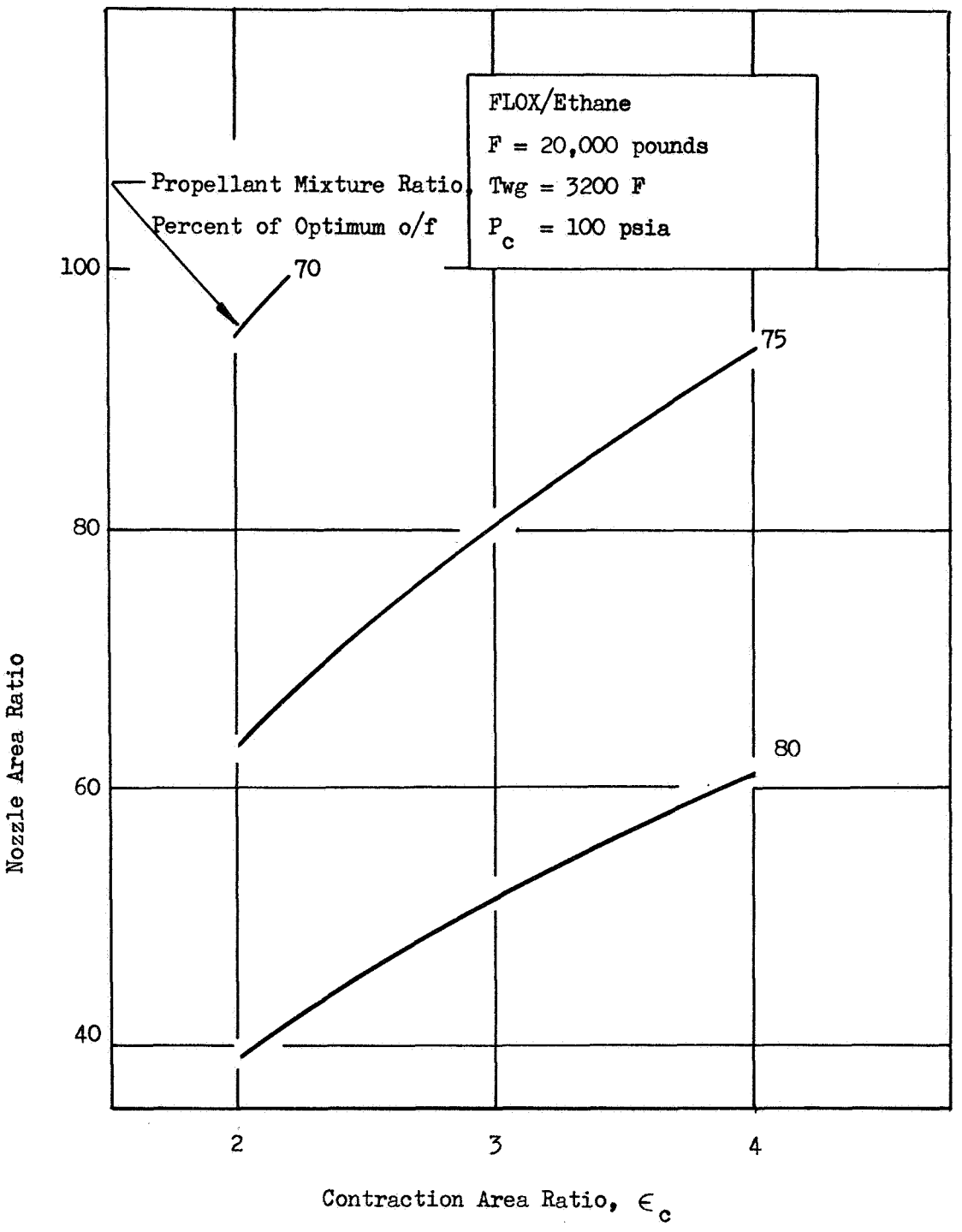

Figure 29. Propellant Mixture Ratio and Geometry Tradeoffs Based on Ethane Boiling Limits With Carbon Layer

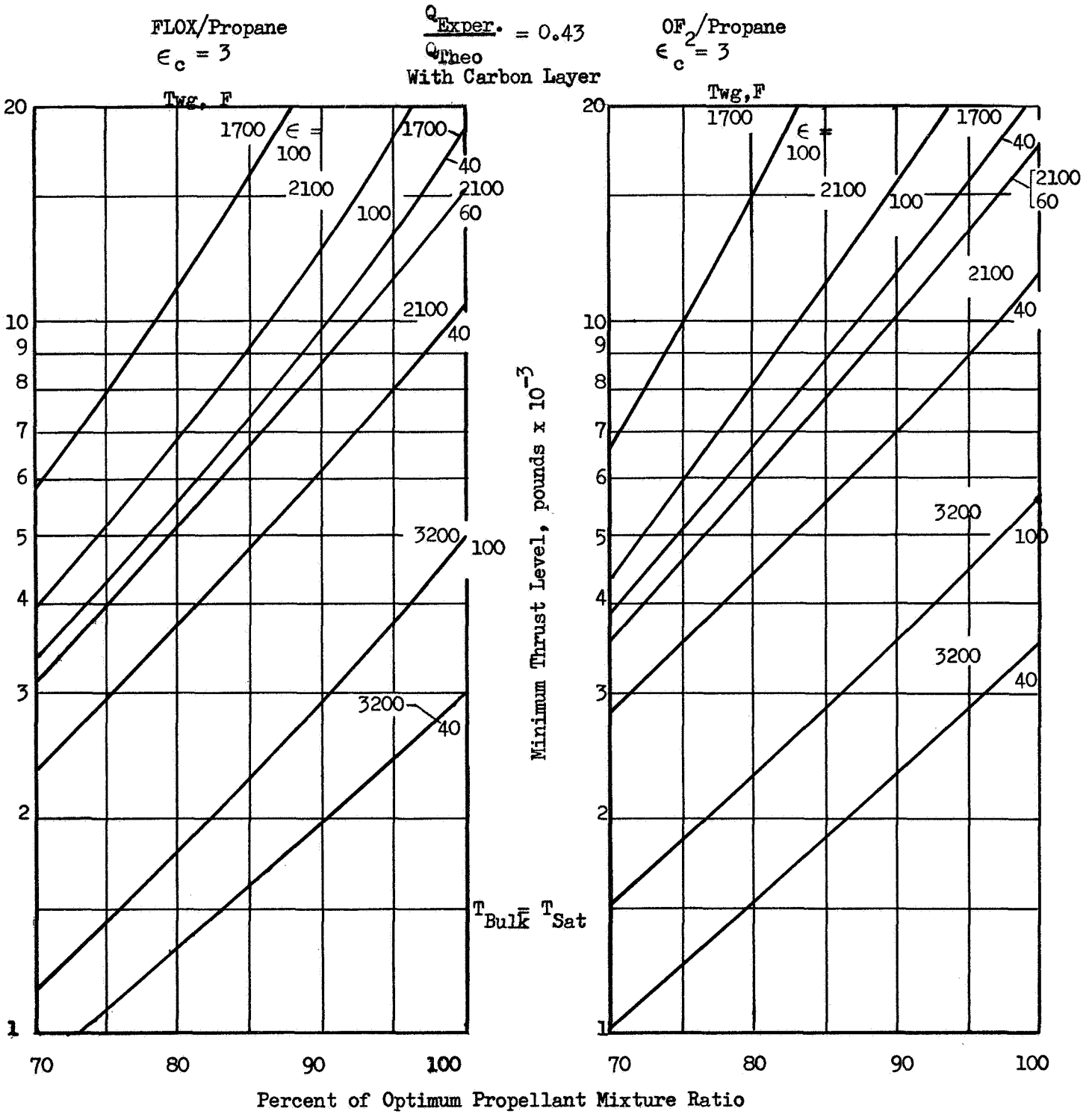

Figure 30 . Minimum Thrust Limits for Propane at P_c = 100 psia

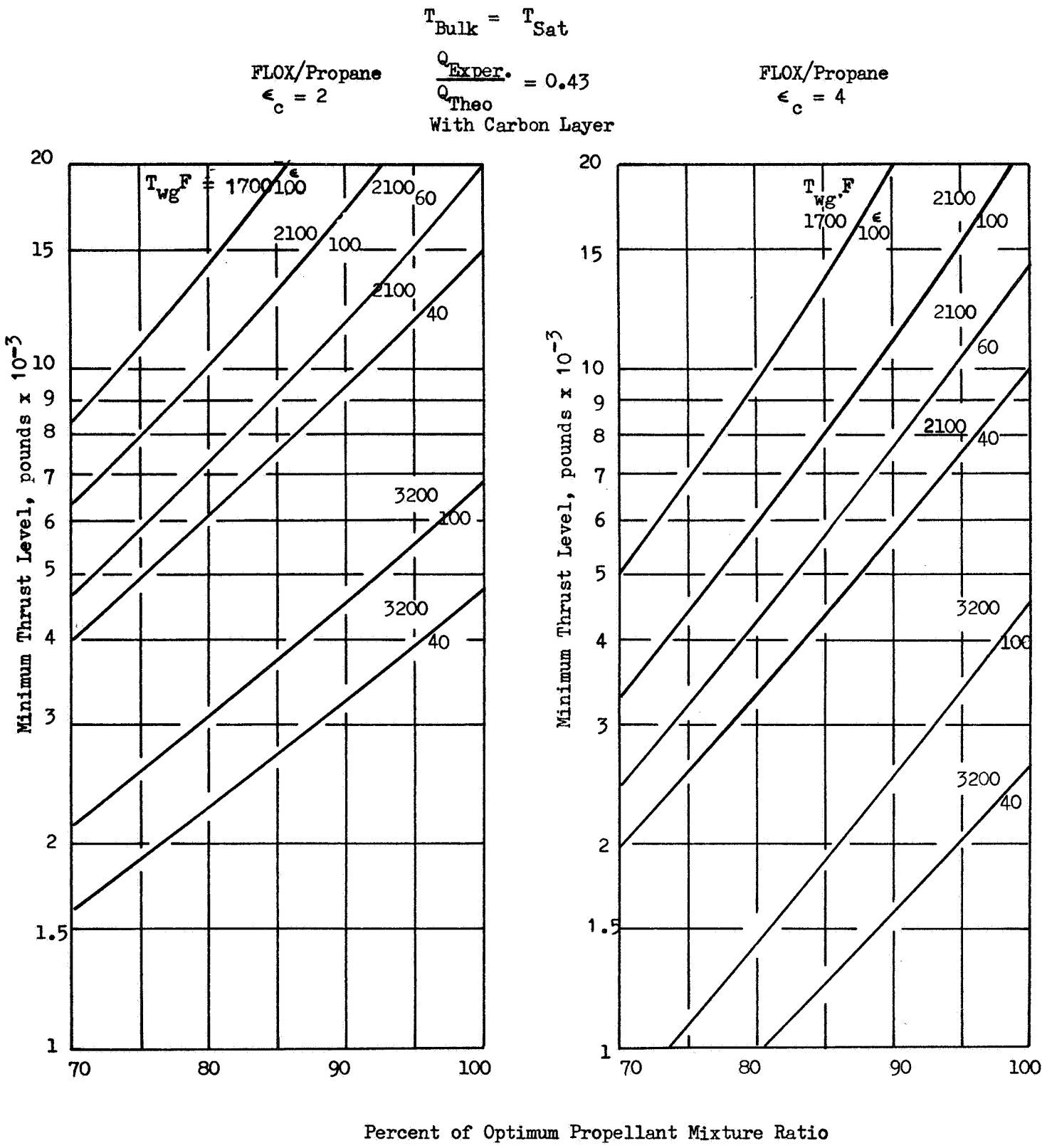

Figure 31 . Minimum Thrust Limits for FLOX/Propane at P_c = 100 psia

T_{wg} must be increased to greater than 2100 F, or ϵ must be reduced to approximately 40, o/f must be reduced to 88 percent of optimum, or various combinations of these compromises may be effected.

The effect of the contraction area ratio on the operating limits is evident from a comparison of the two sets of curves (for ϵ_c = 2 and 4) shown in Fig. 31. This effect, although appreciable, does not alter the general conclusions presented in the previous paragraph. Thus it appears that, if the propane is not allowed to bulk boil, its use would generally be limited to the higher thrust levels. Boiling could not be prevented at any thrust level investigated if the gas-side carbon layer is absent.

1-Butene. Comparison of the heat absorption data with Fig. 28 indicates that the FLOX/1-butene or OF_2/1-butene combinations will not boil at thrust levels of 1000 pounds or greater for the tabulated conditions at a chamber pressure of 100 psia if the assumed gas-side carbon layer is present. Conditions under which the butene could be prevented from boiling at the 1000 pound thrust level are shown in Table 14.

TABLE 14

1-BUTENE BOILING CONDITIONS

ϵ_c	ϵ	T_{wg}, F	o/f, percent	$T_B \leq T_{SAT}$
3	100	1700	100	Yes
2	100	1700	100	No
2	100	1700	85	Yes
2	100	3200	100	Yes
2	40	2100	100	No

F = 1000 pounds, P_c = 100 psia, Carbon Layer

The data shown indicate that 1-butene can be used at the 1000-pound thrust level for all conditions provided that a contraction ratio of 3 or greater is used. The data show the parameter limits necessary to prevent bulk boiling if a contraction ratio of 2 were used. Under this condition, bulk boiling could be prevented by reducing the propellant mixture ratio to 85 percent of the optimum value or by increasing the allowable gas-side wall temperature to 3200 F. Simultaneously decreasing the nozzle area ratio to 40 and increasing the value of T_{wg} to 2100 F would not prevent boiling. The above discussion applies to both FLOX/1-butene and OF_2/1-butene because the heat inputs and optimum propellant mixture ratios are similar for the two propellant combinations.

Without the gas-side carbon layer, the 1-butene propellant mixture ratio would have to be reduced below 90 percent of the optimum value to prevent boiling at even the mildest conditions (Thrust = 20,000 pounds, $\epsilon = 40$, $\epsilon_c = 4$, $T_{wg} = 3200$ F).

<u>Operation at 100-psia Chamber Pressure with Complete Vaporization.</u> For those conditions where it is not possible to prevent bulk boiling, it may be possible to completely vaporize the coolant prior to injection. The use of a vaporized coolant would also facilitate obtaining high C* efficiencies. The coolant flow circuit selection for the complete vaporization cases will depend greatly upon the distribution of heat input between nozzle (low Q/A region) and combustion (high Q/A region) and upon the peak (throat) heat flux level. These various conditions and resulting coolant circuits are summarized in Table 15. If, for example, the chamber peak heat flux is low enough to permit coolant bulk or film boiling (this represents the poorest cooling conditions) without excessive wall temperatures then the coolant may be flowed single-pass in either direction. A nominal limiting

TABLE 15

REGENERATIVE COOLING CIRCUITS FOR SUBCRITICAL OPERATION WITH COMPLETE VAPORIZATION OF COOLANT

Condition	$(Q/\dot{W}_f)$ in Low Flux Region, Btu/lb	$(Q/\dot{W}_f)$ in High Flux Region, Btu/lb	(Q/A) Throat Btu/in.^{2} - sec	Coolant Circuit
1			< 1	Single-Pass Either Direction
2	$> H_{h,v}$		> 1	Single-Pass Counterflow
3		$< H_h$	1 to 3	Single-Pass Parallel Flow
4	$> H_v$	$> H_h$	1 to 3	Two-Pass (Nozzle Exit Return Manifold)

H_h = Heat required to raise the fuel to saturation temperature (liquid)

H_v = Heat required to completely vaporize all of the fuel

$H_{h,v} = H_h + H_v$

heat flux value for this case (condition 1 of Table 15) is approximately 1 Btu/in^2-sec depending on coolant velocity. If the throat heat flux is too high to safely permit film boiling, then the coolant must be either completely vaporized before it reaches the throat (forced convection cooling) or a sufficiently sub-cooled liquid to permit nucleate boiling. In the latter case, the maximum heat flux capability is about 3 Btu/in^2-sec depending on velocity and degree of sub-cooling (see p. 71). Condition 2 of Table 15 represents the case wherein there is sufficient heat input in the nozzle to achieve complete vaporization of the coolant resulting in the selection of a single-pass counterflow circuit. If the throat heat flux is low enough to permit nucleate boiling but too high for film boiling (condition 3), a single-pass parallel circuit may be used if the heat input in high flux region is less than that required to raise the coolant to the boiling point (i.e., coolant is a sub-cooled liquid). Furthermore, there must be sufficient heat input from the low flux region to complete the heating and vaporization of the fuel. Condition 4 differs from the previous condition in that the heat input in the high flux region is more than sufficient to heat the fuel to the boiling point and a two-pass system is required. In this case the fuel is a sub-cooled liquid in the throat on the downpass (nucleate boiling) and a gas in the throat on the uppass return (forced convection cooling).

Methane and Methane-Ethane Blend. Comparison was made of the heat required to heat and completely vaporize the methane with the total heat input in the low-flux region ($<$ 1 Btu/in^2-sec) of the nozzle. This comparison demonstrated that for T_{wg} = 1700 F, ϵ = 40, and Thrust = 20,000 pounds the methane would vaporize completely because of the low-heat-absorption capability and high-heat-input values even with a gas-side carbon layer. Lower values of thrust or higher values of ϵ would, therefore, also result in complete vaporization of the methane in the nozzle.

The methane-ethane blend coolant can be heated and completely vaporized in the nozzle only at the 1000-pound thrust level ($\epsilon = 100$, $T_{wg} = 1700$ F) unless the carbon layer resistance is reduced. With no carbon resistance, one-pass counterflow regenerative cooling with complete vaporization in the nozzle is possible for all thrust levels for $\epsilon = 100$ and $T_{wg} = 3200$ F, or $\epsilon = 40$ and $T_{wg} = 1700$ F.

With the assumed carbon layer resistance, the thrust chamber heat input is sufficient to heat and vaporize the methane-ethane coolant at all thrust levels ($\epsilon_c = 4$, $\epsilon = 40$, $T_{wg} = 1700$ F). The nozzle heat is sufficient to vaporize the coolant at all thrust levels for $\epsilon = 60$ ($T_{wg} = 1700$F).

Only part of the combustion zone heat input is required to heat the methane-ethane coolant to the boiling point so that a two-pass regenerative cooling circuit would be used.

Ethane. Ethane could not be heated and completely vaporized in the nozzle (one-pass counterflow cooling) under any conditions with the assumed carbon resistance. With no carbon resistance, heating and complete vaporization of ethane in the nozzle would be accomplished at all thrust levels with an ϵ of 100 and T_{wg} of 2100 F or less.

Nucleate-boiling liquid ethane could pass through the throat region on the basis of present carbon layer data. A two-pass regenerative cooling circuit could be used under certain conditions. Liquid ethane would enter the injector end of the jacket, pass through the throat region as a liquid and be completely vaporized in the nozzle. Sufficient heat to raise the ethane temperature from near freezing point and completely vaporize the ethane is available only for thrust $\leq$ 10,000 pounds in thrust chambers with $\epsilon_c = 2$, $T_{wg} = 1700$ F, $\epsilon = 100$. At the lowest thrust levels, the combustion-zone heat input is greater than that required to raise the ethane temperature to the boiling point even for $\epsilon_c = 4$. Under these conditions a two-pass system would be required so that the liquid ethane would receive only a portion of the combustion zone heat, the remaining heat would superheat the ethane vapor.

Propane. Heating and complete vaporization of the coolant in the low-heat-flux portion of the nozzle is possible only without the carbon layer for a gas-side wall temperature of 1700 F. Additional restrictions are (1) the area ratio must be 100, the gas-side wall temperature must be 1700 F, and (2) the thrust levels $\leq$ 10,000 pounds. Reducing the area ratio to 60 reduces the maximum thrust to approximately 2000 pounds.

The heat input to the entire thrust chamber with a carbon layer is such that heating and vaporization will occur at thrust levels approximately 2000 pounds with $T_{wg} = 1700$ F, $\epsilon = 100$, and $\epsilon_c = 2$. Under these conditions, the heat input in the high-flux region is too high for single-pass operation so that a two-pass system would be necessary. Single-pass parallel flow cooling is possible with $\epsilon_c = 4$ but the maximum thrust level is 1000 pounds.

Without the gas-side carbon layer, there is sufficient heat in the entire thrust chamber to heat and vaporize the propane at all thrust levels with $\epsilon_c = 4$ and $\epsilon = 40$ with $T_{wg} = 2100$ F. A two-pass cooling circuit would generally be required to prevent bulk boiling in the high-flux region.

1-Butene. Heating and complete vaporization in the nozzle is not possible even without a carbon layer under any of the conditions investigated. Heating and complete vaporization in the entire thrust chamber is also not possible if a carbon layer exists. Without the carbon layer, heating and complete vaporization in the thrust chamber is possible at all thrust levels under the following sets of conditions:

ϵ_c	ϵ	T_{wg}, F
4	60	1700
4	100	2100
2	40	1700
2	60	2100

Single-pass parallel flow cooling circuits are generally applicable for thrust levels greater than 5000 pounds with $\epsilon_c > 2$ because the heat input required to heat the coolant to the boiling point is significantly greater than the heat for vaporization.

Operation at 250-psia Chamber Pressure Without Vaporization. Increasing the chamber pressure from 100 to 250 psia at a fixed thrust level results in higher heat flux values throughout the thrust chamber. However, the saturation temperature is also increased and the net result of the chamber pressure increase is a higher ratio of heat absorption capability (without bulk boiling) to heat input.

Methane and Methane-Ethane Blend. Despite the more favorable heat absorption-to-input ratio at 250 psia, the methane and methane-ethane blend coolants cannot be prevented from bulk boiling under the mildest conditions investigated (Thrust = 20,000 pounds, $\epsilon = 40$, $\epsilon_c = 4$, $T_{wg} = 3200$ F, o/f = 70 percent, gas-side carbon layer).

Ethane. The minimum thrust limits for ethane with a carbon layer are shown in Fig. 32. Under none of the conditions examined can bulk boiling be prevented at thrust levels under 2500 pounds. Specification of a contraction ratio of 2 would require an operating wall temperature of 3200 F and a reduction of propellant mixture ratio for all thrust levels. If the contraction ratio is increased to 4, operation with a 2100 F wall and reduced mixture ratio and area ratio becomes possible for high thrust levels. The difference between results based upon FLOX and OF_2 as oxidizers is fairly small with tht OF_2 propellant combination having a slight advantage because of the lower optimum mixture ratio. Bulk boiling cannot be prevented under any condition without the presence of a gas-side carbon layer.

$$\frac{Q_{Exper.}}{Q_{Theo.}} = 0.5$$

With Carbon Layer

Bulk Temperature = Saturation Temperature

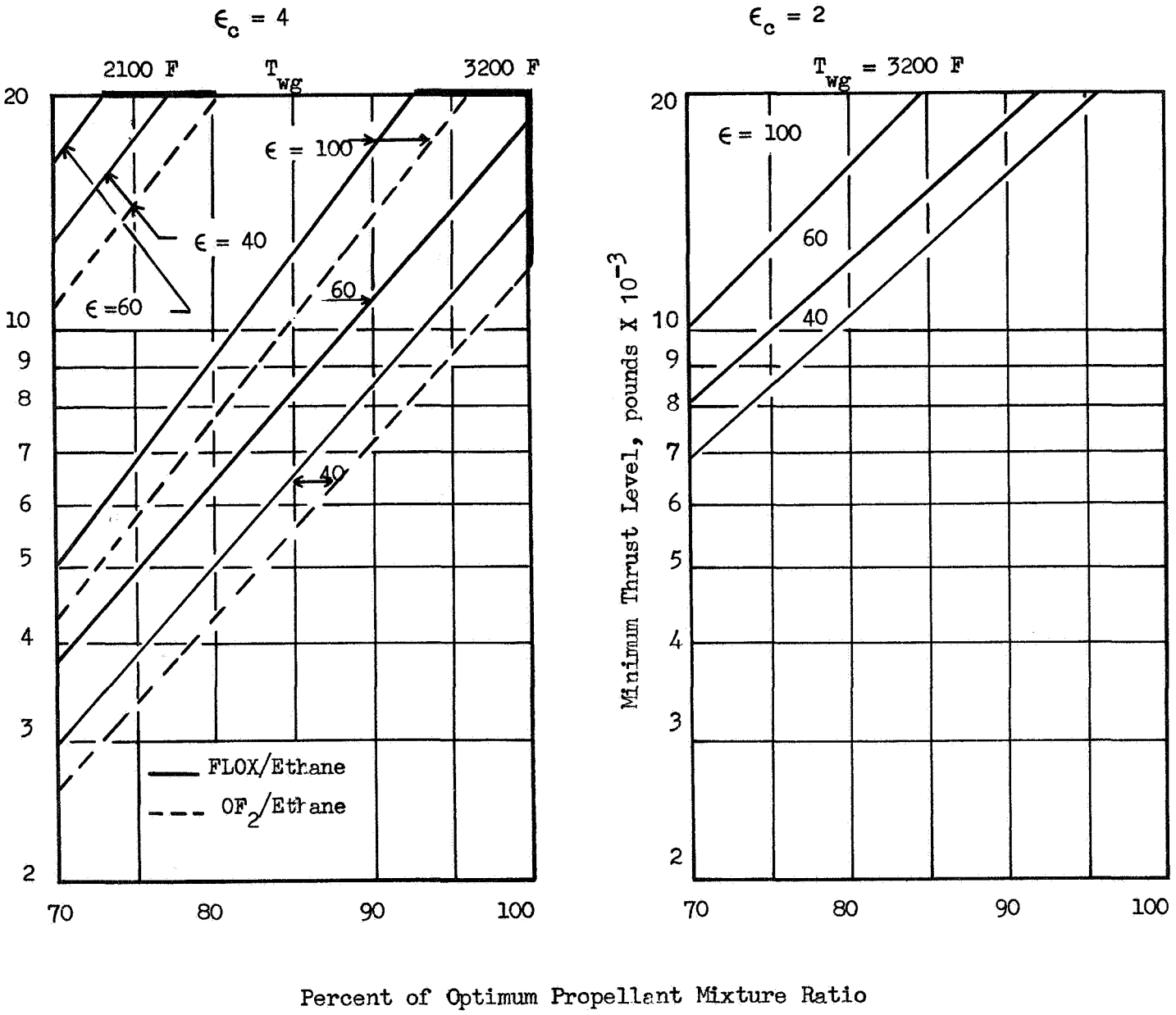

Percent of Optimum Propellant Mixture Ratio

Figure 32. Minimum Thrust Limits for Ethane at Chamber Pressure of 250 psia

Propane. Minimum thrust levels for propane based upon the bulk boiling limit including a gas-side carbon layer are shown in Fig. 33 and 34. For a contraction ratio of 2, operation is possible under all conditions at 1000 pounds. Operation at 1000 pounds thrust is possible with a contraction ratio of 4 but only if a wall temperature of 3200 F is used and the propellant mixture ratio is reduced from the optimum value. Results for OF_2/propane are similar to those with FLOX/propane. The FLOX/propane combination is favored slightly because of its lower optimum mixture ratio and specific impulse (i. e., more fuel is available for cooling at a given set of conditions). Propane cannot be prevented from bulk boiling under any of the investigated conditions if a carbon layer does not exist.

1-Butene. Cooling with liquid 1-butene at 250 psia is generally possible at all thrust levels if a gas-side carbon layer exists. However, for the most severe thrust level examined (1000 pounds), a contraction ratio of 3 or greater would be required to prevent bulk boiling of the coolant without limiting the other parameters. A contraction ratio of 2 with a wall temperature of 3200 F would also prevent bulk boiling at the 1000-pound thrust level. Tradeoffs between nozzle area ratio and propellant mixture ratio for lower values of T_{wg} at $\epsilon_c = 2$ are shown in Table 16 together with a summary of the results discussed in this paragraph. The cooling capabilities of OF_2/1-butene are similar to those of FLOX/1-butene because of the equal optimum mixture ratio values. The slightly higher specific impulse of the OF_2/1-butene would result in a reduction of approximately 2 percent in the maximum mixture ratio values specified in the last four lines of Table 16.

$$\frac{Q_{Exper.}}{Q_{Theo.}} = 0.43$$

With Carbon Layer
Bulk Temperature = Saturation Temperature

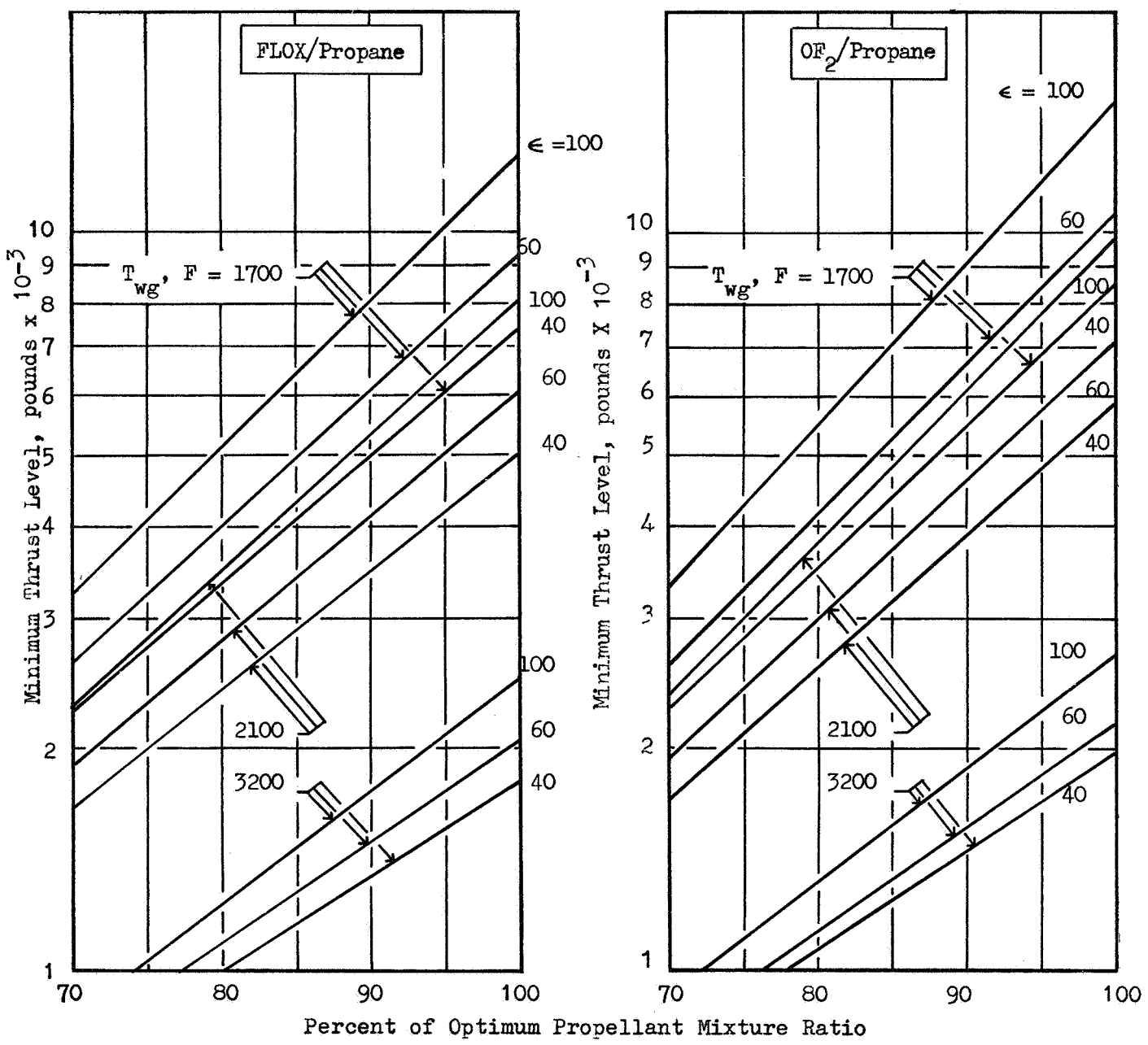

Figure 33. Minimum Thrust Limits for Propane at Chamber Pressure of 250 psia and $\epsilon_c = 3$.

$$\frac{Q_{Exper.}}{Q_{Theo.}} = 0.43$$

With Carbon Layer

Bulk Temperature = Saturation Temperature

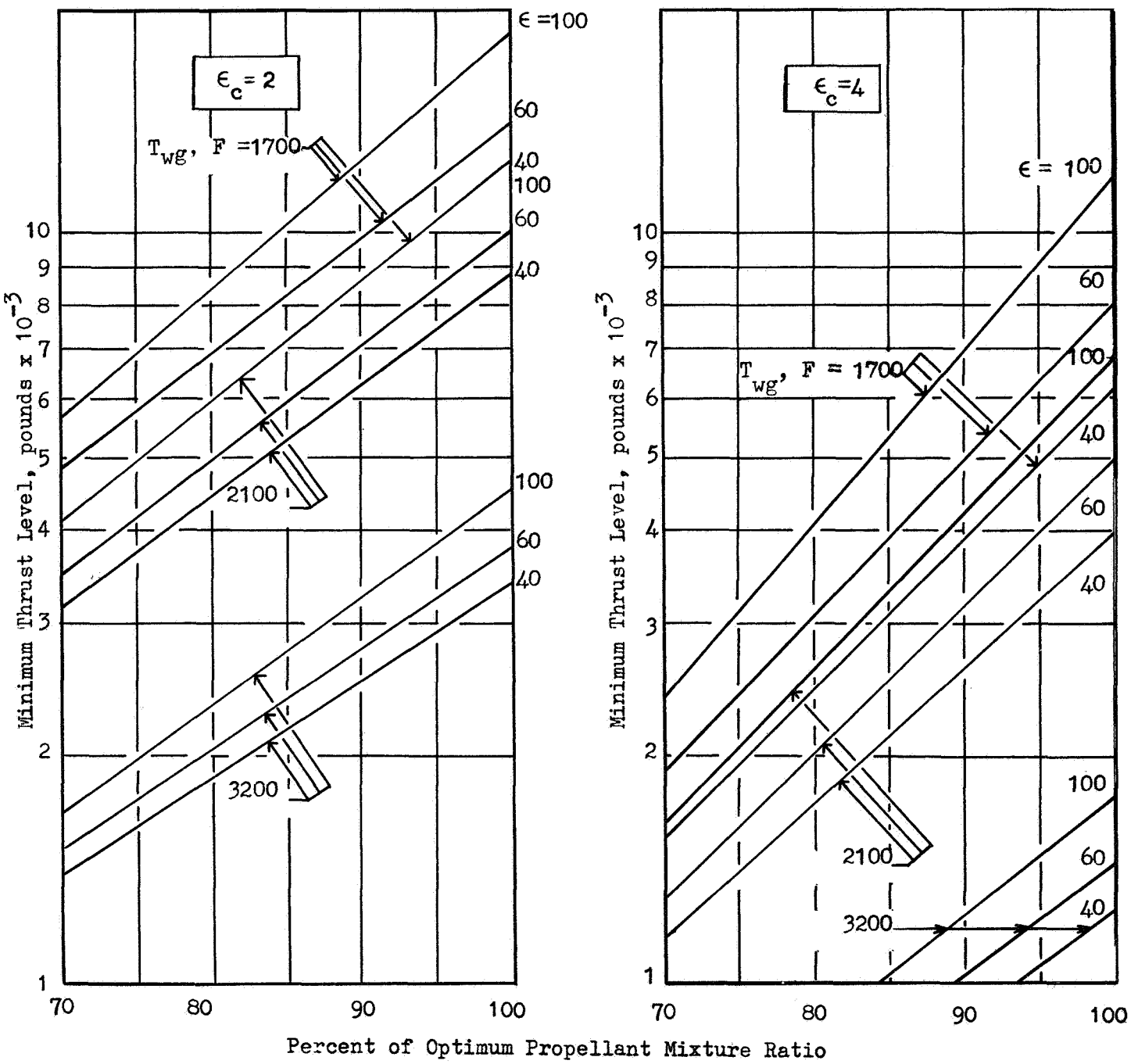

Figure 34. Minimum Thrust Limits for FLOX/Propane at Chamber Pressure of 250 psia.

With no carbon layer resistance, the minimum thrust level to prevent bulk boiling of 1-butene is 3000 pounds (T_{wg} = 3200F, ϵ_c = 4, ϵ = 40, 70 percent o/f). Regenerative cooling is possible at the 20,000-pound thrust level under the following sets of conditions:

ϵ_c	ϵ	T_{wg}, F	o/f, percent
4	40	1700	70
4	60	2100	70
4	40	2100	80
4	50	3200	100

TABLE 16

FLOX/1-BUTENE COOLING LIMITS AT 250 PSIA CHAMBER PRESSURE WITH $T_{BULK} \leq T_{SAT}$

Thrust, lb.	Contraction Ratio, ϵ_c	Gas-Side Wall Temp., T_{wg}, F	Nozzle Area Ratio, ϵ	Propellant Mixture Ratio, o/f, percent of Optimum, o/f
≥5000	*	*	*	*
1000	≥3	*	*	*
1000	2	3200	*	*
1000	2	2100	≤ 60	*
1000	2	2100	100	≤ 95
1000	2	1700	40	≤ 93
1000	2	1700	60	≤ 90
1000	2	1700	100	≤ 87

* All values over the ranges investigated are suitable.

Operation at 250-psia Chamber Pressure with Complete Vaporization. An investigation was made to determine the effects of removal of the bulk temperature limit at 250-psia chamber pressure. To eliminate the potential problems associated with two-phase propellant injection, complete vaporization of the fuel was established as a necessary condition for regenerative cooling applicability. The following results were obtained for optimum propellant mixture ratio and 1700 F wall temperature (except as noted).

Methane and Methane-Ethane Blend. If a gas-side carbon layer exists, there is sufficient heat input to the low heat flux (< 1 Btu/in^2-sec) portion of the nozzle to heat and completely vaporize the methane only if the nozzle area ratio is 100 and the thrust level is 5000 pounds or less. There is sufficient heat in the entire thrust chamber to heat and vaporize the methane under all conditions (even if the wall temperature were increased to 3200 F). However, the throat heat flux is too high for nucleate boiling (Table 13) so that only a portion of the fuel is flowed through a single-pass counterflow coolant circuit such that the coolant is completely vaporized in the low-flux portion of the nozzle, superheated in the high-flux region of the thrust chamber and combined with the remainder of the fuel after exiting the coolant jacket.

The heat absorption and heat input characteristics of the methane-ethane blend are such that heating and vaporization of all of the fuel in the low-flux portion of the nozzle is not possible under any conditions if a gas-side carbon layer exists. Heating and vaporization of all the fuel by the heat of the complete thrust chamber is possible for all conditions investigated with $T_{wg} \leq 2100$ F.

Without the carbon layer, the methane can be heated and completely vaporized in the nozzle under all conditions. The methane-ethane blend can be heated and completely vaporized in the nozzle at all thrust levels if the area ratio is 100, and at thrusts of 10,000 pounds or less if the area ratio is 60. The heat of the entire thrust chamber without a carbon layer is sufficient to heat and vaporize the methane-ethane coolant under all conditions, including T_{wg} = 3200 F.

Ethane. Heating and complete vaporization of the ethane in the nozzle is not possible under any conditions with a carbon layer. Without the carbon layer, heating and vaporization in the nozzle is possible only at thrust levels below 5000 pounds with an area ratio of 100.

There is sufficient heat input form the entire chamber with a carbon layer to heat and vaporize ethane under the following conditions: for thrust = 1000 pounds, all values of ϵ and ϵ_c; for thrust = 5000 pounds, all values except ϵ = 40 and ϵ_c = 4; for thrust = 10,000 pounds, only at ϵ_c = 2 with ϵ = 60 and 100; for thrust = 20,000 pounds complete vaporization was not possible. Without the carbon layer, there is sufficient heat input from the entire thrust chamber to heat and vaporize the ethane under all conditions, including T_{wg} = 3200 F. However, the supercritical analysis results indicated that the minimum thrust level would be approximately 3500 pounds because of the thermal decomposition limit. A two-pass coolant circuit could be used if a carbon layer exists because the throat heat fluxes are probably low enough to permit nucleate boiling.

Propane. Heating and complete vaporization of propane in the low-flux region of the nozzle is not possible under any conditions either with or without a gas-side carbon layer. With a carbon layer, the heat input from the entire thrust chamber is sufficient to vaporize all of the fuel only at the 1000-pound thrust level with $\epsilon = 40$ and $\epsilon_c = 4$, or at thrust levels below 4000 pounds with $\epsilon = 100$ and $\epsilon_c = 2$.

Without the carbon layer, the heat input from the entire thrust chamber is sufficient to heat and vaporize the propane under all conditions including $T_{wg} = 3200$ F. The throat heat flux is greater than the allowable nucleate boiling value so that a single-pass counterflow circuit must be used with only part of the fuel used as coolant. The coolant is superheated in the high-flux region of the thrust chamber. At thrust levels below 5000 pounds (with $T_{wg} = 1700$ F, $\epsilon = 100$, and $\epsilon_c = 2$), the decomposition temperature limit of the propane is reached. The minimum thrust level may be reduced to approximately 2000 pounds by increasing the contraction ratio to 4.

1-Butene. It is not possible to heat and vaporize the 1-butene in the nozzle under any of the conditions investigated. Without a gas-side carbon layer, the thrust chamber heat input is sufficient to heat and vaporize the 1-butene under almost all conditions (maximum thrust = 17,000 pounds for $\epsilon = 40$, $\epsilon_c = 4$, $T_{wg} = 1700$ F). The throat heat flux, without a carbon layer, requires that a counterflow coolant circuit with bypass be used. The maximum portion of the fuel is used as a coolant when $T_{wg} = 1700$ F and $\epsilon = 100$. The maximum superheat occurs when $\epsilon_c = 2$. Under these conditions, the decomposition temperature of the coolant is exceeded at thrust levels below 20,000 pounds.

Operating Limits Summary

The applicable thrust regimes (within the 1000 to 20,000 pound range of the present investigation) for regenerative cooling at 100- and 250-psia chamber pressure are summarized in Tables 17 and 18 respectively. Figure 35 is a more detailed summary for 250 psia chamber pressure operation with a carbon layer. Methane can be used as a regenerative coolant with complete vaporization under all conditions. The same conclusions apply to the methane-ethane blend except that the minimum thrust level is approximately 3500 pounds at 250 psia chamber pressure if a carbon layer does not exist. Ethane can be used as a liquid at the higher thrust levels and completely vaporized at the low thrust levels if a carbon layer exists. Without a carbon layer, ethane can be vaporized at all thrust levels but is decomposition limited to thrust levels above 3500 pounds at 250 psia chamber pressure. Propane may be used as a liquid at all thrust levels with a carbon layer and may be completely vaporized without decomposition at all thrust levels above 5000 pounds without a carbon layer. Butene may be used at all thrust levels with a carbon layer as a liquid and may be completely vaporized at all thrust levels without a carbon layer at 100-psia chamber pressure. Regenerative cooling without a carbon layer at 250-psia chamber pressure is limited to the 20,000 pound thrust level for 1-butene.

At chamber pressures of 500 to 1000 psia, methane may be used as a regenerative coolant at all thrust levels even without a carbon layer. If the assumed gas-side carbon layer exists, all the fuels can be used as regenerative coolants at all thrust levels. Without the carbon layer, all of the fuels except methane are restricted to minimum thrust levels greater than 1000 pounds at optimum propellant mixture ratio and T_{wg} = 1700 F. Relaxation of either of these two constraints to the most favorable values investigated will permit operation at the 1000 pound thrust level.

TABLE 17

APPLICABLE THRUST REGIMES FOR REGENERATIVE COOLING AT 100 PSIA CHAMBER PRESSURE

COOLANT	METHANE	METHANE-ETHANE	ETHANE	PROPANE	1-BUTENE
WITH CARBON LAYER					
NO BULK BOILING	>20K	> 20K	≥10K	1-20K	1-20K
COMPLETE VAPORIZATION	1-20K	1-20K	1-10K	1-2K*	<1K*
WITHOUT CARBON LAYER					
NO BULK BOILING	>20K	> 20K	>20K	> 20K	20K (O/F≤90%)
COMPLETE VAPORIZATION	1-20K	1-20K	1-20K	1-20K	1-20K

CONDITIONS	ϵ	ϵ_c	T_{WG}	O/F
NO BOILING	40	4	3200F	70% OF OPTIMUM
COMPLETE VAPORIZATION	100	2	1700F	OPTIMUM

ROCKETDYNE

TABLE 18

APPLICABLE THRUST REGIMES FOR REGENERATIVE COOLING AT 250 PSIA CHAMBER PRESSURE

COOLANT	METHANE	METHANE-ETHANE	ETHANE	PROPANE	1-BUTENE
WITH CARBON LAYER					
NO BULK BOILING	>20K	>20K	≥3K	≥1K	≥1K
COMPLETE VAPORIZATION	1-20K	1-20K	1-10K ($\epsilon \geq 60$)	1-3K	1K
WITHOUT CARBON LAYER					
NO BULK BOILING	>20K	>20K	>20K	>20K	>3K
COMPLETE VAPORIZATION	1-20K	3.5-20K	3.5-20K	5-20K	20K (ϵ_c=4)

CONDITIONS	ϵ	ϵ_c	T_{WG}	O/F
NO BOILING	40	4	3200F	70% OF OPTIMUM
COMPLETE VAPORIZATION	100	2	1700F	OPTIMUM

ROCKETDYNE

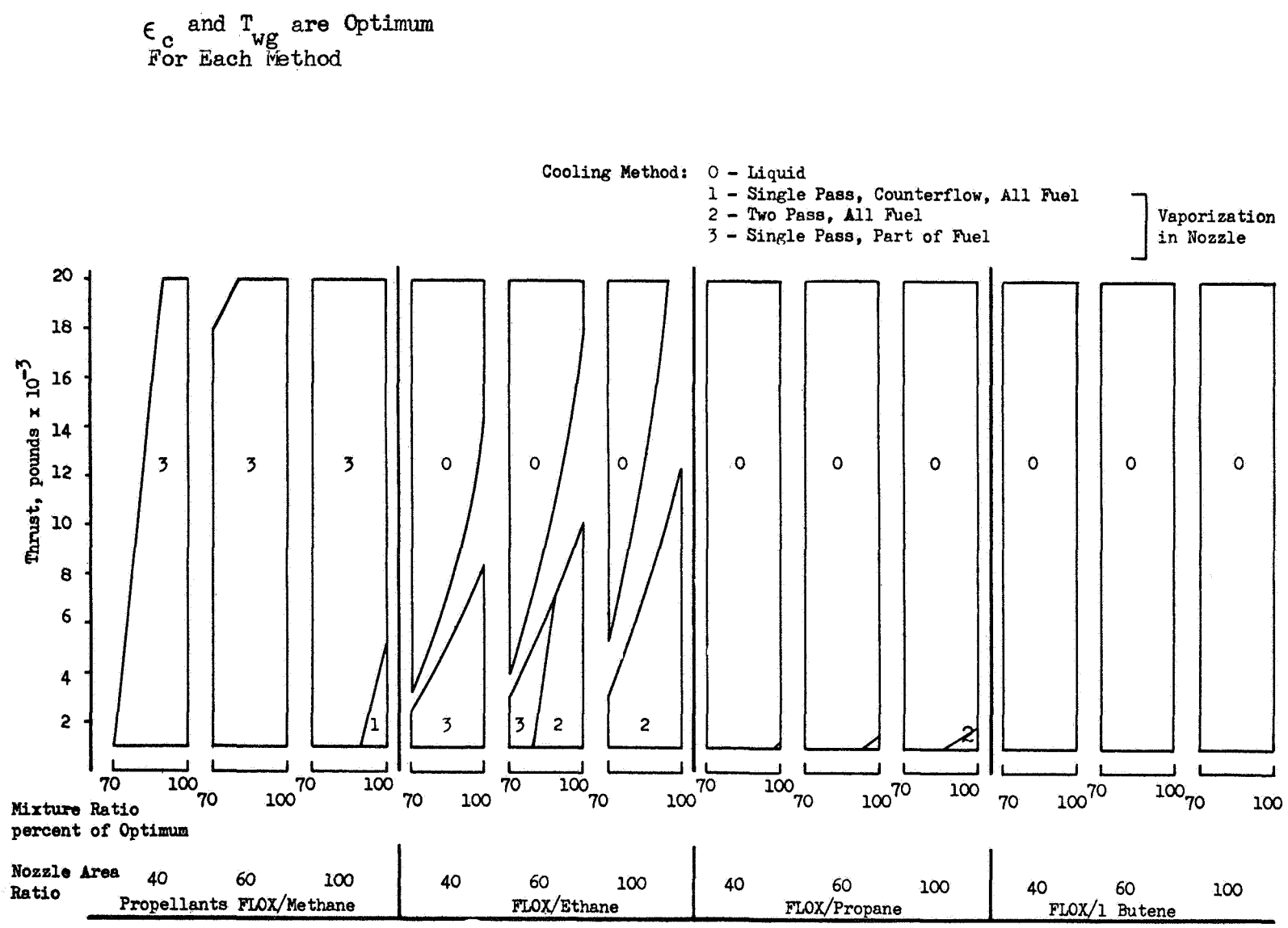

Figure 35. Operating Envelopes at 250 psia Chamber Pressure with Carbon Layer

DETAILED ANALYSIS

The results of the Parametric Analysis were used to select propellant combinations for more detailed regenerative cooling evaluation. The propellant combinations selected at the various thrust levels are presented in Table 19. The range of variation of other pertinent parameters is also summarized in Table 19. A contraction area ratio of 4 was selected to minimize total heat input while maintaining high C* efficiency. Thrust levels of 1000, 5000, and 20,000 pounds were used. Methane was investigated at all thrust levels because of its high performance (specific impulse) and because the Parametric Analysis results indicated methane to be an applicable regenerative coolant under all conditions investigated. Propane was analyzed for the 5000 and 20,000-pound thrust levels because of operating parameter restrictions encountered at the lowest thrust levels investigated in the Parametric Analysis. Butene-1 was evaluated at the 1000 pound thrust level because of its good cooling capability with a gas-side carbon layer. OF_2 was selected as the oxidizer for propane and 1-butene because of the superior performance relative to FLOX. The performance values of OF_2 and FLOX with methane are very similar. FLOX was, therefore, used with methane based upon current availability and cost.

The detailed evaluation consisted of complete thrust chamber regenerative cooling designs to ascertain coolant pressure drops and channel sizes. The results of these analyses are presented in subsequent sections according to propellant combinations.

TABLE 19

OPERATING CONDITIONS FOR DETAILED ANALYSIS

Chamber Pressures, Psia	100 to 1000
Gas-Side Wall Temp., F	1700, 2100, 3200
Contraction Area Ratio	4
Expansion Area Ratio	100 (Maximum)
Propellant Mixture Ratio	Optimum (Maximum)
Coolant Passage Construction	Channel
Coolant Passage Materials	Nickel, Steel, Hastelloy, Coating
Carbon Layer Resistance	Experimental (Fig. 16) and No Carbon
Propellants and Thrust, Pounds	FLOX/Methane : 1000,5000,20,000
	OF_2/Propane : 5000, 20,000
	OF_2/1-Butene : 1000

GROUND RULES AND PRELIMINARY OBSERVATIONS

The feasibility of a given chamber design is based upon whether certain imposed constraints are exceeded. Of necessity, these constraints are somewhat arbitrary. It is important to point out, therefore, the various constraints imposed in this study. In general, there are three areas of concern in establishing feasibility limits: (1) system limitations; (2) coolant limitations, and (3) fabrication limitations. The system limitation is concerned primarily with coolant jacket pressure drop. Coolant limitations arise from decomposition at elevated bulk temperatures and/or wall carbon deposition at elevated coolant-side wall temperatures. Fabrication limits are related to minimum wall thickness and channel size.

Pressure Drop, Geometric, and Thermal Limits

The imposed constraints are summarized in Table 20. The allowable coolant pressure drop was taken as 100 psi at a chamber pressure of 100 psia and increased linearly to a drop of 500 psi at a chamber pressure of 1000 psia.

Channel construction was assumed with a constant land width design. This represents a near-minimum weight design. A 0.050 inch-land width was generally used. Channel splices were required in the nozzle at area ratios of approximately 5 to 20 based upon cooling and stress considerations. Advanced fabrication techniques using channel construction allow for ease of splicing. This is a distinct advantage when compared to tubes which are difficult and expensive to splice. An alternate approach would be to increase the land and wall thickness but this would

increase the chamber weight. The minimum wall thickness of 0.025 inches represents a fabrication limit based on normal tolerance considerations. The minimum channel height of 0.025 inches and channel width of 0.040 inches were selected based upon tolerance and plugging considerations. Channel cross sections were square unless restricted by the minimum width limit. The maximum channel width-to-wall thickness ratio of 5 arises from stress considerations and is fairly conservative.

The coolant bulk decomposition limits were obtained from a literature search as discussed in the Parametric Analysis section. The maximum coolant-side wall temperatures T_{wc} without coking were estimated to be 1500F for propane and 1-butene based upon recent company funded experimental data. Based upon these results and on decomposition rate differences, a value of 2000F was calculated for the maximum T_{wc} for methane cooling. Only under certain extreme conditions do the coolant-side wall temperature constraints come into importance.

The wall temperatures and coolant requirements as calculated by the Rocketdyne digital computer program are based upon one-dimensional heat flow considerations. To ensure that allowable wall temperatures were not exceeded at higher heat flux levels because of two-dimensional effects, a more detailed thermal analysis was performed for selected cases. This was accomplished using a thermal analyzer digital computer program to calculate the two-dimensional temperature distribution in a throat section.

The results of such a detailed analysis are shown in the form of isotherm plots in Fig. 36. The case selected is a methane-cooled nickel channel chamber operating at a thrust of 1000 pounds and chamber pressure of 1000 psia. No carbon layer was assumed so that this represents the most

TABLE 20

LIMITING CONDITIONS FOR REGENERATIVE COOLING

Coolant Jacket Pressure Drop
Variable - 100 psi at 100 psia Chamber Pressure to 500 psi at 1000 psia Chamber Pressure
Minimum Channel Dimensions
0.025 Inch Wall Thickness, T
0.040 Inch Channel Width, W
0.025 Inch Channel Depth, D
0.20 T/W
Coolant Coking
Based on Negligible Coking in 1000 Seconds
T_{wc} = 2000F for Methane
T_{wc} = 1500F for Propane and 1-Butene

ROCKETDYNE

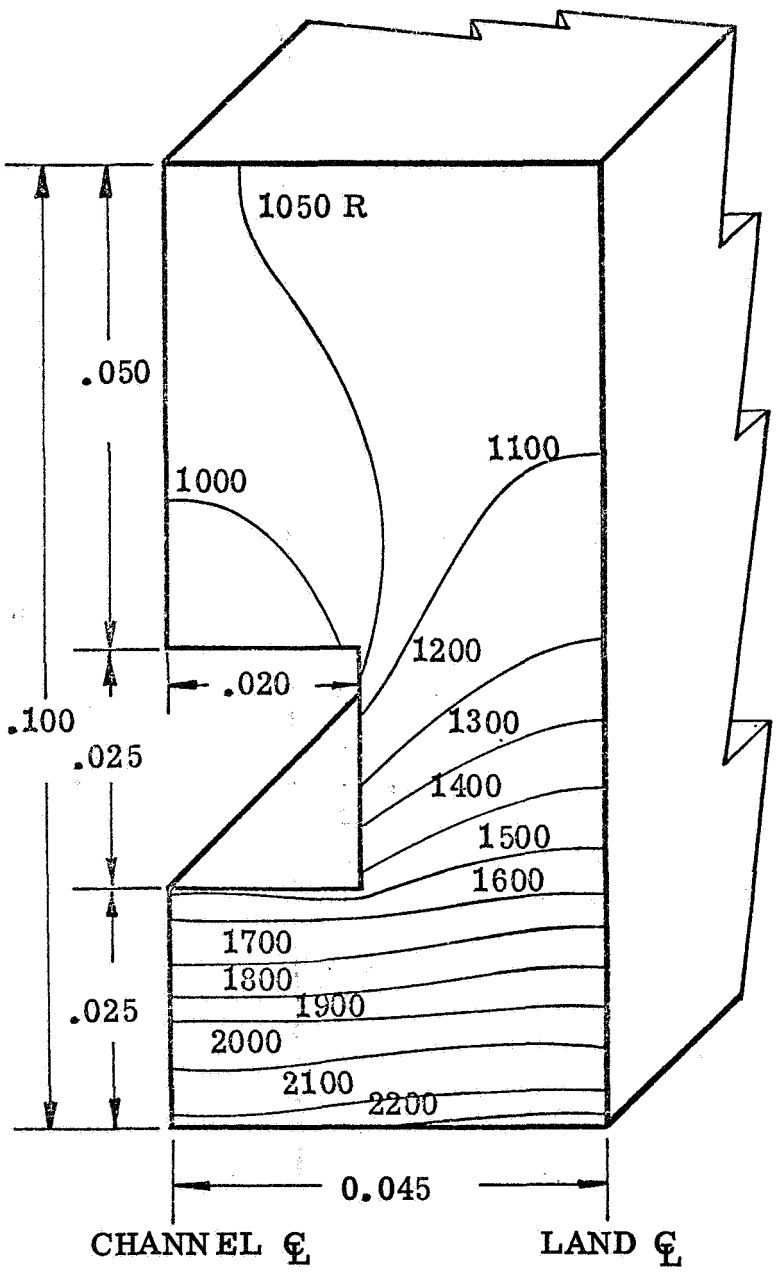

NICKEL 200
FLOX/METHANE
MR = 5.7
T_{AW} = 7723 R
h_g = .00366 BTU/IN^2-SEC R
T_c = 610 R
h_c = .0234 BTU/IN^2-SEC R

P_c = 1000 PSIA
WITHOUT CARBON LAYER

Figure 36. Channel Isotherm Profiles in Throat Region

extreme case considered in terms of heat load. The surface temperature is seen to be slightly higher than 1700F (2160R) at the midland point. The use of Hastelloy X would result in a greater difference between midchannel and midland temperatures due to lower thermal conductivity.

The basic one-dimensional conduction approach appears sufficiently accurate for use in this study. In general, the nickel and steel combustion-side wall temperatures were held at 1600F throughout the chamber to ensure greater cycle life. Only at the throat was the temperature allowed to approach 1700F. Hastelloy X was designed to 2100F throughout. In certain instances the coolant-side wall temperature constraints (nucleate boiling or coking) dictated the combustion-side wall temperatures. In the case of nucleate boiling, the coolant-side wall temperature is only slightly higher than the saturation temperature of the coolant and is in the order of 100-200F. Under these conditions, the combustion-side wall temperatures operate considerably below their maximum allowable values (unless extremely thick walls are utilized).

Thrust Chamber Wall Materials

Three basic materials were selected for evaluation with the light hydrocarbons of interest. These consisted of two conventional materials such as steel and nickel operating at a nominal maximum temperature of 1700F and a more advanced material such as Hastelloy X operating at 2100F. It is possible to make a comparative evaluation of these materials preliminary to the detailed analysis. In order to minimize coolant pressure drop, it is necessary to minimize the coolant mass flux requirements. This can be accomplished by increasing the temperature differential

between the wall (coolant side) and the coolant (forced convection analysis). Since the coolant bulk temperature is essentially fixed at a given station by thrust and chamber pressure levels, it is necessary to raise the coolant-side wall temperature. Conversely, it may be stated that the material which results in the highest allowable coolant-side wall temperature is superior insofar as reducing the jacket pressure losses. That such a material is not necessarily the one with the highest allowable combustion-side wall temperature will be shown directly.

Using the minimum specified wall thickness of 0.025 inches, the steel, nickel, and Hastelloy X were compared in terms of their heat conduction capability. For a fixed combustion-side wall temperature, the coolant-side wall temperature decreases as the heat flux level increases. The slope of this curve is dependent upon the conductivity of the material. This is shown graphically in Fig. 37. It is apparent that the steel is less desirable than the nickel at any heat flux level (i.e., T_{wc} for nickel always higher than for steel). The Hastelloy X appears superior to nickel at heat flux levels of less than 10 Btu/in^2-sec ($P_c \lesssim$ 500 psia for no-carbon layer case).

It can be inferred from Fig. 37 that, at high chamber pressures (high heat flux levels) and low thrust levels (high coolant bulk temperature), the nickel (200) will be superior to the Hastelloy X and steel materials. At lower heat flux levels (low chamber pressure and/or carbon layer) the Hastelloy X appears to be the best choice insofar as heat transfer is concerned. In actuality it will be shown that for low heat flux conditions, the basic material effects on pressure drop are not of enough significance to warrant material selection on this basis.

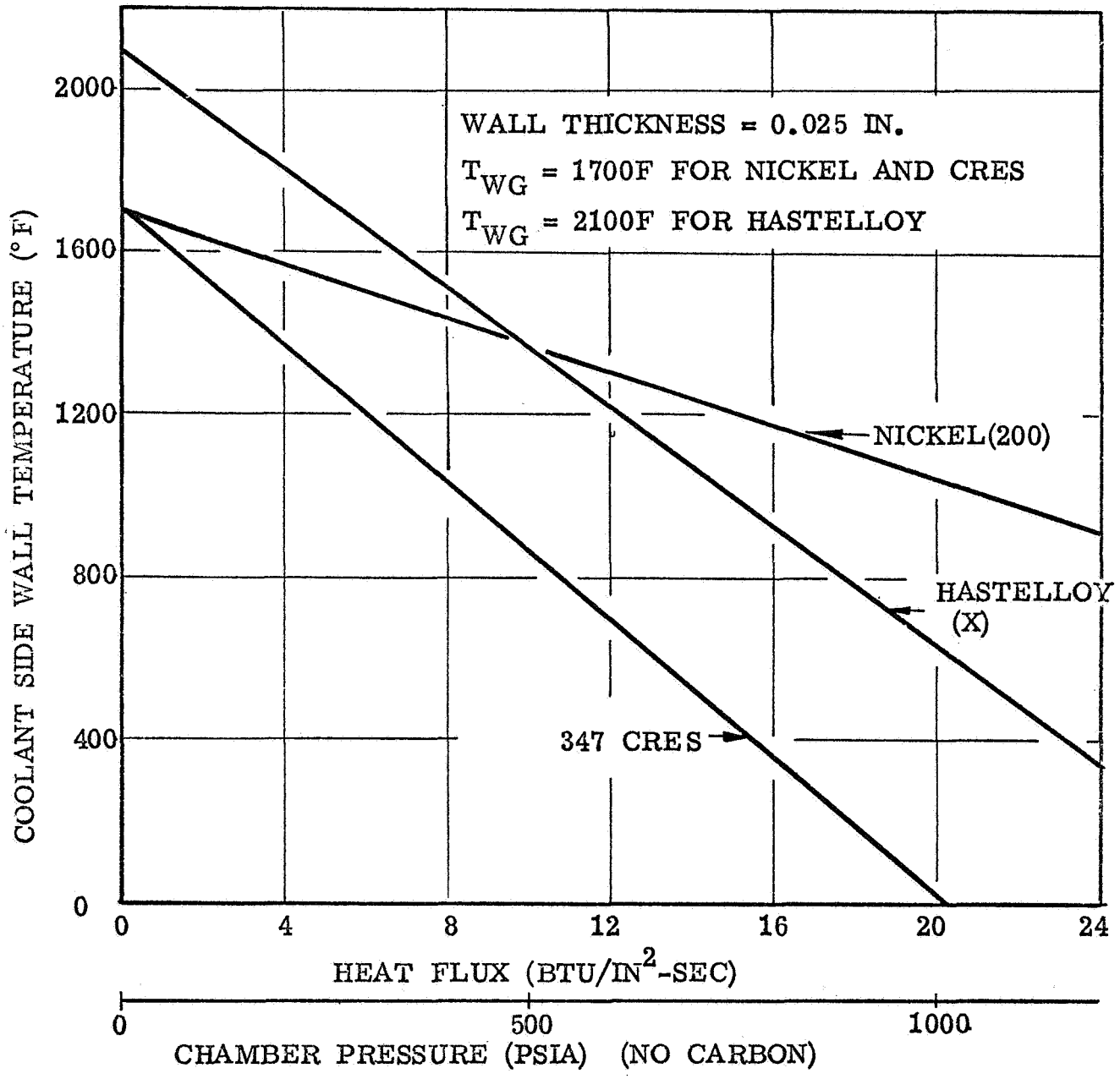

Figure 37. Effect of Material and Heat Flux on Throat Coolant - Side Wall Temperature

Thrust Chamber Wall Coatings

The use of artifically applied coatings (in the case of no carbon layer) were considered in the study. A nominal maximum operating temperature of 3200F was specified for a coating. Insofar as a thrust chamber cooling design (pressure drop and channel sizes) is concerned, only the temperature is of importance. This is used to determine the reduced heat flux profile which in turn is used in the basic design.

Practical considerations concerning the use of coatings, however, require further discussion particularly in regards to thickness requirements. The temperature differential as a function of heat flux for various coatings of 0.010 inch thickness is shown in Fig. 38. Assuming a coating temperature of 3200F with a nickel substrate operating at 1700F requires a temperature drop of 1500F across the coating. From Fig. 38, it is seen that a 0.010-inch-thick tungsten-zirconia oxide composite coating would be adequate at the throat for a chamber pressure of 1000 psia ($Q/A = 15$ Btu/in^2-sec). At higher area ratios (i.e., lower heat flux levels), the coating temperature differential will decrease markedly.

It is apparent therefore that, if maximum use of a coating is to be made, the coating thickness must be varied markedly. This variation is shown in Fig. 39 where the coating thickness required to maintain a fixed temperature differential is shown as a function of heat flux. In the nozzle portion of the chamber where heat flux levels are less than 1 Btu/in^2-sec, coating thicknesses of several tenths of an inch are required. The weight of such a coating would be prohibitive. Practically speaking, therefore, the use of coatings should be limited to the throat, combustion zone, and low area ratio ($\epsilon \lesssim 4$) portions of the nozzle.

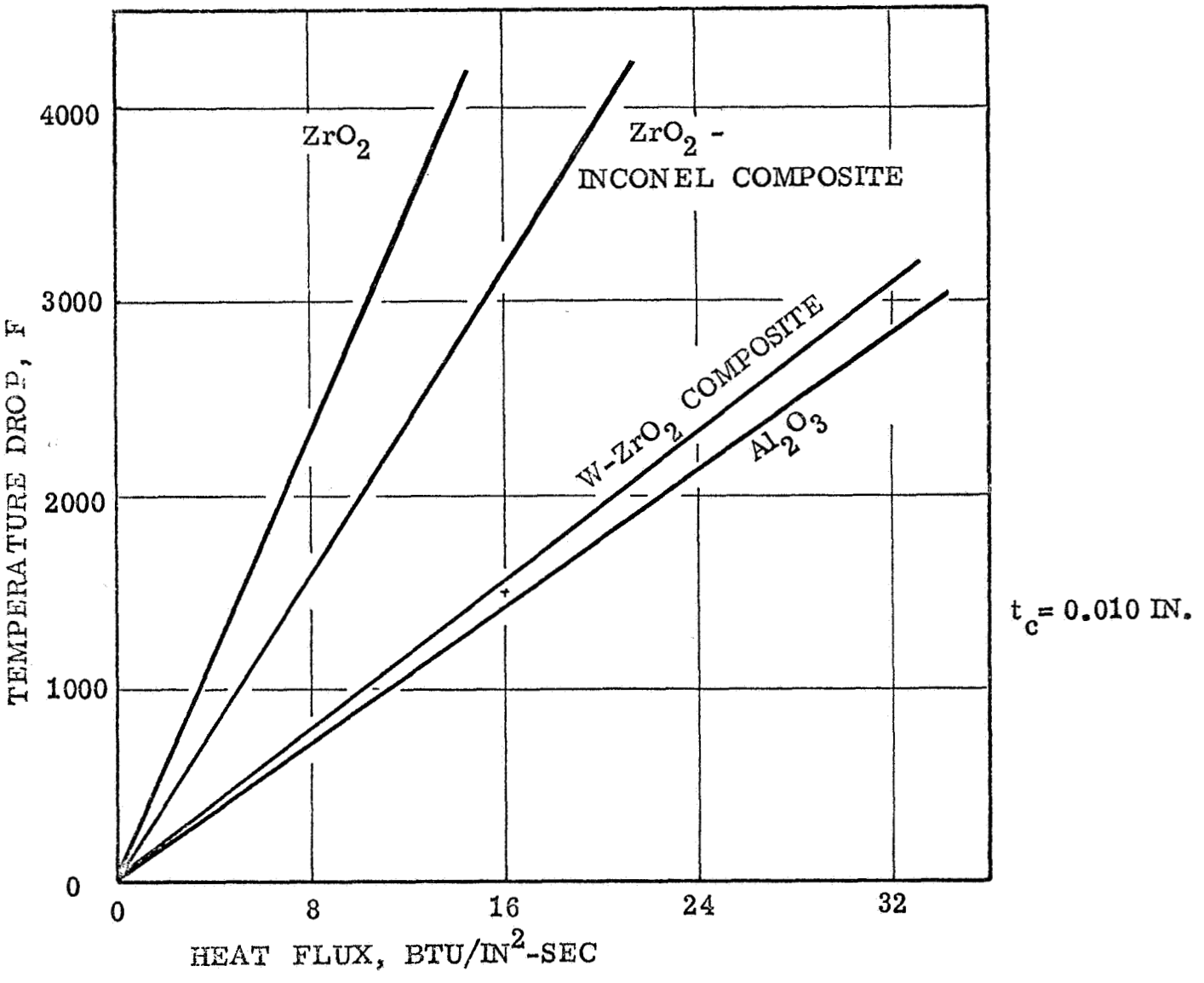

Figure 38. Coating Temperature Drop vs Heat Flux

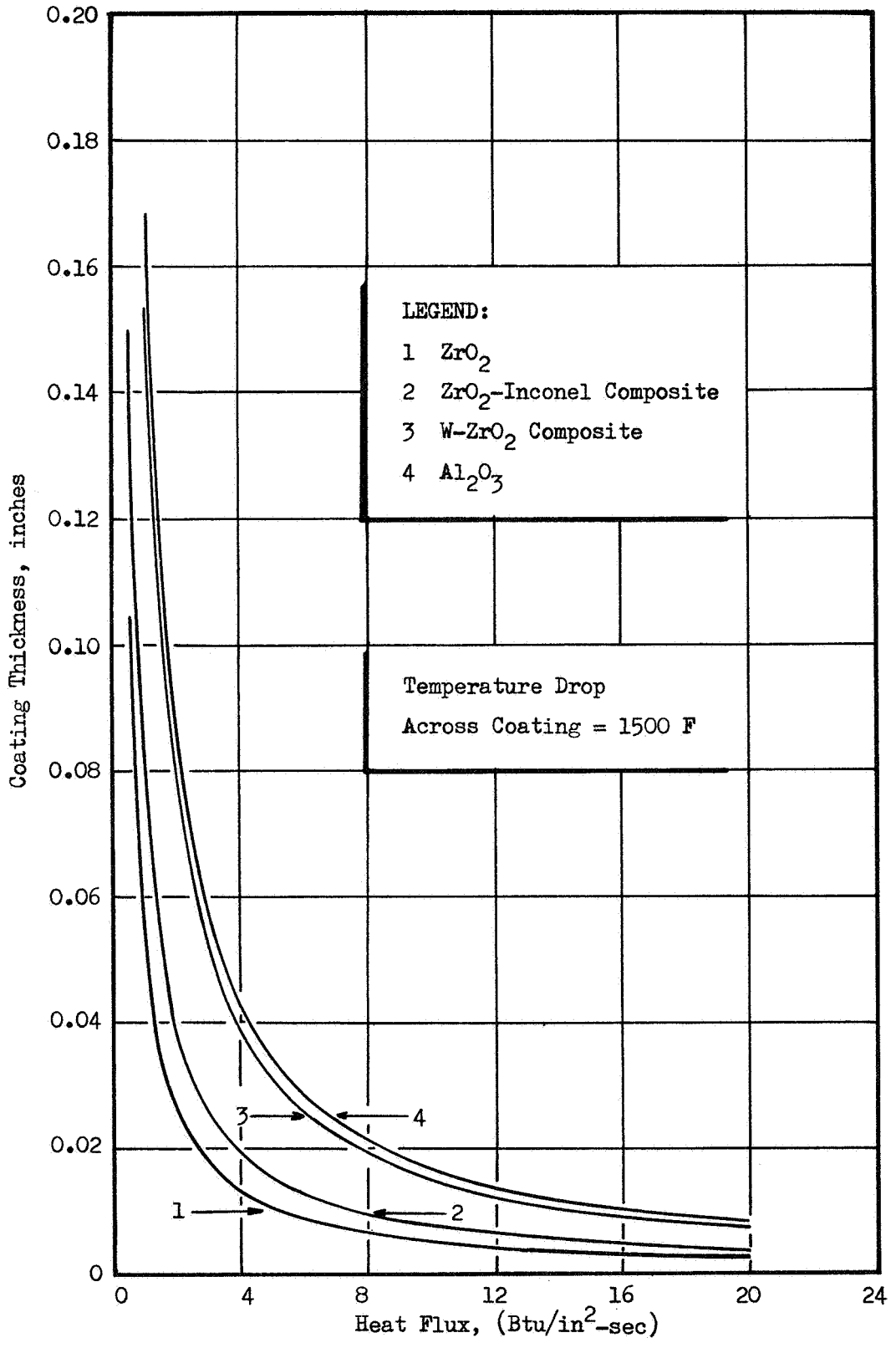

Figure 39. Coating Thickness Requirements as a Function of Heat Flux Level

FLOX/METHANE ANALYSIS RESULTS

Regenerative cooling designs for FLOX/methane thrust chambers were generated using the techniques discussed in Appendix E. Single uppass (counterflow) cooling circuits were used throughout. This pass arrangement was selected so that low-temperature methane (which has poor cooling capability) was utilized in the low-heat-flux region of the nozzle. The use of a downpass (parallel flow) circuit would have resulted in excessively small channel sizes in the combustion zone. The uppass circuit is particularly important for the subcritical pressure conditions since the coolant must be completely vaporized before reaching the higher heat flux (throat) region. Film boiling of the methane, therefore, occurred in the low-heat-flux ($Q/A < 1$ Btu/in^2-sec) region of the nozzle where it can be tolerated without excessive wall temperatures.

Pressure Drops for Nickel Walls

Nickel channel designs assuming a carbon layer were investigated initially. The carbon layer effectiveness was taken as 0.7 as discussed previously in the Parametric Analysis section. This is to say that the carbon layer is such that the heat load is 0.7 times the no-carbon-layer condition. The resulting pressure drops are summarized in Fig. 40 for the three thrust levels of interest. The pressure drops are seen to range from about 150 to 200 psi at a 1000 psia chamber pressure. This is well within the feasibility limits established previously. It is interesting to note that the 20,000-pound thrust design requires the highest pressure drop. Two effects contribute to this result. At the high thrust level, the lower bulk temperature at the throat results in a slightly higher mass flux requirement. The engine size is also reflected in the slightly higher pressure drop.

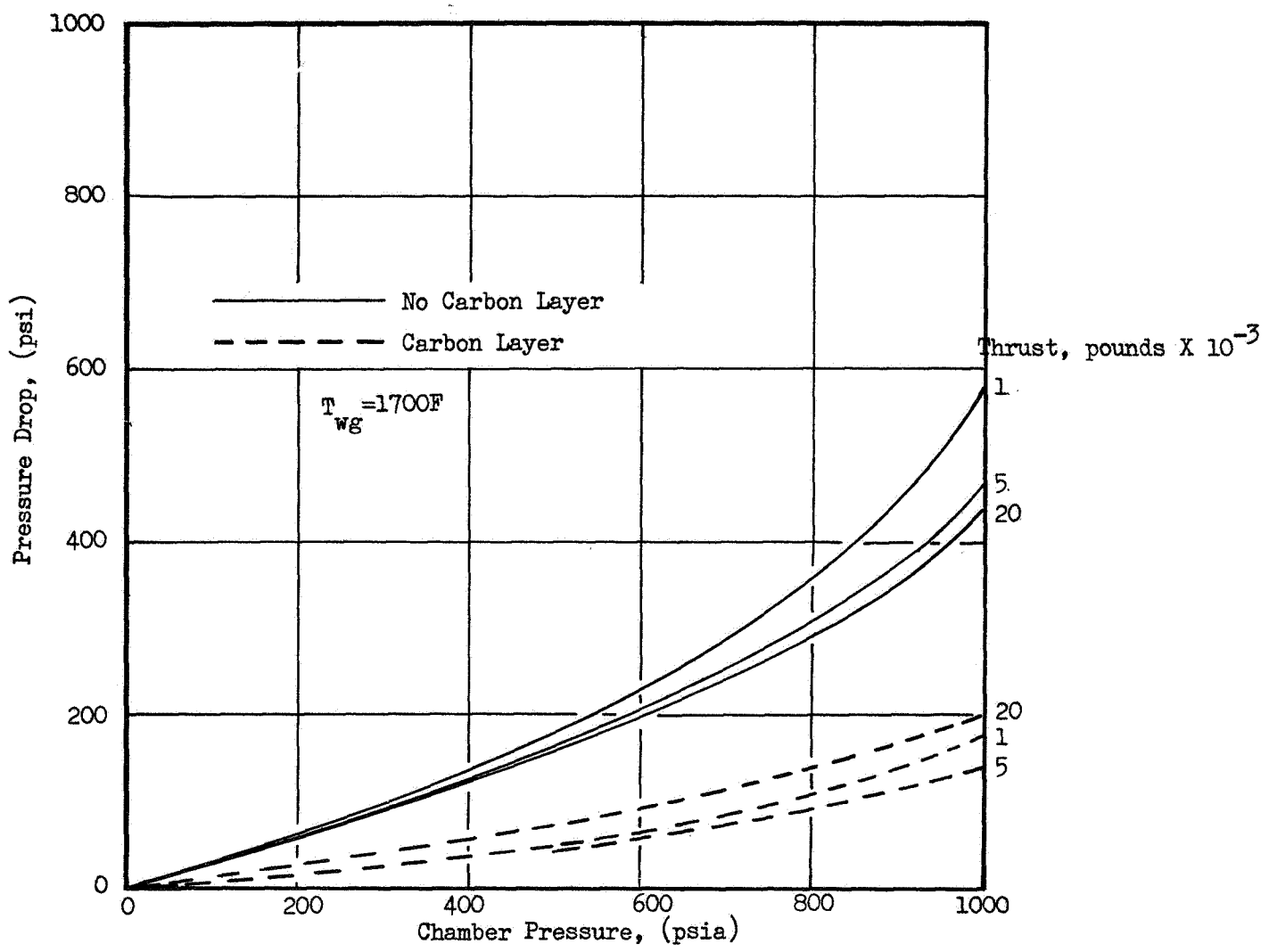

Figure 40. Methane Cooling Jacket Pressure Drop with Nickel Walls

ROCKETDYNE

Previous experience has indicated that high-pressure, high-performance engine designs result in decreasing carbon layer effectiveness (Ref. 7 and 10). For this reason, the propellant combinations of interest were also investigated without the assumption of a gas-side carbon layer. The resulting pressure drops for a nickel-wall chamber are also shown in Fig. 40 for direct comparison with the carbon layer designs. At a chamber pressure of 1000 psia, the resulting pressure drops range from about 440 psi at a thrust of 20000 pounds to a drop of almost 600 psi at the 1000-pound thrust level.

The cause of the large increase in system pressure drop as the carbon layer assumption is removed is three-fold. Primarily, of course, the local heat flux is increased. Also of importance, however, are the facts that the coolant bulk temperature is increased and the coolant-side wall temperature is forced lower. The result of these three effects is that an increased heat flux must be accommodated at a decreased driving potential ($T_{wc} - T_B$), necessitating sharply increased coolant mass flux (i.e., high pressure drop). The lower thrust cases are most drastically affected by increased heat flux levels because of the higher coolant bulk temperatures involved.

As a point of interest, an investigation was conducted to determine the effect on pressure drop of decreasing the maximum allowable wall temperature. A lower wall temperature permits greater cycle life and reliability. The maximum allowable temperature of the nickel was reduced to 1500F. The results are presented in Fig. 41 for the case with a carbon layer. It is seen that the effect on the pressure drop of the design for 1000 pounds thrust is quite significantly increased at P_c = 1000 psia from approximately 175 to 360 psi drop as the wall temperature is decreased. However, even this value represents a reasonable pressure drop. The greater sensitivity of the low-thrust design is caused by the higher coolant bulk temperature.

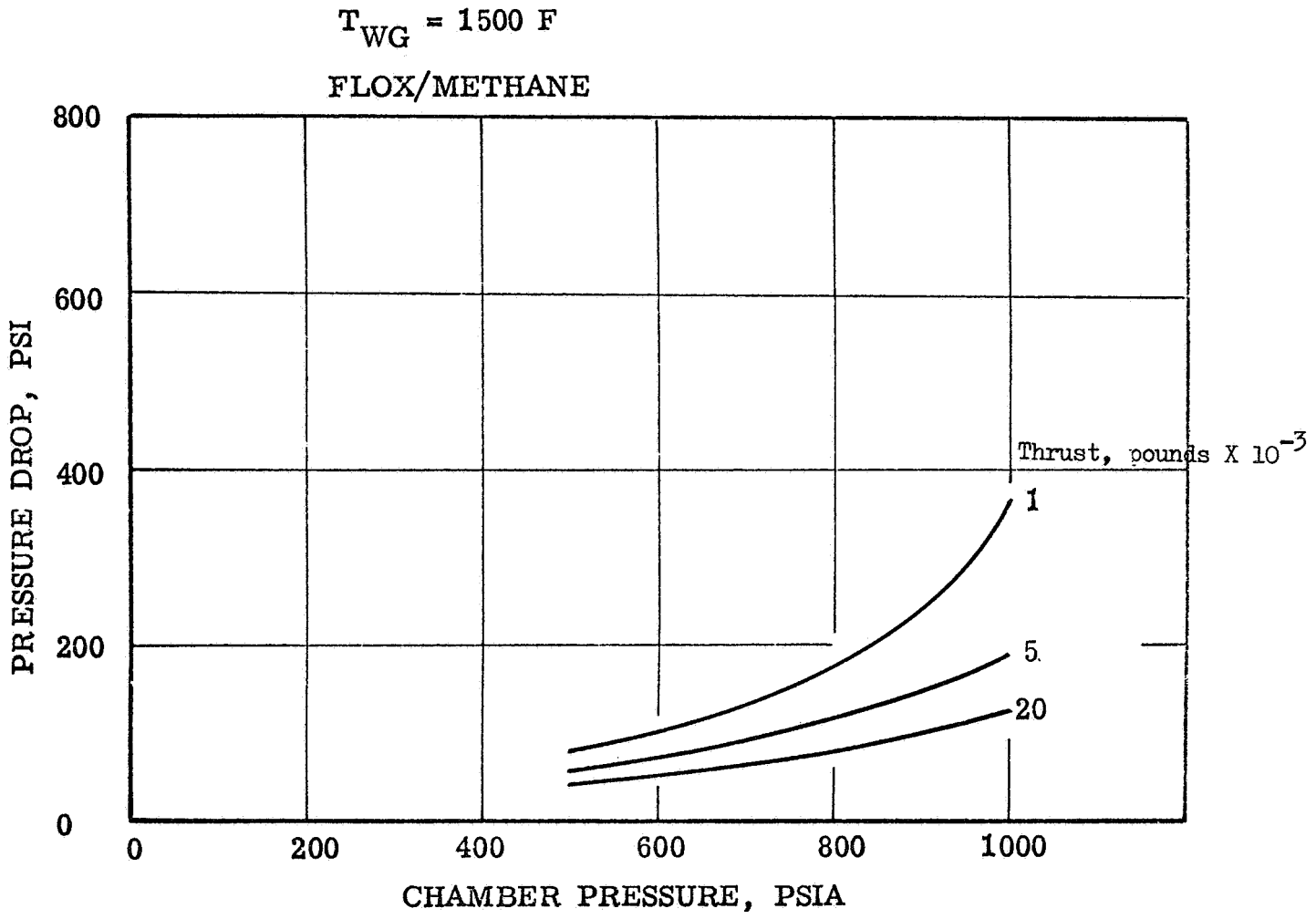

Figure 41. Coolant Jacket Pressure Drop - Nickel Walls with Carbon Layer

Wall Material and Coating Effects

A comparison of nickel (200) and 347 stainless steel was made to ascertain the relative difference in coolant pressure drop. As pointed out previously, the steel was expected to result in higher pressure drops than either the nickel or Hastelloy based upon thermal conductivity considerations. These conclusions were confirmed in the detailed design evaluation as shown in Fig. 42. The selected chamber pressure of 500 psia combined with the carbon layer result in an easily cooled chamber with either nickel or steel. It is noted, however, that the steel design results in approximately double the pressure drop ($\Delta P = 100$ psi) of the nickel design. This difference becomes even more marked at higher heat flux levels. Indeed, at a chamber pressure of 1000 psia without a carbon layer, the heat flux level is such as to approach the conduction limit of the steel. Such a condition implies infinite coolant velocity and pressure drop since the coolant-side wall temperature and bulk temperature are essentially equal (i.e, the driving potential $(T_{wc} - T_B)$ decreases to zero).

Chamber designs utilizing Hastelloy X channel construction were also studied. The resulting pressure drops for the carbon and no-carbon cases are shown in Fig. 43. The Hastelloy X designs with a carbon layer have a somewhat lower pressure drop than the nickel designs because the higher allowable wall temperatures. Even without a carbon layer, the Hastelloy X appears superior at chamber pressures below 500-700 psia. At higher chamber pressures, the relatively poor thermal conductivity of the Hastelloy results in coolant-side wall temperatures lower than nickel. The result is sharply increased pressure drops particularly for low-thrust design conditions. At the 1000 pound thrust level, for example, a coolant pressure drop of approximately 1400 psi was found necessary for adequate cooling. In these particular cases, the use of a thinner (than 0.025 inch) Hastelloy X wall would prove of great benefit in reducing the required pressure drop.

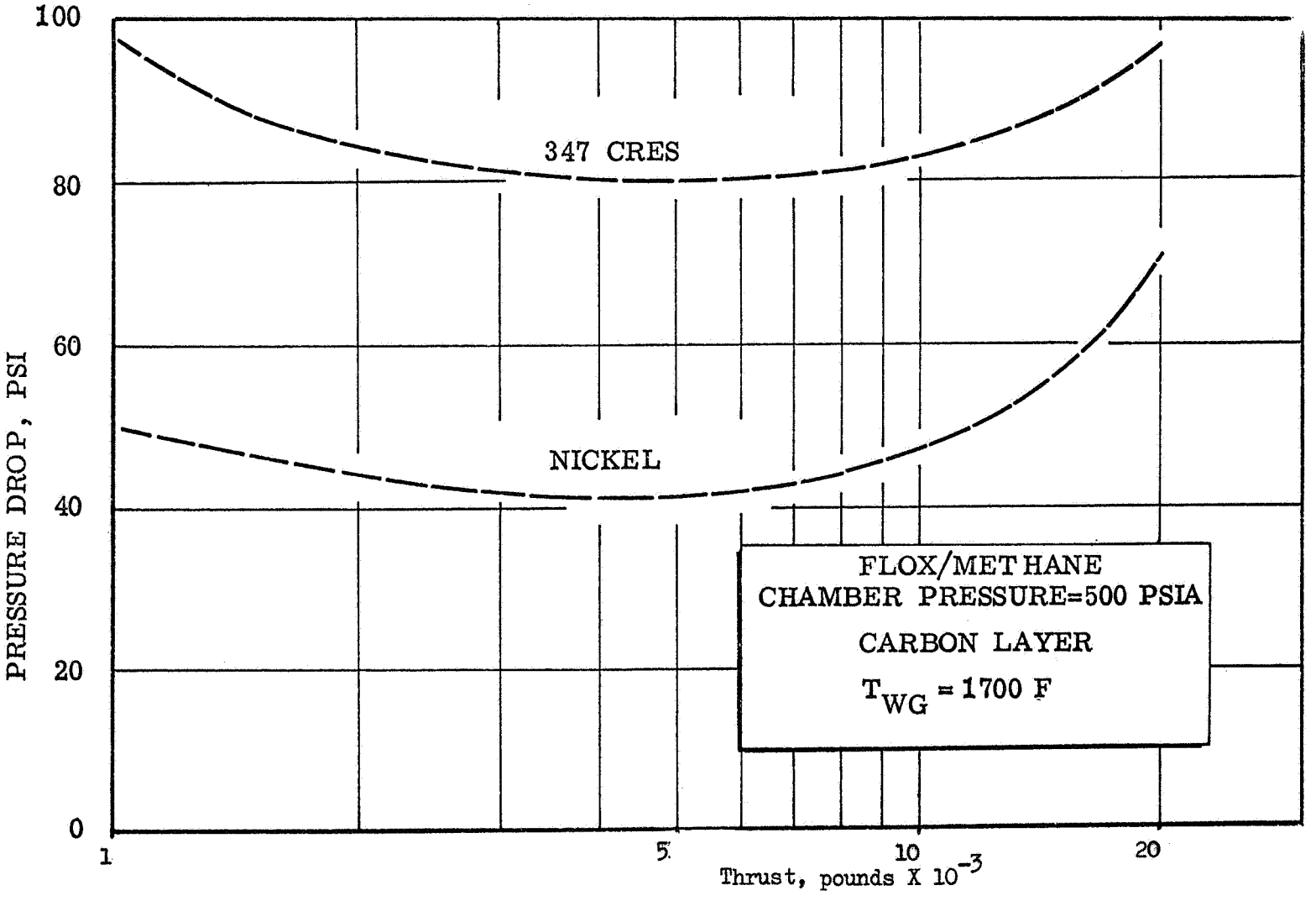

Figure 42 . Comparison of Nickel and Steel Chambers

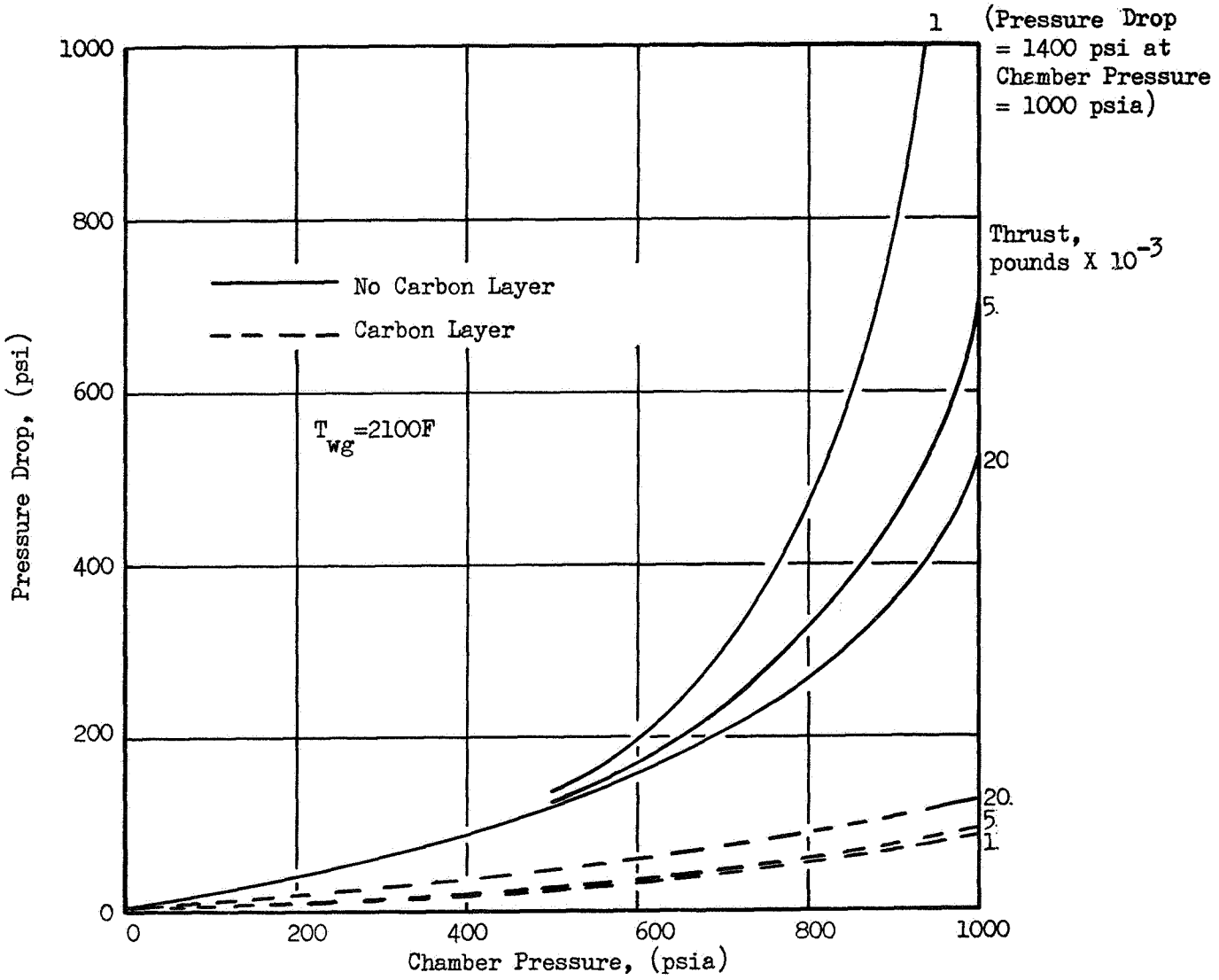

Figure 43. Methane Cooling Jacket Pressure Drop with Hastelloy X Walls

ROCKETDYNE

The use of a coating operating at 3200F was briefly investigated. Such a coating was found to reduce the heat input by 30 percent which is essentially the same effectiveness as the carbon coating for FLOX/methane. The results of the coated chamber designs are therefore exactly the same as the carbon layer results noted previously.

Coolant Temperature and Channel Dimensions

The methane bulk temperature at the coolant jacket exit is shown for the three thrust levels with and without a carbon layer in Fig. 44. The bulk temperature is 1270F and 840F for the no-carbon and carbon cases respectively at 1000 psia chamber pressure. At these high temperatures, particular design attention must be given to injector face cooling. At higher thrust levels, the exit bulk temperatures are considerably lower, e.g., the exit temperature for F = 5000 pounds, P_c = 500 psia is 620F without a carbon layer and 350F with a carbon layer. Different modes of heat transfer to the coolant occur under subcritical and supercritical operating conditions. Therefore, the correlations (described in Appendix E) used for chamber pressures of 250 psia and lower were different from those used for chamber pressures of 500 psia and higher. No analyses were conducted for pressures between these two values. In several cases the data trends in the high- and low-pressure regions did not allow confident interpolation through the 250 to 500 psia region. Operation with methane in this intermediate pressure region appears to be practical.

An area of primary importance in determining a feasible design is the minimum channel size requirements. The minimum channel dimensions for the 1000-pound-thrust FLOX/methane designs are shown in Fig. 45 for the carbon and no-carbon assumptions. The minimum allowable width was taken as 0.040 inches so that minimum dimensions below that value in Fig. 45 refer to

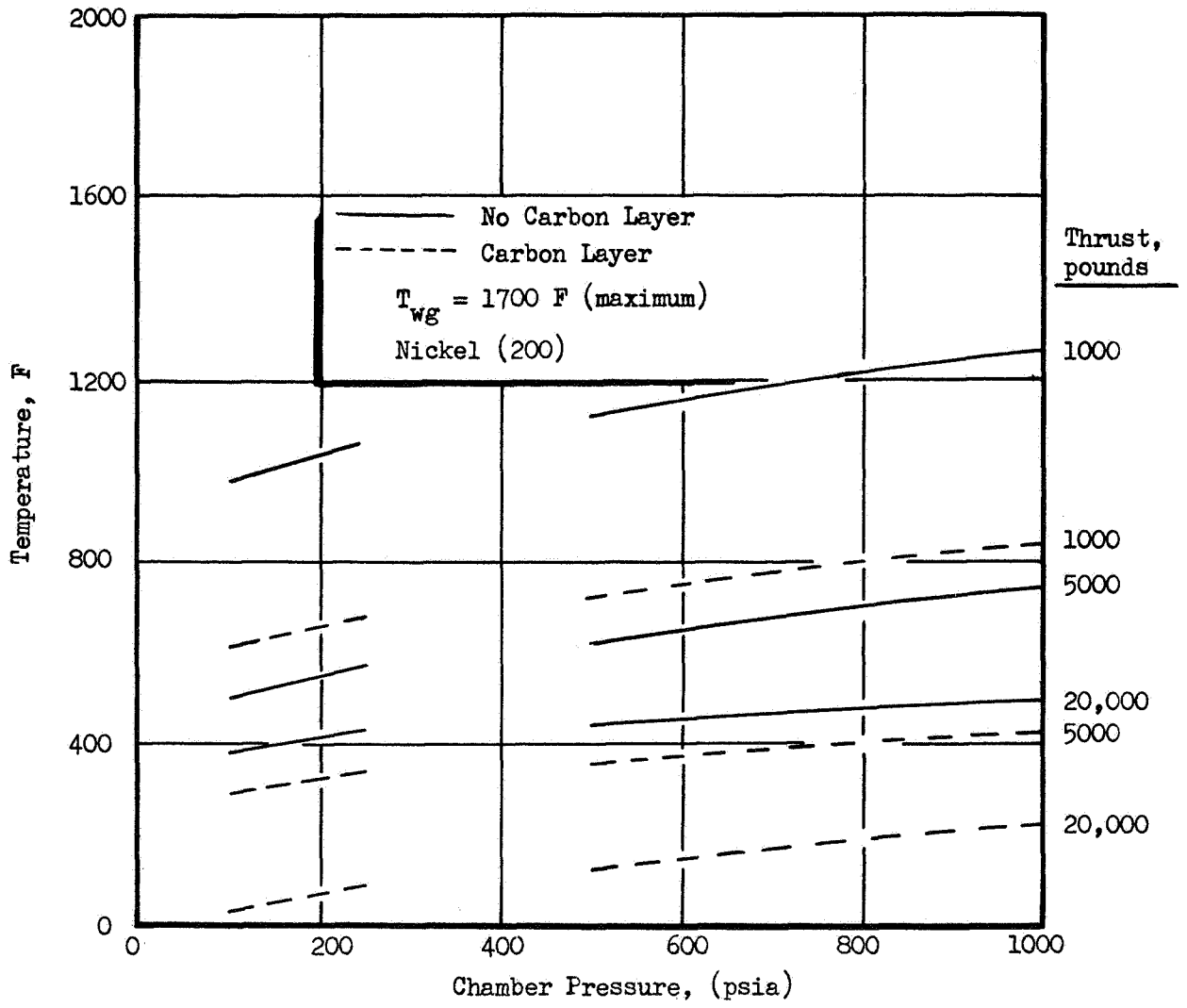

Figure 44. Coolant Exit Bulk Temperature for FLOX/Methane Thrust Chambers

W = H for H $\geq$ 0.040 inches

W = 0.040 inches for H $<$ 0.040 inches

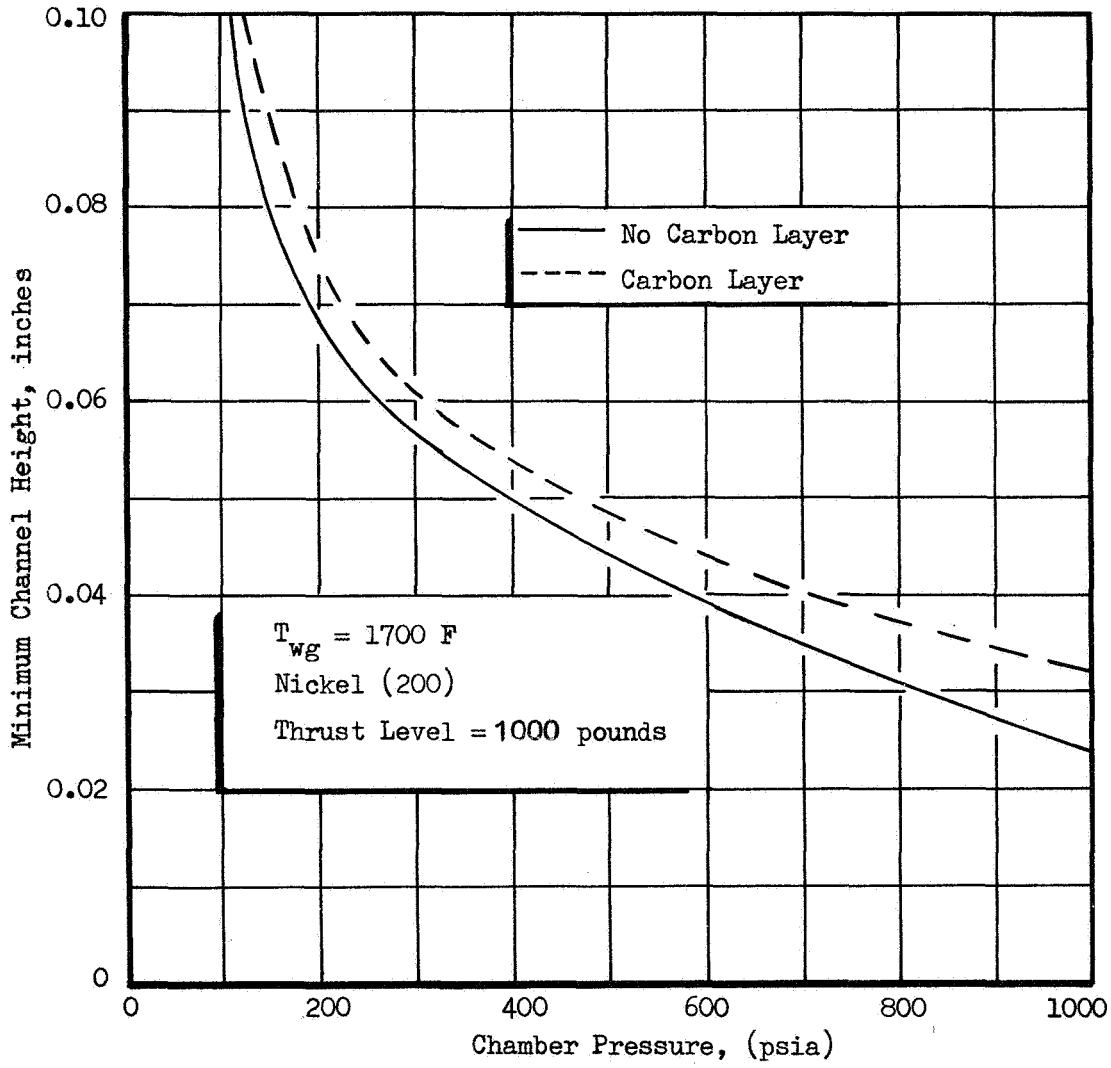

Figure 45. Minimum Channel Dimensions for the FLOX/Methane Regenerative-Cooled Thrust Chambers

channel height. A dimension greater than 0.040 inch in the figure implies a square channel of the stated dimension. The 1000-pound-thrust design at a chamber pressure of 1000 psia without a carbon layer is seen to result in a minimum channel size of 0.040-inch wide by 0.024 inch high. (A two-dimensional thermal analysis of the channel section is given in Fig. 36.). This channel dimension is essentially the feasible minimum value as discussed previously. This particular point represents the most extreme case considered. Increasing the thrust level, decreasing chamber pressure or presence of a carbon layer result in increased channel sizes. This minimum dimension exists only at the throat and increases in the combustion zone and nozzle sections. Furthermore, because of the low thrust and high chamber pressure, the resulting small throat size requires relatively few (29) of these critical coolant passages.

OF_2/PROPANE ANALYSIS RESULTS

The detailed regenerative cooling designs for OF_2/propane were accomplished using the techniques discussed in Appendix E. In general, the propane designs parallel the methane designs discussed previously. A single uppass (counterflow) circuit was used wherever possible because of the basic manifolding simplicity. In certain instances, however, downpass (parallel flow) circuits were required to achieve reasonable pressure drop and channel size.

Pressure Drops for Nickel Walls

The resulting pressure drops for the OF_2/propane chambers utilizing nickel channel construction are presented in Fig. 46 for the 5000- and 20,000-pound-thrust levels of interest. For the supercritical cases ($P_c \geq 500$ psia), single-uppass (counterflow) cooling circuits were utilized. The assumption of a carbon layer or even an applied coating without a carbon layer results

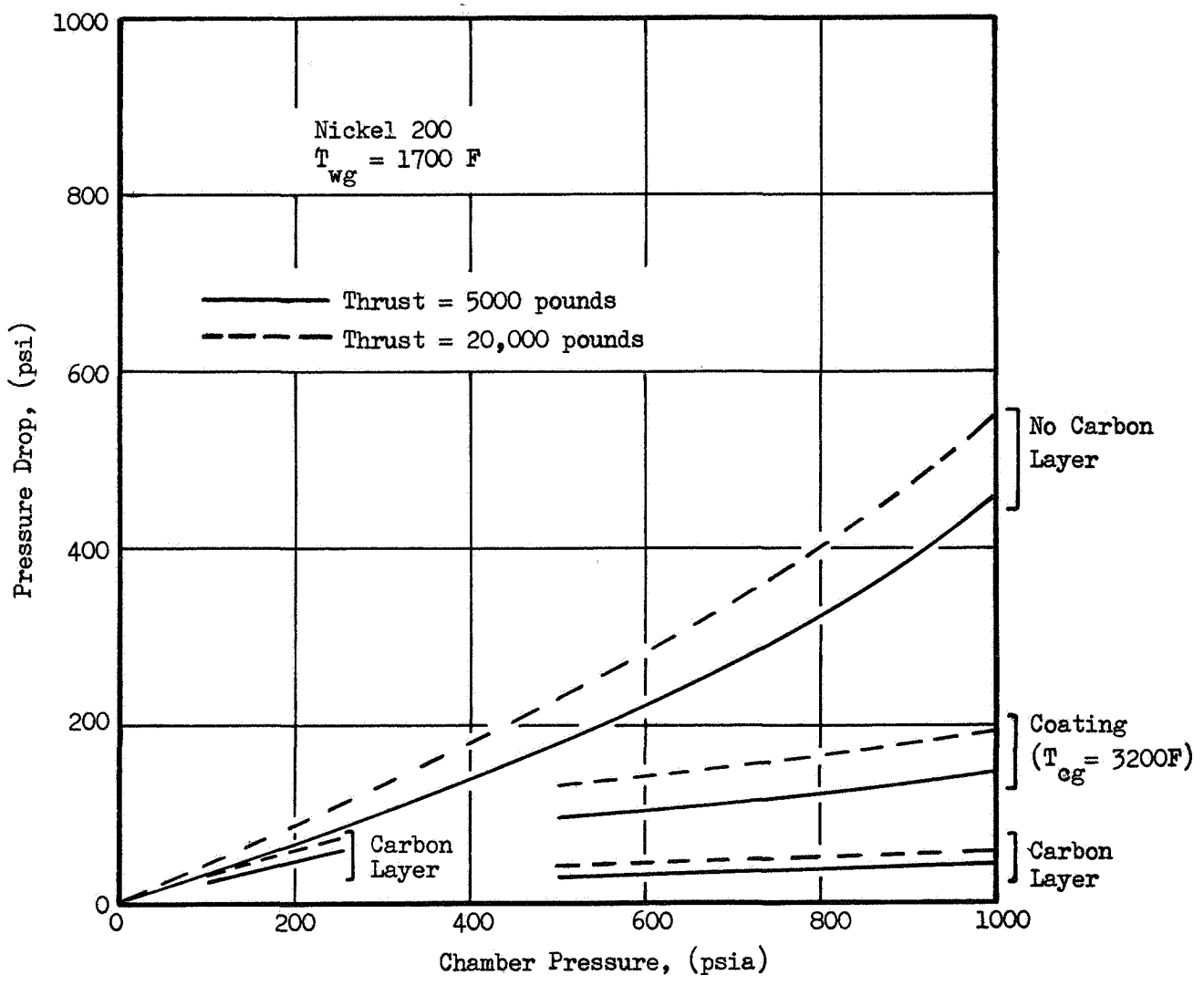

Figure 46. Coolant Jacket Pressure Drops for OF_2/Propane with Nickel Walls

in moderate pressure drops of less than 200 psi at 1000 psia chamber pressure. The no-carbon-layer cases still appear feasible although the pressure drops are near the imposed constraint of 500 psi.

The subcritical cases (P_c < 500 psia) were somewhat more complex to analyze. For the case of no gas-side carbon layer, it was found possible to completely vaporize the propane in the nozzle. This result differs from the result obtained previously in the Parametric Analysis which had indicated that complete vaporization in the nozzle was not possible. This difference arose from the fact that in the nucleate boiling regime the coolant-side wall temperature is nearly equal to the liquid saturation temperature. The resulting combustion-side wall temperatures in the nozzle are, therefore, approximately 200-300F rather than the 1700F assumed in the Parametric Analysis. This lower wall temperature results in approximately a 15- to 20-percent increase in the nozzle heat input which is sufficient for complete vaporization. This complete vaporization of the propane in the nozzle allows the use of an uppass circuit with moderate pressure drops.

In the case of a carbon layer with an effective heat flux reduction of 0.57, it was determined that the 100-psia chamber design could utilize either an uppass or downpass circuit without bulk boiling. The uppass circuit pressure drops were acceptable so that the downpass designs were not pursued further. It is expected that the downpass circuit would result in somewhat lower pressure losses.

A carbon layer assumption for the 250-psia chambers does not allow for complete coolant vaporization in the nozzle so that nucleate boiling occurs in the throat. The propane subcooling at the throat was so low that coolant velocities in excess of 300 ft/sec were required. A downpass circuit, however, allows greater subcooling at the throat because of lower heat input, and coolant velocities of approximately 100 to 130 ft/sec were sufficient for this configuration. Downpass (parallel flow) coolant circuits were, therefore, analyzed at the 250-psia chamber pressure level.

Effects of Wall Coatings and Materials

The use of a coating does not appear necessary at the lower chamber pressures because of the relatively low pressure drops involved. The low heat flux conditions at reduced chamber pressures would require excessively thick coatings to be of benefit. It is believed that the benefits to be obtained do not warrant the excessive weight and increased fabrication effort involved. A coating operating at a gas-side temperature of 3200F would appreciably lower the pressure drops for chamber pressures above 500 psia.

Chamber designs were developed for the Hastelloy X material at supercritical pressures ($P_c \geq 500$ psia). Pressure drop characteristics are shown in Fig. 47. In general, the Hastelloy X appears somewhat superior to the nickel (200) for all cases except the no-carbon-layer cases at high chamber pressures ($P_c \approx 1000$ psia). Even at these extremes there is not a great difference between pressure drops for the two materials. It is interesting to note that for the Hastelloy cases with a carbon layer, the propane coolant-side wall temperature constraint of 1500F is encountered. This is apparent in the typical wall temperature profiles shown in Fig. 48. In essence, full use of the high-temperature capabilities of Hastelloy is not possible in these instances unless the walls are thickened. A weight penalty is, of course, incurred.

Previous results with methane indicated that at low pressures the material selection is not significant. The use of Hastelloy X at subcritical pressures would, therefore, give the same results as the nickel noted in Fig. 46.

Coolant Temperature and Channel Dimensions

The propane exit temperatures and minimum coolant channel sizes are summarized in Fig. 49 and 50 for the minimum thrust case. Exit temperatures range from

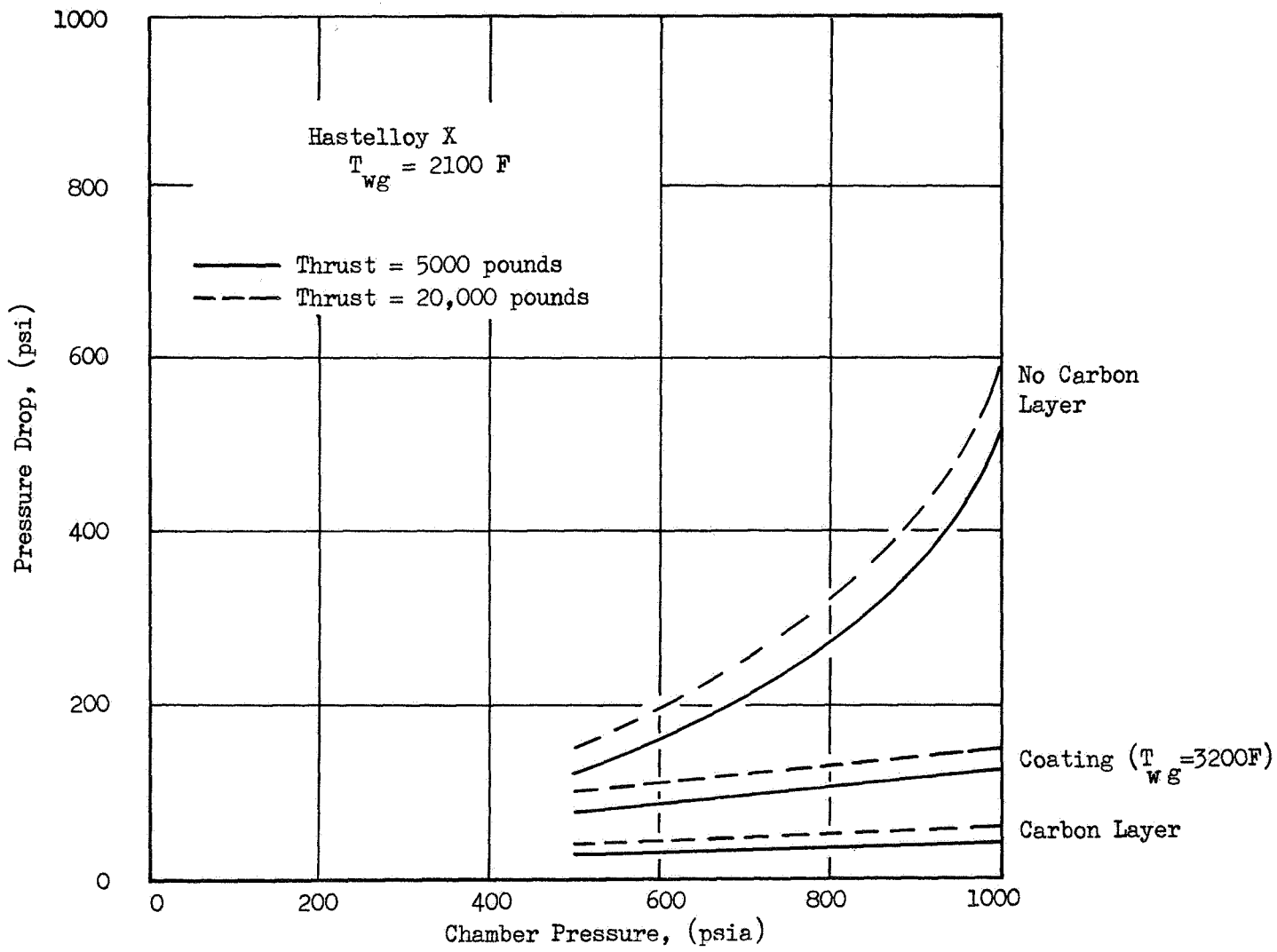

Figure 47. Coolant Jacket Pressure Drops for OF_2/Propane With Hastelloy X Walls.

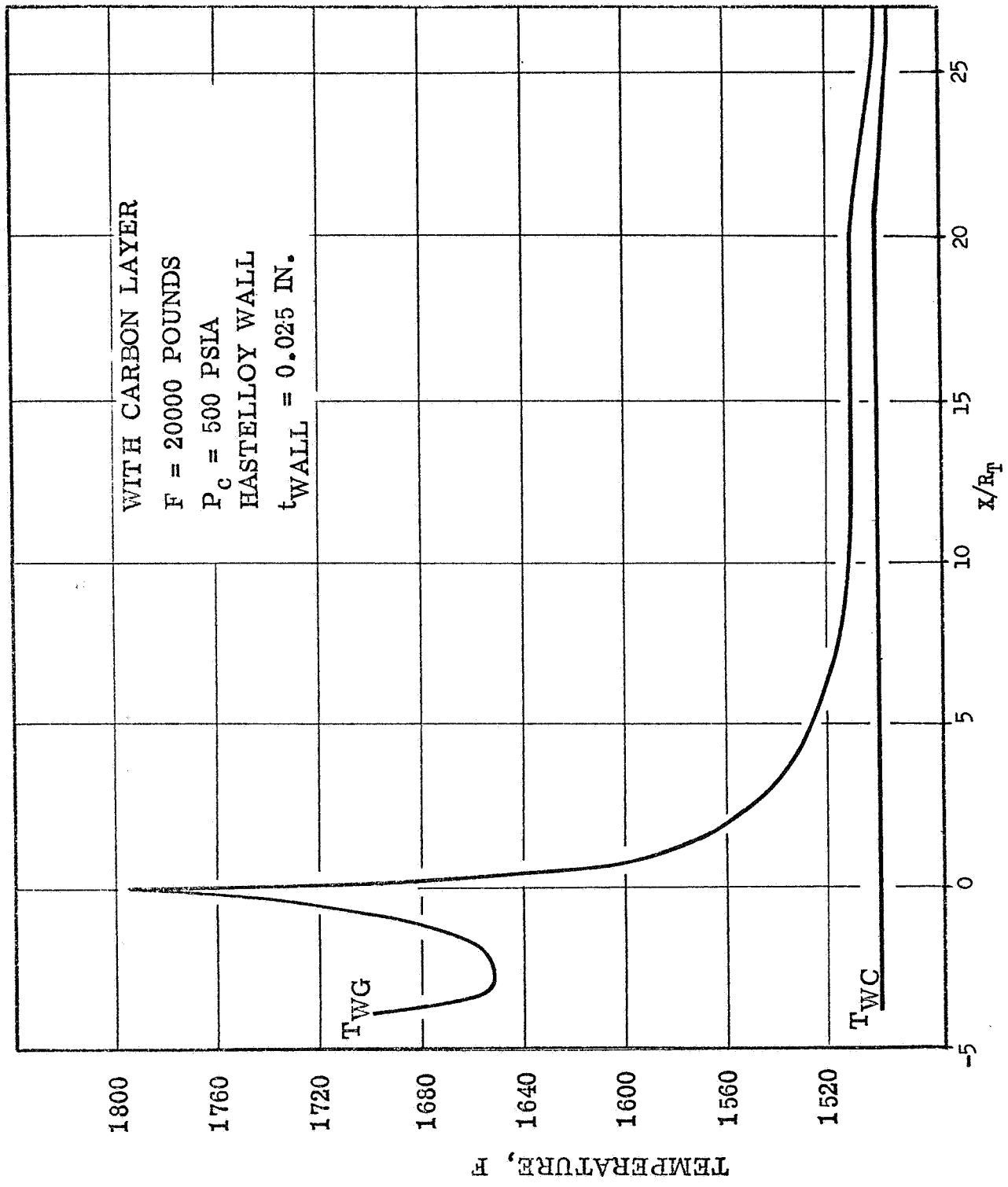

Figure 48. Wall Temperature Profiles for OF_2/Propane

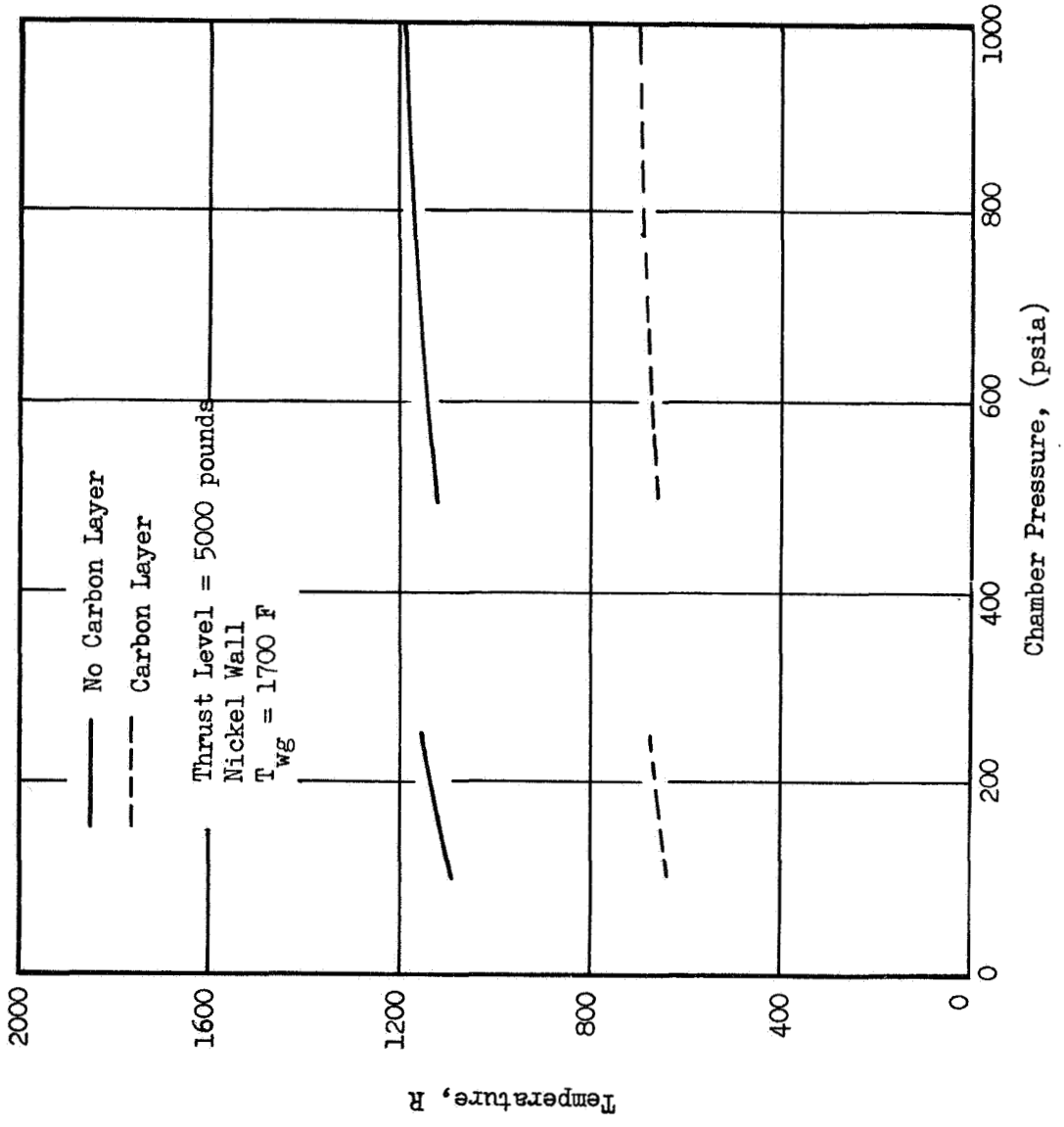

Figure 49. Coolant Exit Bulk Temperatures for OF_2/Propane Chambers

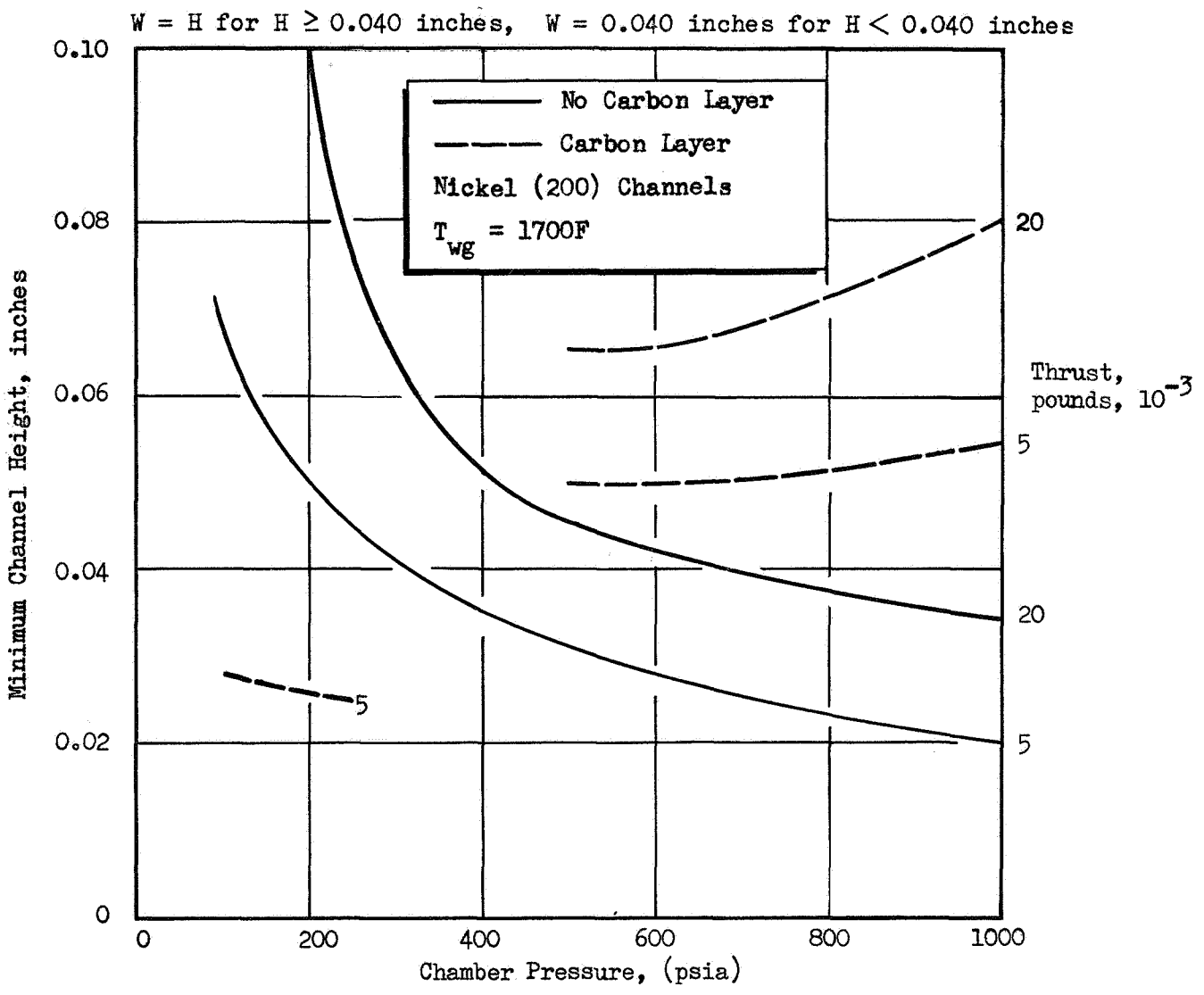

Figure 50. Minimum Channel Dimension for the OF_2/Propane Regenerative Cooled Thrust Chambers

approximately 200F to 700F for carbon and no-carbon assumptions respectively. These values are below the estimated decomposition temperature of propane. The lowest temperature is subcritical and could result in liquid fuel injector design requirements, whereas the higher temperature would result in gaseous fuel injection. Channel sizes are acceptable for nearly all cases. At chamber pressures in excess of 750 psia without a carbon layer, however, the minimum channel dimension falls below the 0.025-inch constraint. Decreasing nozzle area ratio would not significantly increase the channel size. Reduction of the mixture ratio to 74 percent of optimum would increase the channel size to an acceptable level at 1000 psia chamber pressure.

OF_2/1-BUTENE ANALYSIS RESULTS

The OF_2/1-butene propellant combination was analyzed at a thrust level of 1000 pounds to determine regenerative cooling parameters and limits based upon jacket pressure drop, coolant bulk temperature, and minimum channel dimensions. The ground rules were generally the same as those used in the analyses for the methane and propane coolants except that, for the low chamber pressure cases with a gas-side carbon layer, the minimum width of the lands was allowed to increase above the 0.050-inch value used previously. This was done to permit using fewer channels and thus increase the channel dimensions. The larger land width was possible because of the low wall temperatures associated with nucleate boiling. In the following discussion 1000 and 250 psia are referred to as low chamber pressures, and 500 through 1000 psia are referred to as high chamber pressures.

Nickel-200 Wall Material with Carbon Coating

During operation at the low chamber pressures, the coolant is in the subcritical region and, therefore, nucleate boiling is the dominant means of

heat absorption by the coolant. In these analyses, the coolant-side wall temperature was assumed to be 30F above the local saturation temperature of 1-butene. The required coolant velocities at various stations in the the thrust chamber were determined through the use of correlations given by Ref. 4.

During operation at the high chamber pressures the fuel is in the supercritical region and the following equation was used

$$N_{Nu} = 0.023 \quad N_{Re}^{0.8} \quad N_{PR}^{0.4}$$

to determine the mass velocity requirement of the coolant. Differences between experimental and calculated (from the above equation) values of N_{Nu} were reported in Ref. 4. The calculated value was generally conservative and was used for these analyses. A maximum curvature effect of 1.5 was used for enhancement of the liquid-side coefficient in the throat region.

The resulting relationship between pressure drop in the coolant channels and chamber pressure is shown in Fig. 51. Two distinct regions are indicated. The predicted pressure drop is fairly low in the subcritical region but rises very rapidly with chamber pressure because, at 250 psia chamber pressure, the heat input is higher and because the difference between saturation temperature and bulk temperature is less than for the 100-psia chamber pressure case. Therefore, higher coolant velocities are required, as shown in Fig. 52, which lead to pressure drops which are, in fact, higher than the pressure drops for high-chamber-pressure supercritical operation where the forced convection cooling mode predominates. Relationships in the subcritical region are shown as linear which is an approximation because only two chamber pressures (100 and 250 psia) were analyzed.

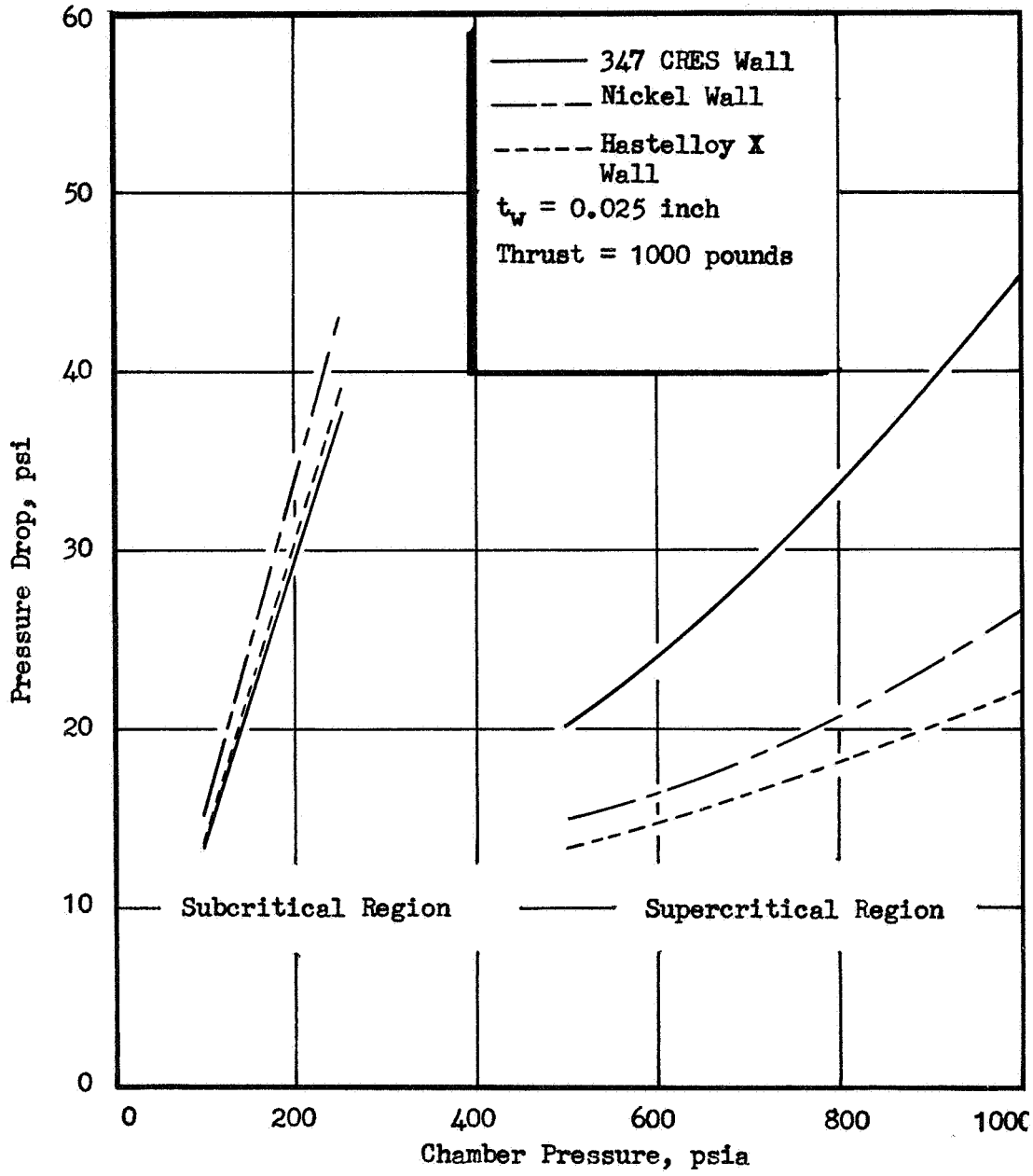

Figure 51.1-Butene Coolant Jacket Pressure Drops with Gas-Side Carbon Layer

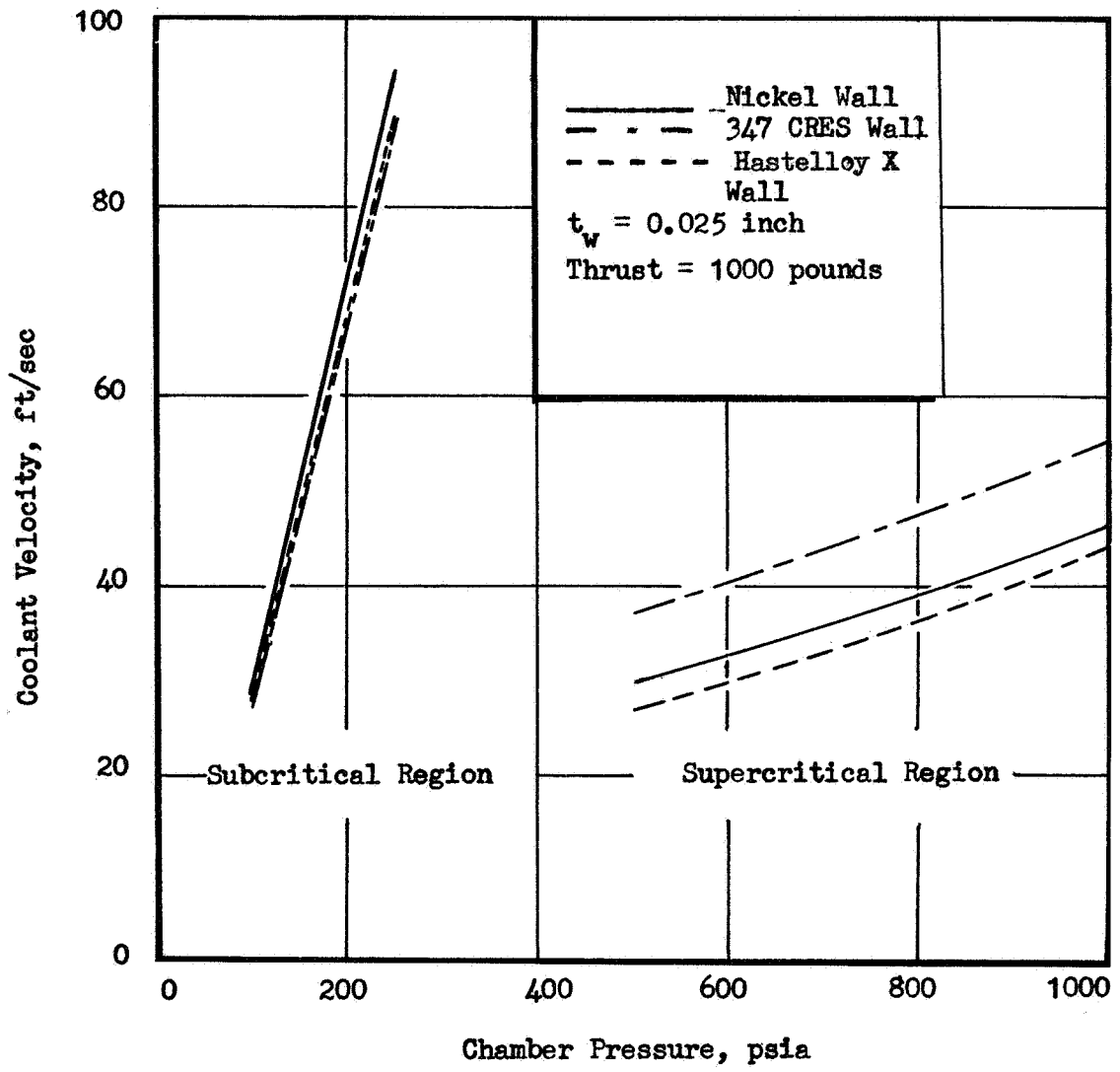

Figure 52. Maximum Coolant Velocity Requirements for 1-Butene with Gas-Side Carbon Layer

In the supercritical region at a chamber pressure of 500 psia, the coolant-side wall temperature is approximately 1600F which is higher than the 1500F limit based upon the decomposition of the 1-butene. However, a slight decrease in the gas-side wall temperature would lower the coolant-side temperature from 1600F to the 1500F limit without causing intolerable coolant jacket pressure drops.

At low chamber pressures, the gas-side wall temperature should not be designed to operate at 1700F because, as mentioned earlier, nucleate boiling is prevalent in this pressure range and the coolant-side wall temperature is fixed by the saturation temperature. Therefore, to keep the gas-side wall temperature at 1700F, an unreasonable wall thickness would be required. For 100-psia chamber pressure, the wall thickness must be approximately 1.3 inches as shown in Fig. 53. Therefore, in the present analysis the minimum wall thickness was chosen on the basis of fabrication tolerances and the hydraulic and thermal stresses with acceptance of the corresponding lower gas-side wall temperatures and slightly higher (approximately 10 to 20 percent) heat inputs.

The low operating wall temperature resulting from nucleate boiling does, however, permit a larger spacing between channels. This results in a larger channel size since the number of channels is reduced. In the current designs at low pressures, the land widths (distance between channels) were selected so as to ensure that the channel depth would not fall below the 0.025-inch constraint (0.040-inch channel width). For example, at a chamber pressure of 250 psia, the required land width was approximately 0.100 inches compared to 0.050 inches at high chamber pressure. Even with this increased spacing the maximum combustion-side wall temperature remained less than about 300F (based upon a two-dimensional thermal analysis). Bulk boiling did not occur even with this low value of T_{wg}. Channel depth vs chamber pressure is shown in Fig. 54.

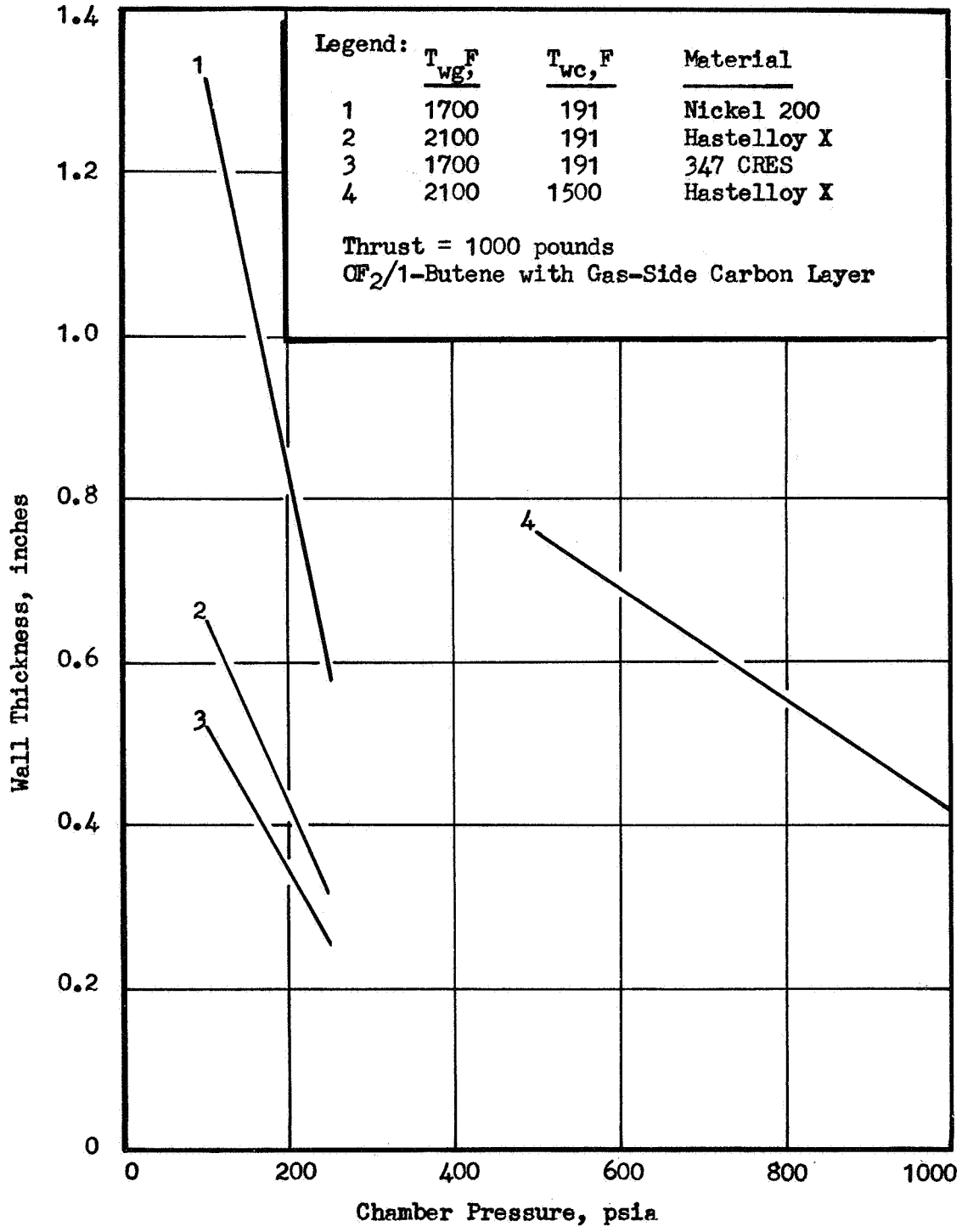

Figure 53. Wall Thickness vs Chamber Pressure for Various Materials

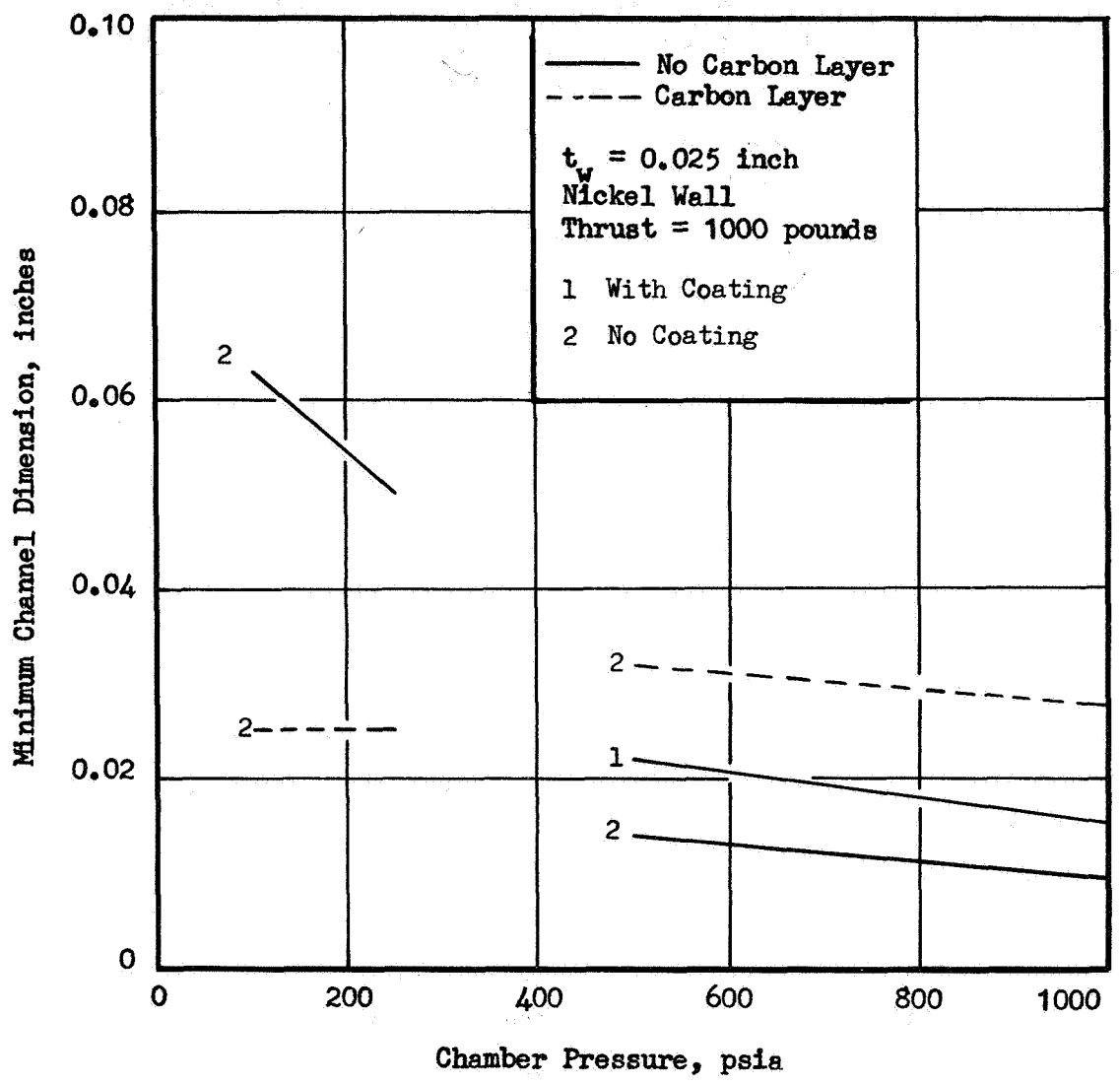

Figure 54. Channel Dimension vs Chamber Pressure for OF_2/1-Butene

Hastelloy-X Wall Materials with Carbon Coating

The evaluation of velocity requirements for both subcritical and supercritical regions were carried out for thrust chambers constructed of Hastelloy X as in the case of nickel previously described. The pressure drop is slightly lower than for nickel (Fig. 51), because the gas-side wall temperature for the Hastelloy-X is higher than that for the nickel wall case. This means slightly lower heat flux, lower velocity, and consequently lower pressure drop for the Hastelloy-X material case. The coolant-side wall temperature was above the 1500F limit in the entire range of high-chamber-pressure cases with T_{wg} = 2100F. In order to lower the coolant-side wall temperature, either the wall thickness must be increased (curve 4 of Fig. 53), or the gas-side wall temperature must be reduced. Reduction of T_{wg} would result in pressure drops nearly identical with those calculated for the nickel case (Fig. 54) because of the similar velocity requirements.

347 CRES Wall Material with Carbon Coating

This case is again very similar to that with the nickel wall. A plot of pressure drop vs chamber pressure for 347 CRES material is shown in Fig. 51. The pressure drop for the 347 CRES wall is lower in the subcritical region than that for nickel. The reverse is true in the supercritical region. In the low-chamber-pressure region, the pressure drop is slightly lower because T_{wc} was determined by the saturation temperature and, since thermal conductivity of 347 CRES is lower than nickel 200, the heat flux was lower. Consequently, the velocity requirements and pressure drops were lower. At high chamber pressure, the same gas-side wall temperature (1700F) was assumed for the nickel and CRES. The lower conductivity of the CRES results in lower coolant-side wall temperatures for the same value of wall thickness. Therefore, a higher coolant velocity is required to maintain the lower T_{wc} for the lower thermal conductivity material. The

ratio of the velocity requirements are related to the ratio of the differences between coolant-side wall temperature and coolant bulk temperature as

$$V_{CRES} = \left[\frac{(T_{wc} - T_B)_{NICKEL}}{(T_{wc} - T_B)_{CRES}} \right]^{1.25} V_{NICKEL}$$

Velocity requirements vs chamber pressure for 347 CRES material are shown in Fig. 52.

The coolant-side wall temperatures ranged from 1460F at 500 psia chamber pressure to 1300F at 1000 psia. These values are below the 1500F limit and coking of the fuel on the wall is not expected. Additionally, the bulk temperature was below the 800F bulk decomposition limit of the fuel (Fig. 55). The channel geometry is similar to that of nickel-200 and Hastelloy-X.

Nickel-200 without Carbon Coating

In this case it was assumed that no carbon deposition would take place on the wall. Therefore, the analytical heat transfer coefficients were used (no reduction in heat flux). In the low chamber pressure operating region, the fuel cools a portion of the nozzle through nucleate boiling. However, the bulk temperature eventually equals the saturation temperature and the fuel undergoes bulk boiling in the low flux portion of the nozzle. The rest of the nozzle, throat region, and the combustion zone are then cooled through forced convection by the totally vaporized fuel. The wall temperatures are low near the exit of the nozzle where nucleate boiling and bulk boiling are taking place. However, the wall temperature was allowed to

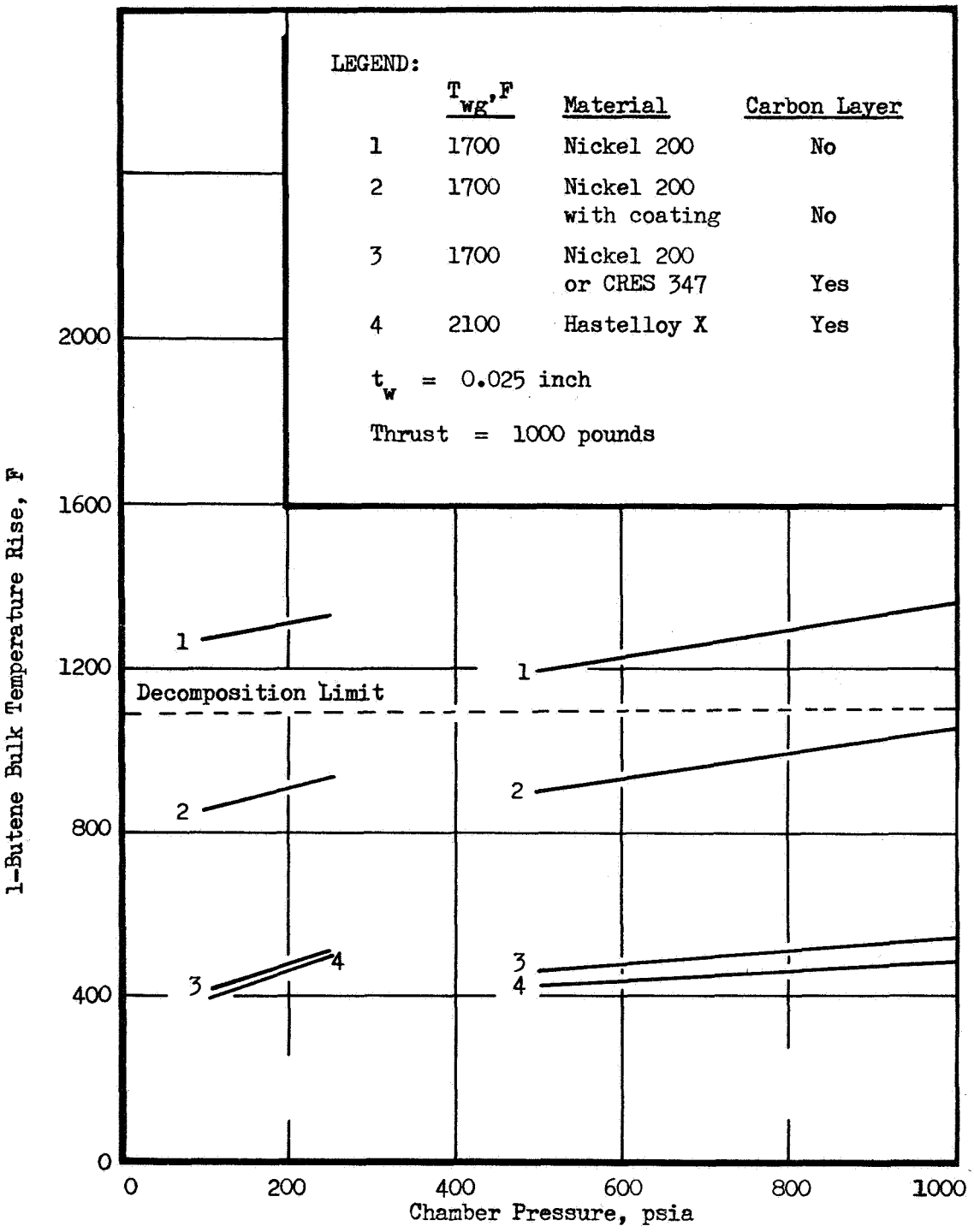

Figure 55. Bulk Temperature Rise vs Chamber Pressure for OF_2/1-Butene

reach higher values in the part of the thrust chamber cooled by the vaporized fuel. In the high chamber pressure operating region, forced convection is predominant throughout the thrust chamber.

When it was assumed that a refractory coating was applied to the gas-side wall (no carbon layer) and the gas-side wall temperature of the coating was kept at 3200F, the heat flux was considerably reduced. However, this heat flux reduction is not as much as the reduction effected by the carbon deposit on the wall. In order to equalize the heat fluxes for the cases of carbon coating and refractory coating, the gas-side wall temperature of the refractory coating must be much higher than 3200F.

The coolant jacket pressure drops for the nickel-200 wall with and without refractory coating are shown in Fig. 56. The pressure drop for the refractory coating case, although much lower than without the coating, is higher than the pressure drop for nickel-200 with carbon deposit (Fig. 51). The predicted pressure drops at 1000 psia chamber pressure are 550 psi for the uncoated wall, 63 psi for the refractory-coated wall, and 27 psi for the carbon-coated wall.

Wall temperatures are shown in Fig. 57 for the cases without a carbon layer. The coolant-side wall temperature at the low chamber pressures is as much as 100F higher than the 1500F limit based upon coolant coking. A slight reduction of T_{wg} could be made which would reduce T_{wc} to 1500F without markedly affecting the coolant-jacket pressure drop. For high chamber pressure operation with or without a refractory coating, the coolant-side wall temperatures are below 1500F. The coolant velocity requirements are high, as shown in Fig. 58 but are easily met by the vaporized coolant.

The minimum channel dimensions are shown in Fig. 54 for a nickel wall without a carbon layer. The channel dimensions are reasonably large for low chamber pressures because of the low heat fluxes and because the coolant is

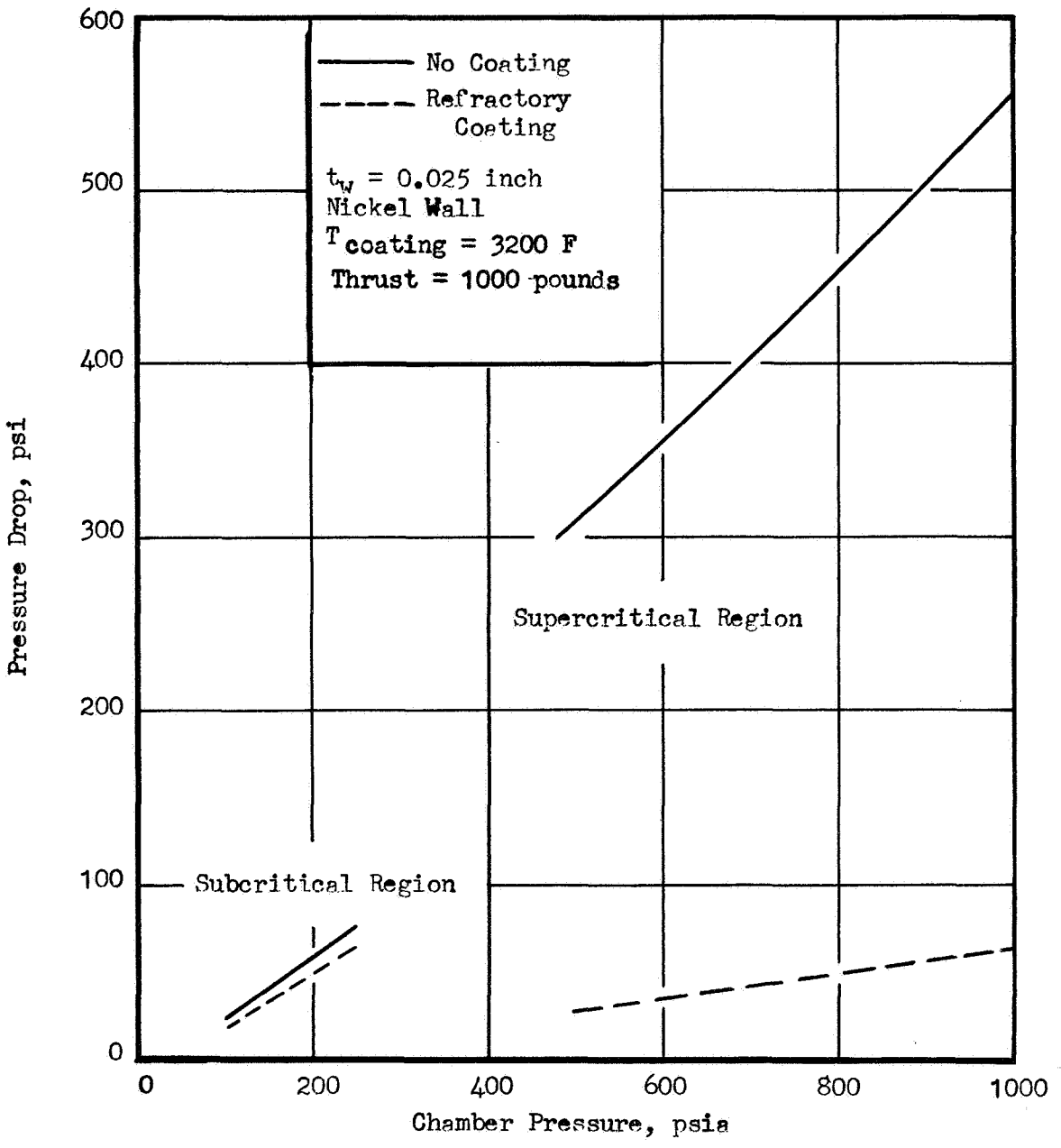

Figure 56 Pressure Drop vs Chamber Pressure For OF_2/1-Butene With No Carbon Layer

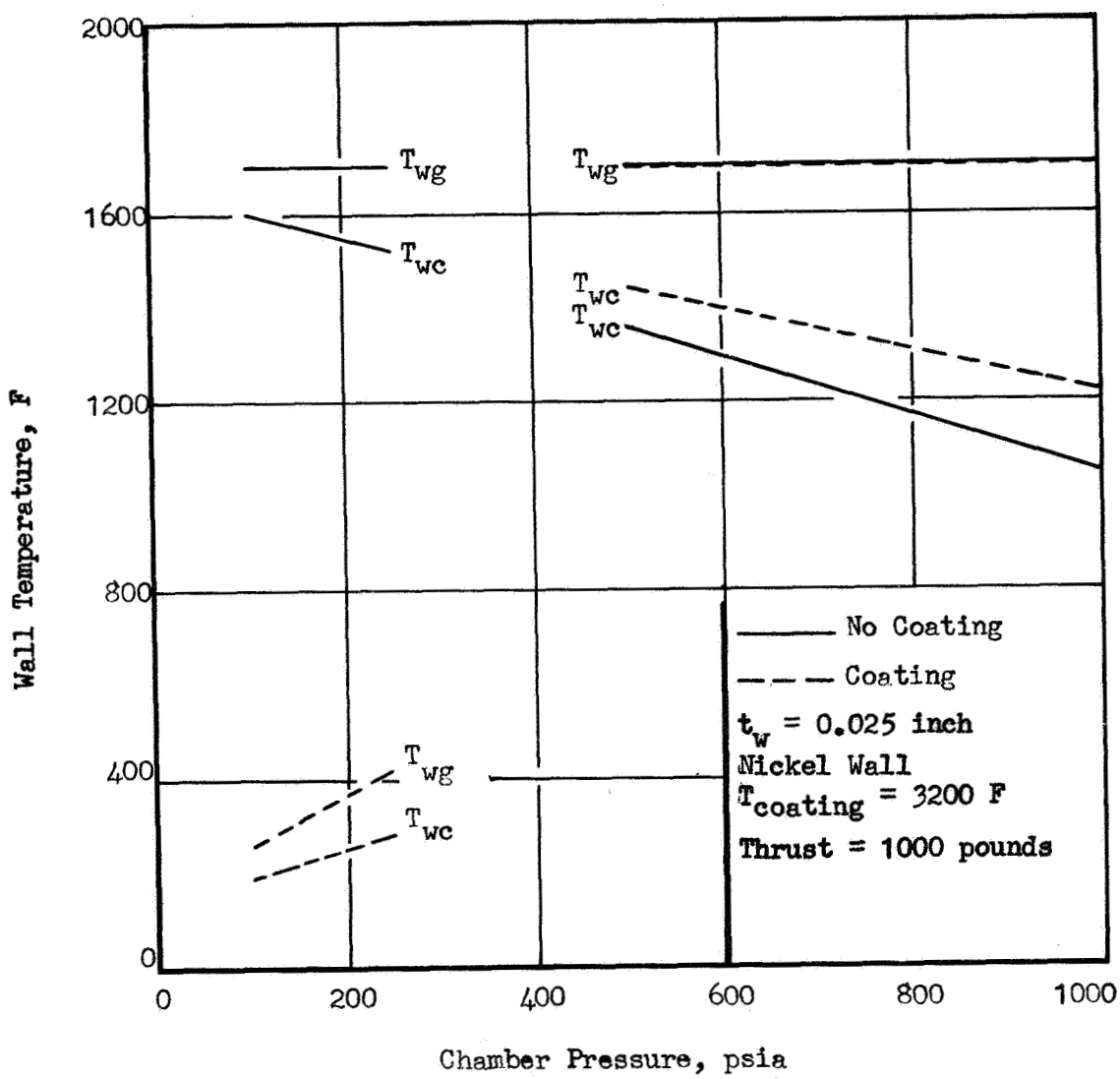

Figure 57. Wall Temperature for 1-Butene with No Carbon Layer

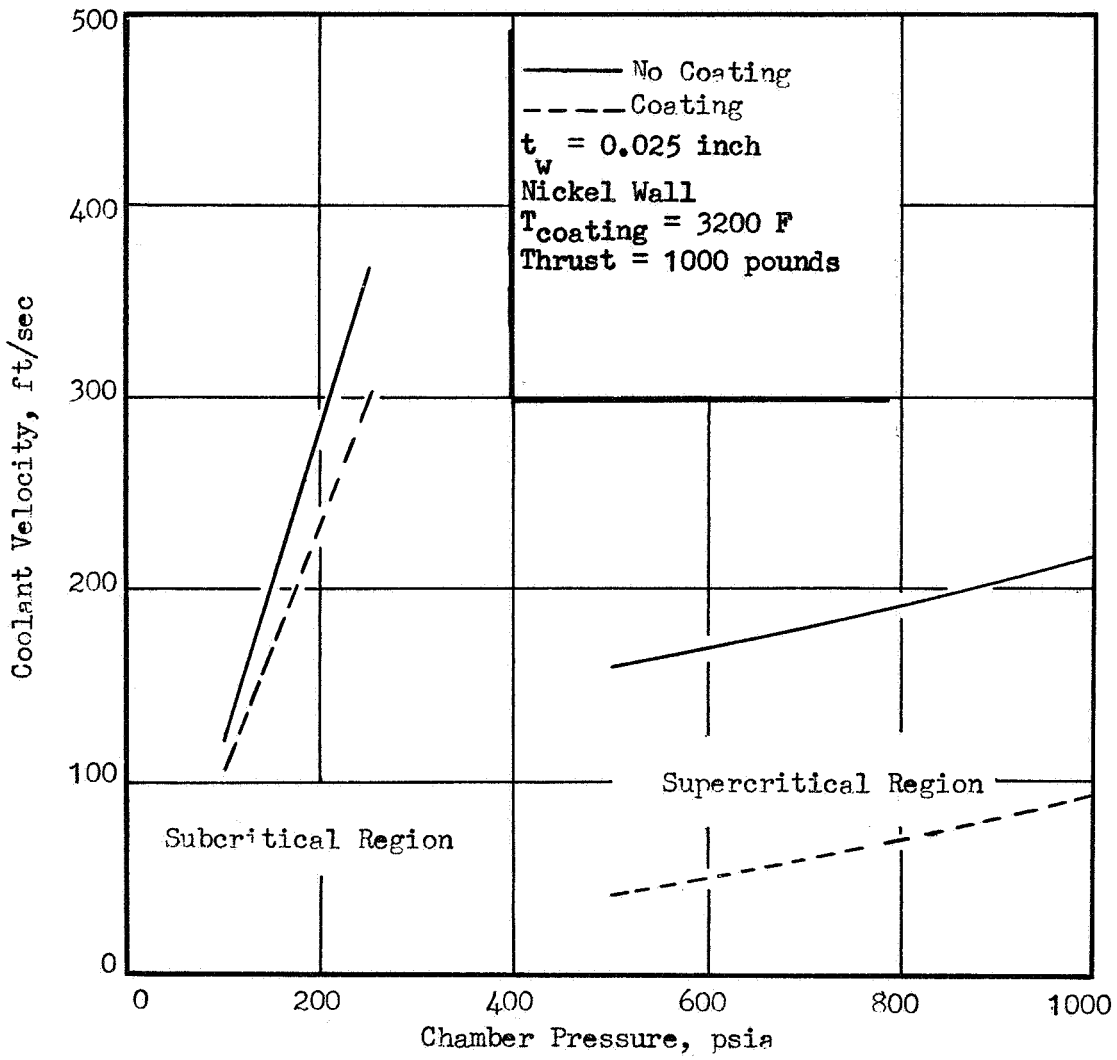

Figure 58. Coolant Velocity Requirements for 1-Butene with No Carbon Layer

vaporized in the high-area-ratio portion of the nozzle prior to reaching the throat region. The channel dimensions for higher chamber pressures are considerably below the minimum limiting values even with a 3200F coating. Reduction of the propellant mixture ratio to 70 percent of the optimum value results in acceptable channel dimensions for chamber pressures less than approximately 700 psia with a refractory coating.

Figure 55 is a plot of the 1-butene bulk temperature rise in the coolant jacket vs the chamber pressure for various cases. The inlet temperature in all cases was 168R, (-292F). In all cases when a carbon coating is assumed, the outlet bulk temperature is below the 800F limit. For a nickel wall without a gas-side carbon layer or a refractory coating, the outlet bulk temperature exceeds the 800F limits. Addition of a refractory coating which operates at a gas-side temperature of 3200F results in acceptable exit temperatures for subcritical-pressure operation. However, it should be noted that these temperatures are close to the decomposition limit and that maintaining a gas-side wall temperature of 3200F results in thick coatings at the high area ratio region of the nozzle. Maintaining a constant-thickness coating based upon throat requirements for a 3200F gas-side coating temperature would result in unacceptable bulk temperatures.

Reduction of the propellant mixture ratio to 70 percent of the optimum value would prevent coolant decomposition even at 1000 psia chamber pressure without a carbon layer or refractory coating.

NOMENCLATURE

A	reaction kinetic constant, sec^{-1}; area, in^2
a	original concentration of component
$C_f/2$	friction coefficient
C_p	specific heat at constant pressure, Btu/lb-R
C_v	specific heat at constant volume, Btu/lb-R
d_E	equivalent hydraulic diameter, inches
E	activation energy, cal/mole
e	surface roughness, inches
F	thrust level, pounds
f	friction factor
$f_1(K)$	pressure gradient factor
G	mass velocity, lb/sec -in^2
g	gravitational constant, ft/sec^2
H	shape factor; enthalpy (when subscripted), Btu/lb
h_c	coolant-side heat transfer coefficient, Btu/in^2-sec
I_s	specific impulse, seconds
I_{vac}	vacuum specific impulse, seconds
k	reaction rate constant, sec^{-1}; thermal conductivity, Btu/in-F-sec
L	length, inches
L^*	characteristic combustion chamber length, inches
M	molecular weight, lb/mole
M^*	wall Mach number
M^*_D	design Mach number referenced to sonic conditions
MR	propellant mixture ratio, o/f
N_{Nu}	Nusselt number
N_{PR}	Prandtl number

N_{Re}	Reynolds number
N_{ST}	Stanton number
n	boundary layer profile exponent
o/f	propellant mixture ratio
P	pressure, psia
P/P^*	ratio of nozzle wall to throat static pressures
P_c	chamber pressure, psia
Q	total heat input, Btu/sec
Q_f	heat absorption capability of fuel, Btu/sec
Q_{ref}	total heat input under reference conditions, Btu/sec
R	gas constant, cal/mole-K
R_1	radius of curvature upstream of throat, inches
R_2	radius of curvature downstream of throat, inches
r	radial coordinate, inches
s	coordinate along surface, inches
T	temperature, R or K
T_f	maximum fuel temperature, F
T_o	mainstream stagnation temperature, R
T^*	static temperature at throat, R
t	time, seconds
t_o	local stagnation temperature (in boundary layer), R
t_w	wall thickness, inches
U	velocity, in./sec
V	velocity, ft/sec
$\dot{W}$	flowrate, lb/sec
$\dot{W}_f$	fuel flowrate lb/sec
x	fraction of component decomposed; depth of carbon layer, inches
X/R_t	nozzle length referenced to throat radius
y	coordinate normal to wall
Y/R_t	nozzle radius referenced to throat radius

Greek Symbols

γ	C_p/C_v
δ	nozzle length, percent of 15-degree conical nozzle
∞	freestream value
δ_T	thermal boundary layer depth, inches
δ_V	velocity boundary layer depth, inches
δ^*	displacement thickness, inches
ϵ	nozzle expansion area ratio
ϵ_c	contraction area ratio
η	heat input influence coefficient
η_c^*	characteristic velocity efficiency
θ	momentum boundary layer thickness, inches
θ_M	maximum nozzle wall angle with axis, degrees
μ	viscosity, lb/ft sec
ρ	density, lb/in^3

Subscripts

θ	based upon momentum boundary layer thickness
ϕ	based upon energy boundary layer thickness

Superscripts

*	throat value, evaluated at atmospheric pressure

REFERENCES

1. Rao, G. V.: Exhaust Nozzle Contour for Optimum Thrust, Jet Propulsion, June 1958.
2. Guderly, G.: On Rao's Method for the Computation of Exhaust Nozzles, Zeitschrift für Flugwissenshaften, December 1959.
3. Bartz, D. R.: "A Simple Equation for Rapid Estimation of Rocket Nozzle Connective Heat Transfer Coefficients", Jet Propulsion, January, 1957.
4. NASA CR-54445, Investigation of Light Hydrocarbon Fuels with Flox Mixtures as Liquid Rocket Propellants, Pratt & Whitney Aircraft, A Division of United Aircraft Corporation, 1 September 1965
5. PWA FR-2107, Flox/Methane Pump-Fed Engine Study Quarterly Progress Report No. 2, Pratt and Whitney Aircraft, A Division of United Aircraft Corporation, 20 October 1966.
6. Landis, R. B., W. R. Wagner, W. R. Studhalter, "Experimental Heat Transfer Rate in Advanced Oxygen/Hydrogen Toroidal Thrust Chamber," 9th Liquid Propulsion Symposium, St. Louis, Missouri, 25-27 October, 1967.
7. R-3999, Investigation of Cooling Problems at High Chamber Pressures, Final Report, Rocketdyne, A Division of North American Aviation, Inc., May, 1963.
8. WADC-TR-59-327, Evaluation of Hydrocarbons for High Temperature Fuels, Part II, Vol. 1, Monsanto Research Corp., Contract AF 33(616)-5799, February, 1962.
9. Fieser, L. F., and M. Fieser, Textbook of Organic Chemistry, D. C. Heath Company, 1950.
10. NASA CR-72147, Investigation of Light Hydrocarbon Fuels with Fluorine-Oxygen as Liquid Rocket Propellants, Pratt and Whitney Aircraft, A Division of United Aircraft Corporation, 15 September 1967.

REFERENCES (continued)

11. Murgulesou, I. G., and I. A. Schneider: "The Thermal Decomposition of Methane Under Dynamic Conditions," (Romanian) Chemical Abstracts Vol. 55, 15067, 1961.

12. Schneider, I. A.: "The Thermal Decomposition of Methane" (Romanian), Chemical Abstracts, Vol. 55, 6996, 1961.

13. Tables of Chemical Kinetics-Homogeneous Reactions, NBS Circular 510, National Bureau of Standards, Washington, D. C., 1951.

14. Kondratiev, V. N.: "Determination of the Rate Constant for Thermal Cracking of Methane by Means of Adiabatic Compression and Expansion," Tenth Symposium International on Combustion, The Combustion Institute, Pittsburg, Pa., 1965.

15. Szwarc, M.: "The Determination of Bond Dissociation Energies by Pyrolytic Methods," Chemical Reviews, Vol. 47, 75, 1950.

16. Laidler, K. H., and B. W. Wojciechowski: Proceedings of the Royal Society, London, A 260, 91, 1961

17. Hougen, O. A. and K. M. Watson: Chemical Process Principles, Vol. 3, John Wiley and Sons, New York, 1943.

18. Laidler, K. J., N. H. Sagert. amd B. W. Wojciechowski: Proceedings of the Royal Society, London, A 270. 242, 1962.

19. Kershenbaum, L. S., and J. J. Martin, American Institute of Chemical Engineers Journal, Vol. 13, 148, 1967.

20. Bryce, W. A. and P. Keburle, Transactions of the Faraday Society, 54, 1660, 1958.

21. Schon, A. and M. Swarc, Proceedings of the Royal Society, London, A 202, 263, 1950.

22. Kerr, J. A., R. Spencer, and A. F. Trotman-Dickenson, Chemical Society Journal, 6652, 1965.

REFERENCES (continued)

23. Stepukhovich, A. D., and I. K. Krol, Zhur. Fiz. Kim., Vol. 30, 1718 (1956), (Russian), Chemical Abstracts, Vol. 51, 7696 (1957).

24. Laidler, K. J., N. H. Sagert, and B. W. Wojciechowski, Proceedings of the Royal Society, London, A 270, 254, 1962.

25. Robinovich, E. Y., and A. V. Rodionov, "Formation of Carbon Filaments During Thermal Decomposition of Hydrocarbons," (Russian) Chemical Abstracts, 54, 13614, 1960.

26. Golder, L., Soc. Chim, France, Chemical Abstracts, 55, 22082, 1961.

27. Greene, E. F., et al Journal of Physical Chemistry, 62, 238, 1958.

28. Rafalkes, I. S., and P. A. Tesner, "Carbon Black Formation in the Decomposition of Hydrocarbons," (Russian) Chemical Abstracts, Vol. 54, 6089, 1960.

29. Syskov, K. I., and E. I. Jelikhovskaya, "On the Formation and Composition of Pyrolytic Carbon," Carbon, Vol. 5, 201, 1967.

30. ASD-TDR-102, Research on the Mechanism of Thermal Decomposition of Hydrocarbon Fuels, Monsanto Research Corp., January 1963.

31. Progress Report No. 2 of above.

32. Weger, E.: An Investigation of Carbon Decomposition, Progress Report No. 3, Washington University, St. Louis, Mo., February 1966.

33. Misic, D. and G. Thodos: "Thermal Conductivity Measurement of Methane in the Dense Gaseous State," Physica, Vol. 32, 1966.

34. Maxwell, J. B.: Data Book on Hydrocarbons, Van Nostrand Company, Inc., New York, 1951.

35. Stiel, L. I., and G. Thodos: "The Prediction of the Transport Properties of Pure Gaseous and Liquid Substances," Progress in International Research on Thermodynamic and Transport Properties, ASME, 1962.

REFERENCES (continued)

36. Huang, E., G. Swift, F. Kurata: "Viscosities of Methane and Propane at Low Temperatures and High Pressures," A.I.Ch.E. Journal Vol. 12, September 1966.

37. Leng, D. E. and E. W. Comings: "Thermal Conductivity of Propane," Industrial and Engineering Chemistry, Vol. 49, American Chemical Society Publications, Washington, D. C., December 1957.

38. Starling, K., B. Eakin, R. Ellington, "Liquid, Gas, and Dense-Fluid Viscosity of Propane, A.I.Ch.E., Journal, September 1960.

39. Owens, E., G. Thodos, "Thermal Conductivity: Reduced State Correlation for Ethylene and its Application to Gaseous Aliphatic Hydrocarbons and their Derivatives at Moderate Pressures,"A.I.Ch.E. Journal, December 1960.

40. Uyehara, O. and K. Watson: National Petroleum News, Technical Section, Vol. 36, October 1944.

41. Vennard, John K.: Elementary Fluid Mechanics, John Wiley and Sons, Inc., New York, 3rd Ed. (1954).

42. Wolf, H. and J. R. McCarthy: Heat Transfer to Hydrogen and Helium with Wall-to-Fluid Temperature Ratios to 11.09, presented at A.I.Ch.E. Annual Meeting, 4 to 7 December 1960.

43. R-5652-4P, Final Program Progress Report for Product Engineering, Volume 2, Rocketdyne, a Division of North American Aviation, Inc., Canoga Park, California, April 1965.

44. Glickstein, M. R. and R. W. Whitesides, Jr.: Forced-Convection Nucleate and Film Boiling of Several Aliphatic Hydrocarbons, A.S.M.E. Paper No. 67-HT-7 presented at the A.S.M.E.-A.I.Ch.E. Heat Transfer Conference, Seattle, Wash., August 6 - 9, 1967.

APPENDIX A

GAS-SIDE HEAT TRANSFER COEFFICIENT CALCULATIONS

The gas-side heat transfer coefficients were determined initially without considering the effects of carbon formation on the thrust chamber wall. The method of calculating the profiles of the heat transfer coefficients was the solution of the integral momentum and energy equations.

Referring to the definition of the momentum thickness and energy thickness, respectively:

$$\theta = \int_0^{\delta_v} \frac{\rho U}{\rho_\infty U_\infty} \left(1 - \frac{U}{U_\infty}\right) dy \qquad (1)$$

$$\phi = \int_0^{\delta_T} \frac{\rho U}{\rho_\infty U_\infty} \left(1 - \frac{t_o - T_{wg}}{T_o - T_{wg}}\right) dy \qquad (2)$$

For a similarity of stagnation temperature and velocity distributions throughout the boundary layer and equal depths of the velocity (δ_v) and thermal (δ_T) layers, the energy and momentum thicknesses might be expected to be equal. However, under variable freestream accelerations and wall cooling or heating conditions, the values of these thicknesses can depart considerably from each other. In general, the rapid acceleration of the flow within the throat vicinity results in greatly diminished momentum layer thickness, with less effect on the thermal boundary layer.

The momentum and energy integral equation forms may be compared for similarity in the following axisymmetric form:

$$\frac{d\theta}{ds} = \frac{C_f}{2} - \theta \left[\frac{1 + H}{U} \left(\frac{dU}{ds} \right) + \frac{1}{\rho U} \left(\frac{d(\rho U)}{ds} \right) + \frac{1}{r} \frac{dr}{ds} \right] \tag{3}$$

$$\frac{d\phi}{ds} = N_{ST} \left(\frac{T_{aw} - T_{wg}}{T_o - T_{wg}} \right) - \phi \left[- \left(\frac{1}{T_o - T_{wg}} \right) \frac{d\, T_{wg}}{ds} + \frac{1}{\rho U} \left(\frac{d(\rho U)}{ds} \right) + \frac{1}{r} \frac{dr}{ds} \right] \tag{4}$$

With the exception of the first term within the right-hand brackets, a near identity of the growth of the momentum and energy thicknesses is observed for near-equivalent relationships for the nondimensional heat transfer coefficient(N_{ST}) and skin friction coefficient ($C_f/2$), respectively. From Eq. 3 it is seen, however, that a strong acceleration at a low flow velocity will result in a controlling influence on the momentum thickness growth and a possible decay of the layer thickness in the throat region. On the other hand, extreme cooling ($H \rightarrow -1$) of the wall will tend to increase the momentum thickness. Similarly, within the bounds of a given combustion chamber geometrical contour, the effect of a substantial wall temperature rise toward the throat is seen to increase the thermal layer thickness.

Study of the component parts of the relationships shown in Eq. 3 and 4 then allows the explanation of the occurrences noted experimentally. For example, if the momentum boundary layer thickness is small in the throat region, either as a result of strong acceleration, short combustor length, or low-freestream mass velocity conditions, the possibility of retention of a laminar boundary layer or a reverse transition from a turbulent to a laminar boundary layer can occur in the throat region. In addition, the damping of initial combustion turbulence within the flow acceleration region can allow for effectively higher critical transition Reynolds numbers.

The solution of the two integral equation forms provided by Eq. 3 and 4 can most easily be accomplished when these relationships are reduced to the form:

$$\frac{d}{ds}(r\,\rho\,U^2\,\theta) = r\rho U^2\left(\frac{C_f}{2}\right) - r\,\rho\,U\,\delta^*\left(\frac{dU}{ds}\right) \tag{5}$$

$$\frac{d}{ds}\left[r\,\rho\,U\,C_p\,(T_o - T_{wg})\phi\right] = r\,\rho\,U\,C_p\,(T_{aw} - T_{wg})\,C_H \tag{6}$$

Because of the variation in the mainstream gas composition with shifting flow behavior, the solution may be expressed in the nondimensional axisymmetric forms:

$$\frac{d}{d\left(\frac{s}{r^*}\right)}\left(\frac{r}{r^*}\,\frac{\rho}{\rho^*}\,M^{*2}\,\frac{\theta}{r^*}\right) = \left(\frac{r}{r^*}\,\frac{\rho}{\rho^*}\,M^{*2}\right)\frac{C_f}{2} - \left(\frac{r}{r^*}\,\frac{\rho}{\rho^*}\,H M^*\,\frac{dM^*}{d\left(\frac{s}{r^*}\right)}\,\frac{\theta}{r^*}\right) \tag{7}$$

$$\frac{d}{d\left(\frac{s}{r^*}\right)}\left[\frac{r}{r^*}\,\frac{\rho}{\rho^*}\,M^*\,(H_o - H_{wg})\frac{\phi}{r^*}\right] = \frac{r}{r^*}\,\frac{\rho}{\rho^*}\,M^*\,(H_{aw} - H_{wg})\,N_{ST} \tag{8}$$

Solution of these equations requires relationships between the Stanton number (C_H) and the energy thickness (ϕ), and between the skin friction coefficient and the momentum thickness (θ). Various semiempirical relations have been established for both laminar and turbulent flow.

For the skin friction coefficient under accelerating flow field conditions, study of laminar, and turbulent flow conditions indicates a dependence on the pressure gradient for equivalent momentum Reynolds number conditions. For the laminar case, the solution employed with corrections for reference temperature coincident with cooled wall and compressible flow conditions was

$$\left(\frac{C_f}{2}\right)_\infty = \frac{f_1(K)}{(Re_\theta)_\infty}\left(\frac{T_\infty}{T_r}\right)\left(\frac{\rho_\infty}{\rho_r}\right)\left(\frac{\mu_r}{\mu_\infty}\right) \tag{9}$$

For the turbulent skin friction, a modified, closed-form solution to include acceleration and shape factor effects on the boundary-layer profile exponent was employed. This form is:

$$\left(\frac{C_f}{2}\right)_r = \frac{0.0023\left(1+\frac{2}{n}\right)^{6.62}}{(Re_\theta)_\infty^{(2/(n+1))}} \left(\frac{T_\infty}{T_r}\right)\left(\frac{\rho_\infty}{\rho_r}\right)^{\left(\frac{2}{n+1}\right)} \left(\frac{\mu_r}{\mu_\infty}\right)^{\left(\frac{2}{n+1}\right)} \tag{10}$$

which reduces for n = 7 (i.e., $U/U_\infty = (y/\delta)^{1/7}$ in outer region turbulent layer) to the form:

$$\left(\frac{C_f}{2}\right)_\infty = \frac{0.0122}{(Re_\theta^{0.25})_\infty} \left(\frac{T_\infty}{T_r}\right)\left(\frac{\rho_\infty}{\rho_r}\right)^{1/4} \left(\frac{\mu_r}{\mu_\infty}\right)^{1/4} \tag{11}$$

For the definition of the local heat transfer coefficient, a similarity between the nondimensional heat transfer coefficient and the skin friction coefficient was assumed, neglecting pressure gradient effects upon the thermal boundary layer profile. For this assumption, these values (based upon energy thickness) become:

$$N_{ST_\infty} = \frac{0.217}{(Re_\phi)_\infty} \left(\frac{T_\infty}{T_r}\right)\left(\frac{\rho_\infty}{\rho_r}\right)\left(\frac{\mu_r}{\mu_\infty}\right)\frac{1}{N_{PR}^{1/2}} \quad \text{(laminar)} \tag{12}$$

$$N_{ST_\infty} = \frac{0.0122}{(Re_\phi)^{.25}} \left(\frac{T_\infty}{T_r}\right)\left(\frac{\rho_\infty}{\rho_r}\right)^{1/4} \left(\frac{\mu_r}{\mu_\infty}\right)^{1/4} \frac{1}{N_{Pr}^{2/3}} \quad \text{(turbulent)} \tag{13}$$

The nondimensional heat transfer coefficients of Eq. 12 and 13 were converted to the actual hot-gas-side heat transfer coefficient by the relation

$$h_g = N_{ST_\infty} \rho U C_p \tag{14}$$

The total heat input to the wall was obtained by numerical integration along the nozzle wall.

$$Q = \int h \left(T_{aw} - T_{wg}\right) d S \tag{15}$$

where

$$T_{aw} = \frac{T_o \left[1 + \sqrt[3]{N_{P-R}} \frac{\gamma - 1}{2} M_\infty^2\right]}{1 + \frac{\gamma - 1}{2} M_\infty^2} \tag{16}$$

The actual combustion temperature, T_o, is related to the ideal (100-percent C* efficiency) combustion temperature by:

$$T_o = T_{o_{IDEAL}} \cdot \eta_{C^*}^2 \tag{17}$$

APPENDIX B

GAS-SIDE CARBON LAYER THERMAL RESISTANCE

The computerized integral energy equations were first applied to experimental data of Ref. 4 taken at a chamber pressure of 100 psia in uncooled thrust chambers. Actual thrust chamber geometrical parameters were used in the analysis. The flow-field behavior in the cylindrical section is difficult to determine because of incomplete combustion, mixing, and freestream turbulence. For the theoretical analysis, therefore, the point of initiation was located one inch downstream of the injector face.

Heat transfer data correlations using either the local heat flux or gas-side flow coefficient have two distinct disadvantages: (1) these parameters are functions of chamber pressure, propellant combustion, mixture ratio, and characteristic velocity efficiency; and (2) these parameters vary strongly with the local mass velocity (area ratio) and therefore increase at a rapid rate in the throat region. A more general correlating parameter can be obtained by nondimensionalizing the heat transfer coefficient by dividing it by $\rho V C_p$ to form the Stanton number and multiplying by $(C_p \mu / k)^{2/3}$, thereby forming the Stanton-Prandtl parameter which is related to Reynolds number, based upon the momentum boundary layer thickness, through the modified Reynolds' analogy

$$N_{ST} \times N_{PR}^{2/3} = \left(\frac{\rho V \theta}{\mu}\right) - 0.25$$

where θ is the momentum boundary layer thickness.

This relation indicates that the Stanton-Prandtl parameter is a weak function of local mass velocity and hence chamber pressure, area ratio, and characteristic velocity efficiency, and also a weak function of combustion product properties. It can be used to provide a direct indication of the local boundary layer development. The distribution of this parameter along a thrust chamber wall surface indicates which regions of the chamber contour are effective in promoting boundary layer growth.

The $N_{ST}N_{PR}^{2/3}$ parameter value at the beginning of the converging section was used to evaluate the gas side theoretical heat transfer coefficient which was then held constant in the cylindrical combustion zone. Theoretical and experimental values of $N_{ST}N_{PR}^{2/3}$ are plotted in Fig. B1 through B4 for the propellant combinations using FLOX with methane, propane, pentane blend, and 1-butene fuels.

The experimental data shown in Fig. B1 sometimes imply boundary layer attachment near the injector (points 1) and at other times near the start of convergence (points 2, 3, 4)as indicated by a decreasing value of the $N_{ST}N_{PR}^{2/3}$ parameter. The theoretical $N_{ST}N_{PR}^{2/3}$ curve is also shown in Fig. B1 and has the same general shape as the experimental curve downstream of the convergent section entrance.

The parameter $N_{ST}N_{PR}^{2/3}$ plotted vs axial coordinate for propellant combinations using FLOX with propane, pentane-blend, and butene-1 as shown in Fig. B2, B3, and B4. It appears in these cases that either the boundary layer attaches near the injector and the film coefficient decreases with length (boundary layer grows with length), or that impingement of the oxidizer on the wall takes place near the injector (swirlers in oxidizer spuds of the injector RL10A-3).

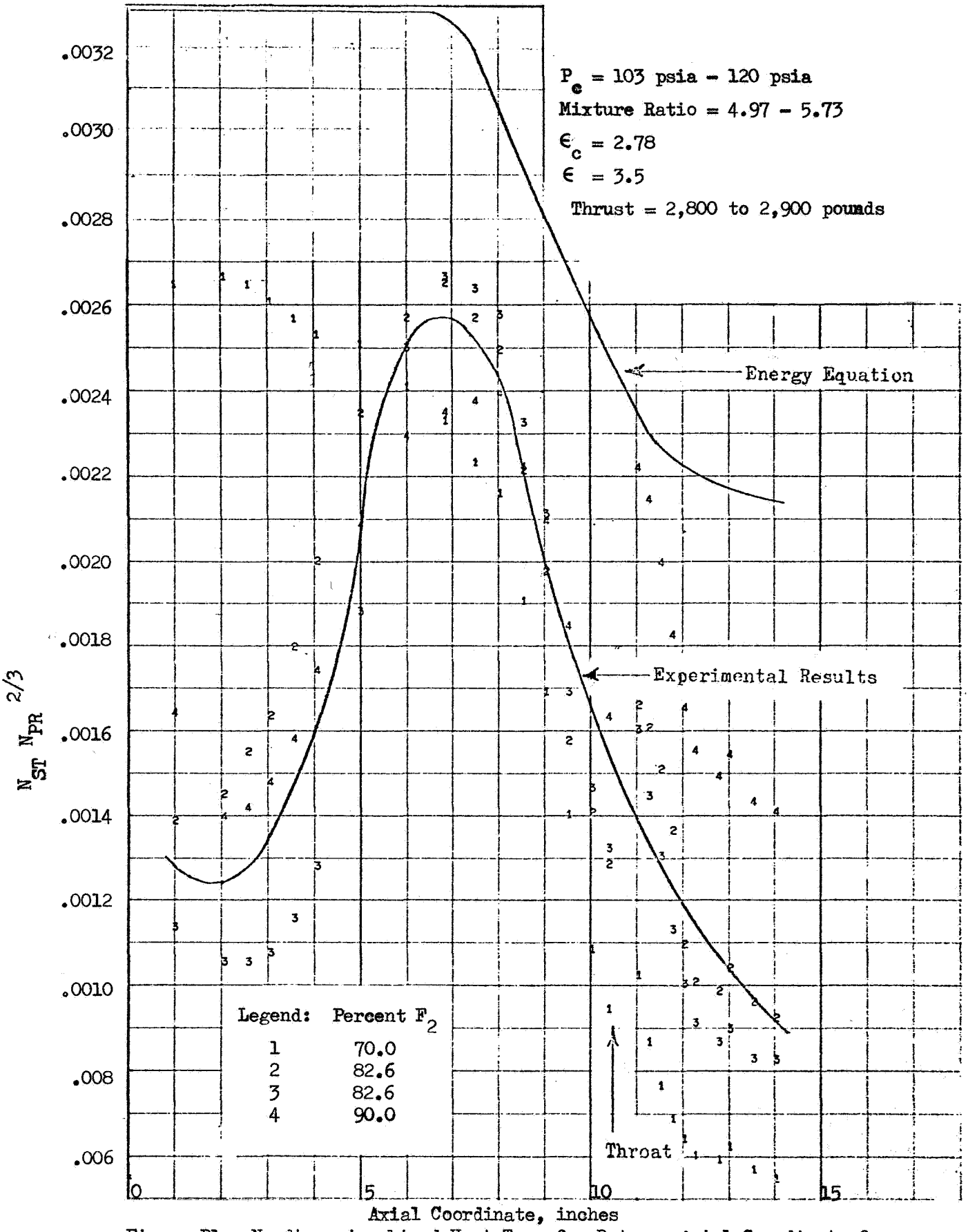

Figure B1. Nondimensionalized Heat Transfer Rate vs Axial Coordinate for FLOX/Methane

Legend:	Thrust, pounds	P_c, psia	MR	Percent F_2
1	2891	108	4.00	75
2	2783	105	4.36	75
3	2727	103	4.68	75

$\epsilon_c = 2.78$
$\epsilon = 3.54$

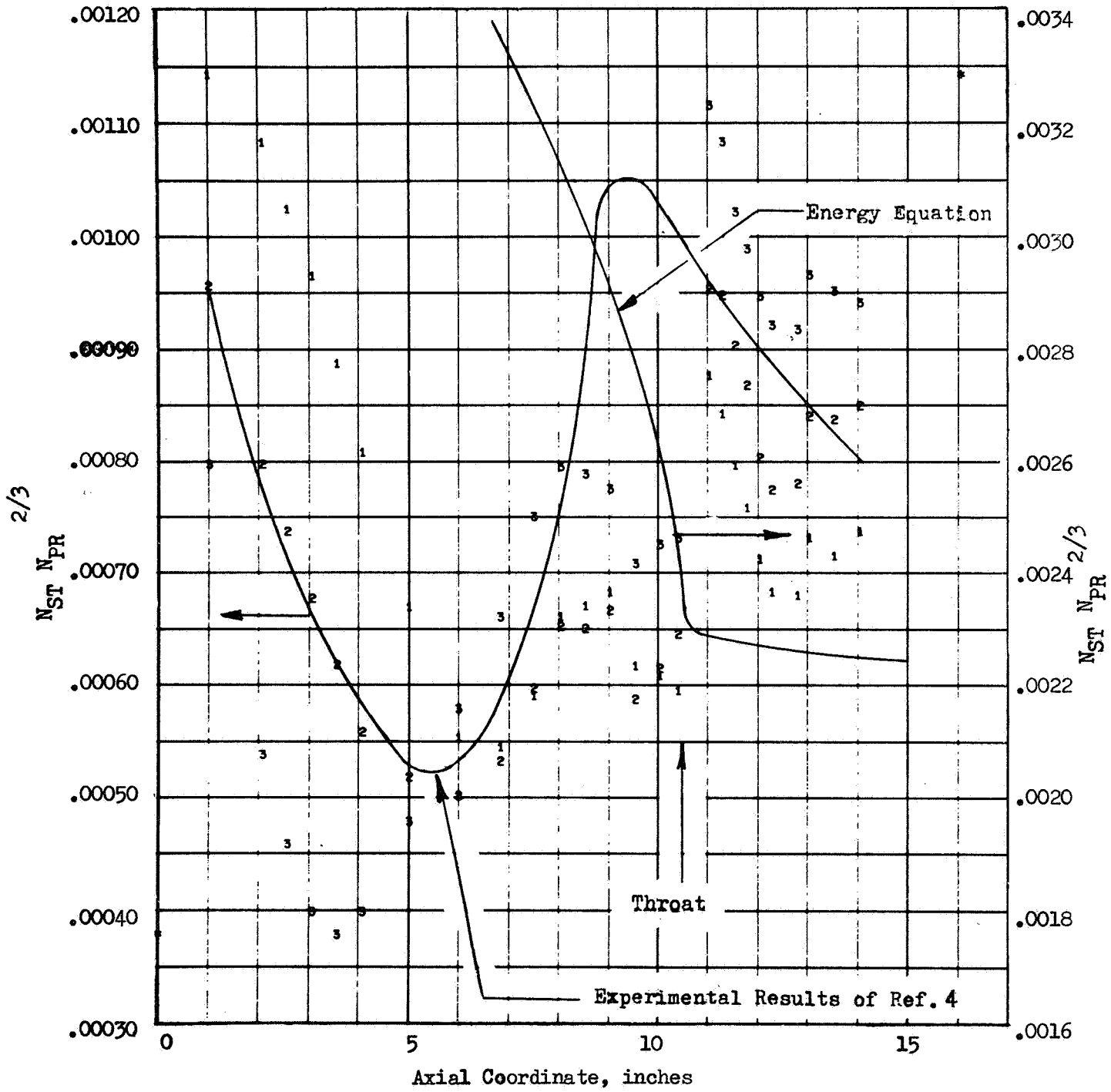

Figure B2 . Nondimensionalized Heat Transfer Rate vs Axial Coordinate for FLOX/Propane

	Legend:	Thrust, pounds	P_c, psia	MR	Percent F_2
$\epsilon_c = 2.78$	1	3182	119	2.73	70.4
$\epsilon = 3.54$	2	3167	117	2.82	70.4
	3	3330	120	3.67	70.4

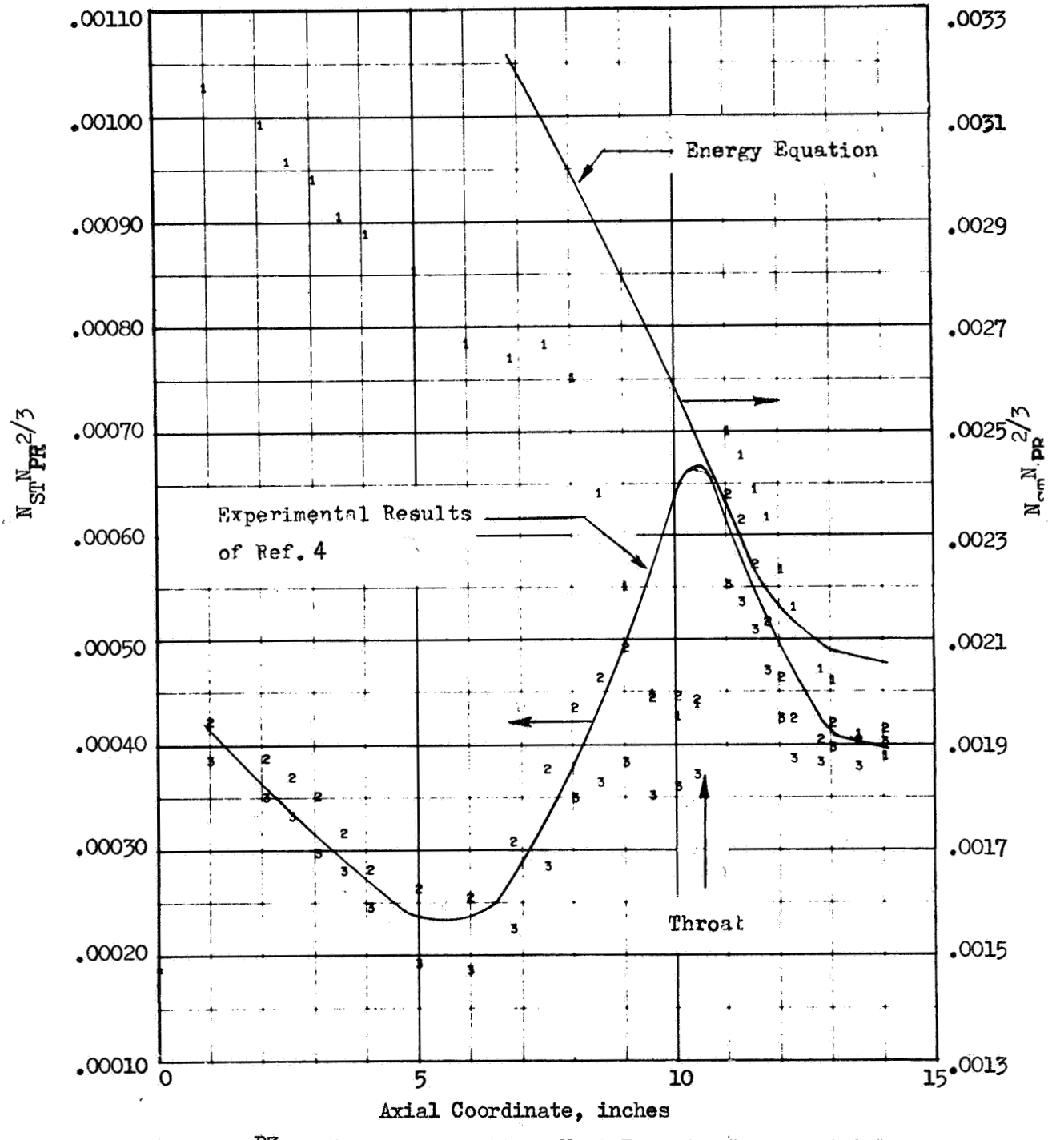

Figure B3. Nondimensionalized Heat Transfer Rate vs Axial Coordinate for FLOX/1-Butene

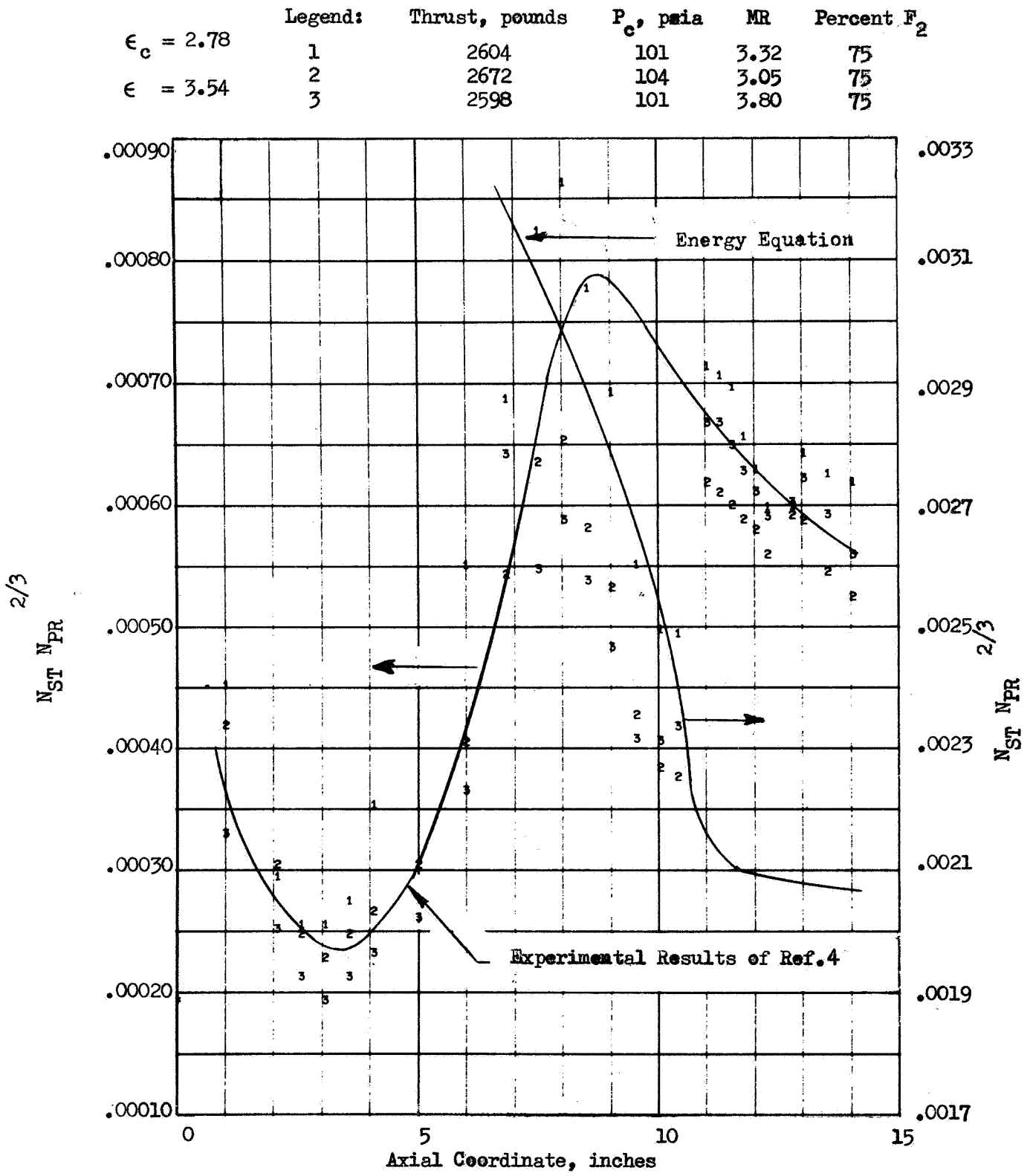

Figure B4 . Nondimensionalized Heat Transfer Rate vs Axial Coordinate for FLOX/Pentane-Blend

The experimental data of Ref. 4 was used to evaluate the carbon layer resistance by assuming that the measured gas side resistance was equal to that of the carbon layer plus the theoretical value.

$$1/h_{exp} = x/k + 1/h_{theo}$$

or

$$x/k = (h_{theo} - h_{exp})/ (h_{theo}) (h_{exp})$$

A plot of x/k, thus calculated, vs local mass velocity is presented in Fig B5 for FLOX/methane at 100 psia chamber pressure and indicates separate correlations for the converging and diverging portions of the nozzle. The equations correlating x/k with the local mass velocity, G, are

$$\ln (x/k) = 6.33 + 1.83G \quad \text{(converging)}$$
$$\ln (x/k) = 12.37 + 12.7\ G \quad \text{(diverging)}$$

In contrast, correlations for the other propellants tested indicated a single function for the entire nozzle. These correlations are as follows:

$$\ln (x/k) = 10.52 - 6.00G \quad \text{(FLOX-Propane)}$$
$$\ln (x/k) = 10.06 - 3.26G \quad \text{(FLOX-Pentane blend)}$$
$$\ln (x/k) = 10.87 - 4.63G \quad \text{(FLOX-Butene-1)}$$

The data upon which these correlations are based are found in Figs. B6 through B8. Since a constant theoretical film coefficient was used in the combustion zone where the mass velocity was assumed to be constant, no definite trend of x/k vs mass velocity exists in this region.

The 250-psia test data for FLOX/methane were also analyzed to determine the carbon thermal resistance layer as a function of local freestream

P_c = 103 psia - 120 psia F = 2.8K - 2.9K

ϵ_c = 2.78 Mixture Ratio = 4.97 - 5.73

ϵ = 3.5

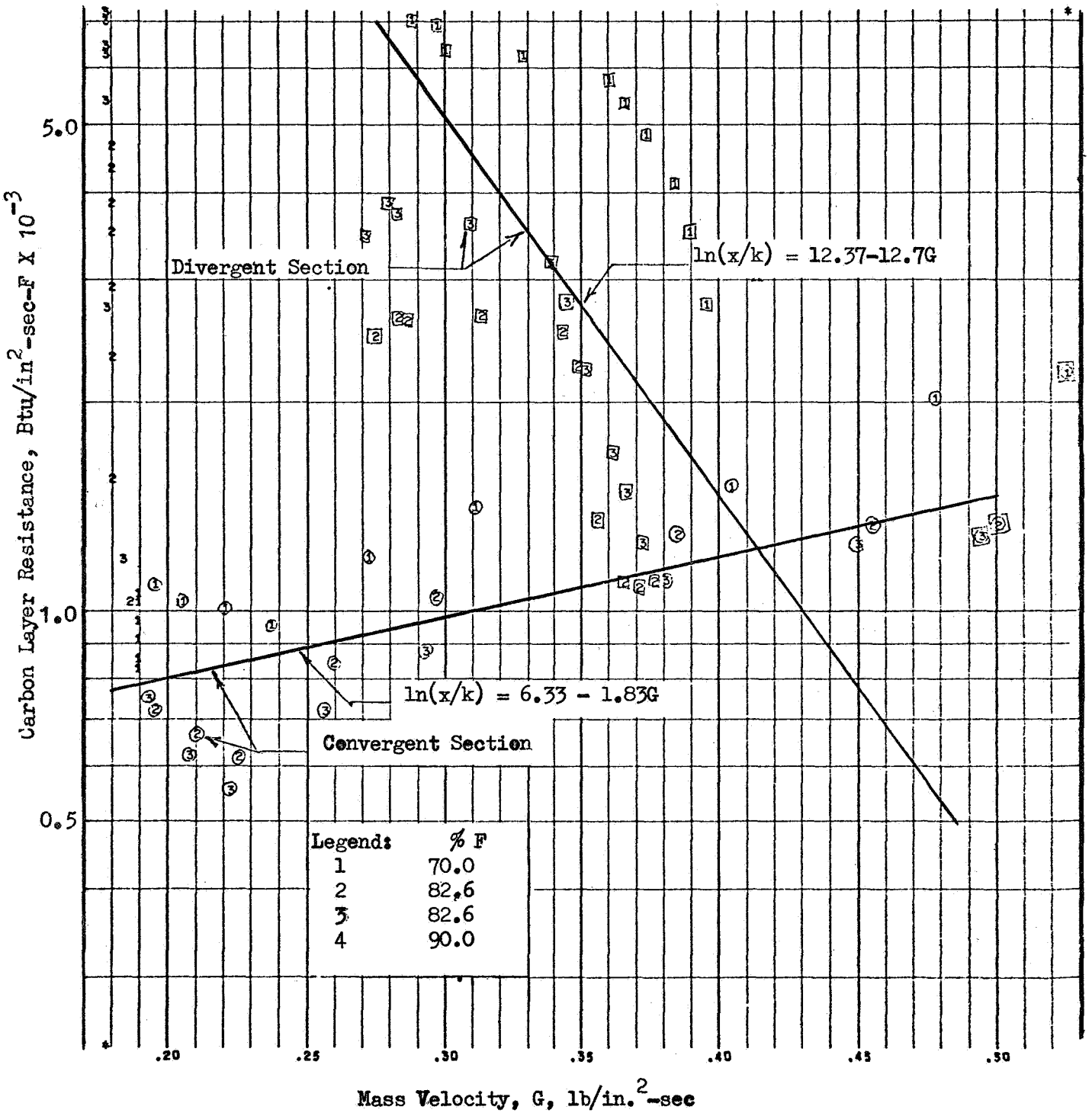

Figure B5. Carbon Layer Resistance Correlation for FLOX/Methane

LEGEND:

$\epsilon_c = 2.78$

$\epsilon = 3.54$

	F, lb	P_c, Psia	MR	Percent F_2
1	2891	108	4.0	75
2	2783	105	4.36	75
3	2727	103	4.68	75

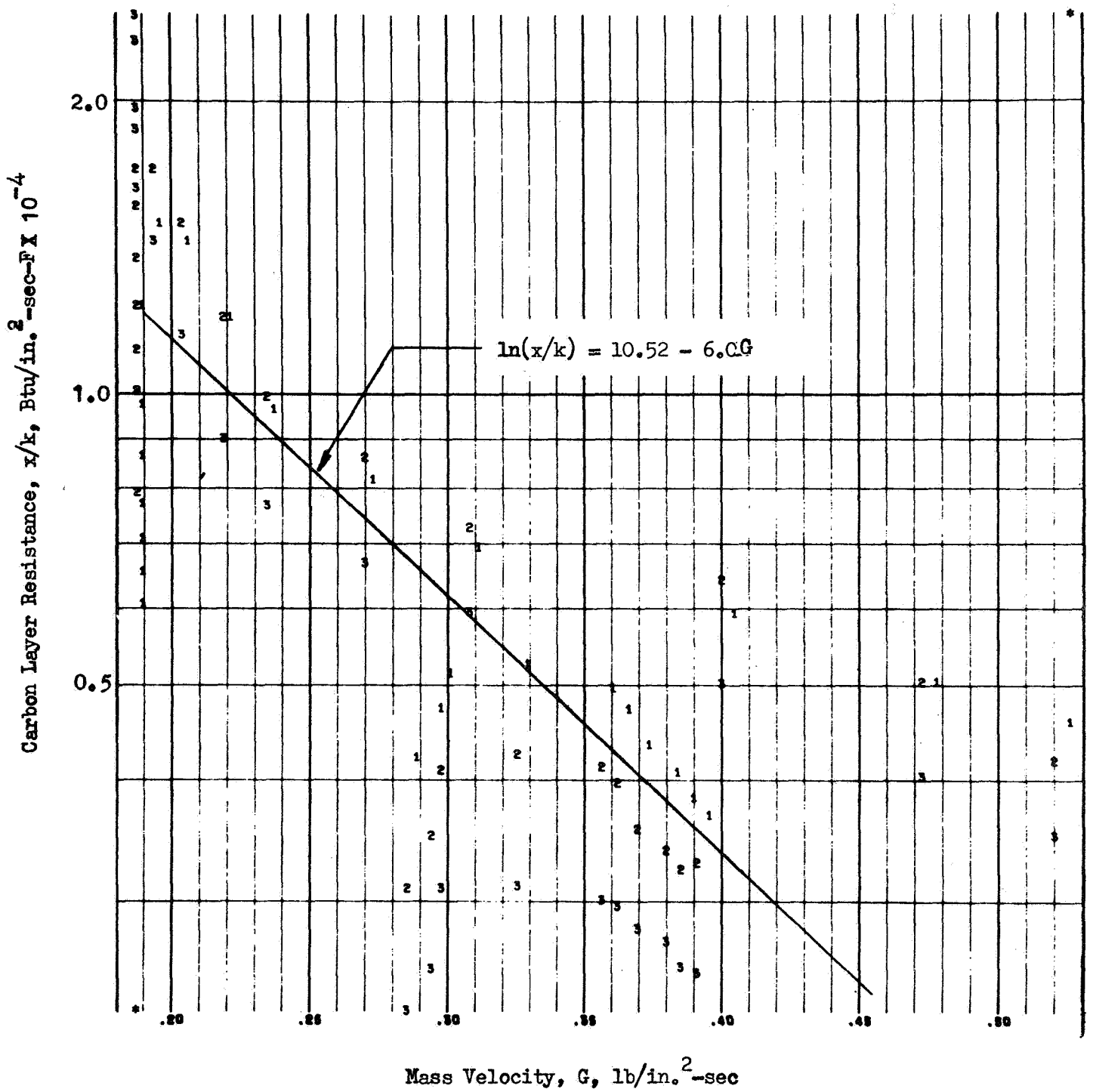

Figure B6 . Carbon Layer Resistance Correlation for FLOX/Propane

	LEGEND:	F, lbs	P_c, psia	MR	% F_2
ϵ_c = 2.78	1	3182	119	2.73	70.4
ϵ = 3.54	2	3167	117	2.82	70.4
	3	3330	120	3.67	70.4

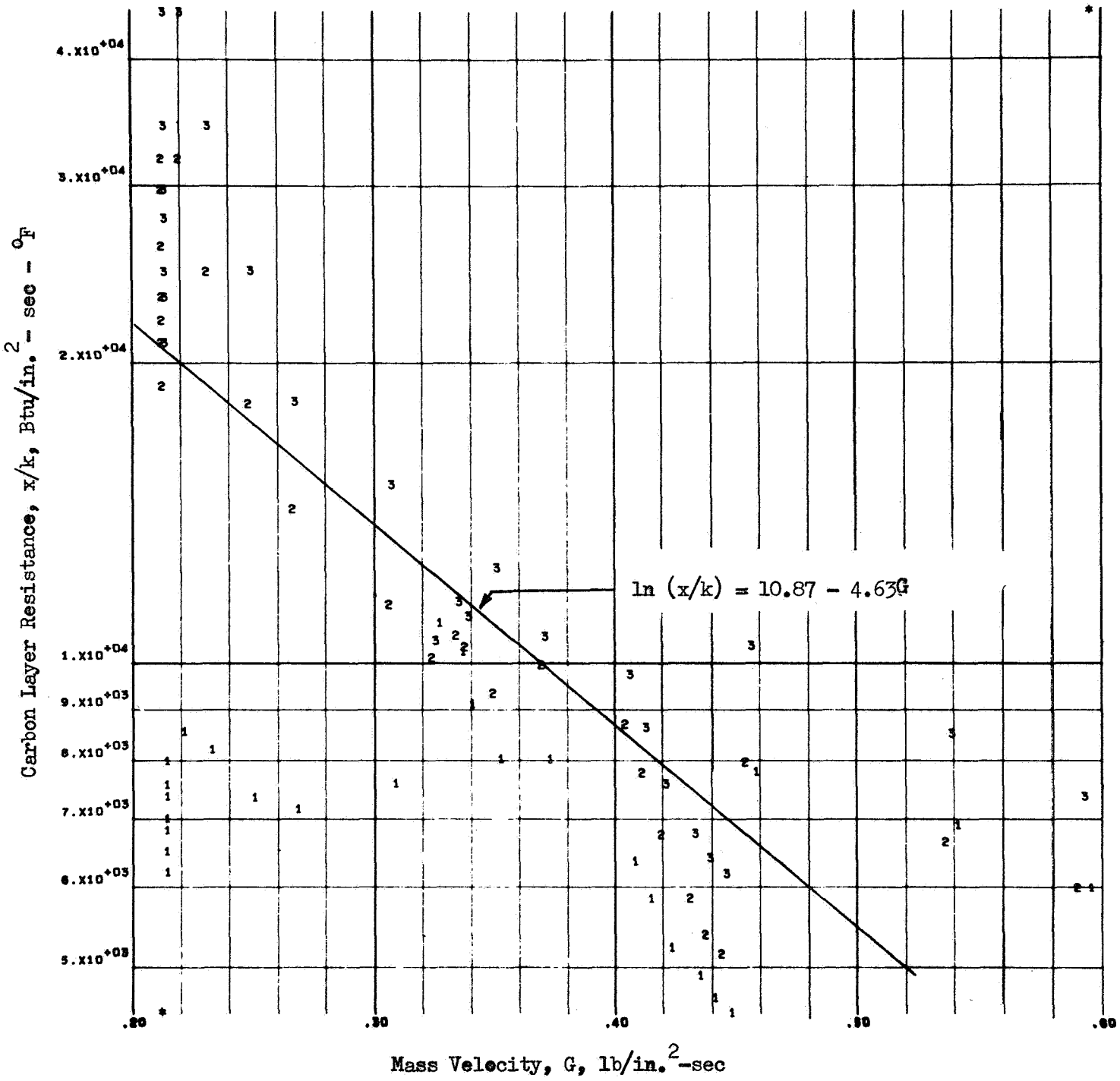

Figure B7. Carbon Layer Resistance Correlation for FLOX/Butene-1

		F, lb	P_c, psia	MR	Percent F_2
	1	2604	101	3.32	75
ϵ_c = 2.78	2	2672	104	3.05	75
	3	2598	101	3.80	75

ϵ = 3.54

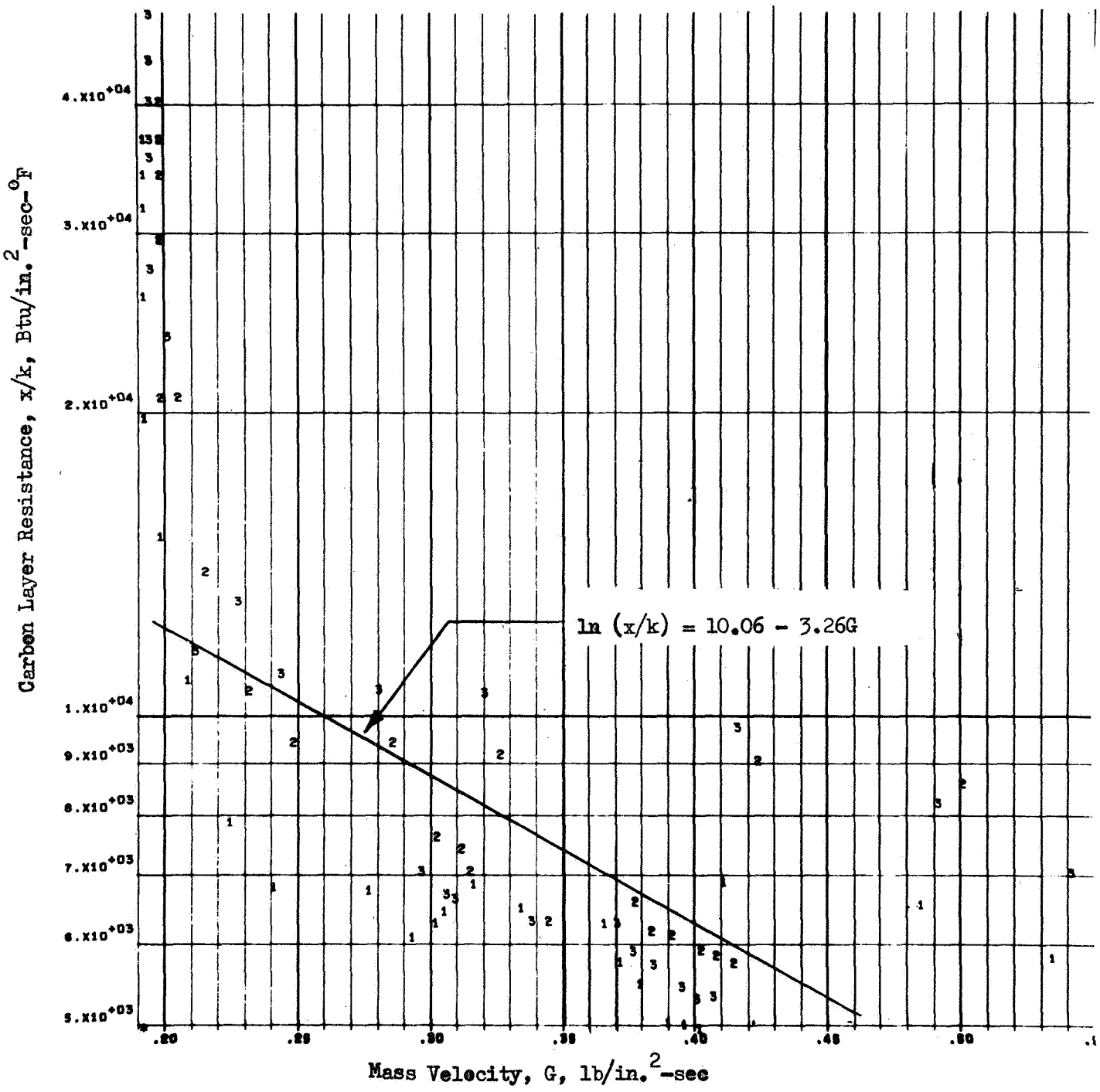

Figure B8 . Carbon Layer Resistance Correlation for FLOX/Pentane-Blend

mass velocity. The results are shown in Fig. B9 . Although the data are scattered (variation in mixture ratio, chamber pressure, combustion efficiency, and injector effects), separate trends existed for the values upstream of the throat and downstream of the throat. The equations for the two lines best representing these trends are:

$$\ln (x/k) = 5.96 + 1.05G \text{ (converging)}$$

and

$$\ln (x/k) = 8.24 - 1.17G \text{ (diverging)}$$

P_c psia = 225 - 272
ϵ_c = 2.78
ϵ = 3.54

F, lbs = 9300 - 11,300
MR = 3.73 - 6.08

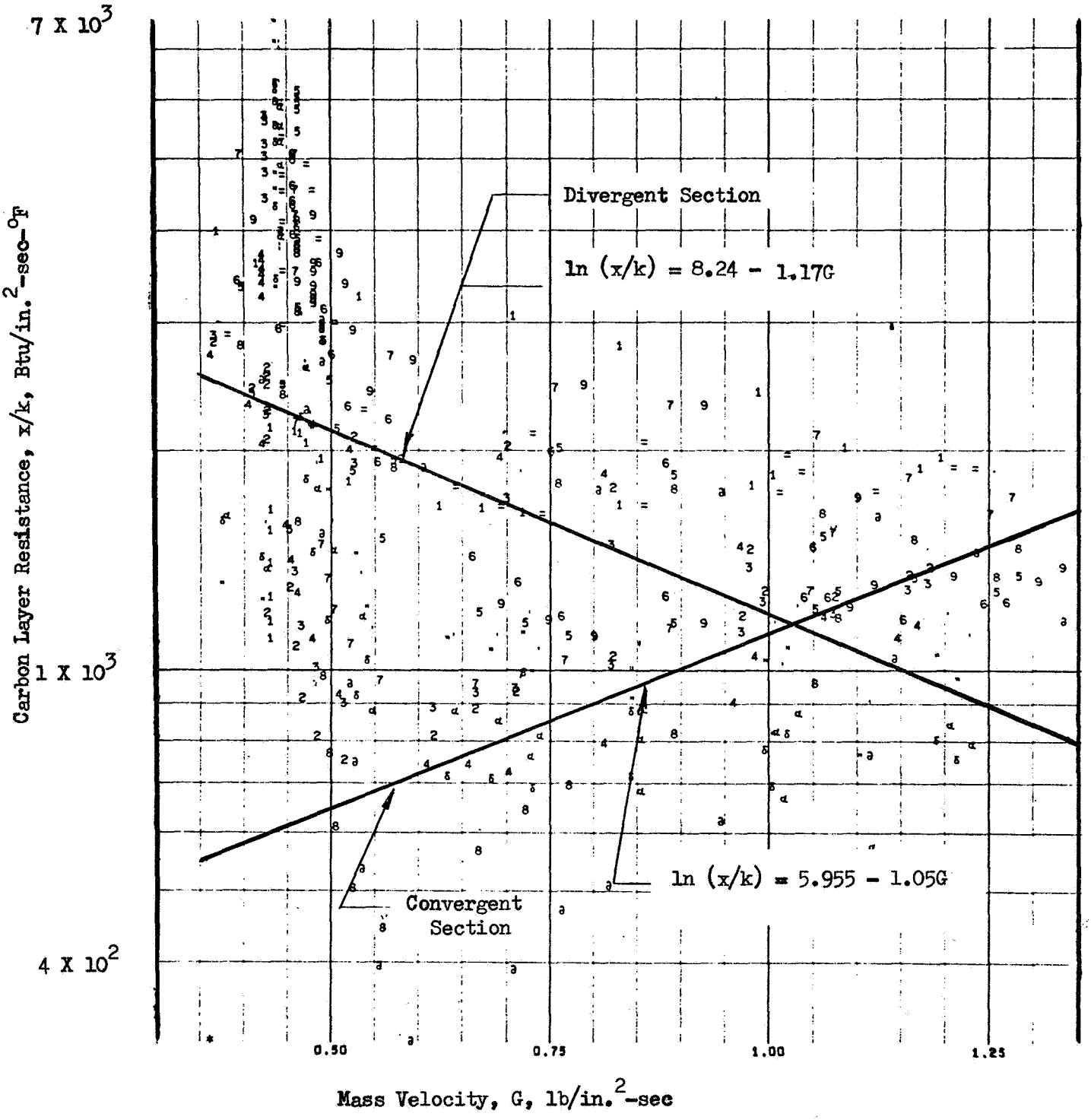

Figure B9 . Carbon Layer Resistance Correlation for FLOX/Methane

APPENDIX C

THERMAL DECOMPOSITION OF LIGHT HYDROCARBONS

The pyrolysis of lower hydrocarbons has been studied over several decades by many investigators, including some eminent physical chemists. Newer studies, utilizing modern techniques, yielded more extensive and, expectedly, more accurate data. For the most part, however, results obtained in relatively old classical studies remain valid.

KINETICS AND PRODUCTS OF PYROLYSIS

For uncatalyzed thermal decomposition, lower hydrocarbons (C_1-C_4) require temperatures of the order of 800 to 1500F. Some studies have been conducted at considerably higher temperatures but with concommitant shorter residence times; e.g., in shock tubes. The products are not only the smaller fragments, down to elemental carbon, but also some larger species. Free-radical type chain reactions are involved. First-order kinetics were found to be obeyed (although, in the case of ethane and propane, 3/2-order was reported to apply for special conditions). Thus, the reaction rates are generally governed by the equation

$$\frac{a}{a - x} = \exp(kt)$$

The initial concentration is a. The concentration decrease in time t is x. The reaction rate constant, k, is dependent upon temperature, T, and is expressed as

$$k = A \exp(E/RT)$$

where R is the universal gas constant and A and E are characteristic constants for the reaction. E is called the activation energy.

Methane, CH_4

On pyrolysis, methane yields hydrogen, ethane, ethylene, acetylene, propylene, and (at higher temperatures) elemental carbon.

In their studies of the pyrolysis of CH_4 by a dynamic method in the temperature range of 1740-2100F, Murgulescu and Schneider (Ref. 11) determined the overall activation energy to be 86.57 Kcal/mole. In another study of Schneider (Ref. 12) under static conditions at 1380 F, the activation energy was 87.25 Kcal/mole.

Data from other studies resulted in different kinetic parameters. An acceptable value for the rate constant of the overall reaction appears to be that determined in 1935 by Kassel (Ref. 13):

$$k = 10^{12} \exp(-79{,}000/RT) \text{ sec}^{-1}$$

The overall activation energy proves to be much lower than that required for the initiation step (considered to be $CH_4 \rightarrow CH_3\cdot + H$). Studying the thermal cracking of methane in an adiabatic compression apparatus within the range of 1590 to 1750K at 20 atm pressure, Kondratiev (Ref. 14) obtained for the primary step

$$k = 10^{15} \exp(-103{,}000/RT) \text{ sec}^{-1}$$

Under Kondratiev's conditions, the reaction was not measurable below 1592K (2407F). The activation energy obtained for the primary step perfectly coincides with the respective bond dissocaition energy

$$D(H_3C - H) = 103 \text{ Kcal/mole}$$

as determined in 1940 by Polanyi, and confirmed in 1950 by Szwarc (Ref. 15).

Ethane, C_2H_6

The decomposition of ethane leads to the formation of ethylene and H_2, followed by the breakdown of the ethylene. both processes involving free radical reactions. Earlier studies (Ref. 13) gave the activation energies of 70 and 74.5 Kcal/mole. The newer work of Laidler and Wojciechowski (Ref. 16) demonstrated that at approximately 1180F there is a transition to 3/2-order kinetics from the usual first order mechanism. The experimental data seemed to support the Kuchler-Theile mechanism (in preference to that of Rice and Herzfeld). The overall rate constant obtained in the extensive investigation of Laidler and Wojciechowski was

$$k = 1.07 \times 10^{15} \exp(-73{,}060/RT) \text{ sec}^{-1}$$

Propane, C_3H_8

The main products of decomposition of propane are CH_4, ethylene, propylene, and H_2 (in approximately equal amounts); the minor products include ethane, methylacetylene, acetylene, carbon and butane. The major reactions follow the stoichiometry

$$C_3H_8 \rightarrow C_3H_6 + H_2$$

and

$$C_3H_8 \rightarrow C_2H_4 + CH_4$$

Earlier studies of Steacie and Puddington (Ref. 13) led to the activation energy of 63.3 Kcal/mole. Similarly, Myers and Weston (quoted in Ref. 17), utilizing the experimental data of other investigators, estimated the activation energy at 63 Kcal/mole. However, in 1962 Laidler et al (Ref. 18) arrived at different values of kinetic parameters and, as in the case of ethane, showed that either first-order kinetics (at lower temperatures,

and high pressures) or 3/2-order kinetics (at higher temperatures, and lower pressures) were obeyed. A free radical mechanism involving six steps was postulated. The activation energies were 67.1 Kcal/mole for the first order region, and 54.5 Kcal/mole for the 3/2-order region. It will be noted that the average of these two values corresponds roughly to the results from earlier studies. However, the most recent (1967) investigation of the pyrolysis of propane by Kershenbaum and Martin (Ref. 19) at the University of Michigan led to the considerably lower value of the activation energy. The overall rate constant was

$$k = 2.4 \times 10^{11} \exp(-52{,}100/RT) \text{ sec}^{-1}$$

1-Butene, C_4H_8

Most of the information on the thermal decomposition of 1-butene derives from the studies in 1958 by Bryce and Kebarle (Ref. 20). Using a static system in the range 914 to 1040F, they found that the first-order kinetics were obeyed; the gaseous products were CH_4, propylene, ethylene, ethane, and some H_2; and the liquid products included cyclohexadiene, cyclopentane, and cyclopentadiene. A representative value of the overall rate constant can be taken as

$$k = 10^{13.2} \exp(-66{,}000/RT)$$

Earlier (1950), studying bond dissociation energies by the toluene carrier gas technique, Sehon and Szwarc (Ref. 21) found that the primary dissociation step in 1-butene has the rate constant

$$k = 10^{13} \exp(-61{,}500/RT) \text{ sec}^{-1}$$

This value was substantiated by recent (1965) studies of Kerr, Spencer, Trotman-Dickenson (Ref. 22). Using the aniline-carrier technique, they investigated the decomposition of 1-butene in the 900 to 990K temperature range and found the rate constant for primary dissociation step; i.e., for the bond rupture yielding the methyl and allyl radicals

$$CH_3CH_2CH = CH_2 \rightarrow CH_3\cdot + CH_2CH = CH_2$$

to be

$$k = 10^{12.71} \exp(-59{,}100/RT) \text{ sec}^{-1}$$

This value was identified with the respective C-C bond dissociation energy.

Since the overall activation energy is usually considerably lower than the activation energy for initiation in this type of processes (compare the results of Kassel and of Konratiev, in the case of methane), it would appear that the value for 1-butene given by Bryce and Kebarle might be too high.

The kinetic parameters for gas-phase thermal decomposition of the four hydrocarbons considered are assembled in Table C-1. It should be borne in mind that these parameters were obtained in different teperature ranges. It should be also noted that lower-activation energies are coupled with consistently lower pre-exponential factors, leading to smaller differences in the predicted rate constants.

DECOMPOSITION TEMPERATURE

The pyrolysis takes place over a range of temperatures. However, for practical reasons, it is important to know at what temperature the decomposition starts; i.e., becomes measurable, or begins to exert some noticeable effects. Such a "decomposition temperature" has to be

TABLE C-1

KINETIC PARAMETERS

Hydrocarbon	Investigators	E, cal/mole	A, sec^{-1}	log A
Methane	1. Kassel (1935)	79,000	10^{12}	12.0000
	*2. Kondratiev (1965)	103,000	10^{15}	15.0000
Ethane	Laidler & Wojciechowski (1961)	73,060	1.07×10^{15}	15.0294
Propane	1. Kershenbaum & Martin (1967)	52,100	2.4×10^{11}	11.3802
	2a. Laidler et al (1962)	54,500	8.5×10^{13}	13.9294
	2b. Laidler et al (1962)	67,100	2.6×10^{14}	14.4150
1-Butene	1. Bryce & Kebarle (1958)	66,000	$10^{13.2}$	13.2000
	2a. Sehon & Szwarc (1950)	61,500	10^{13}	13.0000
	2b. Kerr et al (1965)	59,100	$10^{12.71}$	12.7100

* Primary dissociation step.

defined arbitrarily. In the work at Monsanto Research Corp. (Ref. 8), the thermal decomposition temperature was arbitrarily taken as "that temperature where one mole percent of the material decomposes in one hour". Such a rate is actually rather slow and 1 percent decomposition in 1 minute or even 1 second is of greater interest. Three sets of values of the decomposition temperatures were calculated for comparison. First-order kinetics were used in all of the following calculations; it can be shown that an error of 0.5 in reaction order would only affect the calculated decomposition temperatures by approximately 50F.

The decomposition temperature can be calculated from kinetic parameters in the following manner:

$$k = \frac{1}{t} \ln \frac{a}{a-x} = \frac{2.303}{t} \log \frac{a}{a-x}$$

Hence, for 1-percent decomposition in 1 second

$$k = 2.303 \log \frac{100}{99} = 1.0044 \times 10^{-2} \text{ sec}^{-1} \quad (\log k = -1.9981)$$

For 1-percent decomposition in 1 minute

$$k = \frac{2.303}{60} \log \frac{100}{99} = 1.674 \times 10^{-4} \text{ sec}^{-1} \quad (\log k = -3.7762)$$

and for 1-percent decomposition in 1 hour

$$k = 2.79 \times 10^{-6} \text{ sec}^{-1} \quad (\log K = -5.5544)$$

From the Arrhenius equation

$$k = A \exp(-E/RT); -E = 2.303\, RT\, (\log k - \log A)$$

$$T = \frac{E}{2.303 \times 1.987\, (\log A - \log k)}$$

Therefore:

1. For 1 percent decomposition in 1 second

$$T = \frac{E}{4.576\ (1.9981 + \log A)}$$

2. For 1 percent decomposition in 1 minute

$$T = \frac{E}{4.576\ (3.7762 + \log A)}$$

3. For 1 percent decomposition in 1 hour

$$T = \frac{E}{4.576\ (5.5544 + \log A)}$$

The decomposition temperatures, calculated in this way from the kinetic parameters listed in Table C-1, are given in Table C-2.

TABLE C-2

DECOMPOSITION TEMPERATURES

Hydrocarbon		Calculated temperature, F, for 1 percent decomposition in		
	(Table C-1)	1 hour	1 minute	1 second
Methane	1.	1310	1510	1760
	2.	1512	1697	1928
Ethane		937	1069	1230
Propane	1.	750	892	1072
	2a.	640	752	887
	2b.	861	991	1148
1-Butene	1.	925	1069	1248
	2a.	844	982	1153
	2b.	813	950	1120

INHIBITION AND CATALYSIS

The thermal decomposition of hydrocarbons can be accelerated or, to some extent, inhibited by products of reaction, additives, or surfaces. The catalytic effect of surfaces is of particular interest.

Even in the homogeneous pyrolysis of methane under static conditions Schneider (Ref. 12) noted: (1) an induction period, 2) the "hydrogen effect"; i.e. slowing down of the dissociation by the accumulation of hydrogen; and (3) autocatalytic effect, caused by the accumulating ethane.

Because of the free-radical chain character of decomposition reactions, the process can be markedly inhibited by the addition of free radical acceptors, such as nitric oxide or olefin. Stepukhovich and Krol (Ref. 23) studied the effect of adding 0.5 to 10 percent butenes on the cracking of gaseous alkanes. The inhibiting effect of ethane was observed. It was suggested that the effect may be caused by the decomposition products (propylenes) rather than to butenes. Actually, this inhibitory effect may be quite relevant to the behavior of 1-butene.

The inhibitory effect of the added propylene on the decomposition of propane was studied extensively by Laidler et al (Ref. 24). Recently, the pronounced slowing down of decomposition of propane by the added propylene was demonstrated experimentally by Kershenbaum and Martin (Ref. 19).

The effect of surfaces on the decomposition of methane was investigated by Robinovich and Rodinov (Ref. 25), within their study of the formation of carbon filaments. Copper, porcelain, and pure carbon showed no catalytic effects. Platinum exhibited only a small accelerating effect, but metals of the Fe subgroup showed a marked catalytic activity. Quartz was found to act catalytically only above 1000C (1830F).

Laidler et al (Ref. 18) noted that the rate of propane decomposition in a quartz vessel was lowered approximately 20 percent by an increase in the surface-to-volume ratio by a factor of 12.

The work of Golder (Ref. 26) demonstrated how a catalyst can lower the "decomposition temperature." In the presence of a cobalt catalyst 1-butene yielded H_2, C, CH_4, and C_2H_6 at 350C (662F).

PYROLYTIC CARBON FORMATION

The decomposition of hydrocarbons at high temperatures leads to the formation of pyrolytic carbon on the reactor walls. The phenomenon is often referred to as particle formation (since the solid aggregates need not be pure carbon) or coking. Although higher hydrocarbons, especially with branched structure, yield carbon more readily, much of the useful information on pyrolytic carbon formation was obtained in studies of the pyrolysis of methane.

Greene et al (Ref. 27) studied the decomposition of methane in a shock tube at 1600 to 2500K and concluded that the results supported Porter's acetylene mechanism of carbon formation. Rafalkes and Tesner (Ref. 28) investigated the carbon formation from CH_4 (and other gases) also at high temperatures, 1150 to 1450C. They noted that the hydrogen formed in decomposition slowed down the carbon depostion on the reactor

walls. Robinovich and Rodinov (Ref. 25), in the previously cited work involving the study of catalytic effects, employed lower temperatures, 800 to 1250C (1472 to 2282F). Intensive growth of carbon filaments on metals by decomposition of methane was observed at 925 to 1000C (1700 to 1830F).

A recent (1967) paper by Syskov and Jelikhovskaya (Ref. 29) deals with the mechanism of formation of pyrolytic carbon. Porter's mechanism is not mentioned, and the direct decomposition of hydrocarbon molecules into carbon and hydrogen is dismissed as very unlikely. It is postulated that the formation of pyrolytic carbon occurs through a stage involving the formation of medium-size hydrocarbons in the molten state. These deposited compounds soon form drops because of the tendency for a minimum surface energy. Further development of this process leads to the formation of the globular structure of pryolytic carbon. The main part of the pyrolytic carbon is composed of a mixture of high-molecular hydrocarbons and their free radicals. The temperature of pyrolysis affects the size and composition of the globules. Thus, it was found experimentally from the pyrolysis of CH_4 that the average diameter of the globules was: less than 1μ for 850 C, 3.3μ for 900 C, and 36.0μ for 1000 C. The composition was 99.22 percent C and 0.18 percent H for 850 C, and 99.62 percent C and 0.07 percent H for 1000 C.

A large body of useful information on particle formation in the decomposition of higher molecular weight hydrocarbons has accumulated in the work at Monsanto Research Corp. (Ref. 30). Various polycyclic and higher paraffinic hydrocarbons ($C > 9$) were involved, but many of the conclusions appear to be general.

The following mechanism of particle formation was postulated (Ref. 8, p. 73):

$$A \rightarrow B \rightarrow C \longrightarrow D \longrightarrow E$$

Olefins			Particles
	Conjugated Olefins, Polyolefins	Colored Compounds	

The following evidence supported the above scheme: (1.) Particles appeared only after a substantial conversion of the original hydrocarbon (but their concentration then increases sharply, by many orders of magnitude, over a narrow conversion range). This behavior is characteristic of kinetics in which the product is formed from consecutive reactions. (2.) A plot of the olefin content goes through a well-defined maximum with increasing conversion. The olefins are converted to polymers or other higher structures. (3.) Color appearance always preceded particle formation; this color is presumably caused by the formation of conjugated structures or condensed aromatic ring systems.

A nonrigid polymeric material, immiscible with the hydrocarbon starting material, was believed to be formed prior to the formation of rigid coke particles. It will be recalled that Syskov and Jelikhovskaya (Ref. 29) also assume that the formation of rigid globules of polymeric carbon proceeds through a molten state.

At Monsanto Research Corporation, with the use of a special microcoker unit, the rates of particle formation were specifically studied at temperatures up to 1000F and at 500 psig pressure (Ref. 31). It was found that all the compounds investigated formed particles after 2 to 3 hours of exposure at 800F. A correlation between the ease of decomposition and the formation of particles was sought. An early report stated that "there is a rough correspondence between the resistance

of the initial hydrocarbon to thermal decomposition and the time the hydrocarbon can be held at a specified elevated temperature before particles appear, but the correspondence is far from exact" (Ref. 8). In later reports, however, it was maintained that there was a definite correspondence between these parameters for a homologous series (Ref. 30). A simple relationship was developed (Ref. 31):

$$Kp = a\ Kd$$

where Kp = rate constant of a particle formation
a = a constant for a homologous series
Kd = the rate of decomposition at 50 percent conversion.

It is unknown if this or similar relationship would apply to the series of lower hydrocarbons (in any case, the series is not homologous).

Other results from the Monsanto work which are of particular interest include:

1. Pressure was found to increase the decomposition rate (confirming the early observation of Meyers and Watson that the rate is proportional to the first power of the pressure, as expected from first-order reactions),
2. Alkyl substituents (on rings) usually increase the ease of particle formation,
3. Contacting hydrocarbons with oxygen at temperatures above 250 to 300F (but not lower) considerably decreased their thermal stability toward particle formation (Ref. 8 , p vi),
4. The presence of type 304 stainless steel, as reported earlier, or additional glass surface had no significant effect on the rate of

hydrocarbon decomposition at 800F (Ref. 8 , p. 72). Subsequent work revealed that type 302 stainless steel catalyzes the reactions leading to deposit formation (Ref. 31 , p. 48). The carbon deposit on the aluminum surface appeared at a higher temperature than in the case of type 302 stainless steel, but the deposit extended over a greater length of the reactor.

An investigation of carbon deposition is being carried out by E. Weger at the Washington University, St. Louis, Missouri, under contract AF04(694)-695 (Ref. 32). It involves the use of an induction furnace and temperatures up to 3000K.

At Pratt and Whitney Aircraft Corporation, experimental rocket firings were conducted using FLOX with methane, propane, 1-butene, and an eutectic blend of pentane and isopentane. According to M. R. Glickstein of Pratt and Whitney Aircraft Corporation (Ref. 4), there was no coking problem under normal conditions with methane and ethane, either in the combustion chamber or in cooling passages. However, propane led to various degrees of coking in regenerative cooling systems, and 1-butene was relatively the worst.

The literature data on the thermal decomposition of hydrocarbons were obtained with pure reactants, under well-controlled conditions, usually under reduced pressure, and normally in glass reaction vessels. Conditions in rocket thrust chambers are quite different, particularly with respect to pressure and the nature of the wall surface. Investigations under the actual or closely simulated conditions are, therefore, required to obtain more applicable data on thermal decomposition and coking in regenerative coolant passages.

APPENDIX D

CALCULATION OF COOLANT TRANSPORT PROPERTIES

Semitheoretical methods were used to obtain values of viscosity and thermal conductivity for methane, propane, and 1-butene in the regions where experimental data were lacking. This was particularly necessary for the 1-butene where very few experimental data were available. Reduced state and residual property methods were employed in these calculations.

METHANE

Experimental data were available for the thermal conductivity of methane in the low temperature region in Ref. 33. Values of thermal conductivity of liquid methane at atmospheric pressure, k^*, were available for moderate temperatures in Ref. 34. Values of k^* for higher-temperature methane vapor were also obtained from Ref. 34 and by using the following equation from Ref. 35.

$$k^* = (C_p/\lambda)\,(14.52\,T_R - 5.14)^{2/3} \times 10^{-6} \qquad (1)$$

where C_p is the specific heat at constant pressure, T_R is the reduced temperature, and λ is given by

$$\lambda = \sqrt{M}\,T_c^{1/6}/P_c^{2/3} \qquad (2)$$

where M is the molecular weight, T_c is the critical temperature and P_c is the critical pressure.

The effect of pressure on thermal conductivity was determined by the method of residual conductivity. Application of this procedure is based upon the assumption that the value of the residual thermal conductivity, $k-k^*$, depends uniquely upon the density of the substance. The density, ρ, in turn depends upon temperature and pressure. A graph of $k-k^*$ vs ρ was obtained from Ref. 33.

The same semitheoretical method was used to calculate the viscosity, μ, of methane at high temperatures. Values of μ^* vs temperature were obtained from the experimental data of Ref. 36 and calculated using the equation

$$\mu^* = 34 \times 10^{-5} \phi_{T_R}^{0.94} \tag{3}$$

where $\phi = \sqrt{M}\ P_c^{2/3}/T_c$ (4)

Values of residual viscosity, $(\mu - \mu^*)$, vs ρ were obtained from Ref. 36. The value of μ at any pressure was calculated as $\mu = \mu^* + (\mu - \mu^*)$. Viscosity data for all pressures at temperatures lower than 32F were also obtained from Ref. 36.

PROPANE

Values of k* from 0F to 1000F were obtained for propane from Ref. 34 and extrapolated to -300F. Values of k from Ref. 37 were used to generate a k-k* vs ρ curve which was, in turn, used to obtain values of thermal conductivity for pressures up to 2000 psia.

Propane viscosity data were available in Ref. 38 for all pressures and for temperatures as high as 450F. Viscosities at higher temperatures were obtained by calculating the μ^* values according to Eq. (3) and (4) and adding the residual viscosity values obtained from Ref. 38.

1-BUTENE

The thermal conductivity of 1-butene was calculated according to the method of reduced parameters. The variations of reduced thermal conductivity, k/k_c, with reduced temperature, T/T_c, and reduced pressure, P/P_c, was obtained from Ref. 39 based upon experimental data with ethylene. The critical point conductivity, k_c, was calculated according to

$$k_c = 62.2 \times 10^{-5} \sqrt{M}\ P_c^{2/3} / T_c^{1/6} \text{ cal/cm sec K} \qquad (5)$$

Values of μ^* were calculated for 1-butene using Eq. (3) and (4). These values agreed well with data given in Ref. 34. A graph of $\mu - \mu^*$ vs ρ was prepared using data from p. 177 of Ref. 34, reduced viscosity data from Ref. 40, and from Ref. 4.

APPENDIX E

DETAILED ANALYSIS TECHNIQUE

The detailed thrust chamber regenerative cooling designs were accomplished using the Rocketdyne "Regenerative Cooling Design or Analysis" digital computer program. The thrust chamber contour is divided into a number of axial increments ($\approx$ 75-100) and the required coolant mass flux and channel size to maintain a given wall temperature is determined at each station. The coolant pressure drop and bulk temperature rise between each station are calculated and summed along the contour to obtain total chamber values. A more detailed discussion of the factors entering into the design is presented below.

The case of a supercritical forced convection cooling design is first considered. The gas-side convective film coefficient (h_g) profile is calculated based on the combustion products potential flow field and solution of the integral momentum and energy equations as discussed in Appendix A. The heat flux at a given station is then calculated from the relation

$$Q/A = h_g \left(T_{aw} - T_{wg}\right) \tag{1}$$

where T_{wg} is the design wall temperature (input), and the adiabatic wall temperature (T_{aw}) is obtained for turbulent flow from the relation

$$T_{aw} = \eta_{C^*}^2 \; T_{o_{IDEAL}} \left[\frac{1 + \sqrt[3]{N_{PR}} \; \frac{\gamma - 1}{2} \; M^2}{1 + \frac{\gamma - 1}{2} \; M^2} \right] \tag{2}$$

The coolant-side wall temperature is obtained by integration of the basic one-dimensional conduction equation across the wall

$$\int_{T_{wc}}^{T_{wg}} k(T) \; dT = (Q/A) \; (t_w) \tag{3}$$

where k (T) denotes that the thermal conductivity of the wall material is a function of temperature. The above relation (3) is readily integrated for those materials (such as steel and Hastelloy X) whose thermal conductivities vary linearly with temperature. In the case of a non-linear variation (such as nickel) the relation (3) may be rewritten

$$\int_{T_{REF}}^{T_{wc}} k(T)\, dT = \int_{T_{REF}}^{T_{wg}} k(T)\, dT - (Q/A) \cdot t_w \qquad (4)$$

where T_{REF} denotes some reference temperature. Tabular values of the integral of k(T) dt are input as a function of temperature for the material of interest and solution of (4) for T_{wc} is readily achieved.

The coolant bulk temperature at the station of interest is equal to the value at the previous station plus the temperature increase between stations

$$T_{B_j} = T_{B_{j-1}} + \Delta T_B \qquad (5)$$

where

$$T_B = \frac{\bar{Q}/A \cdot \Delta A_s}{\dot{W}_c \cdot \bar{C}_p} \qquad (6)$$

The above solution for the bulk temperature rise is iterative since the coolant properties are a function of temperature and pressure.

The required coolant convective film coefficient (h_c) is then determined by

$$h_c = \frac{Q/A}{T_{wc} - T_B} \qquad (7)$$

The convective film coefficient is then related to the required coolant mass flux by a semi-empirical relation such as

$$N_{Nu_d} = \frac{h_c d_E}{k} = 0.023\, N_{Re}^{0.8}\, N_{PR}^{0.4}\, \phi_E \phi_C \qquad (8)$$

where the coolant properties are evaluated at a suitable reference temperature as discussed in subsequent paragraphs.

Equation (8) relates the coolant mass flux requirements and channel size (equivalent diameter) based on cooling considerations. The above two parameters are also interrelated based on geometric considerations so that further iteration is required to obtain consistent results.

The coolant pressure change between stations is the sum of the momentum and frictional effects,

$$\Delta P = \Delta P_M + \Delta P_f \qquad (9)$$

where

$$\Delta P_M = \frac{\rho V (\Delta V)}{g} \qquad (10)$$

and

$$\Delta P_f = f \cdot \frac{\Delta L}{d_E} \cdot \frac{G_c^2}{2 g \rho} \qquad (11)$$

The friction factor (f) is calculated from the transcendental Colebrook relation (Ref. 41)

$$\frac{1}{f} = 1.14 - 2 \log_{10} \left[\frac{9.35}{N_{Re} \cdot \sqrt{f}} + \frac{e}{d_E} \right] \qquad (12)$$

A further iteration on the pressure drop is required to account for coolant property dependence on the coolant static pressure.

The coolant pressure drop and bulk temperature rise are summed along the channel to obtain the jacket exit conditions. Iterations on the coolant jacket inlet pressure are normally required for compressible fluids in order to achieve the desired exit pressure. (The desired jacket exit pressure is derived from the chamber pressure and injector pressure drop.)

The chamber cooling design for a nucleate boiling liquid parallels the previous discussion. The primary difference is that the coolant-side wall temperature is fixed by the saturation temperature of the coolant. The combustion-side wall temperature and heat flux are calculated using Eqs. (1) - (3). Coolant velocities and channel sizes are then obtained from a suitable nucleate boiling correlation as discussed in the following paragraphs.

Coolant Correlations

Due to the extreme range of conditions considered in this study, three basic cooling regimes are encountered; (1) forced convection (supercritical cooling); (2) nucleate boiling; and (3) film boiling.

In the forced convection regime, the semi-empirical correlation

$$N_{Nu} = 0.023\, N_{Re}^{0.8} N_{PR}^{0.4}\, \phi_E \phi_C \qquad (13)$$

was utilized. The factors ϕ_E and ϕ_C represent entrance and curvature effects respectively. The entrance effect is determined from the relation (Ref. 42)

$$\phi_E = 1.53 \left(\frac{L}{d}\right)^{-0.15} \qquad \phi_E \geq 1 \qquad (14)$$

The curvature enhancement factor is based on considerable heated curved tube experimental data with hydrogen and nitrogen tetroxide (Ref. 43 and 7). A typical plot of the cooling enhancement on the outer wall as a function of the length to diameter ratio from the start of the curved portion is shown in Fig. E-1 . It is apparent that the coolant capability increases very rapidly once the curve is entered. In the current study the nozzle radius of curvature downstream of the throat was selected so as to achieve a curvature enhancement factor (ϕ_c) of 1.5 at the physical throat for an uppass (counterflow) cooling circuit. Some diminishment of this curvature enhancement might occur for rectangular channels due to changes in the secondary flow patterns. It is possible to make U-shaped or circular channels if necessary at the higher chamber pressures where the curvature factor is of great importance.

In the convective correlation (1) the coolant properties were evaluated at a film temperature which is the arithmetic average of the bulk temperature and coolant-side wall temperature. A comparison was made between this approach and that of evaluating the properties at the coolant bulk temperature. The results of the comparison are shown in Fig. E2 where the required coolant mass flux (G_c) is plotted as a function of bulk temperature for two heat flux levels. It is apparent that at temperatures below about 600R the use of a film temperature correlation results in a considerable increase in the predicted coolant mass flux requirements.

An alternate convective correlation developed for hydrogen (Ref. 42 and 7) including roughness effects is

$$N_{ST} = \frac{h_c}{C_p G_c} = \left[\frac{T_B}{T_{wc}}\right]^{0.55} \frac{f/2}{0.92 + \sqrt{f/2} \cdot \Phi(\varepsilon^*) - 8.48} \qquad (15)$$

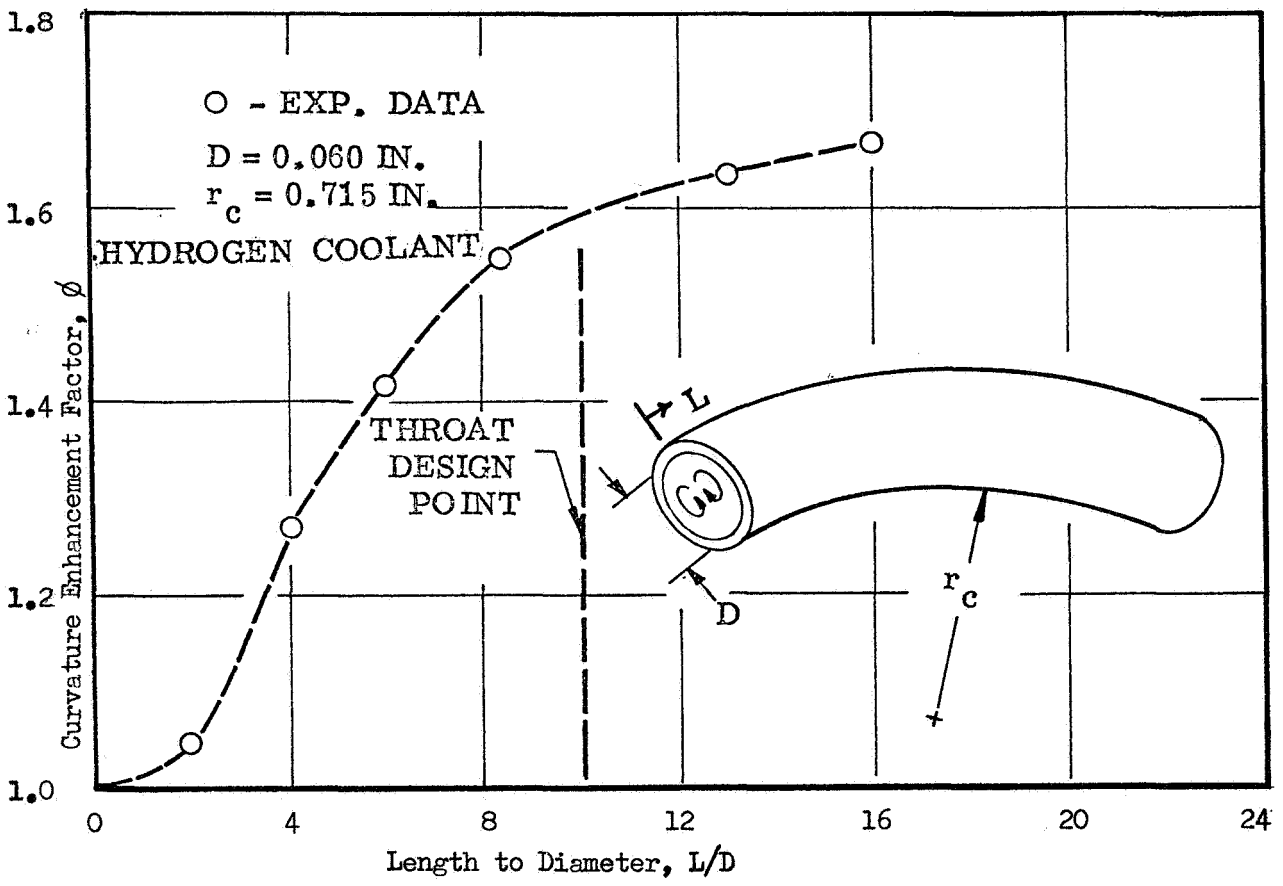

Figure E1. Coolant-Side Curvature Enhancement Factor

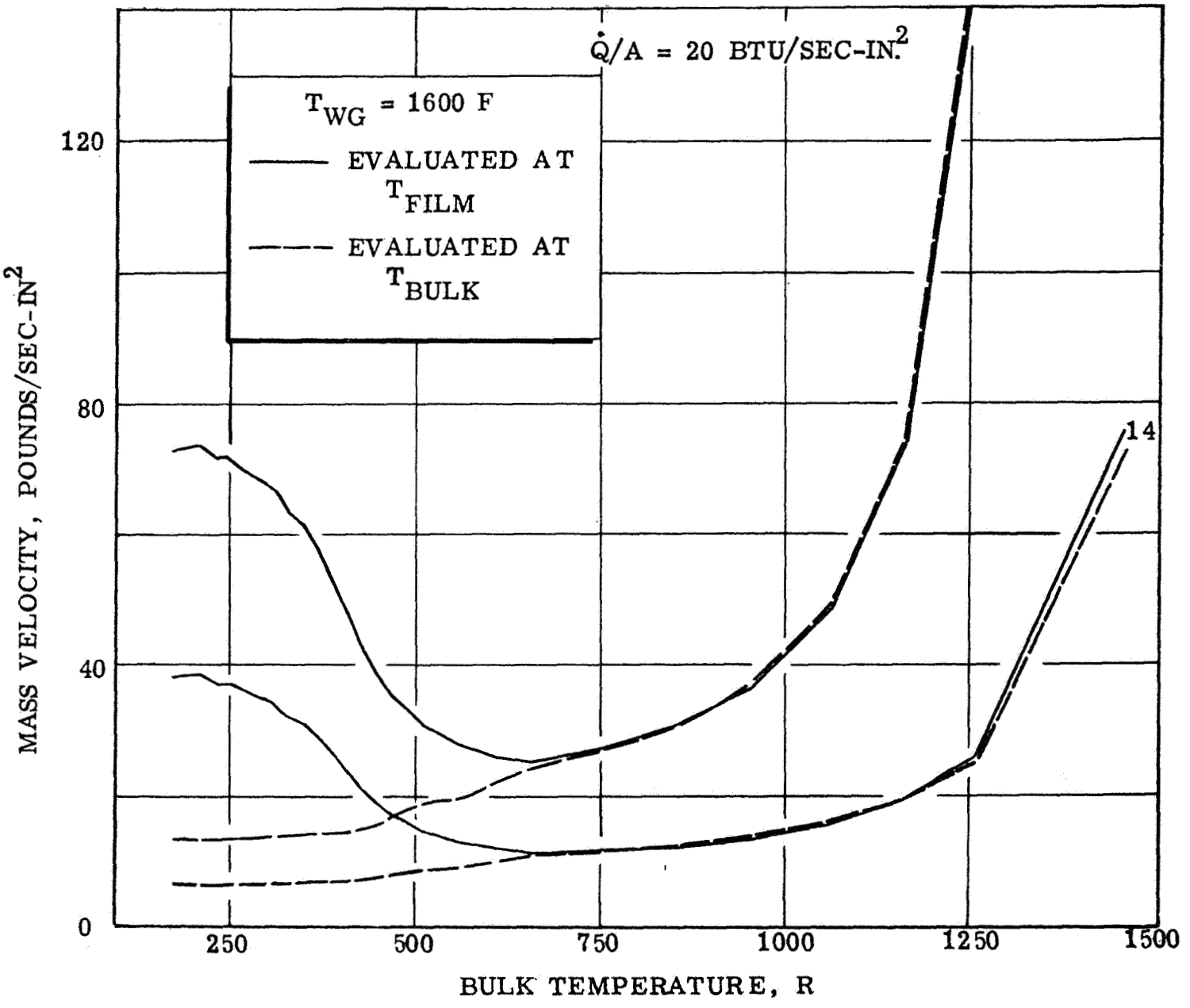

Figure E2. Effect of Temperature on Coolant Mass Velocity Requirements

where $\Phi(\varepsilon^*)$ is a relative roughness parameter (Ref. 7). The coolant properties in the above relation are evaluated at bulk conditions. The inclusion of the roughness factor can account for coolant enhancements of 10 - 30% at higher Reynolds numbers ($> 10^6$). The above relation was not used in this study because of the uncertainty of the exponent on the temperature correction factor for light hydrocarbons. Experimental data for supercritical cooling with light hydrocarbons is needed to more accurately determine the convective cooling correlation. It is believed that the use of equation (13) in this study represents a conservative approach.

In the case of nucleate boiling at sub-critical conditions, the correlation of Ref. 44 was used. This is of the form:

$$(Q/A)_{MAX} = a + b\,(T_{SAT} - T_B)\,V^c\,[d + e\,P] \qquad (16)$$

where the values of the coefficient as taken from Ref. 4 are listed below.

TABLE E-1

CORRELATION CONSTANTS FOR MAXIMUM NUCLEATE BOILING HEAT FLUX

Coolant	a	b	c	d	e
Methane	.2598	4.134×10^{-4}	0.9	1	0
Propane	.3227	9.431×10^{-4}	0.5	1.0376	-2.510×10^{-4}
Butene-1	.2736	7.430×10^{-4}	0.6	1.0619	-4.130×10^{-4}

The above correlation is based on rather low coolant velocities ($V \leq 25$ Ft/sec). Extrapolation to higher velocities as required in some of the chamber designs is somewhat uncertain. Experimental data at higher coolant velocities ($V = 100$ to 200 ft/sec) would be beneficial in the accurate determination of a chamber design.

In the current study the design coolant velocity was increased by 20 percent over the calculated burn-out value as a margin of safety.

In the film boiling regime, use was made of the data of Ref. 4. In general film boiling of the coolant was restricted to the portions of the nozzle having low heat flux values so that the wall temperatures would not become excessive.

APPENDIX F

DISTRIBUTION LIST FOR INTERIM REPORT NASA CR-72360

CONTRACT NAS3-11191

"SPACE STORABLE REGENERATIVE COOLING INVESTIGATION"

ROCKETDYNE DIVISION

NORTH AMERICAN-ROCKWELL CORPORATION

CANOGA PARK, CALIFORNIA

		COPIES
National Aeronautics and Space Administration Lewis Research Center 21000 Brookpark Road Cleveland, Ohio 44135		
Attention:	Contracting Officer, MS 500-210	1
	Liquid Rocket Technology Branch, MS 500-209	8
	Technical Report Control Office, MS 5-5	1
	Technology Utilization Office, MS 3-16	1
	AFSC Liaison Office, MS 4-1	2
	D. L. Nored, MS 500-209	1
	Library	2
	Harold Valentine, MS 501-2	1
	Office of Reliability and Quality Assurance, MS 500-203	1
	Rudolph A Duscha, MS 500-209	1
	E. W. Conrad, MS 100-1	1
	Larry H. Gordon, MS 500-209	1
National Aeronautics and Space Administration Washington, D. C. 20546		
Attention:	Code MT	1
	RPX	2
	RPL	2
	SV	1
	Robert F. Schmidt	1
	RPX, Frank W. Stephenson, Jr.	1
Scientific and Technical Information Facility P. O. Box 33 College Park, Maryland 20740		
Attention:	NASA Representative Code CPT	6

	COPIES
National Aeronautics and Space Administration Ames Research Center Moffett Field, California 94035 Attention: Library	1
C. A. Syvertson	1
National Aeronautics and Space Administration Flight Research Center P. O. Box 273 Edwards, California 93523 Attention: Library	1
National Aeronautics and Space Administration Goddard Space Flight Center Greenbelt, Maryland 20771 Attention: Library	1
C. R. Gunn, Delta	1
National Aeronautics and Space Administration John F. Kennedy Space Center Cocoa Beach, Florida 32931 Attention: Library	1
R. A. Raffaelli	1
National Aeronautics and Space Administration Langley Research Center Langley Station Hampton, Virginia 23365 Attention: Library	1
National Aeronautics and Space Administration Manned Spacecraft Center Houston, Texas 77001 Attention: Library	1
H. J. Brasseaux, PESD-Propulsion	1
W. Hammock	1
National Aeronautics and Space Administration George C. Marshall Space Flight Center Huntsville, Alabama 35812 Attention: Library	1
Keith Chandler, R-P&VE-PA	1
Lee W. Jones, R-PVE-PAS	1
Jet Propulsion Laboratory 4800 Oak Grove Drive Pasadena, California 91103 Attention: Library	1
W. B. Powell	1

	COPIES
Office of the Director of Defense Research & Engineering Washington, D. C. 20301 Attention: Dr. H. W. Schulz, Office of Asst. Dir. (Chem. Technology)	1
Defense Documentation Cameron Station Alexandria, Virginia 22314	1
RTD(RTNP) Bolling Air Force Base Washington, D. C. 20332	1
Arnold Engineering Development Center Air Force Systems Command Tullahoma, Tennessee 37389 Attention: AEOIM	1
Advanced Research Projects Agency Washington, D. C. 20525 Attention: D. E. Mock	1
Aeronautical Systems Division Air Force Systems Command Wright-Patterson Air Force Base Dayton, Ohio Attention: D. L. Schmidt Code ASRCNC-2	1
Air Force Missile Test Center Patrick Air Force Base, Florida Attention: L. J. Ullian	1
Air Force Systems Command (SCLT/Capt. S. W. Bowen)	1
Andrews Air Force Base Washington, D. C. 20332	1
Air Force Rocket Propulsion Laboratory (RPR) Edwards, California 93523	1
Air Force Rocket Propulsion Laboratory (RPM) Edwards, California 93523	1
Air Force FTC (FTAT-2) Edwards Air Force Base, California 93523	1
Attention: Col. J. M. Silk	1
Air Force Office of Scientific Research Washington, D. C. 20333 Attention: SREP, Dr. J. F. Masi	1

	COPIES
Commander Office of Research Analyses (OAR) Holloman Air Force Base, New Mexico 88330 Attention: RRRD	1
U. S. Air Force Washington 25, D. C. Attention: Col. C. K. Stambaugh, Code AFRST	1
Commanding Officer U. S. Army Research Office (Durham) Box CM, Duke Station Durham, North Carolina 27706	1
U. S. Army Missile Command Redstone Scientific Information Center Redstone Arsenal, Alabama 35808 Attention: Chief, Document Section	1
Dr. W. Wharton	1
Bureau of Naval Weapons Department of the Navy Washington, D. C. Attention: J. Kay, Code RTMS-41	1
Commander U. S. Naval Missile Center Point Mugu, California 93041 Attention: Technical Library	1
Commander U. S. Naval Ordnance Test Station China Lake, California 93557 Attention: Code 45	1
Code 753	1
W. F. Thorm, Code 4562	1
Commanding Officer Office of Naval Research 1030 E. Green Street Pasadena, California 91101	1
Director (Code 6180) U. S. Naval Research Laboratory Washington, D. C. 20390 Attention: H. W. Carhart	1
Picatinny Arsenal Dover, New Jersey Attention: I. Forsten, Chief Liquid Propulsion Laboratory	1

	COPIES
Air Force Aero Propulsion Laboratory Research & Technology Division Air Force Systems Command United States Air Force Wright-Patterson AFB, Ohio 45433 Attention: APRP (C. M. Donaldson)	1
Aerojet-General Corporation P. O. Box 296 Azusa, California 91703 Attention: Librarian	1
Aerojet-General Corporation 11711 South Woodruff Avenue Downey, California 90241 Attention: F. M. West, Chief Librarian	1
Aerojet-General Corporation P. O. Box 1947 Sacramento, California 95809 Attention: Technical Library 2484-2015A	1
Dr. C. M. Beighley	1
D. T. Bedsole	1
Aeronutronic Division of Philco Corporation Ford Road Newport Beach, California 92600 Attention: Dr. L. H. Linder, Manager	1
Technical Information Department	1
Aeroprojects, Incorporated 310 East Rosedale Avenue West Chester, Pennsylvania 19380 Attention: C. D. McKinney	1
Aerospace Corporation P. O. Box 95085 Los Angeles, California 90045 Attention: J. G. Wilder, MS-2293	1
Library-Documents	1

	COPIES
Arthur D. Little, Inc. Acorn Park Cambridge 40, Massachusetts Attention: A. C. Tobey	1
Astropower, Incorporated Subs. of Douglas Aircraft Company 2968 Randolph Avenue Costa Mesa, California Attention: Dr. George Moc Director, Research	1
Astrosystems, Incorporated 1275 Bloomfield Avenue Caldwell Township, New Jersey Attention: A. Mendenhall	1
ARO, Incorporated Arnold Engineering Development Center Arnold AF Station, Tennessee 37389 Attention: Dr. B. H. Goethert Chief Scientist	1
Atlantic Research Corporation Shirley Highway & Edsall Road Alexandria, Virginia 22314 Attention: A. Scurlock Security Office for Library	1 1
Battelle Memorial Institute 505 King Avenue Columbus, Ohio 43201 Attention: Report Library, Room 6A	1
Beech Aircraft Corporation Boulder Facility Box 631 Boulder, Colorado Attention: J. H. Rodgers	1
Bell Aerosystems, Inc. Box 1 Buffalo, New York 14205 Attention: T. Reinhardt W. M. Smith	1 1
Bendix Systems Division Bendix Corporation Ann Arbor, Michigan Attention: John M. Bureger	1

	COPIES
The Boeing Company Aero Space Division P. O. Box 3707 Seattle, Washington 98124 Attention: Ruth E. Peerenboom (1190)	1
J. D. Alexander	1
Chemical Propulsion Information Agency Applied Physics Laboratory 8621 Georgia Avenue Silver Spring, Maryland 20910	1
Chrysler Corporation Missile Division Warren, Michigan Attention: John Gates	1
Chrysler Corporation Space Division New Orleans, Louisiana Attention: Librarian	1
Curtiss-Wright Corporation Wright Aeronautical Division Woodridge, New Jersey Attention: G. Kelley	1
University of Denver Denver Research Institute P. O. Box 10127 Denver, Colorado 80210 Attention: Security Office	1
Douglas Aircraft Company, Inc. Santa Monica Division 3000 Ocean Park Blvd. Santa Monica. California 90405 Attention: J. L. Waisman	1
R. W. Hallet	1
G. W. Burge	1
Fairchild Stratos Corporation Aircraft Missiles Division Hagerstown, Maryland Attention: J. S. Kerr	1
General Dynamics/Astronautics P. O. Box 1128 San Diego, California 92112 Attention: F. Dore	1
Library & Information Services (128-00)	1

	COPIES
Convair Division General Dynamics Corporation P. O. Box 1128 San Diego, California 92112 Attention: Mr. W. Fenning Centaur Resident Project Office	1
General Electric Company Re-Entry Systems Department P. O. Box 8555 Philadelphia, Pennsylvania 19101 Attention: F. E. Schultz	1
General Electric Company Flight Propulsion Lab. Department Cincinnati 15, Ohio Attention: D. Suichu	1
Gruman Aircraft Engineering Corporation Bethpage, Long Island New York Attention: Joseph Gavin	1
Hercules Powder Company Allegheny Ballistics Laboratory P. O. Box 210 Cumberland, Maryland 21501 Attention: Library	1
IIT Research Institute Technology Center Chicago, Illinois 60616 Attention: Library	1
Kidde Aero-Space Division Walter Kidde & Company, Inc. 675 Main Street Belleville 9, New Jersey Attention: R. J. Hanville Director of Research Engineering	1
Lockheed Missiles & Space Company P. O. Box 504 Sunnyvale, California Attention: Y. C. Lee	1
Power Systems R&D Technical Information Center	1

	COPIES
Lockheed-California Company 10445 Glen Oaks Blvd. Pacoima, California Attention: G. D. Brewer	1
Lockheed Propulsion Company P. O. Box 111 Redlands, California 92374 Attention: Miss Belle Berlad, Librarian	1
H. L. Thackwell	1
Lockheed Missiles & Space Company Propulsion Engineering Division (D.55-11) 1111 Lockheed Way Sunnyvale, California 94087	1
Marquardt Corporation 16555 Saticoy Street Box 2013 - South Annex Van Nuys, California 91404 Attention: Librarian	1
W. D. Boardman, Jr.	1
Martin-Marietta Corporation Martin Division Baltimore 3, Maryland Attention: John Calathes (3214)	1
McDonnell Aircraft Corporation P. O. Box 6101 Lambert Field, Missouri Attention: R. A. Herzmark	1
North American Rockwell Corporation Space Division 12214 Lakewood Boulevard Downey, California 90242 Attention: Technical Information Center, D/096-722 (AJ01)	1
W. B. Bergen	1
Northrop Space Laboratories 1001 East Broadway Hawthorne, California Attention: Dr. William Howard	1
Purdue University Lafayette, Indiana 47907 Attention: Technical Librarian	1

	COPIES
Radio Corporation of America Astro-Electronics Division Defense Electronic Products Princeton, New Jersey Attention: S. Fairweather	1
Republic Aviation Corporation Farmingdale, Long Island New York Attention: Dr. William O'Donnell	1
Rocket Research Corporation 520 South Portland Street Seattle, Washington 98108	1
Rocketdyne Division of North American Rockwell Corporation 6633 Canoga Avenue Canoga Park, California 91304 Attention: Technical Information Center, Department 086	1
Rohm and Haas Company Redstone Arsenal Research Division Huntsville, Alabama 35808 Attention: Librarian	1
Space-General Corporation 777 Flower Street Glendale, California Attention: C. E. Roth	1
Stanford Research Institute 333 Ravenswood Avenue Menlo Park, California 94025 Attention: Thor Smith	1
Texaco Experiment, Incorporated P. O. Box 1-T Richmond, Virginia 23202 Attention: E. B. Monteath	1
Librarian	1
Thiokol Chemical Corporation Alpha Division, Huntsville Plant Huntsville, Alabama 35800 Attention: Technical Director	1
Thiokol Chemical Corporation Reaction Motors Division Denville, New Jersey 07834 Attention: A. Sherman	1
Librarian	1

	COPIES
Thiokol Chemical Corporation Redstone Division Huntsville, Alabama Attention: John Goodloe	1
TRW Systems, Incorporated 1 Space Park Redondo Beach, California 90200 Attention: G. W. Elverum	1
STL Tech. Lib. Doc. Acquisitions	1
TRW, Incorporated TAPCO Division 23555 Euclid Avenue Cleveland, Ohio 44117 Attention: P. T. Angell	1
United Aircraft Corporation Corporation Library 400 Main Street East Hartford, Connecticut 06118 Attention: Dr. David Rix	1
Erle Martin	1
United Aircraft Corporation Pratt & Whitney Division Florida Research & Development Center P. O. Box 2691 West Palm Beach, Florida 33402 Attention: R. J. Coar	1
Library	1
T. E. Bailey	1
Pete Mitchell	1
United Aircraft Corporation United Technology Center P. O. Box 358 Sunnyvale, California 94088 Attention: Librarian	1
Vought Astronautics Box 5907 Dallas 22, Texas Attention: Warren C. Trent	